University of Alberta

Studies of Troponin C Using NMR: Its Role in Muscle Regulation and Its Interactions with Calcium Modulating Agents.

by ©

Xu Wang

A thesis submitted to the Faculty of Graduate Studies and Research in partial fulfillment of the

requirements for the degree of Doctor of Philosophy

Department of Biochemistry

Edmonton, Alberta

Fall, 2005

Library and
Archives Canada

Published Heritage
Branch

395 Wellington Street
Ottawa ON K1A 0N4
Canada

Bibliothèque et
Archives Canada

Direction du
Patrimoine de l'édition

395, rue Wellington
Ottawa ON K1A 0N4
Canada

0-494-08750-1

Your file Votre référence
ISBN:
Our file Notre reference
ISBN:

NOTICE:
The author has granted a non-exclusive license allowing Library and Archives Canada to reproduce, publish, archive, preserve, conserve, communicate to the public by telecommunication or on the Internet, loan, distribute and sell theses worldwide, for commercial or non-commercial purposes, in microform, paper, electronic and/or any other formats.

The author retains copyright ownership and moral rights in this thesis. Neither the thesis nor substantial extracts from it may be printed or otherwise reproduced without the author's permission.

AVIS:
L'auteur a accordé une licence non exclusive permettant à la Bibliothèque et Archives Canada de reproduire, publier, archiver, sauvegarder, conserver, transmettre au public par télécommunication ou par l'Internet, prêter, distribuer et vendre des thèses partout dans le monde, à des fins commerciales ou autres, sur support microforme, papier, électronique et/ou autres formats.

L'auteur conserve la propriété du droit d'auteur et des droits moraux qui protège cette thèse. Ni la thèse ni des extraits substantiels de celle-ci ne doivent être imprimés ou autrement reproduits sans son autorisation.

In compliance with the Canadian Privacy Act some supporting forms may have been removed from this thesis.

While these forms may be included in the document page count, their removal does not represent any loss of content from the thesis.

Conformément à la loi canadienne sur la protection de la vie privée, quelques formulaires secondaires ont été enlevés de cette thèse.

Bien que ces formulaires aient inclus dans la pagination, il n'y aura aucun contenu manquant.

Canada

Abstract

At the heart of muscle regulation mechanism is troponin C (TnC), the Ca^{2+}-binding component of the troponin (Tn) complex. In Chapter II, interactions of EMD 57033, a Ca^{2+}-sensitizer, with the C-terminal domain of cardiac TnC (cCTnC) is investigated. The structure of cCTnC complexed to EMD 57033 showed that the drug binds to the hydrophobic groove on the domain and the orientation of the binding is such that the methyl group on the stereo centre of the drug makes contacts with residues in the core of the domain. The enantiomer of EMD 57033 was shown to interact differently with cCTnC than EMD 57033.

In Chapter III, the interaction of bepridil, another Ca^{2+}-sensitizer, with the N-terminal domain of cTnC (cNTnC) is studied. Bepridil is shown to weaken cTnC binding to the switch region of cTnI (cSp). The tertiary structure of the cNTnC•cSp•bepridil complex revealed that both bepridil and the N-terminal of cSp bind to the same hydrophobic region on cNTnC such bepridil displaces the N-terminal of cSp from its binding site, weakening the affinity of cSp for cTnC.

In Chapter IV, the effect of phosphorylation at residue S149 of cTnI on cTnI-cTnC interactions is investigated. The phosphorylation of S149 weakens the affinity of cSp for cTnC owing to the disruption of important cTnI-cTnC hydrophobic contacts. However, S149-phosphorylated cTnI showed a significant increase in its affinity for cTnC in the presence of the FHC mutation R161W.

Chapters V to VII are devoted to the development of an *in situ* ^{19}F NMR method that can be applied to myofibrils containing ^{19}F-labelled cTnC. Chapter V explains the

theoretical requirements needed to make the experiment feasible. It also examines the effect of the distribution of Tn on thin filament on the expected result of the experiment. Chapter VI focuses on methods for expressing ^{19}F-labelled proteins. In particular, it examines the correlation between the type of fluorinated amino acid and the degree of perturbation to the TnC structure. In Chapter VII, the structures of two fluorinated Phe-to-Trp mutants of cTnC are closely examined. The mutations themselves are found to produce no significant perturbation to the structure of cTnC. The mutants have a well defined indole ring orientation and are therefore good candidates for use in *in situ* NMR.

Acknowledgements

Throughout my graduate career, I was the fortunate recipient of many people's help and support, without which I would not be able to complete my PhD. On this occasion, I would like to thank a few people whose assistance was vital to the completion of this thesis.

First and foremost, I want to thank my PhD supervisor, Dr. Brian D. Sykes. Brian is the true mentor of my career. Not only did he pass on to me his almost encyclopedic knowledge about NMR, he has helped me to grow and mature as a scientist. NMR is a deep and versatile technique. Throughout my years in his laboratory, Brian has helped me to gain deeper appreciations of NMR. He showed me not only how to apply existing techniques but also how to extend and develop NMR in new applications. Many of the more novel ideas in this thesis (the ^{19}F *in situ* NMR technique, for example) were actually his doing. Furthermore, I want to thank Brian for showing me the way of science. Without his mentoring, I would not have the confidence, the independence and the creativity to become a true scientist.

I also want to thank Dr. Monica X. Li, who has given me much inspiration and support during my years in Brian's laboratory. She was the person who started me on the Ca^{2+} sensitizers and Tn protein phosphorylations/mutations projects. Without her help, it would have taken me considerably longer to get up and going. Her impeccable knowledge of the muscle regulation process has never ceased to amaze me and her fountain of new project ideas seemed inexhaustible.

Prof. Leo Spyracopoulos was also instrumental during my development. Other than Brian, Leo is the person who has taught me the most about science and NMR. His finger prints are on many of the NMR experiments I have used in this thesis, especially the ^{15}N, ^{13}C-filtered experiment used in Chapter II and III. Even after he had already left the laboratory to establish his own group, he never hesitated to extend a helping hand whenever the need arose.

Dr. Pascal Mercier was the senior graduate student in the laboratory when I joined. Over the years he has offered me assistance on many aspects of protein NMR spectroscopy, especially those concerned with data processing and analysis. As the NMRView guru in the laboratory, his presence has reduced the amount of time I spent struggling with the software considerably. Dr. Darrin A. Lindhout also warrants special mention on this occasion. Darrin and I were Brian's students during exactly the same time period. However, he always seemed to be one step ahead of me in everything we did, and he unselfishly passed on to me any practical tips I might need.

I am also indebted to other members of the muscle group including Dr. Tharin Blumenschein, Ryan Hoffman and Grant Gay. All of whom have supplied me with many fresh ideas through the numerous discussions we have had together. Other laboratory members including Dr. Steffen Graether, Erik Saude and Olga Baryshnikova have also lent me their support whenever I needed, and it is truly a pleasure to work with them all.

I want to give a special thanks to all the technologists in the laboratory including David Corson, Gerry McQuaid, Robert Boyco, Jeff Devries, Angela Thiesson, Linda Saltibus and Melissa Rakovszky. David taught me all the practical aspects of protein expression and purification when I first joined the laboratory, and is the most honest and good-natured person I have met. Gerry and Jeff took care of the NMR spectrometers I used. Without them, my life would be very difficult.

A number of non-laboratory members have also provided assistance during my years as a student. I am obliged to Susan Smith, our secretary, who was responsible for all my studentship applications and who diligently reminded me every year when it was time to renew them. Without Sue's help, the amount of time I spent on bureaucratic paper work would be considerably larger. People from NANUC as well as Jan Rainey, the postdoctoral fellow from PENCE also rendered me much assistance over the years.

And finally I want to thank the Alberta Heritage Foundation for Medical Research and Canadian Institutes of Health Research for providing the funding that supported me throughout my graduate studies. I would not have lived so comfortably and be so worry free while pursuing my academic career if it wasn't for their generous support.

Table of Contents

Chapter I Introduction to Muscle Regulation and Its Modulation 1

Historical Background 1

Tn-Mediated Muscle Regulation: The Present 8

Effects of Phosphorylations and Mutations of Cardiac Tn Proteins on Muscle Regulation 18

Calcium Sensitizers & cardiac TnC 22

Tn-Mediated Muscle Regulation: The Future 25

References 27

Chapter II Structure of the C-terminal domain of Human Cardiac Troponin C in Complex with EMD 57033 30

Introduction 30

Experimental Procedures 34

Sample preparation 34

Purification of cCTnC with Reverse-phase HPLC 35

Stability of EMD 57033, 57439 and 73186 in aqueous solution 36

NMR spectroscopy 37

Data Processing and Peak Calibration 37

Structural calculations 38

Results and Discussion 42

Binding Interface between EMD 57033 and cCTnC 47

EMD 57033-induced structural changes 49

Competition of EMD 57033 with $cTnI_{128\text{-}147}$ *and* $cTnI_{34\text{-}71}$ 53

cCTnC as the in situ target of EMD 57033 57

Binding of EMD 57439 and EMD 73186 to cCTnC 58

Conclusion 62

References 64

Chapter III Structure of Regulatory N-Domain of Human Cardiac Troponin C Complexed to Bepridil and Cardiac Troponin I$_{147\text{-}163}$ 67

Introduction 67

Experimental Procedures 70

Sample preparation 70

cTnI$_{147\text{-}163}$ and bepridil titration of ^{15}N-cNTnC•Ca^{2+} 70

NMR spectroscopy 72

Data processing and peak calibration 73

Structure calculations 73

Results and Discussion 77

Effect of bepridil and cTnI$_{147\text{-}163}$ on cNTnC 77

Overall structure 79

Structure of cNTnC 81

Structure of bepridil 84

Structure of cTnI$_{147\text{-}163}$ 87

Comparison of the ternary structure with the binary structure 89

Bepridil's Ca^{2+}-sensitizing activity 92

Conclusion 93

References 96

Chapter IV Effects of S41/S43, S149 Phosphorylations and R161W Mutation on cTnI-cTnC Interactions 98

Introduction 98

Experimental Procedures 101

Protein Sample Preparation 101

Synthetic Peptides 102

Titration of ^{15}N-cTnC•3Ca^{2+} with cRp and cRp-S41P/S43P 102

Titration of ^{15}N-cNTnC•Ca^{2+} with cSp, cSp-S149P, cSp-R161W, and cSp-S149P-R161W 103

NMR Spectroscopy 103

Results 105

Effect of S41/S43 phosphorylation on the interaction of cRp with cTnC•3Ca^{2+} 105

Effect of S149 phosphorylation and R161W mutation 108

Discussion 116

References 122

Chapter V Introduction to in situ ^{19}F NMR of myofibrils 124

Introduction 124

Theoretical Background 128

Distribution of Tn on the thin filament 132

Fluorine-labelling of TnC 134

Concentration of TnC in Myofibrils 136

Effects of Distribution of Tn on Signal Shap 137

Effects of side chain dihedral angle fluctuations on signal shape 140

Other application of the *in situ* NMR system 141

Methods 143

Construction of Tn-actin filament model 143

Spectral simulation 143

References 145

Chapter VI Expression of Fluorinated Proteins and The Effect of Expression System on Expression Level and Protein Structural Integrity 147

Introduction 147

Experimental Details 151

Site directed mutagenesis 151

Expression of 5fW- and 4fW-labelled F104W and F153W mutants in BL21(DE3)pLysS 151

Expression of 5fW- and 4fW-labelled F104W and F153W mutants in W3110TrpA33 152

Purification of the mutants 153

Sample Preparation and Calcium titrations 153

Data acquisition and analysis 154

Results 155

Expression of 5fW-labelled F104W and F153W mutants in BL21 155

Expression of 4fW-labelled F104W and F153W mutants 161

Expression of 5fW-labelled F104W and F153W mutants in W3110TrpA33 163

Discussions 167

Conclusion 168

References 170

Chapter VII Effects of Phe-to-Trp Mutations and 5fW Incorporation on the Solution Structure of Cardiac Trponin C 171

Introduction 171

Experimental Details 175

Site directed mutagenesis 175

Expression of the protein and incorporation of fluorotryptophan 175

Purification of the mutants 176

Sample Preparation and Calcium titrations 177

Data acquisition and analysis 177

Structural determination 178

^{19}F-^{1}H Heteronuclear NOE Determination 179

Molecular dynamics simulations 180

Results 181

Effects of ^{19}F incorporation on Backbone Chemical Shifts 181

Structures of the mutants 183

Discussion 194

Potential use of the mutants as probes in in situ NMR 194

Structures of the F104 and F153 mutants 196

Signal doubling in the F153(5fW) mutant 196

Conclusion 197

References 201

Chapter VIII Conclusion 203

Role of Ca^{2+}-sensitizers in modulating cardiac function 203

Phosphorylations and mutations in cTnI 206

***in situ* ^{19}F NMR of myofibrils** 207

References 210

List of Tables

II-1. NMR spectra acquired and parameters used for structure determination 40

II-2. Structural statistics of the ensemble of 30 structures of cCTnC-EMD 57033 complex 41

II-3. Interhelical angles of various EF hands 53

III-1. NMR spectra acquired and parameters used for structure determination 75

III-2. Structural statistics of the ensemble of 30 ternary structures 76

III-3. Interhelical angles of various EF hands 92

IV-1. K_Ds (μM) and $\Delta G_{binding}$ for peptides binding to cTnC 118

VII-1. NMR spectra acquired and parameters used for structure determination 199

VII-2. Interhelical angles of the C-domain of wild type and mutant TnCs 200

VII-3. Trp and 5fW side chain dihedral angles of the mutants 200

List of Figures

I-1. Organization of the skeletal muscle 3

I-2. Electron micrograph of longitudinal sections of myofibrils 4

I-3. Structure of thick filament and myosin 5

I-4. Schematic diagrams of myofibrils in progressively more contracted states 6

I-5. The Six-step cycle of myosin-actin interaction 6

I-6. Structure of tropomyosin 9

I-7. Schematic representation of the 3-state Tm regulation model 9

I-8. Structure of the skeletal TnC 11

I-9. Structure of the cardiac TnC 13

I-10. The schematic representation of TnI's interactions with other proteins 14

I-11. A model of Ca^{2+}-dependent interactions of the cardiac troponin 16

I-12. Phophorylation and FHC mutation sites on Tn proteins 20

I-13. Chemical structures of Ca^{2+} sensitizers 23

II-1. Chemical structures of EMD 57033, 57439 & 73186 31

II-2. Physiological effects of EMD 57033 & its enantiomer 32

II-3. Titration of Ca^{2+}-saturated cCTnC with EMD 57033 42

II-4. Solution structure of the cCTnC-EMD 57033 binary complex 44

II-5. ^{1}H chemical shift assignments & intramolecular NOEs of EMD 57033 45

II-6. NOE contacts between the protein and the drug 48

II-7. Comparison of cCTnC in the binary complex with other structures 50

II-8. 2D {^{1}H, ^{15}N}-HSQC NMR spectra of the titrations of cCTnC with $cTnI_{34-71}$ in the presence and absence of EMD 57033 54

II-9. Titrations of Ca^{2+}-saturated cCTnC with EMD 57439 and EMD 73186 59

II-10. Back bone atom chemical shift changes during titrations of EMD 57033 and EMD 57439 visualized on the backbone structures of cCTnC 60

III-1. Enhancement of muscle fibre force development by bepridil 68

III-2. Titrations of cNTnC with $cTnI_{147\text{-}163}$ and bepridil 77

III-3. Assigned HSQC spectrum of the uniformly ^{15}N-labelled cNTnC complexed to $cTnI_{147\text{-}163}$ and bepridil 80

III-4. Solution structure of the $cNTnC{\bullet}Ca^{2+}{\bullet}cTnI_{147\text{-}163}{\bullet}$bepridil complex 82

III-5. ^{1}H chemical shift assignments of bepridil and intramolecular NOEs of bepridil and $cTnI_{147\text{-}163}$ 85

III-6. Intermolecular NOEs between bepridil, $cTnI_{147\text{-}163}$ and cNTnC 88

III-7. Comparisons between cNTnC of the ternary structure and that from other complexes 90

III-8. An overview of the effects of bepridil and the $cTnI_{147\text{-}163}$ peptide on cNTnC 94

IV-1. A schematic representation of the phosphorylation and FHC mutation sites on Tn proteins 99

IV-2. Titration of $^{15}N\text{-}cTnC{\bullet}3Ca^{2+}$ with cRp and cRp-S41P/S43P 106

IV-3. Ribbon and surface representations of the structure of $cCTnC{\bullet}2Ca^{2+}{\bullet}$cRp 107

IV-4.1. Titrations of ^{15}N-cNTnC with wild type cSp and cSp-S149P 109

IV-4.2. Titrations of ^{15}N-cNTnC with cSp-R161W and cSp-R161W-S149P 110

IV-5. Comparison of induced chemical shift changes of all titrations 112

IV-6. Chemical shift changed induced in cNTnC by cSp 114

V-1. Coordinate transformations required to obtain protein orientation 132

V-2. Model of the thin filament and its arrangements in sarcomere 133

V-3. Simulated ^{19}F spectra of the 5fW powder pattern and ^{19}F-labelled myofibril 136

V-4. Effects of myofibril orientation and helical Tn distribution on simulated ^{19}F NMR spectra of F104(5fW)-labelled myofibrils 138

V-5. Effects of myofibril orientation and helical Tn distribution on simulated ^{19}F NMR spectra of F153(5fW)-labelled myofibrils 139

V-6. Effects of side chain dihedral angle χ^2 on NMR spectra of myofibrils 142

VI-1. Sites of Phe-to-Trp mutations and the nomenclature of the indole ring 149

VI-2. 1D ^{19}F NMR spectra of non-Ca^{2+}-depeleted samples of the F104(5fW) mutant and the F153(5fW) mutant 156

VI-3. 1D traces from {^{1}H, ^{15}N}-HSQC spectra taken during the Ca^{2+} titrations of BL21-expressed mutants containing L-Trp and 5fW 157

VI-4. {^{1}H, ^{15}N}-HSQC spectra of all wild type and mutants... 159

VI-5. Mass spectra of BL21- and A33-expressed F104(5fW) mutant 160

VI-6. 1D traces from {^{1}H, ^{15}N}-HSQC spectra taken during the Ca^{2+} titrations of the BL21-expressed F104(4fW) and F153(4fW) mutants 162

VI-7. Comparisons between portions of {^{1}H, ^{15}N}-HSQC spectra for F104W and F104(4fW) mutants 164

VI-8. 1D traces from {^{1}H, ^{15}N}-HSQC spectrrum taken during the Ca^{2+} titrations of the A33-expressed F104(4fW) mutant 165

VII-1. Sites of Phe-to-Trp mutations and the nomenclature of the indole ring............. 173

VII-2. {^{1}H, ^{15}N}-HSQC spectra of wild type cTnC and mutants 182

VII-3. Visual representation of the ^{19}F-induced signal doubling of the F153(5fW) mutant 183
VII-4. Ensembles of back bone structures of the mutants........ 186
VII-5. Backbone overlays of the mutants with wild type cTnC........ 187
VII-6. ^{1}H-^{1}H NOEs and ^{19}F-^{1}H NOEs from the F104W and F104(5fW) mutants 189
VII-7. ^{1}H-^{1}H NOEs and ^{19}F-^{1}H NOEs from the F153W and F153(5fW) mutants 192
VII-8. Molecular dynamic simulations of the 5fW indole ring in the F104(5fw) and F153(5fW) mutants 195

List of Abbreviations

4fW	4-fluorotryptophan
5fW	5-fluorotryptophan
ADP	adenosine di-phosphate
ATP	adeneosine tri-phosphate
cAMP	cyclic adenosine monophosphate
(c, s)TnC	(cardiac, skeletal) troponin C
(c, s)TnI	(cardiac, skeletal) troponin I
(c, s)NTnC	(cardiac, skeletal) troponin C, N-terminal domain
(c, s)CTnC	(cardiac, skeletal) troponin C, C-terminal domain
cIp	cardiac troponin I, inhibitory region peptide (residues 129 to 147)
cRp	cardiac troponin I, N-terminal region peptide (residues 34 to 71)
cSp	cardiac troponin I, switch region peptide (residues 147 to 163)
CSA	chemical shift anisotropy
ELC	essential light chain
FHC	Familial Hypertrophic Cardiomyopathy
DTT	dithiothreitol
DSS	2,2-dimethyl-2-silapentane-5-sulfonic acid
HSQC	Heteronuclear Single Quantum Coherence
NOE	Nuclear Overhauser Enhancer
PAK	p21-acivated kinase
PDE	phosphodiesterase

PKA	protein kinase A
PKC	protein kinase C
RLC	regulatory light chain
RMSD	root mean squared deviation
Tm	Tropomyosin
Tn	Troponin

Chapter I

Introduction to Muscle Regulation and Its Modulation

Historical Background

Although all life forms are capable of some type of motility, the ability to harvest and synchronize the power of these micro-movements and convert them into visible, macro-movements is a talent exclusive to a small group of higher organisms. Indeed, it is not an exaggeration to say the development of specialized contractile tissue has changed the course of biology and evolution profoundly. Without muscle, our cardiovascular and digestive systems would be highly compromised. The ingestion and delivery of nutrients over a large system would be difficult, if not impossible. We certainly would not enjoy the benefits of rapid movement provided by skeletal muscle, which means new sources of food would be unexplored, and new territory for habitation would go unoccupied. In fact, most organisms in the animal kingdom probably would never develop beyond the stage of jelly fish without muscle.

It is difficult to know if people ever wondered how muscle contracts before the days of modern science. If they did, the explanation they received was most likely based in mystical and supernatural believes rather than physical observations. However, by the middle of the 19th century, modern science has chipped away that mystic considerably. People begun to realize muscle contraction is no more than a process that converts chemical energy to mechanical energy, with heat being released as a byproduct, a process not very much different than that performed by the steam engine in fact. However, exactly how muscle manage to accomplish this would not become clear for another 100 years. Scientists in the 19th and the beginning of the 20th century conducted many experiments on intact muscles. Data on force generated, amount of heat produced as well as metabolic rates of a host of biochemical processes during muscle contraction were collected and analyzed. A number of models for muscle contractile mechanisms were proposed, and then refuted. The issue was not finally settled (or as settled as the present day knowledge allows) until the 1950s, when new techniques such as X-ray diffraction and electron microscopy were introduced into biological sciences. This turned out to be the deciding factor since the understanding of the muscle micro-structure proved to be the key to solving the mystery.

As far back as the 19th century, people have observed muscle's regular structure under light microscopes. But with the aid of electron microscopy, the investigators were able to gain quantitative information from the picture. They noticed that muscle (striated muscle) had a very regular, striated pattern, consisted of regular repeating units of dark and light bands. Through the measurement of refractive index, they discerned that the arrays of bands are consisted of only two types of fibres interleaved. The thicker filament, they knew, were made out of mostly myosin. They also observed that during contraction, the length of neither type of filaments changed much, what did change is the extent of overlapping between the two fibres, with the overlapping being most extensive during contraction. Based on these observations, Hugh Huxley and Andrew Huxley independently proposed the sliding filament model for muscle contraction in 1954(*5, 6*). It immediately gained wide spread acceptance. Although the modern biochemical picture of muscle contraction is far more complex than the original model proposed by the two Huxleys, the spirit of the sliding filament model continues to be the back bone of muscle contraction mechanism.

Today, our knowledge of the micro-architecture of the muscle paints a more complex picture. Results from modern molecular physiology tell us skeletal muscle is consisted of long bundles of muscle fibres, each 20 to 100μm in diameter. These fibres can often span the entire length of the muscle and are, in fact, single, multinucleated cells. Each fibre is, in turn, composed of parallel bundles of myofibrils which can also extend the entire length of the fibre (Figure I-1). And it is the underlying structure of the myofibril that gives rise to the striation of the muscle.

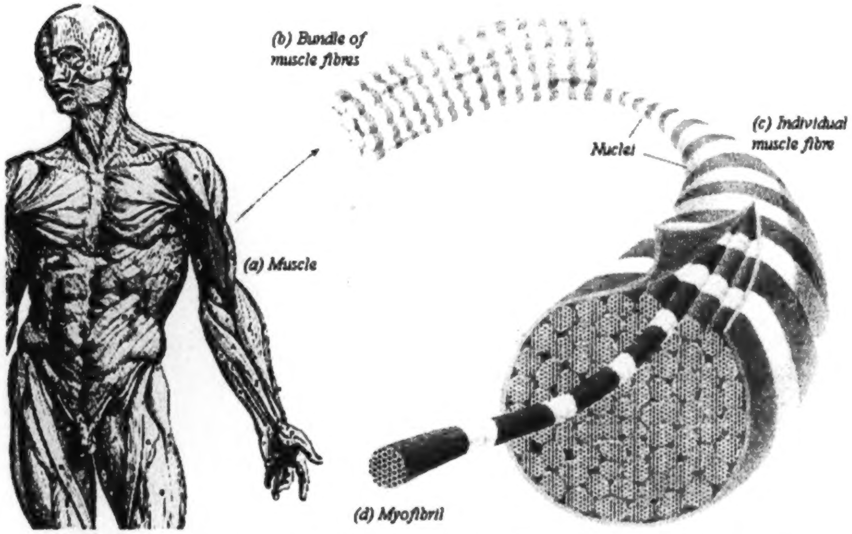

Figure I-1. Organization of skeletal muscles. Skeletal muscle is consisted of well organized muscle fibre bundles. Each muscle fibre is a multinucleated cells containing long myofibrils. Taken from (*1*) with permission.

The darker and lighter regions of myofibrils are termed A bands and I bands, respectively. A bands are centered around a dark line, known as the M disk. Within each A band, there is a region with slightly lighter electron density called the H zone. I bands, on the other hand, are centre on dark bands known as Z disks (Figure I-2). The reason for the darker appearance of A bands lies in the higher electron density of the 150Å-diameter thick filaments composing it. In comparison, I bands are consisted of 75Å-diameter thin filaments only. H zones, it turns out, are lighter than the neighbouring regions of A bands

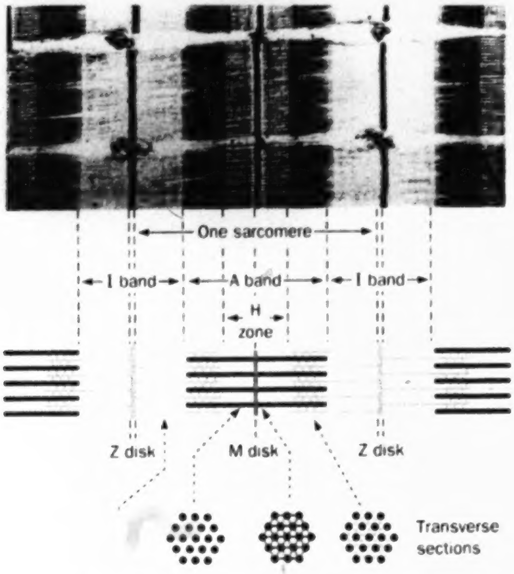

Figure I-2. Electron micrograph of longitudinal sections of myofibrils. The myofibril's major features are shown in the schematic drawing below. Note the hexagonal cross sectional packing of filaments. Taken from (*1*) with permission.

because thick filaments in H zones do not overlap with thin filaments from I bands. Electron micrograph of the muscle cross-section also revealed that the filaments are packed hexagonally with twice as many thin filaments interlocked amongst the thick filaments.

We now know, as did the Huxleys, the thick filaments are consisted of myosin. Myosin is a long rod-shaped molecule with a globular N-terminal domain (Figure I-3a). The N-terminal of myosin contained all the ATPase activity of the myosin as well as the thin filament binding site. The N-terminal is also where the essential light chain (ELC) and the regulatory light chain (RLC) bind to myosin. Owing to its globular structure compared to the rest of myosin, the myosin N-terminal domain is usually referred to as the myosin head. The rest of myosin adopts a continuous α-helical conformation that dimerizes with its counterpart on another myosin molecule to form a long coiled-coil

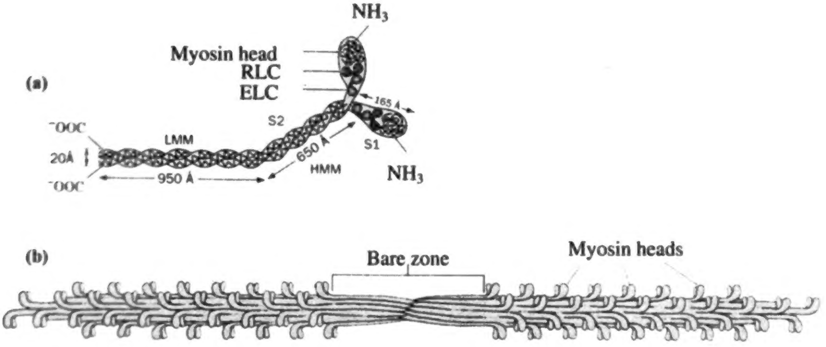

Figure I-3. a) Schematic representation of a myosin dimer. The long α-helical tails of myosins wrap around each other to form the coiled-coil stem of the dimer. An ELC and an RLC chain is bound to the myosin head. b) Schematic representation of a thick filament. Each filament contains several hundred myosin molecules oriented such that their heads point away from the axial centre of the filament. Taken from (*1*) with permission.

stem structure. The dimers then aggregate together through interactions between the stems, creating the basic thick filament (Figure I-3b). The thin filament is consisted of mainly fibrous actin polymer. The structure of the polymer is arranged in a helical pattern, with 14 units of molecule completing a revolution and all 4 domains of the actin contacting neighbouring actin molecules. The thin filament also includes muscle regulatory proteins that are the focus of this thesis.

During muscle contraction, myosin "walks" along the actin filament by utilizing the energy released through ATP hydrolysis. This shortens the lateral distance between adjacent filaments of similar type, achieving muscle shortening (Figure I-4). The present day biochemical knowledge is consistent with a 6-step cycle for each myosin step on the thin filament (Figure I-5). At the beginning of each cycle, myosin head is apo and tightly bound to actin on the thin filament. Upon binding an ATP molecule, a conformation change on the N-terminal of myosin causes myosin to be released from actin. Then the ATP-bound to the myosin head is hydrolyzed, inducing a major conformation change in the myosin N-terminal, changing the angle between the myosin head and the thick

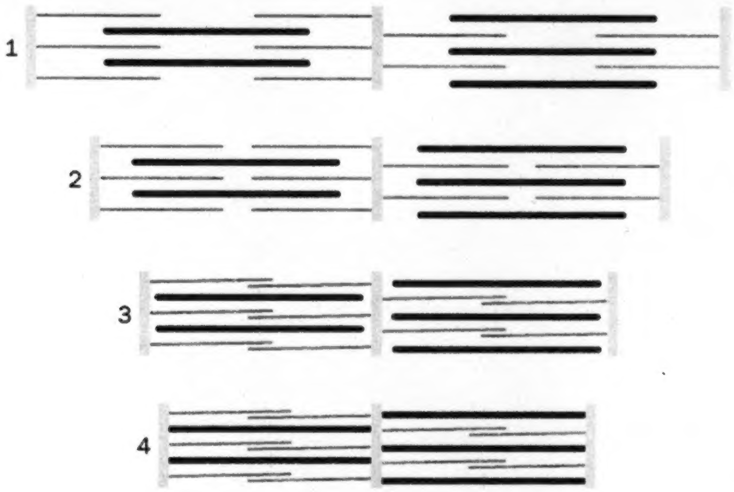

Figure I-4. Schematic diagrams of myofibrils in progressively more contracted states(1-4). The colouring scheme is similar to that used in Figure 2. The width of I bands and H zones decrease upon contraction but the lengths of thick and thin filaments remain constant. Note the overlap between neighbouring thin filaments in states 3 and 4. Taken from (*1*) with permission.

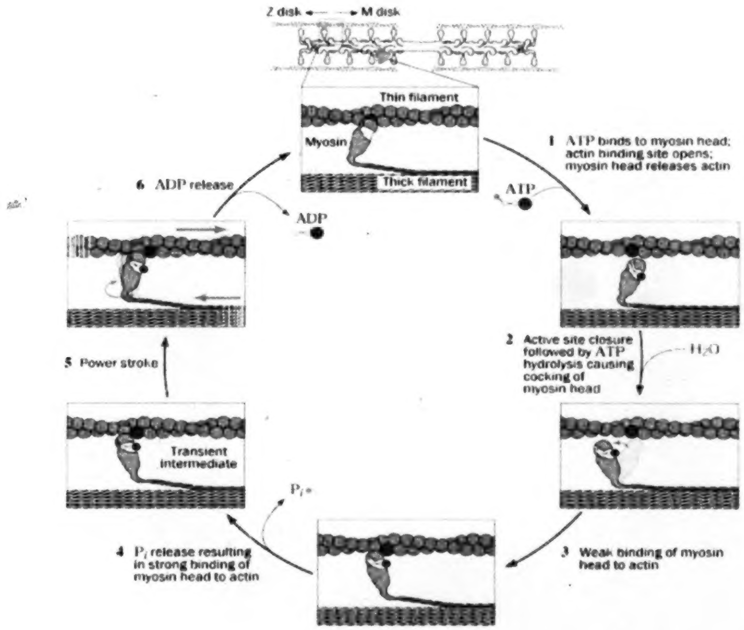
Z disk
M disk
Thin filament
Myosin
Thick filament
1 ATP binds to myosin head; actin binding site opens; myosin head releases actin
ATP
6 ADP release
ADP
2 Active site closure followed by ATP hydrolysis causing cocking of myosin head
H₂O
5 Power stroke
Transient intermediate
Pᵢ
4 Pᵢ release resulting in strong binding of myosin head to actin
3 Weak binding of myosin head to actin

Figure I-5. The Six-step cycle of myosin-actin interaction. Taken from (*1*) with permission.

filament. The myosin head then binds weakly to another actin molecule on the thin filament. The weak binding is strengthened greatly when the inorganic phosphate group is released. This is followed by another conformation change in the myosin head, leading to the pulling of the thin filament towards the M-disk by almost 6 nm. Afterwards, ADP bound to the myosin head is released and myosin head adopts the conformation it has at the start of the cycle, and the whole cycle is ready to be repeated if necessary. It is estimated that each myosin is capable of completing 5 cycles every second.

Notwithstanding people's fascination with the mechanisms of muscle contraction, many of us have taken for granted our intricate ability to regulate the activity of the muscle. Only when we lose our grip on muscle regulation, as in instances where we are infected by some exotic poison or inflicted by a certain unfortunate disease, do we become keenly aware of its vital impact.

About ten years after the two Huxleys proposed the sliding filament model, an important discovery was made in the field of muscle regulation research – Setsuro Ebashi proved unambiguously that troponin (Tn) and tropomyosin (Tm) are the mediators for Ca^{2+}-dependent muscle regulation(*7*). Ca^{2+} has been implemented in muscle activity as early as the 19th century(*8-11*), and in the 1940s, biochemist Heilbrunn was the first to connect Ca^{2+} with the regulation of muscle contraction(*12*). Not only did Heilbrunn have a clear idea on the role played by Ca^{2+} in muscle activation, he also hinted at the source of Ca^{2+} used for the activation and the mechanism of its release. But owing to the low concentration of Ca^{2+} required to trigger muscle contraction, people remained skeptical about the results. Ebashi was able to show skinned muscle fibre containing no troponin and tropomyosin was active irrespective of the Ca^{2+} concentration where as fibres with troponin and tropomyosin demonstrated Ca^{2+}-dependent activation(*7, 13*). Furthermore, neither tropomyosin nor troponin alone was able to achieve this Ca^{2+}-dependent regulation. A few years after Ebashi's publication, researchers realized troponin was a complex of proteins rather than a single homogenous protein, as Ebashi has believed(*14-19*). It would be another few years before it was certain whether troponin is a complex of two or three proteins. When the dust finally settled, troponin had three subunits. One of the components, troponin C (TnC) is responsible for all the Ca^{2+}-sensitizing activity of troponin, while another component, troponin I (TnI) is responsible for the inhibitory activity of troponin. The third members of complex, troponin T (TnT) is responsible for connecting the troponin proteins with tropomyosin.

Tn-Mediated Muscle Regulation: The Present

Our knowledge of muscle regulation has developed tremendously since Ebashi's discovery. Extensive biochemical as well as biophysical studies on interactions of Tn proteins with each other as well as with actin and tropomyosin were conducted. These studies, although lacking in high resolution structural information, helped to map out regions of Tn proteins important for functions of Tn. In the last 10 years, high resolution techniques, such as X-ray crystallography and solution NMR, also had impressive successes investigating Tn protein interactions in relaxed and activated muscle, especially that between TnI and TnC. As more information becomes available, it is surprising to discover that much of the rigorous and robust process of muscle regulation depends on subtle and minute shifts in protein conformational equilibrium, a point we are just beginning to appreciate.

Before people even realized the existence of troponin, tropomyosin was thought to be the major player in muscle regulation. Tropomyosin is a 284-residue protein that exists

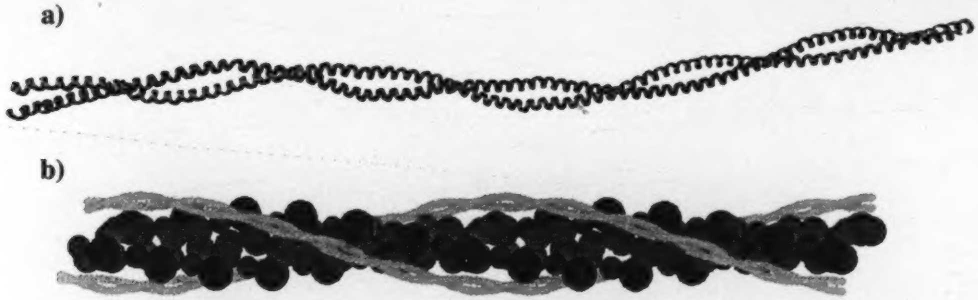

Figure I-6. a) X-ray crystal structure of the porcine skeletal tropomyosin dimer (PDB access code 1C1G). b) The schematic diagram of actin polymer (red spheres with subdomain 1 of actins being dark red) complexed to tropomyosin dimers (green strands). Taken from (*3*).

as a dimmer (Figure I-6a). Two isoforms of Tm are produced by the body and their expression levels vary according to tissue type. In skeletal muscle, both α- and β-isoforms are expressed and Tm exists primarily as a heterodimer, where as in cardiac muscle, expression of α-form is dominant and Tm exists as a homodimer. Both isoforms adopt the conformation of a single, long α-helix with the dimer being a coiled-coil structure approx. 42nm long, enough to span 7 actin molecules on the thin filament (Figure I-6b). Neighbouring modules of tropomyosin are believed to overlap in a head-to-tail fashion, forming a long contiguous strand. It is also believed that Tm binds to actin filaments mainly through electrostatic interactions. The tightness of binding is

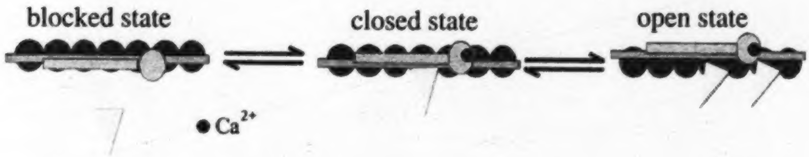

Figure I-7. Schematic representation of the 3-state Tm regulation model. The actin filament is represented by red spheres. Tm is represented by the green stick. Tn is represented by the light blue globular head with tail. Myosin head is represented by yellow triangles and Ca^{2+} ion is represented by the black circle. Taken from (*3*).

determined by many factors, including the isoform of Tm, existence of other proteins such as myosin and troponin, and most importantly, whether Tm can form a contiguous strand on the actin filament. Tm has long been known to inhibit the actin-myosin interaction by blocking the myosin-binding sites on actin. The inhibition is released when Tm rotates away from the interaction sites. More detailed kinetic analysis showed three states of Tm movement exist, usually termed blocked, closed, and open states(*20*). In the blocked state, Tm is positioned such that most myosin-binding sites on actin are blocked and myosin-actin interactions are impossible. In the closed state, Tm is believed to rotate 25° to 30° away from its original position, exposing some hydrophobic interaction sites on actin and allowing weak binding of the myosin head to actin(*21, 22*). Tm rotates a further 10° in the switch from the closed to open state, exposing even more interaction sites and leading to strong binding of the myosin head to actin(*23-26*) (Figure I-7). CryoEM as well as kinetic studies showed that Ca^{2+}-binding to troponin helps to switch Tm from blocked to closed state, and binding of myosin head to actin changes Tm to the open state, during which strong binding of myosin head to actin takes place and force generation occurs(*21-26*). There is considerable argument as to whether Tm dynamics exist as the clear cut three-state model, or can it adopt any position in between states. But it is clear that troponin and Ca^{2+} play a crucial role in controlling the state of Tm on the filament.

Compared with Tm, which spans continuously the entire thin filament, the existence of Tn, which is only distributed one unit every seven actin molecules, on the thin filament is rather insubstantial. The core domain of Tn, which includes TnC, TnI and T2 region of TnT, is situated approx. 15nm away from the amino terminal end of Tm. However, the tail of Tn, the T1 region of TnT, extends all the way to the overlapping region between the two neighbouring Tm. Besides Tm, Tn also interacts with actin and inhibits the actomyosin ATPase in an one-to-one manner. In almost all cases, interactions between Tn and other proteins occurs in a Ca^{2+}-dependent manner, making Tn the initiator of Ca^{2+}-dependent muscle regulatory activity.

TnC, the Ca^{2+}-sensor of Tn, is a regular EF-hand protein, whose sequence bears high-homology to many other EF-hand proteins. From the very beginning of Tn research, the importance of TnC in sensing $[Ca^{2+}]$ change has been recognized. EDTA extraction of TnC from skinned muscle fibres prevents muscle activation by Ca^{2+}. Only after the fibres are reconstituted with TnC, is the Ca^{2+}-dependent activity of muscle restored(*27*). The first high-resolution structure of skeletal TnC (sTnC) was solved by Herzberg & James in 1985(*28*) (Figure I-8a). The structure shows that TnC adopts a dumb-bell shape composed of two globular domains connected by a straight α-helix. Each globular domain contains two Ca^{2+}-binding EF-hand motifs. Biochemical analysis showed the two

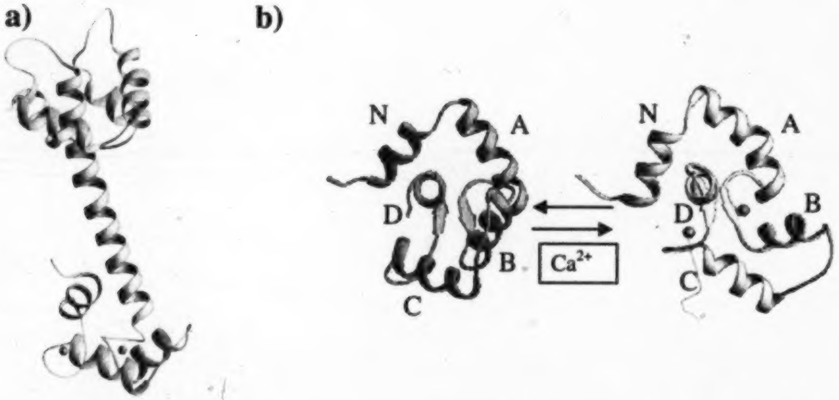

Figure I-8. a) The ribbon representation of the skeletal TnC structure solved by Herzberg & James (PDB access code 5TNC). The N-terminal domain of the molecule is in the apo state while the C-terminal domain is Ca^{2+} saturated. Ca^{2+} ions are represented by green spheres. b) The N-terminal domain of TnC in different Ca^{2+} states. Note the conformational changed induced by Ca^{2+} binding (PDB access code 1TNP and 1TNQ).

EF-hand motifs in the C-terminal globular domain possessed very high Ca^{2+} affinity (K_D ~0.1μM), which implies the C-terminal domain remains Ca^{2+}-saturated even when the cell is in its most Ca^{2+}-depleted state. Thus the C-terminal domain can not be involved in Ca^{2+}-dependent regulation if its Ca^{2+} state does not change with the change in cytoplasmic Ca^{2+} concentration. The N-terminal domain, on the other hand, has relatively low Ca^{2+} affinity (K_D ~10μM) and is most likely apo when Ca^{2+} concentration in the cytoplasm is low. But it will become Ca^{2+}-saturated after Ca^{2+} ions sequestered in the sarcoplasmic reticulum is released into the cytoplasm. The apo structure of the N-terminal domain adopts a so called "closed" conformation, in which helices A/B and helices C/D are collapsed together, hiding the hydrophobic core of the protein(*29*). Upon binding Ca^{2+}, the beginning of helix B undergoes a conformation change from coil to α-helix. This results in changes in the interhelical angles between helices A/B and C/D, causing the hydrophobic core to be exposed and available for interactions with TnI, essentially adopting the same conformation as the C-terminal domain of TnC(*29*). This conformational transition, it turns out, is crucial for the muscle regulation mechanism, and is the first step in a cascade of protein interactions that initiate muscle contraction (Figure I-8b).

The solution structure of sTnC for various species has also been solved using NMR techniques. The biggest difference between the solution structure and the crystal structure lies in the conformation of the central linker connecting the two domains. In the crystal structure, central linker adopts a rigid α-helical conformation, fixing the orientation between N- and C-terminal domains. However, in the solution structure, the central linker is unstructured and flexible, making the N- and C-terminal domains behave completely independent of each other(*30*). More and more evidence from other studies

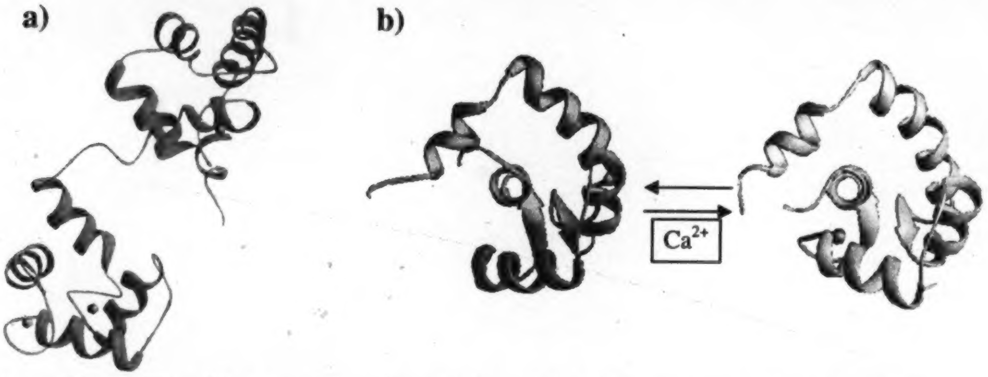

Figure I-9. a) The ribbon representation of the cardiac TnC structure solved by Sia et al. (PDB access code 1AJ4). Both domains of the molecule are Ca^{2+} saturated. Ca^{2+} ions are represented by green spheres. b) The N-terminal domain of cTnC in different Ca^{2+} states. Note the the lack of conformational changed induced by Ca^{2+} binding (PDB access codes for the apo and Ca^{2+}-bound state structures are 1SKT and 1AP4, respectively).

seem to indicate that the conformation adopted by the central linker in the Tn complex is Ca^{2+}-dependent, with the linker being unstructured and flexible in the apo state, and long and α-helical in the Ca^{2+}-bound state(*31*).

Cardiac TnC (cTnC) is translated from the same gene as that of slow skeletal TnC, thus shares high sequence homology with sTnC. However, there is one important difference between them: amino acid substitutions at three places in the first Ca^{2+}-binding site of cTnC destroyed the pentagonal bipyramidal side chain coordination required to complex the Ca^{2+} ion, making the site defunct as a Ca^{2+} binder. The first high-resolution structure of cTnC was solved in 1997 by Sia et al. using solution NMR techniques(*32*) (Figure I-9a). It revealed the impact of these mutations on the structure of cTnC. In particular, it showed that the N-terminal domain of cTnC adopts a "closed" conformation even in the Ca^{2+}-saturated state(*32*) (Figure I-9b). This lack of conformation change upon binding Ca^{2+} would have important physiological consequences on the activity of muscle. Specifically, the hydrophobic surface on TnC required to interact with TnI is not automatically available in the case of cardiac TnC (see the section on cTnC-cTnI interaction for more detail). Although it would be eventually proven that TnC-TnI interactions can still take place and TnI was able to force open the N-terminal domain upon binding(*33*), the energetics of the interaction under those situations is distinctively unfavourable.

The Tn protein with whom TnC interacts the most is TnI. TnI is single handedly responsible for all the inhibitory activity exhibited by Tn on actomyosin ATPase activity. Skeletal TnI (sTnI) is a 176-residue protein consisted of mostly α-helical segments. The cardiac version of TnI (cTnI) is highly homologous to sTnI with the exception of a 33-residue N-terminal insert. Mutagenesis study showed that cTnI devoid of the N-terminal extension is still functional (*34*). However, there are two PKA phosphorylation sites in this region. Absence of this region can have an effect on the modulation of cardiac muscle activity during special circumstances. Various biochemical studies have

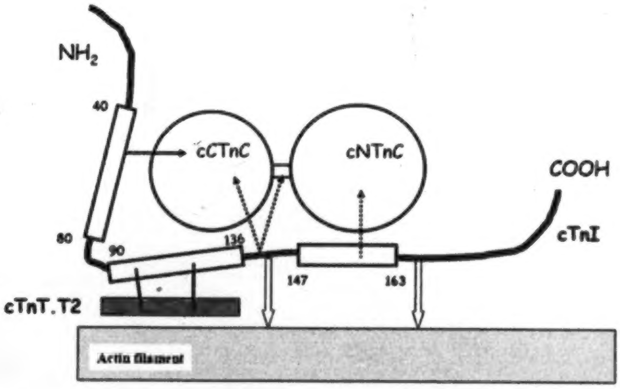

Figure I-10. The schematic representation of TnI's interactions with other Tn proteins and actin. TnI is represented in red with α-helices represented by boxed segments. TnC is represented by the green dumb-bell shaped structure. T2 region of cTnT is represented by the light blue box. Solid arrows represent Ca^{2+}-independent interactions. Dashed arrows represent interactions in the presence of Ca^{2+}. Block arrows represent interactions in the absence of Ca^{2+}. Residue numbers of TnI are marked along the schematic representation.

identified two regions of TnI that interact extensively with actin molecules during the apo state. Only one of these segments, consisted of residues 127 to 143 (all TnI numbering schemes used in this volume will be that of cTnI with the N-terminal extension), is needed to inhibit all myosin-binding to actin and activation of actomyosin ATPase in a one-to-one manner(*35*) (Figure I-10). This region is thus termed the inhibitory region. The residues C-terminal to the inhibitory region, residues 173 to 182, make up the second actin-binding region on TnI(*36*). Whether this segment of TnI is directly involved in inhibiting muscle activity is unclear. However, both segments are instrumental in anchoring Tn to the thin filament during muscle relaxation.

Owing to their physiological importance, interactions between TnC and TnI have been extensively studied. Knowledge accumulated from various biochemical and structural studies have allowed us to have a very good understanding of how changes in these interactions activate the muscle. Two segments of TnI are involved in majority of TnI-TnC interactions. The N-terminal of TnI, residues 34 to 71, binds tightly to the hydrophobic groove on the C-terminal of TnC (*37*). Cross-linking study as well as high resolution structure of Tn core domain, both in the presence and absence of Ca^{2+}, indicate the interactions between the C-terminal domain of TnC and the N-terminal of TnI is constant and independent of Ca^{2+} concentration (*4, 31, 38*). Thus it is reasonable to conclude that this region of TnI serves only to structurally connect TnC and TnI (Figure I-10). A second region of TnI, residues 147 to 163, exhibit Ca^{2+}-dependent interactions with TnC(*36*). When Ca^{2+} concentration is low and the N-terminal domain of TnC is apo, this region does not interact with TnC at all. However, when the N-terminal domain becomes Ca^{2+}-saturated, this region of TnI binds to the N-terminal hydrophobic patch with a K_D in μM range (Figure I-10). Even in the case of cardiac TnC, where the N-terminal domain remains "closed" after Ca^{2+}-saturation, binding of Ca^{2+} lowers the energetic barrier for TnC-TnI interaction enough that $TnI_{147-163}$ was able to bind to the N-terminal domain of TnC and force open the domain to expose the hydrophobic patch on the surface (*33*). However, this lack of Ca^{2+}-induced conformational change on cTnC does have an impact on the affinity of $TnI_{147-163}$ of cTnI for cTnC, and subsequently, the physiological function of the muscle.

There is an extensive body of biochemical data regarding changes in TnC-TnI interactions during muscle activation. In the last ten years, high-resolution structures elucidated using both NMR and X-ray techniques have helped to establish the dynamics of Tn protein interactions during muscle activation more clearly. The recent publication of X-ray crystal structures of both cardiac Tn and skeletal Tn core domain validated and summarized the work done by many laboratories over the years(*4, 31*). We now have unequivocal snap shots of the Tn core structure, both in the presence and absence of Ca^{2+}.

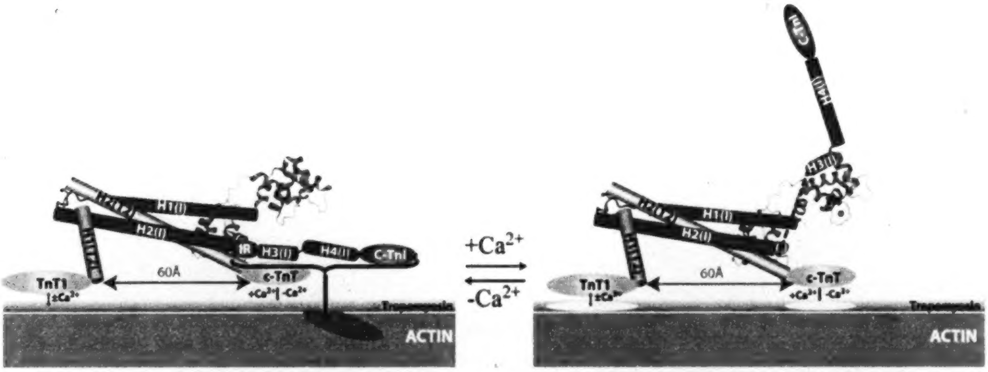

Figure I-11. A model of Ca^{2+}-dependent interactions of cardiac troponin in the context of the thin filament regulation. cTnC (gray) is shown in ribbon representation and the bound Ca^{2+} ions are represented by gray spheres. cTnI (green) and cTnT (yellow) are schematically drawn by rods and ellipsoids. Actin is blue and tropomyosin is gold. In contracting state, the structure is based on the atomic model of Takeda *et al.* (*4*); the N-domain of cTnC is Ca^{2+}-filled and is bound to the switch region of cTnI. In relaxing state, the N-domain of cTnC is replaced by NMR structure of cNTnC in Ca^{2+}-free state but the relative orientation of the two lobes of cTnC is the same as in the X-ray structure of cTnC•$3Ca^{2+}$•cTnI31-210•cTnT183-288 (PDB 1J1E). Taken from (2).

And we now know the key difference between Ca^{2+}-saturated Tn and Ca^{2+}-depleted Ca^{2+} is the location of the C-terminal region of TnI, especially that of residues 127-167. In the absence of Ca^{2+}, both segments of TnI known to interact with actin are bound to actin, locking Tm in the blocked state as well as directly inhibiting actomyosin ATPase activity. Since $TnI_{147-163}$ is flanked by the two actin binding regions, it is localized to actin simply by its proximity to the two actin-binding segments (Figure I-11). Whether it interacts with actin is not clear. However, when the N-terminal domain of TnC becomes Ca^{2+}-saturated, $TnI_{147-163}$ migrates from actin to the N-terminal domain of TnC. This migration also removes two actin-binding regions of cTnI from actin, allowing the Tm to switch from blocked to closed state and myosin-actin interactions to proceed (Figure I-11). Because $TnI_{147-163}$ switches from actin to TnC during muscle activation, this region of TnI is also termed the switch region of TnI. Besides the switch region of TnI, the inhibitory region also interacts electrostatically with the central linker and the C-terminal domain of TnC during the activated state, an interaction that maybe crucial in stabilizing the active state of Tn (*39*).

TnI is also known to interact extensively with T2 regions of TnT (see next section). It has long been predicted, and now proven with the Tn core domain structures, that residues 89 to 133 of TnI form a coiled-coil structure with a segment of TnT. The function of this "IT" coiled-coil arm appears to be purely structural, connecting TnI with TnT(*4, 31*). It remains to be seen whether it plays any role in transmitting the Ca^{2+}-induced signal down stream to Tm.

Despite the large amount of structural data available for the TnC and TnI, not too much information is known about the structure of TnT, especially that of the very flexible T1 region of TnT. TnT is the largest of the three proteins composing the Tn complex.

Owing to alternative exon-splicing during the transcription of the TnI gene, many isoforms of TnI exist. However, all isoforms are structurally similar. They all are rod-shaped molecules with a long N-terminal tail, termed the T1 region, that makes extensive contact with Tm, and a globular C-terminal region, termed the T2 region, that makes contacts with TnI and TnC. Because TnT interacts with all the protein in the Tn-Tm-actin complex, it is referred to as the "glue" of the complex(*40*). Owing to its flexibility, no structural information, other than it is 68% α-helix, exist for the T1 region of TnT. Structure of the T2 region of TnT has been solved as part of the Tn core domain structure. In these structures, residues 202 to 221 and residue 226 to 276 of TnT (the residue numbering system used here is that of cardiac TnT with 288 residues) form two α-helices, with the longer α-helix involved in the coiled-coil interaction with residues 89 to 133 of cTnI, forming the IT arm. There is also some evidence indicating that the short helix in the T2 of TnT is responsible for interaction with the C-terminal domain of TnC(*41*).

Because the substantial interactions TnT makes with other proteins, it is in the position to be the key link in Tm's switch from the blocked to the closed state after Ca^{2+}-binding to the N-terminal domain of TnC. However, many interactions involving TnT are not Ca^{2+}-dependent(*36*). Functionally, TnT appears to increase the inhibition of actomyosin ATPase in the absence of Ca^{2+} and stimulate it in the presence of Ca^{2+}(*42-45*). Not surprisingly, T1 is absolutely required for cooperative activation of muscle(*46*) while T2s is required for interaction with TnI and TnC(*47*).

Effects of Phosphorylations and Mutations of Cardiac Tn Proteins on Muscle Regulation

Phosphorylation plays an important role in modulating muscle activity. Owing to their physiological importance, effects of phosphorylation of cardiac Tn proteins have been the focus of many studies (for reviews of the subject, please see (*48, 49*)). So far six phosphorylation sites have been discovered on cTnI and four sites have been found on the T2 region of cTnT(*2*). However, understanding the effects of phosphorylation on Tn proteins have proven to be difficult because of the transient nature of the modification as well as multiple signaling pathways the phosphorylating enzyme is usually involved in(*2*). As a result, more often than not, data from biochemical studies of phosphorylated Tn proteins can not fully explain the physiological effects observed when the enzyme responsible for phosphorylating the Tn proteins is activated *in vivo.*

Of the 6 phosphorylation sites on cTnI, S22 and S23 are believed to be phosphorylated by protein kinase A (PKA), S41, S43 and T142 are believed to be phosphorylated by protein kinase C (PKC) and S149 is believed to be phosphorylated by p21-activated kinase (PAK)(*2*) (Figure I-12). Evidence indicates that PKA phosphorylation on the two serine residues in the N-terminal insert of cTnI results in reduction of Ca^{2+}-sensitivity and acceleration of muscle relaxation rate(*49, 50*). Although the N-terminal of cTnI is not in the cardiac Tn core structure, it is believed to be very close to the hydrophobic groove on the N-terminal domain of cTnC, and is reportedly capable of influencing conformational exchange in the N-terminal domain by shifting the equilibrium to favour an "closed" state(*2*).

Owing to multiple signaling pathways PKC is involved in, the physiological role of the PKC phosphorylation of cardiac Tn protein is difficult to ascertain. *in vitro* studies involving phosphorylated TnI at these sites showed that the cardiac muscle contractility as well as actomyosin ATPase activity is down regulated by the phosphorylation(*48, 49*). Of the three PKC phosphorylation sites, S41 and S42 are located in the region just N-

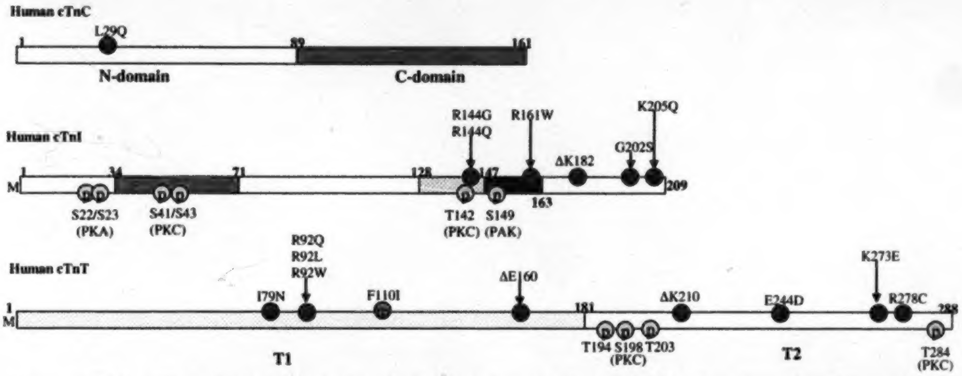
Human cTnC
1
L29Q
89
161
N-domain
C-domain
Human cTnI
R144G
R144Q
R161W
K205Q
G202S
ΔK182
M
1
34
71
128
147
163
209
S22/S23
(PKA)
S41/S43
(PKC)
T142 S149
(PKC) (PAK)
Human cTnT
R92Q
R92L
R92W
K273E
I79N
F110I
ΔE160
ΔK210
E244D
R278C
1
M
181
288
T194 S198 T203
(PKC)
T1
T2
T284
(PKC)

Figure I-12. The phosphorylation (gold) and mutation (pink) sites are identifies on the primary sequences of human cTnC, cTnI and cTnT). For each phosphorylation site, the name of the phosphorylating enzyme is also indicated below. Different functional segments of each Tn protein are indicated by different hatch marks. Taken from (*2*).

terminal to the TnI segment responsible for binding the C-terminal domain of TnC. There is no evidence that the phosphorylation at these two sites disrupt interactions between the N-terminal of TnI and the C-terminal of TnC(*51*) (Figure I-12). However, the location of these two serines does place them in close proximity to helix A of the N-terminal of TnC, thus it is possible that phosphorylation at these two sites might influence cTnC N-terminal domain conformational equilibrium. Residue T142 is located in the inhibitory region of TnI (Figure I-12), therefore its phosphorylation would have a huge impact on TnI's interaction with both TnC and actin. A recent *in vitro* NMR study using phosphorylated cTnI segments showed phosphorylation at T142 weakened inhibitory peptide's affinity for the C-terminal domain of TnC by 14 folds(*52*). PKC is also responsible for the phosphorylation of all 4 sites (T194, S198, T203, T284) on T2 region of TnT. Biochemical studies showed that phosphorylation of these sites by PKC led to a decrease in actomyosin ATPase activity(*53*). None of the sites lay in the two regions of TnT that form the two helices in the Tn core domain. Thus the effect of these phosphorylations on interactions between cTnI and cTnT is difficult to infer from structural information alone. In the case of PAK phosphorylation of TnI, myocytes showed increased maximum force and Ca^{2+}-sensitivity after PAK activation(*54*). However, it is unclear whether this is due to cTnI phosphorylation or PAK phosphorylation of other proteins. Chapter 4 of this thesis will examine in detail the effects of S149 on interactions between cTnC and cTnI, as well as how genetic mutations in cTnI modulate its impact.

Besides phosphorylation, mutations in Tn proteins also possess great physiological importance. Over the years, a number of naturally occurring mutations in cTnT, cTnI, and most recently, in cTnC are linked to a disease known as familial hypertrophic cardiomyopathy (FHC), an autosomal dominant disease whose main symptoms include cardiac hypertrophy, myofibril disarray and sudden cardiac death. There exists an extensive body of literature on the physiological effects of FHC mutations in Tn proteins (for reviews of this topic, please refer to (*2, 55, 56*)). I will not attempt to reproduce all the information in this short introduction. It suffices to say that there is still much work to be done to fully understand how these mutations are able to elicit their clinical symptoms. Of the three troponin proteins, cTnT possesses the highest number of known mutations. Almost all of them are localized to the T1 region of TnT (Figure I-12), which is responsible for interacting with Tm. Extensive physiological studies have been conducted to understand the effects of the mutations on muscle function, but have failed to produce any consistent trends from which effects of other cTnT mutations can be extrapolated. Lack of detailed structural information for both T1 region of TnT and the T1-Tm complex means almost none of the results can be rationalized on the basis of protein structure. For the time being, we can only satisfy ourselves with the knowledge of the existence of these mutations.

Almost all mutations on cTnI are localized to the C-terminal of cTnI, the portion of cTnI involved in regulatory switching between actin and cTnC. Amongst these FHC mutations, only R144G and R161W have been extensively studied. Physiologically both R144G and R161W mutants can reduce the inhibition of actomyosin ATPase activity and increase Ca^{2+}-sensitivity in skinned muscle fibres. However, *in vitro* NMR study conducted by Lindhout et al. showed the R144G mutation in fact weakens the affinity of the TnI inhibitory region for the C-terminal domain of TnC(*2, 52*). This implies that actin-TnI interactions must be weakened even more by the mutation in order for it to have the known physiological effects. Chapter 4 will discuss extensively how R161W change the TnI-TnC interaction and its implication on muscle regulation.

Calcium Sensitizers & cardiac TnC

Given the importance of TnC in regulating muscle contraction, it shouldn't be a surprise to find out that it is the possible target of many pharmaceutical compounds known to enhance muscle function. The purpose of these drugs is usually to enhance cardiac muscle contractility during the onset of congestive heart failure. The drugs usually work by one of several mechanisms known to improve muscle contractility. The simplest mechanism involves increasing the intra-cellular Ca^{2+} concentration. Since muscle contractile force is a Ca^{2+}-dependent event, any compound capable of inducing the release of Ca^{2+} from sarcoplasmic reticulum will enhance the contractility of cardiac muscle. The most effective way to do this is by raising the intra-cellular cAMP concentration, which will activate Ca^{2+} channels on the cytoplasmic membrane. Either inhibiting PDE III, which breaks down cAMP, or stimulating β-adrenergic receptors, which activate adenylate cyclases that produce cAMP, will achieve the goal. Drugs working through this mechanism are known as positive inotropic compounds. The drawback of this type of drugs, however, is the intracellular Ca^{2+}-overload produced by the spontaneous Ca^{2+} release increases the danger of arrhythmia, which can be deadly if the heart is already damaged by congestive heart failure(*57*). A second type of drugs works not by increasing intracellular Ca^{2+} concentration but by allowing myofibrils to generate more force for a fixed amount of cytoplasmic Ca^{2+}. Owing to the mode of their action, this class of drugs is termed Ca^{2+}-sensitizers. Over the past 20 years, many such compounds have been developed (Figure I-13). Some old Ca^{2+}-flux modulators are also proven to have Ca^{2+}-sensitizing activity. Bepridil, the subject of detailed analysis in

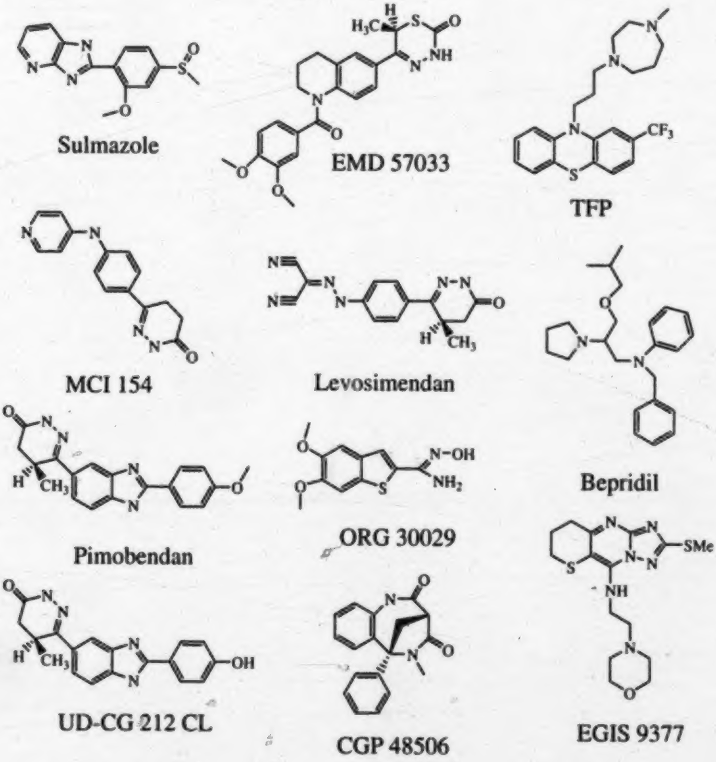
Sulmazole
EMD 57033
TFP
MCI 154
Levosimendan
Bepridil
Pimobendan
ORG 30029
UD-CG 212 CL
CGP 48506
EGIS 9377

Figure I-13. Chemical structures of a few Ca^{2+}-sensitizing drugs.

Chapter 3 of this thesis, is one of them(*58*). Of the newer Ca^{2+}-sensitizers developed, many of them, including levosimendan, the only commercially available Ca^{2+}-sensitizer, EMD57033, pimobendan and others, possess a common diazinone functional group (Figure I-13). The significance of this function group could lay in its specificity for binding the target protein, although this has not been thoroughly proven. Not surprisingly, almost all the Ca^{2+}-sensitizers examined in known biochemical studies have some affinity for cTnC. In particular, of the Ca^{2+}-sensitizers for which high-resolution structural information is available, all have their cTnC binding sites located in the hydrophobic groove on either the N-terminal domain or the C-terminal domain(*59-61*). Thus it is clear that most of them interact with cTnC through hydrophobic rather than electrostatic interactions. The exact mechanisms of these drugs have yet to be concretely proven. Few Ca^{2+}-sensitizers are known to directly increase the Ca^{2+} affinity of cTnC, a concept that has been naturally proposed as one of the possible mechanisms of Ca^{2+}-sensitizers. In fact, many Ca^{2+}-sensitizers only bind to cTnC in the presence of Ca^{2+}. However, many Ca^{2+}-sensitizers have either been shown to modulate cTnC-cTnI interactions or have great potential of influencing cTnC-cTnI interactions(*62-64*), thus the ability to alter cTnC-cTnI interactions maybe the major component in Ca^{2+}-sensitizing mechanism. Another possibility is that TnC may not be the site of interaction for these drugs at all. The interface between myosin and actin has been proposed as the site of activity for EMD 57033(*65*). And given the fact that RLC is also an EF-hand protein with very similar structural properties as cTnC, there is a high probability that Ca^{2+}-sensitizers can also bind to RLC. However, very few techniques today have the capability of probing drug-protein interactions *in situ*.

Tn-Mediated Muscle Regulation: The Future

With the elucidation of both skeletal and cardiac Tn core structures, many questions have been answered, more are raised, but most importantly, many new research projects have been made possible. Specifically, people are now shifting their attention to the investigation of dynamics of Tn protein complexed to other thin filament proteins. However, traditional high-resolution structural technique such as X-ray crystallography and solution NMR are powerless when dealing with the fibrous nature of the thin filament. New techniques would need to be developed to obtain detailed structural information. So far, most success seems to be from cryoelectron microscopy and polarized fluorescence studies of Tn on the thin filament. CryoEM had a long history in the muscle regulatory protein field. This was the first technique used to visualize the actin filament as well as Tm implanted on the thin filament. Observation of the movement of Tm on the thin filament in different Ca^{2+} state of Tn as well as in the presence and absence of myosin head using CryoEM was the first to lend structural proof to the existence of the 3-state muscle activation. However, visualizing Tn on the thin filament proved to be much tougher. Compared to Tm, existence of Tn on the thin filament is quite unsubstantial. The difficulty is exaggerated by the discontinuous distribution of Tn along the thin filament, which proved to be the biggest barrier in observing electron density from Tn. Nevertheless, Bill Lehman's group has made some headway in this area. They were successful in observing electron densities on the thin filament that can not be accounted for simply by actin and Tm(*66*). Even though the resolution was low, they were able to construct models of Tn core attached to the thin filament by incorporating the CryoEM data with both the high-resolution X-ray crystal structure of Tn core domain as well as TnC orientation information from fluorescence polarization studies done by David Trentham's group. Trentham's group has ingeniously obtained the orientation of TnC in the thin filament by attaching bifunctional rhodamine groups on several helices in the N-terminal domain of TnC. Since the fluorescence signal given off by the bifunctional rhodamine is dependent on its orientation relative to the excitation light source, and Tn on the thin filament aligns naturally along the thin filament axis, they were able to extrapolate the orientation of TnC on the thin filament through the analysis of the fluorescence signal from the rhodamine(*67*). This information proved to be rather helpful because it is the only orientational restraint the CryoEM group can use to orient the crystal structure on the thin filament. However, fluorescence polarization is not the only technique capable of giving orientational information. Many interactions in NMR are orientation dependent, including chemical shift anisotropy (for a good review on the subject, please see reference (*68*)). In the last part of this thesis, we explore the possibility of obtaining TnC orientation on the thin filament by utilizing the wide chemical shift anisotropy of fluorine atom. Our strategy is to reconstitute fluorine-labelled TnC into skinned muscle fibre and extrapolate the orientation of TnC by observing the shape of fluorine NMR signal from the fluorine-labelled TnC. ^{19}F NMR may also be useful in probing *in situ* interactions between Ca^{2+}-sensitizers and proteins. By titrating fluorine labelled drug into skinned muscle fibres reconstituted with ^{19}F-labelled TnC, distance as well as orientational information between the two fluorine groups can be obtained using several NMR techniques. Whether the drugs bind cTnC *in situ* can thus be determined.

References

1. Voet, D., and Voet, J. G. (1995) *Biochemistry*, 2nd Ed. ed., John Wiley & Sons, New York.
2. Li, M. X., Wang, X., and Sykes, B. D. (2004) *J Muscle Res Cell Motil 25*, 559-79.
3. Squire, J. M., and Morris, E. P. (1998) *Faseb J 12*, 761-71.
4. Takeda, S., Yamashita, A., Maeda, K., and Maeda, Y. (2003) *Nature 424*, 35-41.
5. Huxley, H., and Hanson, J. (1954) *Nature 173*, 973-6.
6. Huxley, A. F., and Niedergerke, R. (1954) *Nature 173*, 971-3.
7. Ebashi, S. (1963) *Nature 200*, 1010.
8. Ringer, S. (1883) *J. Physiol. (London) 4*, 29-42.
9. Ringer, S. (1886) *J. Physiol. (London) 7*.
10. Ringer, S. (1887) *J. Physiol. (London) 8*, 15-19.
11. Ringer, S. (1887) *J. Physiol. (London) 8*, 20-24.
12. Heilbrunn, L. V., and Wiercinski, F. J. (1947) *Journal of Cellular and Comparative Physiology 29*, 15-32.
13. Ebashi, S., and Kodama, A. (1965) *J Biochem (Tokyo) 58*, 107-8.
14. Hartshorne, D. J., and Mueller, H. (1968) *Biochem Biophys Res Commun 31*, 647-53.
15. Greaser, M. L., and Gergely, J. (1971) *J Biol Chem 246*, 4226-33.
16. Ebashi, S., Wakabayashi, T., and Ebashi, F. (1971) *J Biochem (Tokyo) 69*, 441-5.
17. Schaub, M. C., and Perry, S. V. (1969) *Biochem J 115*, 993-1004.
18. Schaub, M. C., and Perry, S. V. (1971) *Biochem J 123*, 367-77.
19. Drabikowski, W., Rafalowska, U., Dabrowska, R., Szpacenko, A., and Barylko, B. (1971) *FEBS Lett 19*, 259-263.
20. McKillop, D. F., and Geeves, M. A. (1993) *Biophys J 65*, 693-701.
21. Xu, C., Craig, R., Tobacman, L., Horowitz, R., and Lehman, W. (1999) *Biophys J 77*, 985-92.
22. Vibert, P., Craig, R., and Lehman, W. (1997) *J Mol Biol 266*, 8-14.
23. Moss, R. L., Lauer, M. R., Giulian, G. G., and Greaser, M. L. (1986) *J Biol Chem 261*, 6096-9.
24. Moss, R. L., Allen, J. D., and Greaser, M. L. (1986) *J Gen Physiol 87*, 761-74.
25. Moss, R. L., Giulian, G. G., and Greaser, M. L. (1985) *J Gen Physiol 86*, 585-600.
26. Moss, R. L., Diffee, G. M., and Greaser, M. L. (1995) *Rev Physiol Biochem Pharmacol 126*, 1-63.
27. Zot, H. G., and Potter, J. D. (1982) *J Biol Chem 257*, 7678-83.
28. Herzberg, O., and James, M. N. G. (1985) *Nature 313*, 653-659.
29. Gagné, S. M., Tsuda, S., Li, M. X., Smillie, L. B., and Sykes, B. D. (1995) *Nat. Struct. Biol. 2*, 784-789.
30. Slupsky, C. M., and Sykes, B. D. (1995) *Biochemistry 34*, 15953-15964.
31. Vinogradova, M. V., Stone, D. B., Malanina, G. G., Karatzaferi, C., Cooke, R., Mendelson, R. A., and Fletterick, R. J. (2005) *Proc Natl Acad Sci U S A 102*, 5038-43.
32. Sia, S. K., Li, M. X., Spyracopoulos, L., Gagné, S. M., Liu, W., Putkey, J. A., and Sykes, B. D. (1997) *J. Biol. Chem. 272*, 18216-18221.
33. Li, M. X., Spyracopoulos, L., and Sykes, B. D. (1999) *Biochemistry 38*, 8289-98.
34. Guo, X., Wattanapermpool, J., Palmiter, K. A., Murphy, A. M., and Solaro, R. J. (1994) *J Biol Chem 269*, 15210-6.

35. Syska, H., Wilkinson, J. M., Grand, R. J., and Perry, S. V. (1976) *Biochem J 153*, 375-87.
36. Tripet, B. P., Van Eyk, J. E., and Hodges, R. S. (1997) *J. Mol. Biol. 271*, 728-750.
37. Vassylyev, D. G., Takeda, S., Wakatsuki, S., Maeda, K., and Maeda, Y. (1998) *Proc. Natl. Acad. Sci. U.S.A. 95*, 4847-4852.
38. Luo, Y., Wu, J. L., Li, B., Langsetmo, K., Gergely, J., and Tao, T. (2000) *J. Mol. Biol. 296*, 899-910.
39. Lindhout, D. A., and Sykes, B. D. (2003) *J Biol Chem 278*, 27024-34.
40. Tobacman, L. S. (1996) *Annual Review of Physiology 58*, 447-481.
41. Blumenschein, T. M., Tripet, B. P., Hodges, R. S., and Sykes, B. D. (2001) *J Biol Chem 276*, 36606-12.
42. Van Eyk, J. E., Thomas, L. T., Tripet, B. P., Wiesner, R. J., Pearlstone, J. R., Farah, C. S., Reinach, F. C., and Hodges, R. S. (1997) *Journal of Biological Chemistry 272*, 10529-10537.
43. Potter, J. D., Sheng, Z., Pan, B. S., and Zhao, J. (1995) *J Biol Chem 270*, 2557-62.
44. Greaser, M. L., and Gergely, J. (1973) *Journal of Biological Chemistry 248*, 2125-2133.
45. Farah, C. S., Miyamoto, C. A., Ramos, C. H. I., da Silva, A. C. R., Quaggio, R. B., Fujimori, K., Smillie, L. B., and Reinach, F. C. (1994) *Journal of Biological Chemistry 269*, 5230-5240.
46. Schaertl, S., Lehrer, S. S., and Geeves, M. A. (1995) *Biochemistry 34*, 15890-4.
47. Pearlstone, J. R., and Smillie, L. B. (1983) *J Biol Chem 258*, 2534-42.
48. Metzger, J. M., and Westfall, M. V. (2004) *Circ Res 94*, 146-58.
49. Solaro, R. J., and Rarick, H. M. (1998) *Circ. Res. 83*, 471-80.
50. Rarick, H. M., Tang, H. P., Guo, X. D., Martin, A. F., and Solaro, R. J. (1999) *J Mol Cell Cardiol 31*, 363-75.
51. Li, M. X., Wang, X., Lindhout, D. A., Buscemi, N., Van Eyk, J. E., and Sykes, B. D. (2003) *Biochemistry 42*, 14460-8.
52. Lindhout, D. A., Li, M. X., Schieve, D., and Sykes, B. D. (2002) *Biochemistry 41*, 7267-74.
53. Noland, T. A., Jr., Raynor, R. L., and Kuo, J. F. (1989) *J Biol Chem 264*, 20778-85.
54. Buscemi, N., Foster, D. B., Neverova, I., and Van Eyk, J. E. (2002) *Circ Res 91*, 509-16.
55. Hernandez, O. M., Housmans, P. R., and Potter, J. D. (2001) *J Appl Physiol 90*, 1125-36.
56. Redwood, C. S., Moolman-Smook, J. C., and Watkins, H. (1999) *Cardiovasc Res 44*, 20-36.
57. Haikala, H., and Linden, I. B. (1995) *J Cardiovasc Pharmacol 26 Suppl 1*, S10-9.
58. Solaro, R. J., Bousquet, P., and Johnson, J. D. (1986) *J Pharmacol Exp Ther 238*, 502-7.
59. Sorsa, T., Heikkinen, S., Abbott, M. B., Abusamhadneh, E., Laakso, T., Tilgmann, C., Serimaa, R., Annila, A., Rosevear, P. R., Drakenberg, T., Pollesello, P., and Kilpelainen, I. (2001) *J Biol Chem 276*, 9337-43.
60. Li, M. X., Spyracopoulos, L., Beier, N., Putkey, J. A., and Sykes, B. D. (2000) *Biochemistry 39*, 8782-90.
61. Li, Y., Love, M. L., Putkey, J. A., and Cohen, C. (2000) *Proc. Natl. Acad. Sci. U. S. A. 97*, 5140-5.

62. Rosevear, P. R., and Finley, N. (2003) *J Mol Cell Cardiol 35*, 1011-5.
63. Wang, X., Li, M. X., Spyracopoulos, L., Beier, N., Chandra, M., Solaro, R. J., and Sykes, B. D. (2001) *J Biol Chem 276*, 25456-66.
64. Wang, X., Li, M. X., and Sykes, B. D. (2002) *J Biol Chem 277*, 31124-33.
65. Solaro, R. J., Gambassi, G., Warshaw, D. M., Keller, M. R., Spurgeon, H. A., Beier, N., and Lakatta, E. G. (1993) *Circ. Res. 73*, 981-90.
66. Pirani, A., Xu, C., Hatch, V., Craig, R., Tobacman, L. S., and Lehman, W. (2005) *J Mol Biol 346*, 761-72.
67. Ferguson, R. E., Sun, Y. B., Mercier, P., Brack, A. S., Sykes, B. D., Corrie, J. E., Trentham, D. R., and Irving, M. (2003) *Mol Cell 11*, 865-74.
68. Ulrich, A. S. (2005) *Progress in Nuclear Magnetic Resonance Spectroscopy 46*, 1-21.

Chapter II

Structure of the C-terminal domain of Human Cardiac Troponin C in Complex with EMD 57033[†]

Introduction

In order to function properly, heart muscle must respond efficiently to the transient increases in cytosolic Ca^{2+} levels in the myocardial cell. During the onset of congestive heart failure, there is strong evidence that the amount of Ca^{2+} available for contraction is depressed as is the maximum force generating capability of the myofilaments (for reviews, see ref. (*3-5*)). Treating this condition by elevating intracellular Ca^{2+} has the potential threat of inducing arrhythmias. In contrast, the ability to sensitize cardiac muscle to Ca^{2+} and increase cardiac contractility has the considerable advantage of increasing tension with little or no change in intracellular Ca^{2+} concentration and thus no increase in the energy required to release and transport Ca^{2+} (for a review, see ref. (*3*)). A logical target for such Ca^{2+} sensitizing drugs is cardiac troponin C (cTnC) owing to its role as the Ca^{2+} sensor on the thin filament of cardiac muscle.

In view of the importance of the exposed hydrophobic surfaces on both domains of cTnC for the binding of cTnI, it is clear that one way to enhance the Ca^{2+} sensitivity of cardiac muscle would be to stabilize the interaction of cTnC and cTnI by amplifying the hydrophobic cTnI-binding interface on cTnC. This can be accomplished by employing certain pharmacological agents that bind to the hydrophobic cleft but do not interfere with cTnC-cTnI interaction. Indeed, a variety of small hydrophobic compounds including the

---

[†] The results from this chapter is mainly taken from Wang, X., Li, M. X., Spyracopoulos, L., Beier, N., Chandra, M., Solaro, R. J. and Sykes, B. D. *J. Biol. Chem.* 276(27):25456-66, 2001. The exceptions include the results on the binding of EMD 57439 and EMD 73186 to cCTnC.

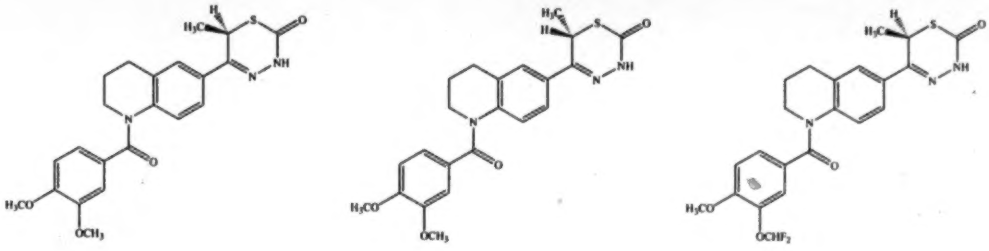

EMD 57033 EMD 57439 EMD 73186

Figure II-1. Chemical structures of EMD 57033, its enantiomer EMD 57439 and the fluorinated version of EMD 57033, EMD 73186.

calmodulin antagonists bepridil, trifluoperazine, and calmidazolium have been shown to increase the Ca^{2+} sensitivity of cardiac muscle preparations (for a review, see ref. (*3*)). However, most of these compounds are not good Ca^{2+}-sensitizers because their non-specific interaction with a host of other proteins. This led to a search for new generations of Ca^{2+}-sensitizing compounds. The thiadiazinone derivative EMD 57033 (*6, 7*) was one of the drugs discovered in this effort (Figure II-1).

Amongst the newer Ca^{2+}-sensitizers in existence, EMD 57033 is perhaps the most extensively studied. This is probably because of its potency as a Ca^{2+}-sensitizer. As little as 3μM of EMD 57033 is enough to elicit an increase in maximum force generated by skinned muscle fibres (Figure II-2a) (2). Many *in vivo* studies involving perfused hearts also verified EMD 57033's efficacy in intact tissues *(8-11)*. The most interesting aspect of this drug is the stereo-specific nature of its Ca^{2+}-sensitizing activity. EMD 57033 is the (+)-enantiomer in an enantiomeric pair (*R* in the Cahn-Ingold-Prelog nomenclature). The (-) enantiomer in the pair is referred to as EMD 57439, and the racemic mixture of the two is known as EMD 53998. Intriguingly, EMD 57033 is the only enantiomer in the pair to have Ca^{2+}-sensitizing activity (Figure II-2a) (2). EMD 57439 has little if any Ca^{2+}-sensitzing activity but possesses a much higher phosphodiesterase III (PDE III) inhibition activity (Figure II-2b). As mentioned in Chapter I, inhibiting PDE III leads to increased intracellular cAMP concentration, which results in higher cytoplasmic free Ca^{2+} concentration during muscle activation and enhanced muscle contractility. But this mode of action is less desirable owing to the higher chance of arrhythmia associated with it. Thus it is more beneficial to have a compound with only Ca^{2+}-sensitizing activity. However, most Ca^{2+}-sensitzers have both PDE III inhibition and Ca^{2+}-sensitizing activity (*5*). The fact that EMD 53998's Ca^{2+}-sensitizing and PDE III-inhibition activities reside in different enantiomers makes EMD 57033 a much more attractive therapeutic compound.

There has been much speculation on the mechanism of EMD 57033's Ca^{2+}-sensitizing activity. One of the earlier physiological studies investigating the effect of EMD 57033 on skinned muscle fibres showed EMD 57033 was able to enhance actomyosin ATPase activity even in the absence of TnC (*12*). From this observation, they inferred that EMD 57033 might be active at the interface between myosin and actin.

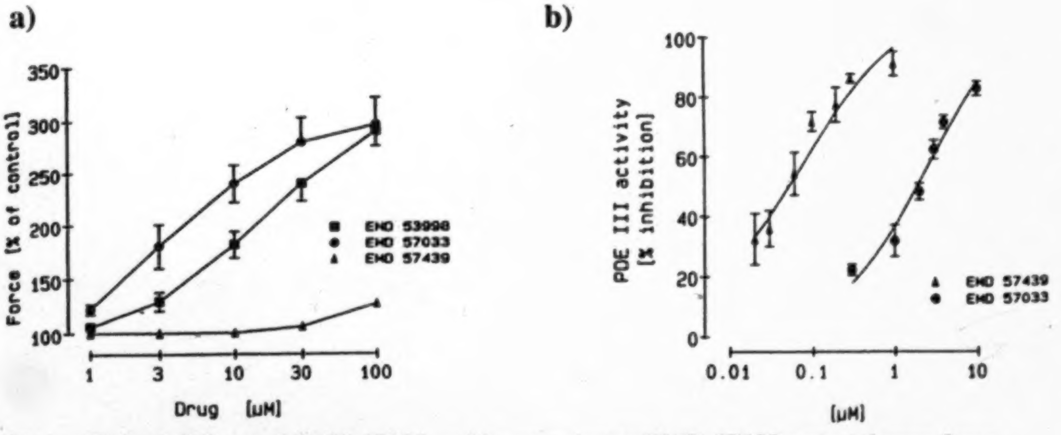

Figure II-2. a) Effects of EMD 57033 and its enantiomer EMD 57439 on maximum force generated by skinned ventricular fibres. EMD 53998 is the racemic mixture of two enantiomers. b) PDE III-inhibitory activity of EMD 57033 and EMD 57439. The horizontal axis is concentration of the drug. Taken from (2).

However, a subsequent fluorescence study demonstrated that EMD 57033 interacts with isolated cTnC in a Ca^{2+}-dependent and stereo-selective manner (*13*). A NMR study has shown that EMD 57033 induces chemical shift changes of Met methyl groups in the C-domain of cTnC (*14*). Using NMR chemical shift mapping, Li et al. showed that the EMD 57033 binding site is in the hydrophobic pocket of the C-domain of Ca^{2+}-saturated cTnC and that this drug does not interfere with the binding of the inhibitory region of cTnI to cTnC (*15*). These findings suggest that EMD 57033 may exert its positive inotropic effect by binding to the structural domain of cTnC, modulating the interaction between cTnC and other thin filament proteins, rather than directly enhancing Ca^{2+} binding to the regulatory domain of cTnC.

In order to delineate the molecular basis of the interaction between cTnC and EMD 57033, we have determined NMR solution structure of the 1:1 complex between the Ca^{2+}-saturated C-domain of human cTnC and EMD 57033. In the present structure, the drug molecule is oriented such that the chiral group of EMD fits deep in the hydrophobic pocket and makes several key contacts with the protein. This stereospecific interaction explains why the (-) enantiomer of EMD 57033 is inactive. This structure provides a structural basis for the Ca^{2+}-sensitizing effect of EMD 57033. We also examined the possible competition of the drug with cTnI peptides and found that the drug does not share common binding epitope with the inhibitory region of cTnI but is displaced completely by the N-terminal region of cTnI. These results have important implications in understanding the mechanism underlining Ca^{2+}-sensitizing effects of EMD 57033 in cardiac muscle contraction.

Experimental Procedures

Sample preparation: The engineering of the pET-3a expression vector for the cCTnC (91-161) protein was as described in Chandra *et al.* (*16*). Expression of the protein was carried out in *E. coli* strain BL21(DE3)pLysS using conventional protocols. In particular, cells containing the vector were first plated on LB agar plate containing 50 μg of ampicillin per ml of media and incubated at 37 °C for 18 hours. A single colony was picked from the plate and used to inoculate 15 ml of LB starter culture. Once the O.D.$_{600}$ of the culture has reached 1.0, 10 mls of the starter culture was used to seed one litre of either minimal media or normal LB media, depending on needs. The culture was induced with 0.5 mM of IPTG as soon as the culture has reached an O.D.$_{600}$ of 1.0 and harvested 3 hours after induction. The protein was purified by first lysing the cell using French press and then loading the supernatant onto a DEAE-sepharose (DE52, Whatman) column equilibrated with buffer containing 50 mM Tris, 0.1 M KCl, pH 8.0. After extensive washing of the column with equilibration buffer, the protein was eluted with a 0.1 M KCl to 0.4 M KCl gradient. The fractions containing the protein were then pooled and desalted using a G25 column and subsequently lyophilized. The protein was then dissolved in 2 ml of a buffer containing 50 mM Tris, 0.15 M NaCl and purified by gel-filtration using a Superdex-75 (Pharmacia) column equilibrated with the same buffer. The handling and characterization of the stock solutions of EMD 57033 are as described in Li *et al.* (*15*). Two stock solutions (94 mM and 53 mM, respectively) of EMD 57033 in DMSO-d$_6$ (Cambridge Isotopes Inc.) were prepared. 50mM stock solutions of EMD 57439 and EMD73186 were prepared in a similar manner as EMD 57033. The synthetic peptides, cTnI$_{128-147}$, acetyl-TQKIFDLRGKFKRPTLRRVR-amide, and cTnI$_{34-71}$, acetyl-

AKKKSKISASRKLQLKTLLLQIAKQELEREAEERRGEK-amide, were prepared as described for sTnI$_{96-115}$ and sTnI$_{1-40}$ in Tripet *et al.* (*17*). Solid peptides were dissolved in double distilled water to make stock solutions. The concentrations were 60 mM for cTnI$_{128-147}$ and 32 mM for cTnI$_{34-71}$, respectively, as determined by amino acid analysis. All NMR samples were 500 μL in volume. The buffer conditions were 100 mM KCl, 10 mM imidazole, 0.2 mM DSS, and 0.01% NaN_3 in 90% H_2O/10% D_2O, and the pH was 6.7. For structure determination, NMR samples contained 1 – 2 mM of ^{15}N-cCTnC or ^{15}N/^{13}C-cCTnC saturated with ~ 10 mM $CaCl_2$. EMD 57033, 57439 and 73186 were titrated to the Ca^{2+}-saturated cCTnC until ratios reached 1:1. The NMR samples used for titrations with cTnI$_{128-147}$ or cTnI$_{34-71}$ were prepared in a similar manner as described above. The titrations of cCTnC by cTnI$_{128-147}$ or cTnI$_{34-71}$ follow the procedures as described previously (*15*).

Purification of cCTnC with Reverse-phase HPLC: cCTnC was also purified using reverse-phase HPLC to rid of unlabelled impurities that were interfering with the analysis of ^{15}N, ^{13}C-filtered NOESY and TOCSY spectra. Owing to the lower solubility of cCTnC at low pH, the C8 reverse-phase column used to purify cCTnC was equilibrated at pH 6.5 using a buffer of 25mM ammonium acetate and 1.25mM EDTA. After the sample was loaded onto the column, the column was washed for 20min with the aforementioned buffer. The protein was eluted with a linear increasing acetonitrile gradient at a rate of 2%/min until the total concentration of acetonitrile has reached 26%. After which, the linear gradient was slowed down to an increase of 0.5%/min until the final concentration of acetonitrile has reached 50%. The column was then washed with 50% acetonitrile for

20 more minutes to ensure complete elution. Owing to the irreversible binding of cCTnC to the C8 reverse-phase column, the column must be washed with two or three aliquots of 500µl trifluoroethanol (TFE) after each run.

Stability of EMD 57033, 57439 and 73186 in aqueous solution: The thiadiazinone drugs are only marginally soluble in aqueous solutions (~2 µM). However, once it is bound to cCTnC, the complex is soluble and stable for 4 – 5 days, which is long enough for a typical 3D NMR experiment. 2D {^{1}H, ^{15}N}-HSQC NMR spectra acquired before and after every 3D NMR experiment were compared and their identity was taken as an indication of sample stability throughout the 3D NMR experiment. However, EMD 57033 tends to dissociate from the complex and precipitates out of the aqueous environment after 4 – 5 days. This is reflected in the disappearance of the EMD 57033-induced chemical shift changes (Figure II-3), which, however, can be reproduced upon the addition of more EMD 57033. This indicates that the protein is still intact and it is the drug that is disappearing from the solution. ^{15}N-filtered-DIPSI spectra of EMD 57033 in the cCTnC-EMD 57033 NMR sample detected no new resonances except those of intact EMD 57033, implying that the drug is not breaking down, but precipitating out of the solution. This conclusion was further supported by evidence from Mass Spectrometry measurements (T. Ta, unpublished data). ^{1}H-NMR spectra were used to check any possible modification of EMD 57033 by chemicals present in the NMR buffer, such as imidazole and NaN_3, which have been shown to interact with levosimendan (*18*), and the results show no sign of reaction between EMD 57033 and the chemical reagents.

NMR spectroscopy: Most NMR data used in this study were collected at 30 °C using Varian Unity 600 MHz, Unity Inova 500 MHz, and Inova 800 MHz spectrometers. All three spectrometers are equipped with triple resonance probes and Z-axis pulsed field gradients (XYZ gradients for the 800 MHz). A Varian Unity 300 spectrometer was also used to collect the spectra of EMD 57033 in DMSO-d_6. 2D {^{1}H, ^{15}N}-HSQC NMR spectra were acquired using the sensitivity-enhanced gradient pulse scheme developed by Lewis E. Kay and co-workers (*19, 20*). For cCTnC in the cCTnC-EMD 57033 complex, the chemical shift assignments of the backbone and side chain atoms and NOE interproton distance restraints were determined using 2D and 3D NMR experiments described in Table II-1. For the bound EMD 57033, the proton chemical shifts of the drug were assigned by using 2D-^{15}N/^{13}C filtered-NOESY (80 ms mixing time) and 2D-^{15}N/^{13}C filtered-DIPSI experiments (43.2 ms spinlock time). The pulse sequences for these two experiments were based on Ogura *et al.* (*21*) with extensive modifications done in this lab (Leo Spyracopoulos, University of Alberta). 1D ^{1}H and 2D DIPSI spectra of EMD 57033 in DMSO-d_6 were obtained using the Unity 300 MHz spectrometer. The intermolecular proton distances were obtained using 3D ^{15}N/^{13}C F_1-filtered, F_3-edited-NOESY HSQC experiments employing linear frequency ramped broadband inversion pulses for ^{13}C (80 ms mixing time) (22).

Data Processing and Peak Calibration: All 2D and 3D NMR data was processed using NMRPipe (*23*), and all 1D NMR data were processed using VNMR (Varian Associates). The spectra were analyzed using NMRView (*24*). For cCTnC in the complex, intramolecular distance restraints obtained from the NOESY experiments were calibrated according to Gagné *et al.* (*25*). Intramolecular proton distances for EMD 57033 in the complex were calibrated based on NOEs corresponding to known distances (neighboring protons on aromatic ring are separated by 2.48 Å). Intermolecular NOEs obtained from the $^{15}N/^{13}C$-filtered/edited experiment were categorized as either strong (1.8-3.0Å), medium (1.8 to 4.0Å), or weak (1.8 to 5.5Å). Dihedral angle restraints were derived from data obtained from HNHA, HNHB, and NOESY-HSQC experiments according to Sia *et al.* (*26*).

Structural calculations: Using an initial set of intramolecular NOE restraints for cCTnC, 100 structures of cCTnC without EMD 57033 were calculated starting from an extended conformation. The calculations were done using simulated annealing protocol implemented in X-PLOR (*27*) with 10,000 high-temperature steps (time step of 30 ps) and 6000 cooling steps (time step of 30 ps). Approximately 50% of the initial structures converged. These structures were used as templates for further rounds of refinements. Dihedral angle restraints and twelve artificial distance restraints from chelating oxygens to the two Ca^{2+} ions were added at later stages of the refinement process. Structures of the cCTnC-EMD 57033 complex were calculated starting from the extended conformations of cCTnC and EMD 57033 using simulated annealing protocol with the same conditions as above. The calculations were carried out using the distance and dihedral restraints for cCTnC, twelve distance restraints to Ca^{2+} ions, fourteen intermolecular distance restraints between cCTnC and EMD 57033 as well as eight intramolecular distance restraints for the bound EMD 57033 molecule (see Table II-2).

The final family of solution structures presented in this paper consists of thirty lowest energy structures.

Coordinates. The coordinates for the structure have been deposited in the RCSB Protein Data Bank (1IH0). Chemical shifts assignments for cCTnC and EMD 57033 have been deposited in the BioMagResBank (4994).

Table II-1. NMR Spectra Acquired and Experimental Conditions Used to Obtain Assignments and NOE Restraints.

Experiment name	Nuclei[a]	^{1}H freq[b].	nt[c]	*x*-pts[d]	*y*-pts	*z*-pts	*x*-sw	*y*-sw	*z*-sw	mix[e]	Ref.
2D {^{1}H, ^{13}C}-HSQC	^{1}H, ^{13}C	500	32	1024	128		7000	3771			*(28)*
2D {^{1}H,^{15}N}-HSQC	^{1}H,^{15}N	600	8	960	96		7500	1800			*(19, 20)*
3D ^{15}N-edited DIPSI-HSQC	^{1}H,^{1}H,^{15}N	600	8	960	128	32	7500	6400	1642	80.2	*(20)*
3D ^{15}N-edited NOESY-HSQC	^{1}H,^{1}H,^{15}N	500	16	1024	128	32	7000	5500	1500	80	*(20)*
HNHA	^{1}H,^{1}H,^{15}N	500	8	896	48	48	7000	4000	1408		*(29)*
HNHB	^{1}H,^{1}H,^{15}N	500	8	1024	96	32	7000	5400	1408		*(30)*
CBCA(CO)NNH	^{1}H,^{13}C,^{15}N	500	16	768	50	32	6000	7794	1500		*(31)*
HNCACB	^{1}H,^{13}C,^{15}N	500	16	888	50	32	6000	7794	1500		*(31)*
HCCH-TOCSY	^{1}H,^{1}H,^{13}C	500	16	768	128	32	6000	3000	3000	19.6	*(32)*
3D ^{13}C/^{15}N-edited NOESY	^{1}H,^{1}H,^{15}N/^{13}C	600	16	810	128	32	7500	6500	3165	80	*(33)*
2D ^{13}C/^{15}N-filtered NOESY	^{1}H(^{14}N/^{12}C),^{1}H (^{14}N/^{12}C)	500	32	4096	512		6200	6200		80	*(21)*
2D ^{13}C/^{15}N-filtered DIPSI	^{1}H(^{14}N/^{12}C),^{1}H (^{14}N/^{12}C)	500	32	4096	512		6200	6200		43.2	*(21)*
3D ^{13}C/^{15}N-filtered/edited NOESY	^{1}H(^{14}N/^{12}C),^{1}H ,^{15}N/^{13}C	500	16	640	128	32	6000	5000	3000	80	*(22)*

[a] The nucleus acquired in each dimension (e.g. ^{1}H, ^{15}N indicates proton in *x*-dimension and ^{15}N in *y*-dimension).

[b] The frequency of ^{1}H in MHz.

[c] The number of transients acquired for each FID.

[d] *x,y,z*-pts and sw is the number of complex points and sweep width in each respective dimension (*x* is the directly detected dimension).

[e] Mixing times are given in milliseconds. In the case of DIPSI or TOCSY experiments, this is the spin-locking time.

Table II-2: Structural Statistics of the family of the 30 structures calculated.

	Backbone Atoms	Heavy Atoms
R.M.S.D. from the average structure (Å)[a]		
Well-defined residues	0.67±0.13	1.2±0.14
Helices	0.28±0.06	0.63±0.11
NOE restraints		
Total	1000(approx. 14/residue)	
Intra-residue	432	
Sequential ($\|i-j\|=1$)	251	
Medium-range($2\leq\|i-j\|\leq4$)	197	
Long-range ($\|i-j\|\geq5$)	120	
Artificial restraints to Ca^{2+}	12	
Intermolecular NOEs	14	
Intramolecular NOEs in EMD 57033	8	
Dihedral Restraints		
Total	61	
ϕ	30	
ψ	31	
χ_1	11	
Energies[b]		
E_{total}	66±3	
E_{NOE}	1.4±0.7	
$E_{dihedral}$	0.08±0.06	
R.M.S.D. from idealized geometry		
Bond length (Å)	0.0008±8e-05	
Bond angle (°)	0.364±0.004	
Impropers (°)	0.428±0.003	
Restraint Violations[c]		
Distance >0.1Å but <0.2Å	1(0.03/strucure)	
Dihedral>1°	0	
ϕ, ψ in core or allowed regions[d]	97.2%	

[a] 67 residues have well defined backbone atoms. This include residues 94-123, 128, 130-160. The R.M.S.D. for helices are calculated from the average of the R.M.S.D. of individual helices.

[b] The final K_{NOE} and $K_{dihedral}$ used were 50 kcalmol^{-1} and 200 kcalmol^{-1}rad^{-2}, respectively.

[c] There were no distance violations over 0.2 Å.

[d] As determined using PROCHECK (*34*).

Results and Discussion

Structure of the cCTnC-EMD 57033 complex

We have shown clearly that EMD 57033 forms a 1:1 complex ($K_D \sim 8$ μM) with intact cTnC and the binding site resides in the C-domain (*15*). For the purpose of this study, we have made a complex between an isolated Ca^{2+}-saturated C-domain (residues

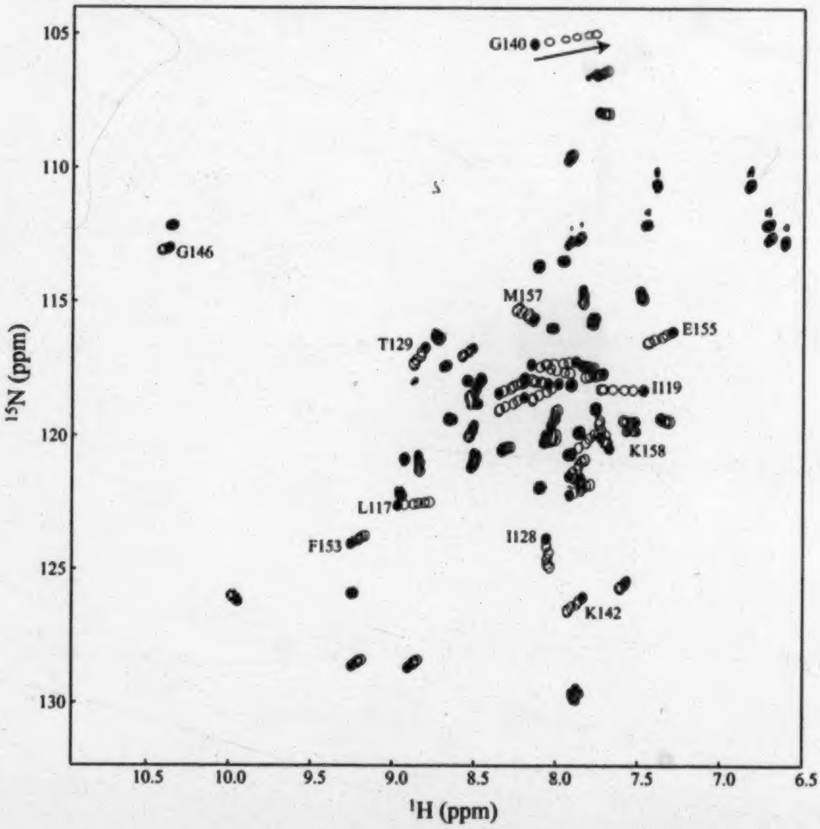

Figure II-3. Titration of Ca^{2+}-saturated cCTnC with EMD 57033. 2D {^{1}H, ^{15}N}-HSQC NMR spectra arising from the backbone NH and side chain NH_2 groups of cTnC are superimposed for various EMD 57033 additions. Each titration point represents the addition of 1μl of 94 mM EMD 57033 stock solution to a NMR sample containing 0.92 mM of ^{15}N-labeled cCTnC. Assignments of the cross peaks are indicated. Cross peaks corresponding to free cCTnC with no drug added are shown as multiple contours. Cross peaks from subsequent spectra are shown as single contours. The arrow indicates the direction of the movement of cross peak for Gly^{140} with increasing EMD 57033 concentrations.

91-161) of human cTnC and EMD 57033. This reduces the NMR spectral overlap and facilitates the structure determination process. The 2D {^{1}H, ^{15}N}-HSQC NMR spectrum of the Ca^{2+}-saturated cCTnC, shown in Figure II-3, indicates that it is a well-structured domain characterized by the dispersion of amide proton signals. Titration of EMD 57033 induces progressive shifts of the cross peaks. All chemical shift changes fall into the fast exchange limit on the NMR time scale. The linear movement of the cross peaks indicates that EMD 57033 binding to cCTnC occurs with a 1:1 stoichiometry. At the end of titration, a stable 1:1 cCTnC:EMD 57033 complex ($K_D \sim 10\ \mu M$) formed.

The 2D {^{1}H, ^{15}N}-HSQC NMR spectrum (Figure II-3) of cCTnC in the cCTnC-EMD 57033 complex was highly resolved, which allowed the chemical shifts of the backbone and the side chain atoms to be readily assigned using ^{15}N- or ^{15}N/^{13}C-labeled protein. Distance restraints for cCTnC in the cCTnC-EMD 57033 complex were obtained by analyzing 3D ^{15}N- or ^{15}N/^{13}C-NOESY experiments. Dihedral angle restraints for cCTnC in the cCTnC-EMD 57033 complex were obtained from 3D HNHA and HNHB experiments. The NMR experiments performed are summarized in Table II-1.

The proton NMR chemical shifts assignments and intramolecular distance restraints for the bound EMD 57033 required the collection of ^{15}N/^{13}C filtered 2D-DIPSI and 2D-NOESY experiments using unlabeled drug bound to ^{15}N/^{13}C labeled cCTnC. These experiments removed all of the resonances arising from ^{15}N/^{13}C labeled cCTnC. 1D-^{1}H and 2D-DIPSI NMR spectra of free EMD 57033 in DMSO-d_6 were also analyzed to aid the assignments. Intermolecular NOE correlations between cCTnC and EMD 57033 were determined from 3D-^{15}N/^{13}C-filtered, ^{15}N/^{13}C-edited NOESY data. These experiments were optimized (L. Spyracopoulos, unpublished data) for detecting NOEs between protons attached to $^{14}N/^{12}C$ and protons attached to $^{15}N/^{13}C$, thereby editing out all the intramolecular NOEs. A total of 1000 experimental distance restraints (approx. 14 restraints per residue) including 974 for cCTnC, 8 for EMD 57033, 14 intermolecular contacts between cCTnC and EMD 57033, 61 dihedral restraints for cCTnC, and 12 restraints to Ca^{2+} were used to calculate the high resolution structure of the cCTnC-EMD 57033 complex. Figure II-4a depicts the ensemble of 30 lowest energy structures of the cCTnC-EMD 57033 complex in stereo view, with overall structural statistics and conformational energies for the ensemble of solution structures provided in Table II-2. The ribbon and the surface representations of the structure of cCTnC-EMD 57033 complex are shown in Figure II-4B and 2C, respectively.

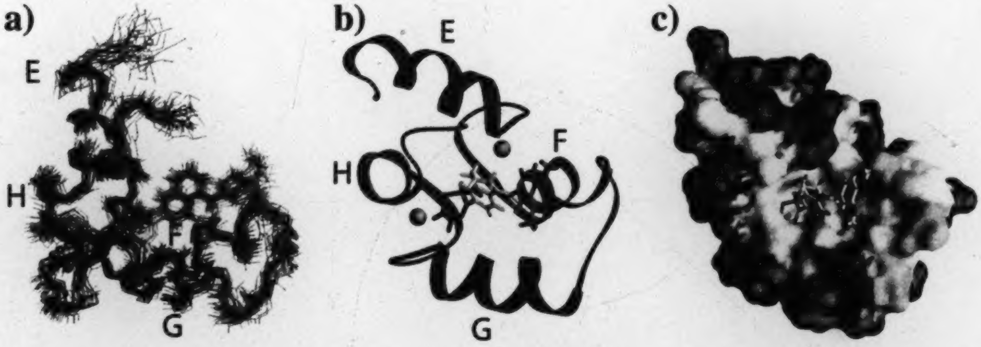

Figure II-4. a) The solution structure of the cCTnC-EMD 57033 complex. The backbones (N, Cα, C') of a family of 30 structures are shown in blue. The assembly of EMD 57033 structures is shown in red. The Ca^{2+} ions are shown as green spheres. b) The ribbon representation of the cCTnC-EMD 57033 complex. The protein is shown in dark red and Ca^{2+} ions are shown as cyan spheres. The thiadiazinone functional group of the drug is colored in blue; the tetrahydroquinolyl group of the drug is colored in gold; and the dimethoxybenzoyl group is shown in gray. c) Molecular surface of cCTnC in the cCTnC-EMD 57033 complex. The side chain atoms of hydrophobic residues (Ala, Ile, Leu Met, Phe, and Val) are shown in yellow. Negatively charged residues (Asp and Glu) in red, positively charged residues (Arg and Lys) in blue. Polar residues (Ser, Thr and Tyr) are shown in cyan. EMD 57033 is embedded in the hydrophobic cleft of the protein. The orientation of the complex is the same as in (b). Figure C was created with the program GRASP (*1*).

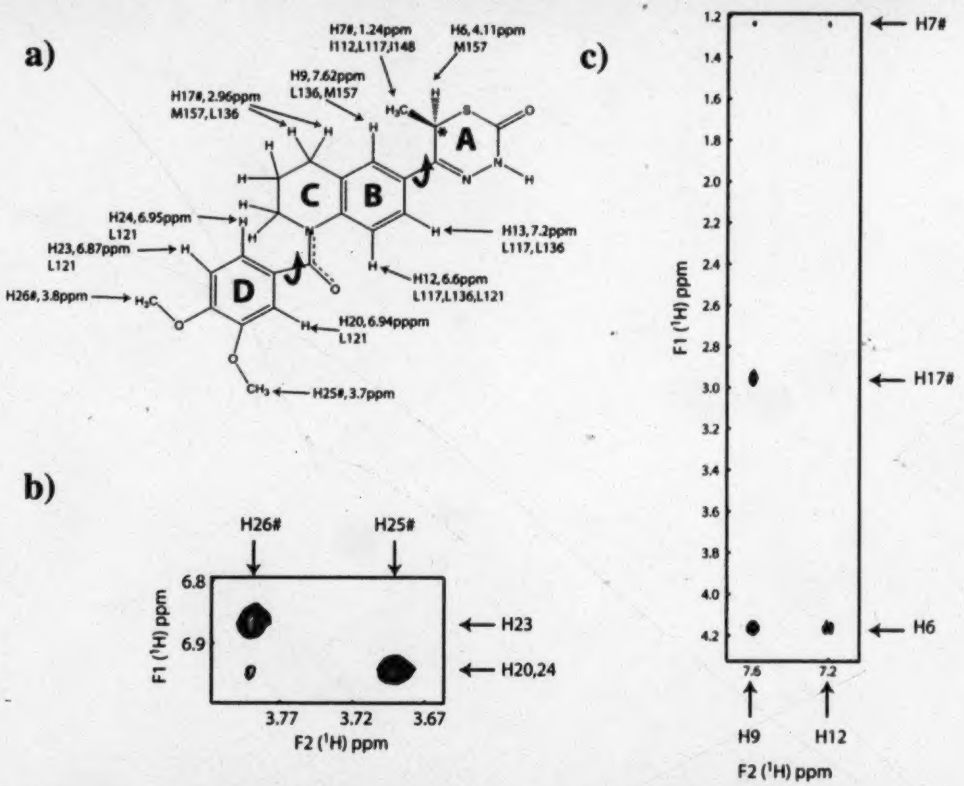
a)
H7#, 1.24ppm
I112,L117,I148
H6, 4.11ppm
M157
H9, 7.62ppm
L136, M157
H17#, 2.96ppm
M157, L136
A
B
C
D
H24, 6.95ppm
L121
H23, 6.87ppm
L121
H26#, 3.8ppm
H13, 7.2ppm
L117, L136
H12, 6.6ppm
L117, L136, L121
H20, 6.94pppm
L121
H25#, 3.7ppm
b)
H26#
H25#
H23
H20,24
F1 (¹H) ppm
F2 (¹H) ppm
c)
H7#
H17#
H6
H9
H12
F1 (¹H) ppm
F2 (¹H) ppm

Figure II-5. a) The chemical structure of EMD 57033. The four rings that form the three functional groups are labeled as A-D. The two bonds that connect the three units are indicated by curved arrows to emphasize their ability to rotate freely. The number designation and the chemical shift assignments of most protons of the drug are indicated. The residues of cCTnC, which are involved in interacting with protons of EMD 57033, are also indicated. b, c) strips from the 2D-$^{15}N/^{13}C$-filtered-NOESY NMR experiment showing the intramolecular NOE contacts of EMD 57033.

cCTnC in the present structure exhibits an overall fold resembling other Ca^{2+}-bound domains in the EF-hand family, such as the C-domain of sTnC and N- and C-domains of CaM. The four helices, E, F, G, and H, are well defined, superimposing with individual backbone RMSDs of 0.23 ± 0.06Å (E, residues 95-103), 0.27 ± 0.09Å (F, residues 114-123), 0.36 ± 0.11Å (G, residues 130-140), 0.26 ± 0.07Å (H, residues 150-156). The two EF-hands are joined by a short twisted antiparallel β-sheet. The two Ca^{2+} binding sites are relatively well defined with backbone RMSD of ~ 0.61 Å. The β-sheet (residues 111-

113, 147-149) is well defined with a backbone RMSD of 0.29 ± 0.08 Å. The N- and C-terminal residues (residues 91-94, and 158-161) are less well defined (RMSD, 1.4 ± 0.4) than the helices and the β-sheet. EMD 57033 consists of three main organic groups, which are the thiadiazinone (A ring in Figure II-5a), the tetrahydroquinolinyl (B and C rings in Figure II-5a), and the dimethoxybenzoyl (D ring in Figure II-5a) moieties, respectively. The three functional groups have rigid conformations. The bond that connects the thiadiazinone-tetrahydroquinolinyl units is most likely not freely rotatable owing to the steric interactions between the two groups where as the bond that connects the tetrahydroquinolinyl-dimethoxybenzoyl units does have freedom of rotation (see Figure II-5a). The drug molecule is completely assigned and the chemical shifts for all the protons are labeled in Figure II-5a. Eight intramolecular NOEs of the bound drug were observed and shown in Figure II-5b, c. The relative orientations of the three moieties in the cCTnC-EMD 57033 complex are determined by both the intramolecular NOEs within the drug molecule and the intermolecular NOEs between cCTnC and the drug. In the ensemble of structures (Figure II-4a), the interplanetary angles for the thiadiazinone-tetrahydroquinolinyl and the tetrahydroquinolinyl-dimethoxybenzoyl units are 44° ± 21°and 69°± 14°, respectively. When the heavy atoms of EMD 57033 superimpose onto the average structure in the cCTnC-EMD complex, the average RMSD is 0.29 ± 0.07 Å. This RMSD increases to 1.15 Å when the backbone atoms of residues 95-158 of cCTnC in the ensemble of solution structures for the cCTnC-EMD 57033 complex are superimposed onto the average cCTnC structure. As a result, the stereochemical quality of the drug molecule assembly is slightly lower than the structures of cCTnC in the cCTnC-EMD 57033 complex. This is due in part to the loosely imposed intermolecular restraints between cCTnC and EMD 57033 because of a lack objective calibration scheme for those NOEs (see Experimental Procedures).

Binding Interface between EMD 57033 and cCTnC in the cCTnC-EMD 57033 complex

Strip plots taken from the 3D $^{15}N/^{13}C$ F_1-filtered, F_3-edited spectrum of the cCTnC-EMD 57033 complex are shown in Figure II-6a. In this spectrum, only NOEs arising from the drug protons (attached to ^{12}C) and terminating on protein protons (attached to ^{13}C) are observed. For example, the H7# methyl protons from the thiadiazinone unit show strong NOE contacts with the protons attached to the methyl groups of Leu 117 located in the F-helix (Figure II-6b-III) and of Ile 112 and Ile 148 located in the β-sheet of cCTnC (Figure II-6b-I); the H9, H12, and H13 protons from the B ring (Figure II-5a) show NOE contacts with the protons attached to the methyl groups of Leu 136 located in the G-helix (Figure II-6b-II); and the two H17 protons from the C ring (Figure II-5a) show NOE contacts with the protons attached to the methyl groups of Met 157 located in the H-helix (Figure II-6b-IV). These experimental intermolecular restraints serve to orient the drug molecule in the cCTnC-EMD 57033 complex. As a result, the thiadiazinone group is located at the bottom of the cCTnC pocket in a small hydrophobic cavity (Figure II-4c). It seems that the strong contacts between the chiral methyl group and three residues of cCTnC (Ile 112, Leu 117, and Ile 148) serve as the primary anchoring site for this drug molecule (see below for biological implications). The dimethoxybenzoyl group protrudes toward outside of the hydrophobic pocket (Figure II-4c). Although most interactions between cCTnC and EMD 57033 are hydrophobic in nature, the fact that the chiral methyl (H7#) group delves deep into the hydrophobic

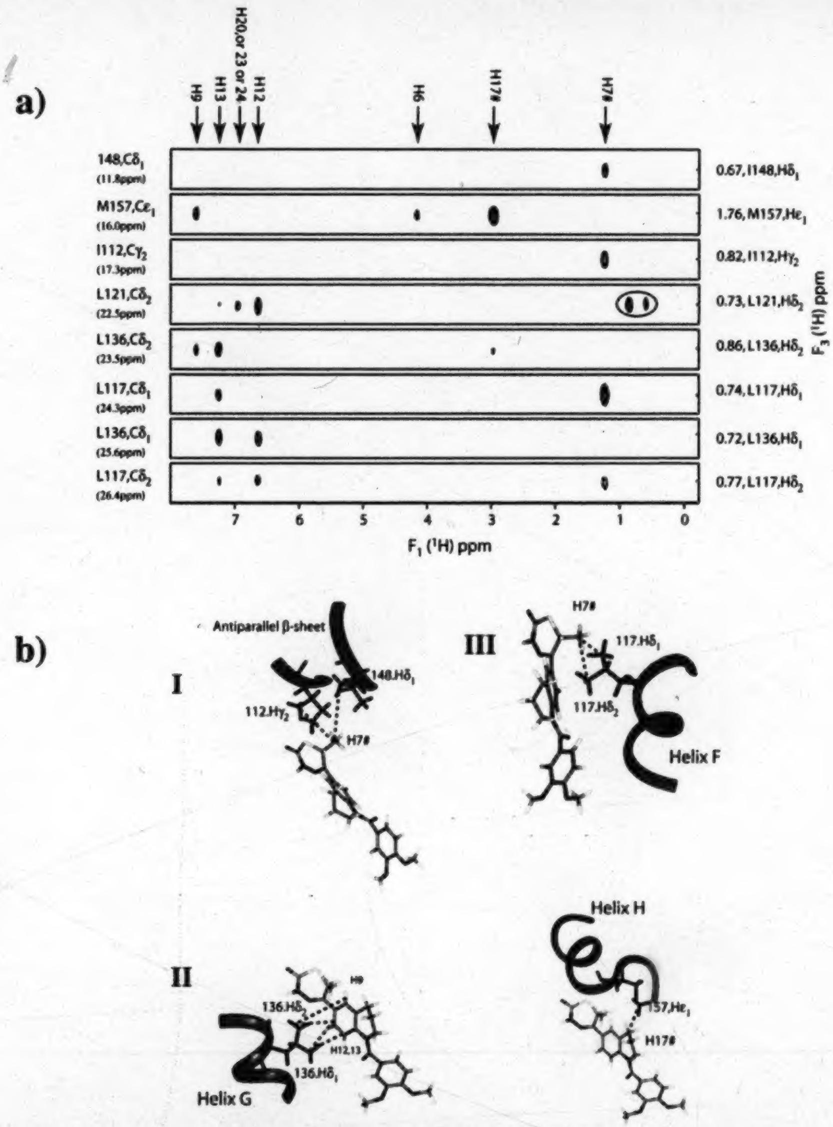

Figure II-6. NOE contacts between the protein and the drug. a) Strip plots from ^{13}C portion of the 3D-$^{15}N/^{13}C$-filtered/edited-NOESY NMR experiment illustrating the NOEs between cCTnC and EMD 57033. The carbon chemical shift is shown on the left. The cCTnC proton to which the strip corresponds to is labeled on the right. The proton chemical shifts of the drug are indicated at the top. The two peaks circled in the Leu^{121}.Cδ_2 strip are artifacts in the spectra. b) Detailed views of the interactions between EMD 57033 and cCTnC. Dotted lines represent the NOE distances observed in a).

pocket of cCTnC while the two methoxy moieties, despite their hydrophobic nature, stick out indicates the interaction is specific. Another important interaction is between the methyl group of Met 157 located in the C-terminal G-helix and H17# protons from ring C (Figure II-5a) of EMD 57033. This contact serves mainly to hold the plane formed by rings B and C of the drug in an orientation that is almost perpendicular to the plane formed by ring A, and to allow the residues on helix G (Leu 136) and at the end of helix H (Met 157) to interact with the same proton (H9) on ring B. The contacts between the protons (H12 and H13) on ring B and the methyl groups of Leu 117 and Leu 136 help the drug bound to the protein firmly. Leu 121 located on the C-terminal of F-helix makes only weak NOE contacts with aromatic protons on both ring B (H12) and ring D (H20, H23, and H24) of EMD 57033, which also play a role in binding the drug to cCTnC. Overall, the protons from EMD 57033 make 14 NOE contacts with protons of the methyl groups from six hydrophobic residues (Ile 112, Leu 117, Leu 121, Leu 136, Ile 148, and Met 157) of cCTnC and these interactions keep the drug molecule fit snuggly in the hydrophobic cavity of Ca^{2+}-saturated cCTnC (Figure II-4c). The total "exposed" nonpolar accessible surface area for residues 95-158 of cCTnC, excluding the drug, in the cCTnC-EMD 57033 complex is ~ 2689 Å^2, as measured by GRASP (*1*) and the drug molecule shields ~ 740 Å^2 of the apolar surface from the solvent.

EMD 57033-induced structural changes in cCTnC

The overall fold of cCTnC in the cCTnC-EMD 57033 complex is similar to the structure of the C-domain of intact cTnC determined by solution NMR spectroscopy (*26*), with a RMSD of ~ 1.7 Å for backbone overlay (Figure II-7a). There are several EMD

57033-induced structural changes. Among the most notable ones, the cCTnC in the cCTnC-EMD 57033 complex is more 'open', *i.e.*, the F/G helix unit is farther away from the E/H helix unit, than the free C-domain of cTnC. This is mostly due to the strong interactions of the drug with residues Leu 117 and Leu 121 located on the F helix, which pulls helix F away from helix E and toward helix G. This is quantified by a decrease in the E/F interhelical angles (from 115 ± 4° for the C-domain in cTnC to 92 ± 4° for cCTnC in the cCTnC-EMD 57033 complex). The interhelical angle between G and H also showed a slight decrease (from 121 ± 4° for the C-domain in cTnC to 113 ± 7° for

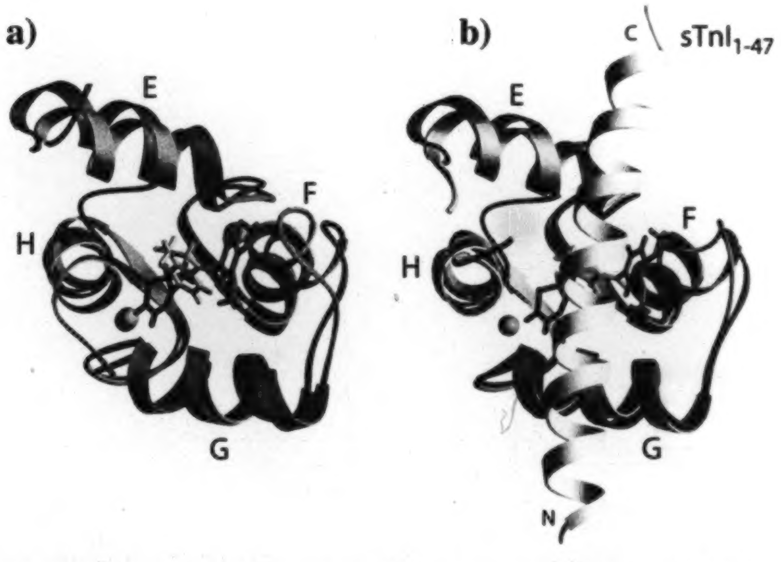

Figure II-7. a) The backbone overlay of cCTnC in the cCTnC-EMD 57033 complex (dark red) and the free C-domain of cTnC (green), PDB accession code 1AJ4. The two Ca^{2+} ions are shown as cyan-colored spheres. The three units of the drug are colored in the same scheme as Figure 2B. Note the slight opening of helix E and F as well as the unwinding of the C-terminal helix. b) The backbone overlay of cCTnC in the cCTnC-EMD 57033 complex (dark red) with the C-domain of skeletal TnC (purple), bound to $sTnI_{1-47}$ (light green), PDB accession code 1A2X. The Ca^{2+} ions and EMD 57033 are colored in the same scheme as in (a). The overlay shows that the binding of EMD 57033 to cCTnC mimics the binding of $sTnI_{1-47}$ to sCTnC.

cCTnC in the cCTnC-EMD 57033 complex) (see Table II-3). The slight opening of cCTnC and movement of F/G-helix unit away from E/H-helix unit was also observed by the binding of $cTnI_{33-80}$ peptide to cCTnC (*35*). It seems that these movements are necessary for the C-domain of cTnC to provide a binding site for cTnI or a drug molecule. The degree of EMD 57033–induced structural opening of cCTnC is also measured by an increase of ~ 20 $Å^2$ of 'exposed' apolar surface area for cCTnC in the cCTnC-EMD 57033 complex, compared to the free C-domain of cTnC. Although EMD 57033 induced little G/H interhelical angle changes, the multiple contacts between Leu 136 of the G-helix with several ring protons of EMD 57033 resulted in a more flexible G-helix in the present structure than the C-domain in the cTnC structure (RMSDs of 0.36 Å for cCTnC in the cCTnC-EMD 57033 *vs.* 0.24 Å for the C-domain in cTnC). Another significant EMD-induced change on cCTnC is the unwinding of residues 156-161 at the end of helix H. This last helix is well defined at the C-terminal end in many EF-hand domains such as sNTnC (9,48), cNTnC (*36*), and CaM domains (*37*). However, in this complex, helix H ends at residue 156, the last portion of the C-terminal residues (157-161) forms an extended structure and appears to be more flexible than usual. This can be attributed to the interactions between EMD 57033 and residue Met 157 of cCTnC. Interestingly, the same extended conformation at the end of the H helix was observed in the C-domain of sTnC bound to the N-terminal region of sTnI ($sTnI_{1-47}$) (*38*). This suggests that the nature of the interactions between EMD 57033 and cCTnC may be similar to that between $sTnI_{1-47}$ and sTnC. An overlay (Figure II-7b) of the cCTnC in the cCTnC-EMD complex and sCTnC in the sCTnC-$sTnI_{1-47}$ complex shows that the backbones of cCTnC and sCTnC adopt very similar conformations (RMSD = 1.3 Å). It also shows that the binding of EMD 57033 to cCTnC possesses similar features as the binding of $sTnI_{1-47}$ to sCTnC. In fact, residues Ile 110, Leu 115, Phe 119, Leu 134, Ileu 146, and Met 155 of sCTnC, corresponding to the six EMD 57033-contacting residues in cCTnC, are all involved in the interaction with $sTnI_{1-47}$ (*38*). It is interesting to notice that binding of $sTnI_{1-47}$ to sCTnC does not greatly perturb the fold of this domain from a peptide free conformation. In the free state, sCTnC exhibits E/F and G/H interhelical angles of ~ 105° and ~115°, respectively (Table II-3). These angles do not change very much upon $sTnI_{1-47}$ binding to sCTnC. On the other hand, both EMD 57033 and $cTnI_{33-80}$ induce interhelical angle changes in cCTnC and the bound cCTnC exhibits a more open conformation. This is analogous to the ligand induced structural changes in the N-domain of sTnC and cTnC. Ca^{2+} binding switches sNTnC from a 'closed' to 'open' conformation (*39*) and the 'open' sNTnC is ready to bind $sTnI_{115-131}$ with no need to open further (*40*). On the other hand, Ca^{2+} binding to cNTnC induces little structural changes but sets the stage for cTnI binding and cNTnC undergoes a large 'closed' to 'open' transition upon binding $cTnI_{147-163}$ (*39*) or Bepridil (*15*). Thus, the interaction of both domains of cTnC with cTnI would require more free energy than those of sTnC with sTnI, because cTnI has to overcome the energy barrier of opening the domains of cTnC (see discussions in McKay *et al.* (*41*)). This energy cost may be compensated by employing pharmacological agents, which bind to both domains of cTnC and thereby help to stabilize the open conformation of cTnC. The ideal situation would be that the interaction between the drug and cTnC occurs without interfering with cTnI binding to cTnC. The analysis presented herein raises issues about the effect of EMD 57033 on the interaction of cCTnC and cTnI. Since two regions of cTnI ($cTnI_{128-147}$ and $cTnI_{34-71}$)

were identified to interact with the C-terminal domain of cTnC (*17*), we examined the binding of these two synthetic peptides ($cTnI_{128-147}$ and $cTnI_{34-71}$) to the cCTnC-EMD 57033 complex as discussed below.

Table II-3. Interhelical angles of various EF hands.

Calcium Binding Protein[a]	Interhelical angles(°)[b]		Accession Code (PDB)
	E-F	G-H	
cCTnC ($2Ca^{2+}$)-EMD 57033	92±4	113±7	N/A
C-domain of Ca^{2+} saturated cTnC ($2Ca^{2+}$)	115±4	121±4	1AJ4
C-domain of Ca^{2+} saturated sTnC ($2Ca^{2+}$)	105±6	111±7	5TNC
cCTnC ($2Ca^{2+}$) bound to $cTnI_{33-80}$	94 ± 8	89±9	1FI5
C-domain of sTnC ($2Ca^{2+}$) bound to $sTnI_{1-47}$	99	109	1A2X

[a] The parentheses indicate the number of the Ca^{2+} ions contained in the domain.

[b] A large angle defines a "closed" conformation, whereas a small angle defines an "open" conformation. The axis for an α-helix is defined by two points, taken as the average coordinates of the first and last 11 backbone atoms of the α-helix.

Competition of EMD 57033 with $cTnI_{128-147}$ and $cTnI_{34-71}$

Previously, we have shown that both EMD 57033 and $cTnI_{128-147}$ bind with a 1:1 stoichiometry to cTnC but do not compete for the same binding sites on cTnC (*15*). EMD 57033 binding is not affected by $cTnI_{128-147}$ nor does the drug affect $cTnI_{128-147}$ binding. In the end, a stable ternary cTnC-EMD 57033-$cTnI_{128-147}$ complex is formed. In the present work, similar titrations were performed on cCTnC and similar conclusions were obtained (data not shown). Both EMD 57033 and $cTnI_{128-147}$ can bind to cCTnC simultaneously and the binding affinities (K_D ~ 10 μM for EMD 57033 and K_D ~ 100 μM for $cTnI_{128-147}$) are similar to those determined from binding to intact cTnC (*15*). However, unlike $cTnI_{128-147}$, the N-terminal region of cTnI, $cTnI_{34-71}$, can displace EMD 57033 completely from cCTnC. When the 38-residue $cTnI_{34-71}$ peptide is titrated to the

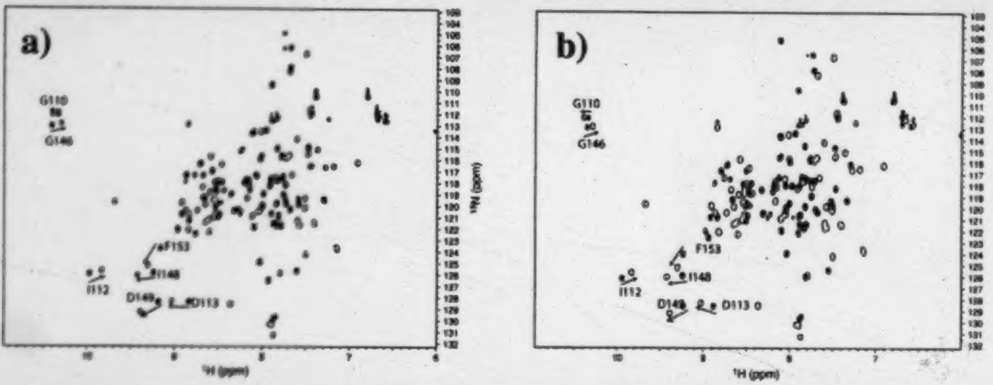

Figure II-8. 2D {^{1}H, ^{15}N}-HSQC NMR spectra of the titrations of a) cCTnC with cTnI$_{34-71}$, b) the cCTnC-EMD 57033 complex with cTnI$_{34-71}$. A) The cross peaks corresponding to free cCTnC are shown in multiple contours, whereas the peaks corresponding to the cCTnC-cTnI$_{34-71}$ complex are shown as single contours. B) The cross peaks corresponding to the cCTnC·EMD 57033 complex are shown as multiple contours, whereas cross peaks corresponding to the cCTnC·cTnI$_{34-71}$ complex are shown as single contours.

Ca^{2+}-saturated cCTnC, it binds tightly ($K_D \leq 1\mu M$) to form a stable cCTnC-cTnI$_{34-71}$ complex. Figure II-8a shows a superimposition of the 2D {^{1}H, ^{15}N}-HSQC NMR spectra of cCTnC and the cCTnC-cTnI$_{34-71}$ complex. Similar to sTnI$_{1-40}$ binding to sCTnC (*42*), cTnI$_{34-71}$ binding to cCTnC occurs with slow exchange kinetics on the NMR time scale. Thus, as the titration progresses, the resonance peaks corresponding to cCTnC becomes less intense while those corresponding to cCTnC-cTnI$_{34-71}$ grow. When the cTnI$_{34-71}$:cCTnC ratio reaches 1:1, all cross peaks corresponding to cCTnC have completely disappeared while those corresponding to cCTnC-cTnI$_{34-71}$ attain maximum intensity. When cTnI$_{34-71}$ is titrated to the cCTnC-EMD 57033 complex, EMD 57033 is displaced completely by cTnI$_{34-71}$ and a stable cCTnC-cTnI$_{34-71}$ complex forms ($K_D \leq 1\mu M$). The binding behavior of cTnI$_{34-71}$ to the cCTnC-EMD complex is very similar to that of cTnI$_{34-71}$ to cCTnC (Figure II-8a) and is illustrated in Figure II-8b, which shows a superimposition of the 2D {^{1}H,^{15}N}-HSQC NMR spectra of cCTnC-EMD 57033 and cCTnC-cTnI$_{34-71}$. The only difference between Figure II-8a and Figure II-8b is the starting spectra. The former started with the spectrum of cCTnC and the latter started with the spectrum of cCTnC-EMD 57033. The end spectra are identical and represent that of the cCTnC-cTnI$_{34-71}$ complex. Thus, cTnI$_{34-71}$ associates tightly with cCTnC regardless of the presence of EMD 57033.

It is necessary to put these results into perspective with respect to the interaction of cTnC and cTnI. The noncompetitive binding sites of cTnI$_{128-147}$ and EMD 57033 on cTnC (*15*) or cCTnC (present data) suggest that the inhibitory region of cTnI does not block the binding of EMD 57033 to cTnC, and *vice versa*. This conclusion is important in terms of addressing the Ca^{2+}-sensitizing role of EMD 57033 because the inhibitory region of cTnI constitutes a major switch between muscle contraction/relaxation by moving between cTnC and actin-tropomyosin (*43*). A good Ca^{2+}-sensitizer would not interfere with the inhibitory function of cTnI. A pertinent question is whether this is also the case with intact cTnI, especially considering the present clear-cut results that EMD 57033 can not compete with cTnI$_{34-71}$ for cCTnC. The very tight association of sTnI$_{1-40}$ and the sCTnC has been shown by several groups. In addition to the sTnC-sTnI$_{1-47}$ crystal structure (*38*), early functional studies of this region by Ngai and Hodges (*44*) have shown that sTnI$_{1-40}$ can effectively competes with sTnI or sTnI$_{96-115}$ ihhibitory peptide for sTnC and a recent NMR study has shown that sTnI$_{1-40}$ binds strongly to sCTnC with a K_D of ~ 2 μM and can displace sTnI$_{96-115}$ completely (*42*). This raises questions regarding how the inhibitory region binds to TnC to release inhibition if the N-terminal region of TnI is always present. In order to rationalize these results, two models have been proposed for the interaction of TnC and TnI. One suggests that these two regions of TnI share overlapping binding sites on the C-domain of TnC, which are alternatively occupied by either one or the other depending on the interactions between the N-domain of TnC and the C-domain of TnI or the C-domain of TnT (*17*). The second model proposes that the N-terminal region of TnI always binds to the C-domain of TnC, regardless of the Ca^{2+}-dependent interactions between the N-domain of TnC and the C-domain of TnI (*38, 45, 46*), while the inhibitory region interacts with the central helix area (including part of the D helix in the N-domain and part of the E-helix in the C-domain) of TnC in a Ca^{2+}-dependent manner. The later model does not adequately explain the experimental data (*15, 47-51*) supporting a binding site for the inhibitory region of TnI primarily in the C-domain of TnC, especially when only isolated C-domains of TnC were used in the study (*42, 49*). Based on our titration data of $cTnI_{128-147}$ binding to cTnC (*15*) and cCTnC (present work) and the competitive binding of $sTnI_{1-40}$ and $sTnI_{96-115}$ to sCTnC (*42*), we suggest that $cTnI_{128-147}$ binds primarily to the C-domain of cTnC and in order for this binding to occur, the interaction between $cTnI_{34-71}$ and cCTnC has to be weakened. This can be accomplished by the mechanisms proposed by the first model (*17*). Since cTnC does not act alone, and the contractile proteins work in a highly organized and cooperative manner in muscle contraction, it is possible that cCTnC in myofilaments may have a lower affinity for $cTnI_{34-71}$ than it does in isolation. Although EMD 57033 alone is too small to compete with the extensive contacts between the long α-helix of $cTnI_{34-71}$ and cCTnC, the fact that EMD 57033 interacts with many of the same residues on cCTnC as $sTnI_{1-47}$ on sCTnC suggests that the drug may play a role in disrupting and therefore weakening the interaction of $cTnI_{34-71}$ with cCTnC in the myofilaments, and consequently, in enhancing the binding of the inhibitory region of TnI to TnC. Since this interaction is Ca^{2+}-dependent, the apparent Ca^{2+} sensitivity of the contractile system can be modulated by EMD 57033.

cCTnC as the in situ target of EMD 57033

The question of *in situ* target of EMD 57033 has been clarified indirectly by two recent physiological studies involving EMD 57033 (*52*, *53*). First, Burkart et al. uncovered that a combination of cTnI N-terminal phosphorylation (S43/S45) and Tm mutation had an effect on EMD 57033's potency (*52*). It was difficult to conclude that EMD 57033 acted directly on cTnC from these results alone. However, it is evident that Tn proteins have a direct connection to EMD 57033's Ca^{2+}-sensitizing activity. A more recent study by Lipscomb et al. was more informative (*53*). By replacing the TnC isoform in skinned muscle fibres with either sTnC or cTnC, they showed that EMD 57033 had greater Ca^{2+}-sensitizing activity in fibres containing cTnC than those containing sTnC. This directly implicated TnC in EMD 57033's Ca^{2+}-sensitizing mechanism. In the light of these results, cTnC is most likely EMD 57033's *in situ* target. However, as noted by Lipscomb et al., EMD 57033's Ca^{2+}-sensitizing activity was not completely nullified in fibres with only sTnC. This could be an indication that EMD 57033 does not have a single mechanism for Ca^{2+}-sensitization. Although weak, EMD 57033 does possess some PDE III-inhibition activity (*2*), and as noted by Solaro et al., actomyosin ATPase activity was boosted by EMD 57033 even in the absence of TnC(*12*). Therefore, EMD 57033 could enhance muscle contractility through multiple mechanisms.

Binding of EMD 57439 and EMD 73186 to cCTnC

EMD 57033's stereo-specific interactions with cTnC were first confirmed by Pan & Johnson using fluorescence techniques (*13*). They revealed that, compared with EMD 57033, a much higher concentration of EMD 57439 was needed to suppress cTnC's Tyr fluorescence. To investigate how EMD 57439's interactions with cTnC differ from that between EMD 57033 and cTnC, we titrated EMD 57439 into cTnC and monitored the titration using {^{1}H, ^{15}N}-HSQC (Figure II-9a). Differences in patterns of chemical shift changes induced by the drugs revealed that the two drugs interacted with cTnC in dissimilar manners. The number of residues in the {^{1}H, ^{15}N}-HSQC exhibiting drug-induced chemical shift changes as well as the magnitudes of those changes are much less for EMD 57439 than EMD 57033 (Figure II-9a). The patterns of chemical shift changes produced by the two enantiomers are also quite different. In the case of EMD 57033, the major chemical shift changes occurred around helices F, G and H (residues 117, 119, 121, 136, 137, 140, 141, 154 and 155) (Figure II-10). But for EMD 57439, it is residues in the linker region that showed the most chemical shift changes (residues 122, 124, 125, 127, 128, 129), with residues on the helices showing only minor chemical shift changes (Figure II-10). Because the structure of cCTnC is quite rigid, neither EMD 57033 nor EMD 57439 should produce significant structural changes. Thus the chemical shift change pattern is expected to reflect accurately the binding site of the drug. The fact that EMD 57439 elicited the most amide nitrogen/proton chemical shift changes from residues in the linker region means EMD 57439 was not able to penetrate deep into the hydrophobic pocket the way EMD 57033 did and only made fleeting contacts with hydrophobic residues on the surface of the protein.

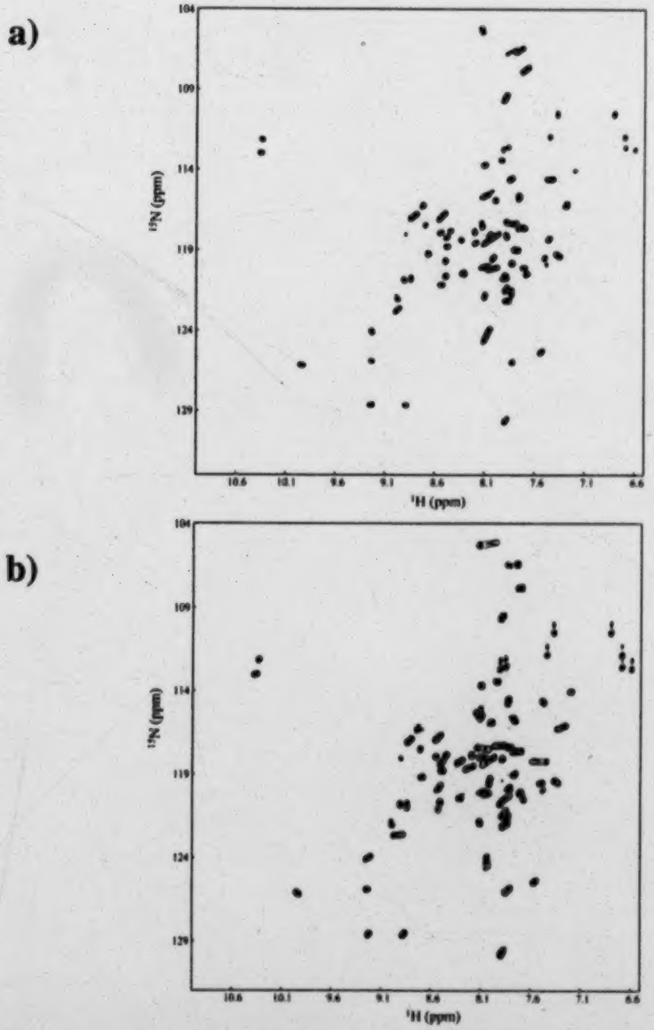

Figure II-9. Titrations of Ca^{2+}-saturated cCTnC with a) EMD 57439 and b) EMD 73186. 2D {^{1}H, ^{15}N}-HSQC NMR spectra arising from the backbone NH and side chain NH_2 groups of cTnC are superimposed for various EMD 57439 additions. Each titration point represents the addition of 1µl of 50 mM stock solution. Crossp eaks corresponding to free cCTnC with no drug added are shown as multiple contours. Cross peaks from subsequent spectra are shown as single contours.

EMD 73186 is a fluorinated version of EMD 57033 in which one of the methoxy group is replaced by a difluoromethoxy group (Figure II-1). Our interest in the drug stems mostly from a desire to investigate interactions between drugs and proteins *in situ*. In our proposed methodology, the fluorine –labelled drug will be titrated into intact tissue containing fluorine-labelled protein. Then, the fluorine homonuclear dipolar interaction between fluorine-labelled drug and protein will be measured using a variety of solid-state NMR techniques and the distance as well as the orientation of the drug relative to the target protein can be accurately quantitated. However, results from this type of investigation are only valid if the fluorine label on the drug does not disturb its

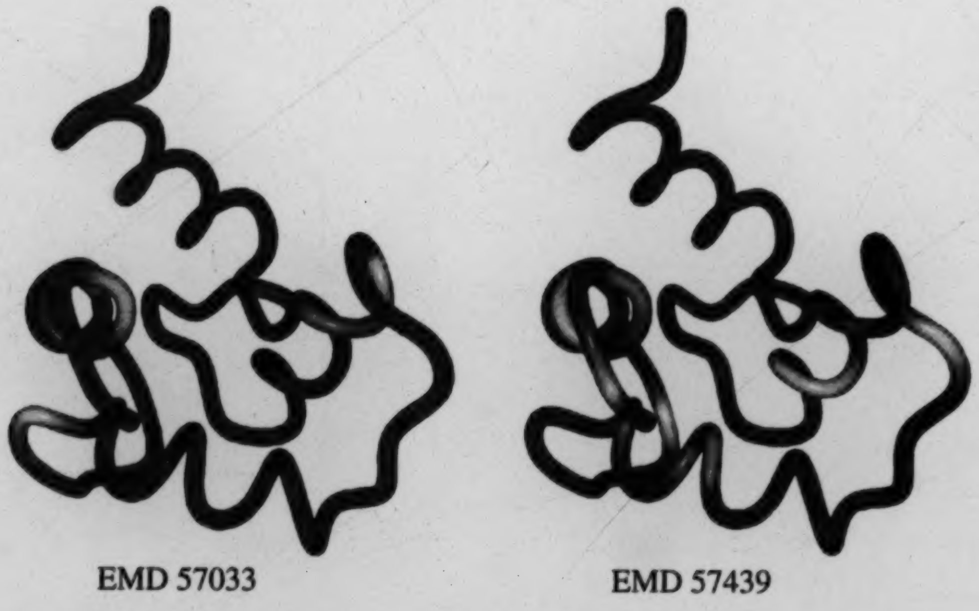

Figure II-10. Schematic backbone structures of cCTnC colored to reflect the normalized back bone amide nitrogen/proton chemical shift changes during titrations of EMD 57033 and EMD 57439. Residues with chemical shift changes less than 150% of the average change are colored green. Residues with chemical shift changes greater than 150% of the average changes are colored with a white-to-red color gradient with dark red being the residue with the biggest change in chemical shifts.

interaction with the protein. To determine the fluorines perturbation on EMD57033-cCTnC interactions, we titrated cCTnC with EMD 73186. Figure II-9b shows the overlay of {^{1}H, ^{15}N}-HSQC spectra taken during the titration. The pattern of chemical shift changes induced by EMD 73186 is almost identical to that induced by EMD 57033, suggesting EMD 73186 interacts with EMD 57033 in a similar manner. However, the magnitudes of EMD 73186-induced chemical shift changes are small compared to that of EMD 57033. This is best explained as a reduction in either the solubility or the cCTnC affinity of EMD 73186 as compared to EMD 57033. Indeed, during the titration of cCTnC with EMD 73186, precipitations were observed at a much earlier stage than that seen with EMD 57033 and chemical shift changes ceased soon after that. It would be surprising if the solubility of EMD 57186 is lower than that of EMD 57033 since fluorinated drugs are usually much more soluble than that of their non-fluorinated counterpart. However, I must point out that owing to the low solubility of the thiadiazinone drugs as well as its relatively low affinity for cTnC, a small variation in experimental condition (such as salt concentration and pH) can alter the drugs solubility greatly. It is possible the low solubility observed for EMD 73186 is the result of non-uniform experimental conditions rather than the inherent property of the fluorinated drug. An alternative explanation could be that the fluorination reduced the drug's affinity for cTnC, thus more drugs are required to produce the same magnitude of chemical shift changes. But because of the low solubility of the drug, the concentration required to saturate the protein is never reached, therefore producing low-magnitude chemical shift changes.

Conclusion

The number of patients suffering from congestive heart failure is rising accompanying the aging of baby boomers. Ca^{2+}-sensitizers have been proposed as a treatment for this common disease. These agents increase myocardial contractility by generating more force for a given amount of cytosolic free Ca^{2+}. This allows an achievement of positive inotropic effect more economically as compared to other positive inotropic drugs that exert effect by simply enhancing Ca^{2+} influx into myocytes and therefore add intracellular Ca^{2+} overload. Numerous studies have documented the Ca^{2+}-sensitizing effects of this class of agents under *in vivo* and *in vitro* conditions (for a review, see ref. (*3*)). Among which, EMD 57033 is one of the most potent and selective Ca^{2+}-sensitizers available. Earlier physiological studies have shown that EMD 57033 exerts detectable positive inotropic effects on isolated cardiac myocytes at concentrations as low as 1 μM (*12*), and in skinned cardiac muscle fibers, 3 μM of EMD 57033 induced significant Ca^{2+} sensitivity of force development (*2*). In a recent study, 0.3 – 1 μM of EMD 57033 is shown to have positive inotropic effects on both normal and failing cardiac myocytes (*11*). The cCTnC-EMD 57033 complex structure presented in this work provided a structural basis for the understanding of the mechanism underlining the Ca^{2+}-sensitizing effect of EMD 57033 in cardiac muscle contraction. In the present structure of the cCTnC-EMD 57033 complex, the drug molecule is orientated such that the chiral group of EMD 57033 fits deep in the hydrophobic pocket and makes several key contacts with the protein. This stereospecific interaction explains why the (-) enantiomer of EMD 57033 is inactive (*12*). Since the methyl group attached to the chiral carbon of EMD 57033 makes extensive contacts with methyl groups of Ile 112, Ile 117, and Ile 148, these contacts may be weakened or lost if the stereospecificity of the chiral carbon is changed. This is especially true for the interactions between residues on the short β-sheet and the drug. These interactions would be eliminated if the chirality of the drug has reversed, not even the rotation of ring A can completely restore all the contacts between the drug and these residues. Results from this and other studies laid the ground work for understand Ca^{2+}-sensitizing mechanisms of thiadiazinone-derived drugs such as EMD 57033 and levosimendan.

References

1. Nicholls, A. (1992) *GRASP: graphical representation and analysis of surface properties*, Columbia University, New York.
2. Lues, I., Beier, N., Jonas, R., Klockow, M., and Haeusler, G. (1993) *J. Cardiovasc. Pharmacol. 21*, 883-92.
3. Endoh, M. (1995) *Gen. Pharmacol. 26*, 1-31.
4. Varro, A., and Papp, J. G. (1995) *J. Cardiovasc. Pharmacol. 26*, S32-44.
5. Nielsen-Kudsk, J. E., and Aldershvile, J. (1995) *J. Cardiovasc. Pharmacol. 26*, S77-84.
6. Ventura, C., Miller, R., Wolf, H. P., Beier, N., Jonas, R., Klockow, M., Lues, I., Hano, O., Spurgeon, H. A., Lakatta, E. G., and et al. (1992) *Circ. Res. 70*, 1081-90.
7. Gross, T., Lues, I., and Daut, J. (1993) *J. Mol. Cell. Cardiol. 25*, 239-44.
8. de Zeeuw, S., Trines, S. A., Krams, R., Verdouw, P. D., and Duncker, D. J. (2000) *Br. J. Pharmacol. 129*, 1413-22.
9. Haeusler, G., Jonas, R., Minck, K. O., Schliep, H. J., Schelling, P., Weygandt, H., and Lues, I. (1997) *J. Cardiovasc. Pharmacol. 29*, 647-55.
10. Senzaki, H., Isoda, T., Paolocci, N., Ekelund, U., Hare, J. M., and Kass, D. A. (2000) *Circulation 101*, 1040-8.
11. Tsutsui, H., Kinugawa, S., Ide, T., Hayashidani, S., Suematsu, N., Satoh, S., Nakamura, R., Egashira, K., and Takeshita, A. (2001) *J. Cardiovasc. Pharmacol. 37*, 16-24.
12. Solaro, R. J., Gambassi, G., Warshaw, D. M., Keller, M. R., Spurgeon, H. A., Beier, N., and Lakatta, E. G. (1993) *Circ. Res. 73*, 981-90.
13. Pan, B.-S., and Johnson, J., R. G. (1996) *J. Biol. Chem. 271*, 817-823.
14. Kleerekoper, Q., and Putkey, J. A. (1999) *J. Biol. Chem. 274*, 23932-9.
15. Li, M. X., Spyracopoulos, L., Beier, N., Putkey, J. A., and Sykes, B. D. (2000) *Biochemistry 39*, 8782-90.
16. Chandra, M., Dong, W. J., Pan, B. S., Cheung, H. C., and Solaro, R. J. (1997) *Biochemistry 36*, 13305-13311.
17. Tripet, B. P., Van Eyk, J. E., and Hodges, R. S. (1997) *J. Mol. Biol. 271*, 728-750.
18. Levijoki, J., Pollesello, P., Kaivola, J., Tilgmann, C., Sorsa, T., Annila, A., Kilpelainen, I., and Haikala, H. (2000) *J Mol Cell Cardiol 32*, 479-91.
19. Kay, L. E., Keifer, P., and Saarinen, T. (1992) *J. Am. Chem. Soc. 114*, 10663-10665.
20. Zhang, O., Kay, L. E., Olivier, J. P., and Forman-Kay, J. D. (1994) *J. Biomol. NMR 4*, 845-858.
21. Ogura, K., Terasawa, H., and Inagaki, F. (1996) *J. Biomol. NMR 8*, 492-498.
22. Zwahlen, C., Legault, P., Vincent, S. J. F., Greenblatt, J., Konrat, R., and Kay, L. E. (1997) *J. Am. Chem. Soc. 119*, 6711-6721.
23. Delaglio, F., Grzesiek, S., Vuister, G. W., Zhu, G., Pfeifer, J., and Bax, A. (1995) *J. Biomol. NMR 6*, 277-293.
24. Johnson, B. A., and Blevins, R. A. (1994) *J. Biomol. NMR 4*, 603-614.
25. Gagné, S. M., Tsuda, S., Li, M. X., Smillie, L. B., and Sykes, B. D. (1995) *Nat. Struct. Biol. 2*, 784-789.

26. Sia, S. K., Li, M. X., Spyracopoulos, L., Gagné, S. M., Liu, W., Putkey, J. A., and Sykes, B. D. (1997) *J. Biol. Chem. 272*, 18216-18221.
27. Brünger, A. T. (1992) *X-PLOR Version 3.1 A system for X-ray Crystallography and NMR*, Yale University Press, New Haven.
28. Neri, D., Szyperski, T., Otting, G., Senn, H., and Wuthrich, K. (1989) *Biochemistry 28*, 7510-7516.
29. Kuboniwa, H., Grzesiek, S., Delaglio, F., and Bax, A. (1994) *J. Biomol. NMR 4*, 871-8.
30. Archer, S. J., Ikura, N. I., Torchia, D. A., and Bax, A. (1991) *J. Magn. Reson. 95*, 636-641.
31. Muhandiram, D. R., and Kay, L. E. (1994) *J. Magn. Reson. B103*, 203-216.
32. Kay, L. E., Xu, G. Y., Singer, A. U., Muhandiram, D. R., and Forman-Kay, J. D. (1993) *J. Magn. Reson. B101*, 333-337.
33. Pascal, S. M., Muhandiram, D. R., Yamazaki, T., Forman-Kay, J. D., and Kay, L. E. (1994) *J. Magn. Reson. B103*, 197-201.
34. Laskowski, R. A., MacArthur, M. W., Moss, D. S., and Thorton, J. M. (1993) *J. Appl. Crystallogr. 26*, 283-290.
35. Gasmi-Seabrook, G. M., Howarth, J. W., Finley, N., Abusamhadneh, E., Gaponenko, V., Brito, R. M., Solaro, R. J., and Rosevear, P. R. (1999) *Biochemistry 38*, 8313-22.
36. Spyracopoulos, L., Li, M. X., Sia, S. K., Gagné, S. M., Chandra, M., Solaro, R. J., and Sykes, B. D. (1997) *Biochemistry 36*, 12138-12146.
37. Finn, B. E., Evenas, J., Drakenberg, T., Waltho, J. P., Thulin, E., and Forsen, S. (1995) *Nat. Struct. Biol. 2*, 777-83.
38. Vassylyev, D. G., Takeda, S., Wakatsuki, S., Maeda, K., and Maeda, Y. (1998) *Proc. Natl. Acad. Sci. U.S.A. 95*, 4847-4852.
39. Li, M. X., Spyracopoulos, L., and Sykes, B. D. (1999) *Biochemistry 38*, 8289-98.
40. McKay, R. T., Tripet, B. P., Hodges, R. S., and Sykes, B. D. (1997) *J. Biol. Chem. 272*, 28494-28500.
41. McKay, R. T., Saltibus, L. F., Li, M. X., and Sykes, B. D. (2000) *Biochemistry 39*, 12731-12738.
42. Mercier, P., Li, M. X., and Sykes, B. D. (2000) *Biochemistry 39*, 2902-11.
43. Van Eyk, J. E., and Hodges, R. S. (1988) *J. Biol. Chem. 263*, 1726-1732.
44. Ngai, S.-M., and Hodges, R. S. (1992) *J. Biol. Chem. 267*, 15715-15720.
45. Tung, C. S., Wall, M. E., Gallagher, S. C., and Trewhella, J. (2000) *Protein. Sci. 9*, 1312-26.
46. Luo, Y., Leszyk, J., Li, B., Gergely, J., and Tao, T. (2000) *Biochemistry 39*, 15306-15.
47. Lan, J., Albaugh, S., and Steiner, R. F. (1989) *Biochemistry 28*, 7380-7385.
48. Campbell, A. P., and Sykes, B. D. (1991) *J. Mol. Biol. 222*, 405-421.
49. Swenson, C. A., and Fredricksen, R. S. (1992) *Biochemistry 31*, 3420-9.
50. Ngai, S.-M., Sönnichsen, F. D., and Hodges, R. S. (1994) *J. Biol. Chem. 269*, 2165-2172.
51. Howarth, J. W., Krudy, G. A., Lin, X., Putkey, J. A., and Rosevear, P. R. (1995) *Protein Sci. 4*, 671-680.

52. Burkart, E. M., Arteaga, G. M., Sumandea, M. P., Prabhakar, R., Wieczorek, D. F., and Solaro, R. J. (2003) *J Mol Cell Cardiol 35*, 1285-93.
53. Lipscomb, S., Preston, L. C., Robinson, P., Redwood, C. S., Mulligan, I. P., and Ashley, C. C. (2005) *Biochem J.*

Chapter III

Structure of Regulatory N-Domain of Human Cardiac Troponin C Complexed to Bepridil and Cardiac Troponin I$_{147-163}$[†]

Introduction

The essential role of cTnC in the regulation of heart muscle contraction makes it an attractive target for cardiotonic drugs in the therapy of heart diseases. These drugs are expected to tune the cardiac function by modulating the Ca^{2+}-sensitivity of the myofilaments and the myofilament protein interactions. In the early days of the search for Ca^{2+}-sensitizers, many drugs known to modulate Ca^{2+}-flux in myocytes were screened for Ca^{2+}-sensitizing activity. Most were inert. However, one of them, bepridil, was able to induce modest Ca^{2+}-sensitization in skinned cardiac muscle fibres (*1*).

Bepridil is a well-known Ca^{2+}-antagonist, i.e. a compound capable of inhibiting the cytosolic Ca^{2+}-influx during muscle activation. In the case of bepridil, this is accomplished mainly through the inhibition of voltage-dependent Ca^{2+} channels in the cytoplasmic membrane. Besides Ca^{2+} channels, bepridil is also known to slightly depress the fast Na^+ channel as well as slow the release of Ca^{2+} from SR. The overall effect of the drug is to decrease myocardial oxygen consumption and reduce the chances of arrhythmia. In fact, bepridil has been commercially available as a treatment for hypertension for some time. But by reducing the Ca^{2+}-influx during activation, bepridil reduces muscle activity *in vivo*, not enhance it. However, Solaro et al. showed that in the absence of membrane systems controlling the flow of Ca^{2+}, bepridil had weak Ca^{2+}-

---

[†] The results in this chapter are taken from Wang, X., Li, M. X. and Sykes, B. D., *J. Biol. Chem.* 277(34):31124-33, 2002.

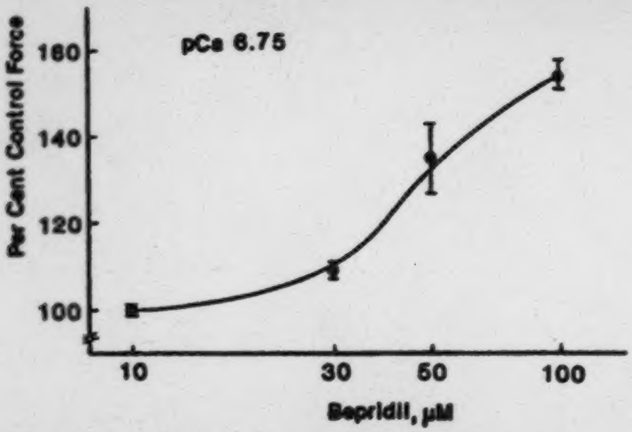

Figure III-1. Relationship between the normalized force generated by muscle fibres and the concentration of bepridil in solution. Taken from (*1*).

sensitizing effect on myofibrils (Figure III-1) (*1*). Despite this observation, the plethora of interactions bepridil has with other proteins undermines its potential as an ideal Ca^{2+}-sensitizer. Instead, it has developed into a popular model compound for investigating Ca^{2+}-sensitizing mechanisms. A series of biochemical studies showed that bepridil binds to isolated cTnC with a K_D of ~ 10 μM (*2*) and to the cTnC-cTnI complex with a K_D of ~ 140 μM (*3*). A NMR study, using Met residues as markers, identified three bepridil binding sites in cTnC (*4*). Interest in bepridil was boosted once gain in the year 2000 when Carolyn Cohen's group solved the X-ray crystal structure of bepridil complexed to cTnC. In the X-ray structure of the cTnC•3Ca^{2+}•3bepridil complex (*5*), two bepridil molecules located in the hydrophobic cavity between domains pull the domains close together to result in a compact structure for cTnC and a third bepridil appears to stabilize an open regulatory domain conformation by binding to the center of the hydrophobic pocket, much like the switch region of cTnI, cTnI$_{147-163}$ (please refer to Chapter I for detailed discussion of Tn-mediated muscle activation). This is the first physical evidence showing that compounds with Ca^{2+}-sensitizing activity are capable of stabilizing the active conformation of TnC, a very plausible Ca^{2+}-sensitizing mechanism.

The fact that both cTnI$_{147-163}$ and bepridil can induce a structural 'opening' in the N-domain of cTnC by interacting with the hydrophobic patch of the domain prompted us to explore whether cTnI$_{147-163}$ and bepridil compete for cNTnC•Ca^{2+}. In order to address this issue, we used 2D {^{1}H, ^{15}N} HSQC NMR spectroscopy to examine the binding of bepridil to cNTnC•Ca^{2+} in the absence and presence of cTnI$_{147-163}$ and of cTnI$_{147-163}$ to cNTnC•Ca^{2+} in the absence and presence of bepridil. The results show that the drug and the cTnI$_{147-163}$ peptide bind to cNTnC•Ca^{2+} simultaneously, but with negative cooperativity. The affinity of cTnI$_{147-163}$ for cNTnC•Ca^{2+} is reduced ~ 3.5 fold by bepridil and *vice versa*. Using multinuclear and multidimensional NMR spectroscopy, we have determined the structure of the ternary cNTnC•Ca^{2+}•cTnI$_{147-163}$•bepridil complex. The structure reveals a binding site for cTnI$_{147-163}$ primarily located on the A/B interhelical interface and a binding site for bepridil in the hydrophobic core of cNTnC•Ca^{2+}. In the structure, the N-terminus of the peptide clashes with part of the bepridil molecule. This explains the observed negative cooperativity between cTnI$_{147-163}$ and bepridil for cNTnC•Ca^{2+}. The current structure provides insights into the features that are important for the design of cTnC-specific cardiotonic drugs, which may be used to tune the cardiac function by modulating the Ca^{2+}-sensitivity of the myofilaments and the myofilament protein interactions.

Experimental Procedures

Sample preparation: The engineering of the expression vector of cNTnC (1-89) mutant was as described in Chandra *et al.* (*6*). The procedure used to express of ^{15}N- and ^{15}N/^{13}C-labeled cNTnC in *E. coli* strain BL21(DE3)pLysS was the same as that described for the expression of cCTnC in Chapter II. The purification of the protein is similar to that described previously (*7*). However, an additional purification step using Superdex-75 gel-filtration column (Pharmacia) was added. The condition for the column was also the same as that for the purification of cCTnC described in Chapter II. The synthetic peptide cTnI$_{147-163}$, Acetyl-RISADAMMQALLGARAK-Amide, was prepared and characterized as described previously (*8*). Bepridil was purchased from Sigma-Aldrich. Stock solutions (93 mM and 46.5 mM, respectively) of bepridil in DMSO-d$_6$ (Cambridge Isotopes Inc.) were prepared and the vials containing the solutions were wrapped in aluminum foil due to its sensitivity to light. All NMR samples were 500 μL in volume. The buffer conditions were 100 mM KCl, 10 mM imidazole in 90% H_2O/10% D_2O, 15 mM dithiothreitol (DTT), and the pH was 6.8. Two bepridil titrations were performed, one to a cNTnC•Ca^{2+} sample and the other to a cNTnC•Ca^{2+}•cTnI$_{147-163}$ complex sample. Two cTnI$_{147-163}$ titrations were performed, one using ^{15}N-cNTnC•Ca^{2+} and the other with the ^{15}N-cNTnC•Ca^{2+}•bepridil complex. For structure determination, NMR samples contain 1 - 2 mM cNTnC, 6 - 8 mM Ca^{2+}, 1 - 2 mM bepridil, and 3 - 6 mM cTnI$_{147-163}$.

cTnI$_{147-163}$ and bepridil titration of ^{15}N-cNTnC•Ca^{2+} monitored by 2D [^{1}H,^{15}N]-HSQC NMR spectra:

(A) Titration of ^{15}N-cNTnC•Ca^{2+} with cTnI$_{147-163}$: This titration reproduces the titration reported previously (*8*). cTnI$_{147-163}$ peptide is highly soluble in aqueous solution but tends to form a gel at high concentrations (>50 mM), likely due to aggregation. Thus, no stock peptide solution was prepared; instead, solid peptide was added at every titration point. To a NMR tube containing 500 μL sample of 0.56 mM of ^{15}N-cNTnC•Ca^{2+}, solid cTnI$_{147-163}$ was added for the seven titration points. The sample was mixed thoroughly with each addition. 2 μL of sample were taken at every titration point for amino acid analysis to determine the peptide/protein ratios. Changes in pH associated with cTnI$_{147-163}$ additions were compensated by adjusting to pH 6.8 at every titration point.

(B) Titration of ^{15}N-cNTnC•Ca^{2+} with bepridil: To a NMR tube containing a 500 μL sample of 0.50 mM ^{15}N-cNTnC•Ca^{2+}, aliquots of 0.5 μL of 93 mM bepridil in DMSO-d$_6$ were added for the nine titration points. The sample was mixed thoroughly with each addition. The total volume increase was 4.5 μL and the change in protein concentration due to dilution was taken into account for data analysis. The change in pH from bepridil addition was negligible. As a control experiment, a 2D {^{1}H, ^{15}N}-HSQC NMR spectrum of ^{15}N-cNTnC•Ca^{2+} in the presence of 4.5 μL of pure DMSO-d$_6$ was acquired to confirm that DMSO-d$_6$ has no effect on ^{15}N-cNTnC•Ca^{2+}.

(C) Titration of ^{15}N-cNTnC•cTnI$_{147-163}$ with bepridil: To a 500 μL NMR sample containing 0.58 mM of ^{15}N-cNTnC•Ca^{2+} and 2.0 mM of cTnI$_{147-163}$, aliquots of 1 μL of 46.5 mM bepridil in DMSO-d$_6$ were added for the six titration points. The sample was mixed thoroughly after each addition and no precipitation was observed. The change in pH from the addition of bepridil was negligible. The total volume increase was 6 μL and the change in protein concentration due to dilution was taken into account for data analysis.

(D) Titration of ^{15}N-cNTnC•Ca^{2+}•bepridil with cTnI$_{147-163}$: To a 500 µL NMR sample containing 0.50 mM ^{15}N-cNTnC•Ca^{2+}, aliquots of 6 µl of 46.5 mM bepridil in DMSO-d$_6$ was added to obtain a 1:1 ^{15}N-cNTnC•Ca^{2+}:bepridil complex. Solid cTnI$_{147-163}$ peptide was added at every titration point. The sample was mixed thoroughly with each addition. 2 µL of sample were taken at every titration point for amino acid analysis to determine the peptide/protein ratios. Changes in pH associated with cTnI$_{147-163}$ additions were compensated by adjusting to pH 6.8 at every titration point. Precipitation of free bepridil was not observed during the titration.

NMR spectroscopy: Most NMR data used in this study were collected at 30°C using Unity 600 MHz and Unity Inova 500 MHz spectrometers. Both spectrometers are equipped with triple resonance probes and Z-pulsed field gradients. 2D {^{1}H, ^{15}N}-HSQC spectra were acquired using the sensitivity enhanced gradient pulse scheme developed by Lewis E. Kay and coworkers (*9, 10*). For cNTnC in the ternary complex, the chemical shift assignments of the backbone and side chain atoms and NOE interproton distance restraints were determined using 2D and 3D NMR experiments described in Table III-1. For the bound cTnI$_{147-163}$ peptide, the proton chemical shifts of the peptide were assigned using 2D-^{15}N/^{13}C filtered-NOESY (250 ms mixing time) and 2D-^{15}N/^{13}C filtered-DIPSI experiments (43.2 ms spinlock time). The pulse sequences for these two experiments were based on Ogura *et al.* (*11*) with extensive modifications by Leo Spyracopoulos to optimize solvent suppression, pulse timing and calibration (L. Spyracopoulos, unpublished data). 1D ^{1}H and 2D DIPSI spectra of free bepridil in DMSO-d$_6$ and in H_2O were obtained to help in the assignment of the bepridil in the ternary complex. The intermolecular proton distances between cNTnC and cTnI$_{147-163}$ and bepridil were obtained using 3D ^{15}N/^{13}C F$_1$-filtered, F$_3$-edited-NOESY HSQC experiments employing linear frequency ramped broadband inversion pulses for ^{13}C (150 ms mixing time) (*12*).

Data processing and peak calibration: All 2D and 3D NMR data was processed using NMRPipe (*13*) and all 1D NMR data were processed using VNMR (Varian Associates). The spectra were analyzed using NMRView (*14*). For cNTnC in the complex, intramolecular distance restraints obtained from the NOESY experiments were calibrated according to Gagné *et al.* (*15*). Intramolecular proton distances for the peptide and bepridil in the complex were calibrated by classifying NOE intensities as strong (2 Å - 4 Å), medium (3 Å – 5 Å), and weak (4 Å – 6 Å). Intermolecular NOEs between bepridil and cNTnC, between cTnI$_{147-163}$ and cNTnC, and between bepridil and cTnI$_{147-163}$ were obtained from the ^{15}N/^{13}C-filtered and the ^{15}N/^{13}C-filtered/edited experiments. Dihedral angle restraints for cNTnC in the complex were derived from data obtained from HNHA, HNHB, and NOESY-HSQC experiments according to Sia *et al.* (*16*). For bound cTnI$_{147-163}$, dihedral restraints of $-60° \pm 25°$ and $-30° \pm 25°$ for ϕ and ψ, respectively, were obtained from the chemical shift indices (CSI) of the peptide ^{1}Hα protons for residues which showed α-helical CSI values (*17*).

Structure calculations: Using an initial set of intramolecular NOE restraints for cNTnC, 100 structures of cNTnC alone were calculated starting from an extended conformation.

The calculations were done using simulated annealing protocol implemented in X-PLOR (*18*) with 10,000 high-temperature steps (time step of 30 ps) and 6000 cooling steps (time step of 30 ps). Approximately 50% of the initial structures converged. These structures were used as templates for further rounds of refinements. Dihedral angle restraints and six artificial distance restraints from chelating oxygen atoms to Ca^{2+} ion were added at later stages of the refinement process. The structure of the ternary complex was calculated starting from the extended conformations of cNTnC, bepridil, and cTnI$_{147-163}$ peptide using simulated annealing protocol with the same conditions as above. The calculations were carried out using the distance and the ϕ, ψ, and χ_1 dihedral restraints for cNTnC and for cTnI$_{147-163}$ (see Table III-2), 6 distance restraints to the Ca^{2+} ion, 28 intermolecular distance restraints between cNTnC and bepridil, 30 intermolecular distance restraints between cNTnC and cTnI$_{147-163}$ peptide, 24 intramolecular distance restrains for the bound cTnI$_{147-163}$ peptide as well as an intermolecular distance restraint between bepridil and cTnI$_{147-163}$ (see Table III-2). The final family of solution structures presented in this paper consists of thirty lowest energy structures.

Table III-1. NMR Spectra Acquired and Experimental Conditions Used to Obtain Assignments and NOE Restraints.

Experiment name	Nuclei[a]	^{1}H freq[b].	nt[c]	*x*-pts[d]	*y*-pts	*z*-pts	*x*-sw	*y*-sw	*z*-sw	mix[e]	Ref.
3D ^{15}N-edited DIPSI-HSQC	^{1}H,^{1}H,^{15}N	600	36	900	116	30	7500	6400	1700	86.5	*(10)*
3D ^{15}N-edited NOESY-HSQC	^{1}H,^{1}H,^{15}N	500	16	896	120	30	7000	5748	1322	75	*(10)*
HNHA	^{1}H,^{1}H,^{15}N	500	16	896	64	48	7000	4000	1500		*(19)*
HNHB	^{1}H,^{1}H,^{15}N	500	16	950	82	32	6500	5400	1390		*(20)*
CBCA(CO)NNH	^{1}H,^{13}C,^{15}N	500	16	832	50	32	6500	7794	1250		*(21)*
HNCACB	^{1}H,^{13}C,^{15}N	500	32	832	50	30	6500	7794	1250		*(21)*
HCCH-TOCSY	^{1}H,^{1}H,^{13}C	500	16	832	128	32	6000	3000	3000	19.6	*(22)*
3D ^{13}C/^{15}N-edited NOESY	^{1}H,^{1}H,^{15}N/^{13}C	500	16	650	128	32	6500	5500	3000	75	*(23)*
2D ^{13}C/^{15}N-filtered NOESY	^{1}H(^{14}N/^{12}C),^{1}H(^{14}N/^{12}C)	500	24	4096	512		6200	6200		250	*(11)*
2D ^{13}C/^{15}N-filtered DIPSI	^{1}H(^{14}N/^{12}C),^{1}H(^{14}N/^{12}C)	500	32	4096	512		6000	6000		43.2	*(11)*
3D ^{13}C/^{15}N-filtered/edited NOESY	^{1}H(^{14}N/^{12}C),^{1}H,^{15}N/^{13}C	500	16	746	106	30	7000	5500	3000	250	*(12)*

[a] The nucleus acquired in each dimension (e.g. ^{1}H, ^{15}N indicates proton in *x*-dimension and ^{15}N in *y*-dimension).

[b] The frequency of ^{1}H in MHz.

[c] The number of transients acquired for each FID.

[d] *x*,*y*,*z*-pts and sw is the number of complex points and sweep width in each respective dimension (*x* is the directly detected dimension).

[e] Mixing times are given in milliseconds. In the case of DIPSI or TOCSY experiments, this is the spin-locking time.

Table III-2: Structural Statistics of the family of the 30 structures calculated.

	Backbone Atoms	Heavy Atoms
R.M.S.D. from the average structure (Å)[a]		
Well-defined residues	0.58±0.08	0.98±0.07
Helices	0.22±0.04	0.69±0.09
NOE restraints		
Total	1169(approx. 13/residue)	
Intra-residue	535	
Sequential ($\|i-j\|=1$)	284	
Medium-range($2\leq\|i-j\|\leq4$)	229	
Long-range ($\|i-j\|\geq5$)	121	
Artificial restraints to Ca^{2+}	6	
Intermolecular NOEs between cNTnC and bepridil	28	
Intermolecular NOEs between cNTnC and the cTnI$_{147-163}$ peptide	30	
Intramolecular restraints in cTnI$_{147-163}$ peptide		
NOEs	24	
ϕ angle restraints	6	
ψ angle restraints	6	
Dihedral Restraints in cNTnC		
Total	88	
ϕ	29	
ψ	39	
χ_1	20	
Energies[b]		
E_{total}	124±9	
E_{NOE}	2.8±0.2	
$E_{dihedral}$	0.08±0.01	
R.M.S.D. from idealized geometry		
Bond length (Å)	0.001±1e-05	
Bond angle (°)	0.47±0.09	
Impropers (°)	0.26±0.05	
Restraint Violations		
Distance >0.2Å	0	
Dihedral>1°	0	
ϕ, ψ in core or allowed regions[d]	98.8%	

[a] 81 residues have well defined backbone atoms. This includes residues 5-85. The R.M.S.D. for helices are calculated from the average of the R.M.S.D. of individual helices.

[b] The final K_{NOE} and $K_{dihedral}$ used were 50 kcalmol^{-1} and 200 kcalmol^{-1}rad^{-2}, respectively.

[c] As determined using PROCHECK (*24*).

Results and Discussion

Effect of bepridil and cTnI$_{147-163}$ on cNTnC•Ca^{2+}

The assigned 2D {^{1}H, ^{15}N}-HSQC NMR spectrum of cNTnC•Ca^{2+} (*25*) was used to monitor the binding of bepridil and/or cTnI$_{147-163}$ to cNTnC•Ca^{2+}, the assigned 2D {^{1}H, ^{15}N}-HSQC NMR spectrum of cNTnC•Ca^{2+}•cTnI$_{147-163}$ (*8*) was used to monitor bepridil binding to cNTnC•Ca^{2+}•cTnI$_{147-163}$, and the assigned 2D {^{1}H, ^{15}N}-HSQC NMR spectrum of cNTnC•Ca^{2+}•bepridil (unpublished) was used to monitor the binding of cTnI$_{147-163}$ to cNTnC•Ca^{2+}•bepridil. Using residues Leu 29 and Glu 66 of cNTnC as examples, Figure

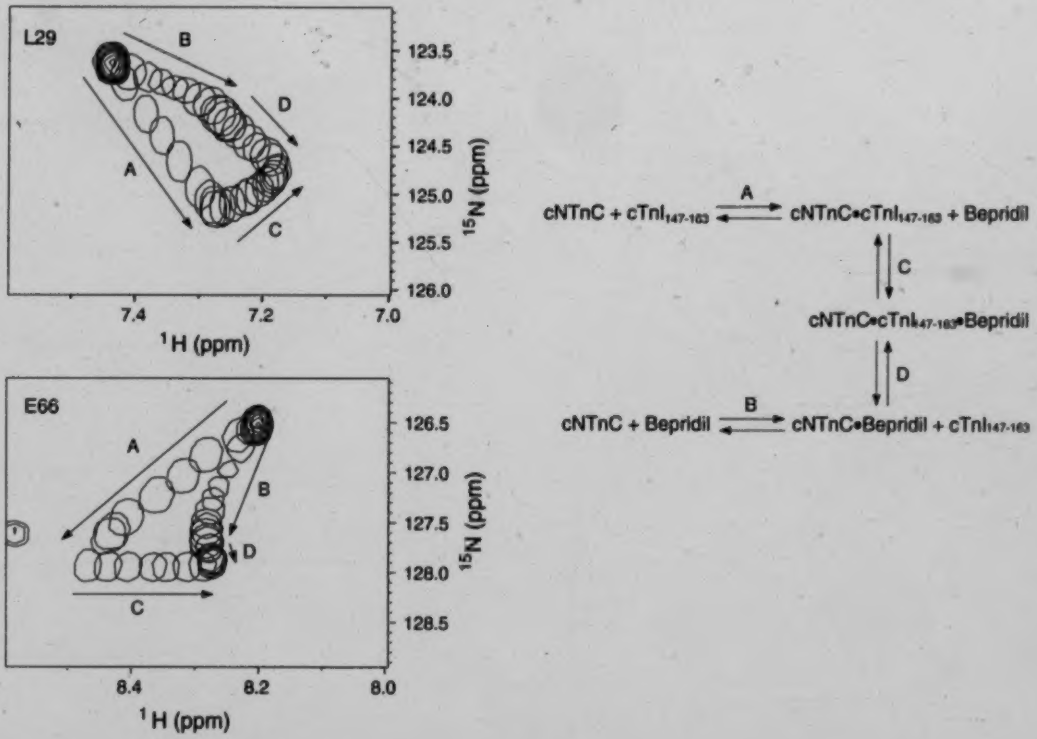

Figure III-2. Titration of (A) cNTnC•Ca^{2+} with cTnI$_{147-163}$, (B) cNTnC•Ca^{2+} with bepridil, (C) cNTnC•Ca^{2+}•cTnI$_{147-163}$ with bepridil, and (D) cNTnC•Ca^{2+}•bepridil with cTnI$_{147-163}$. 2D {^{1}H, ^{15}N}-HSQC NMR spectra for residues Leu 29 and Glu 66 of cNTnC at various bepridil and cTnI$_{147-163}$ additions are superimposed, showing the progressive shift of peaks with increasing bepridil or cTnI$_{147-163}$ concentrations. The corresponding equilibria for titrations A-D are also shown.

III-2 depicts the cTnI$_{147-163}$-induced peak shifts on cNTnC•Ca^{2+} (arrow A), the bepridil-induced peak shifts on cNTnC•Ca^{2+} (arrow B), the bepridil-induced peak shifts on cNTnC•Ca^{2+}•cTnI$_{147-163}$ (arrow C), and the cTnI$_{147-163}$-induced peak shifts on cNTnC•Ca^{2+}•bepridil (arrow D). It is important to point out that these two residues do exemplify all of the residues in the protein, which undergoes backbone amide ^{1}H or ^{15}N chemical shift changes during titrations. In Figure III-2, arrows A and D represent the binding of cTnI$_{147-163}$ to cNTnC•Ca^{2+} in the absence and presence of bepridil, respectively, whereas arrows B and C represent the binding of bepridil to cNTnC•Ca^{2+} in the absence and presence of cTnI$_{147-163}$, respectively. It is interesting to notice that arrows A and B point to different directions, but arrows C and D point to the same end position. This indicates that a stable ternary cNTnC•Ca^{2+}•cTnI$_{147-163}$•bepridil complex forms in the end regardless whether bepridil was added first followed by cTnI$_{147-163}$ or *vice versa*. This observation is reminiscent of our previous work on EMD 57033 and cTnI$_{128-147}$ binding to cTnC•3Ca^{2+}, where we demonstrated that both EMD 57033 and cTnI$_{128-147}$ bind cTnC•3Ca^{2+} in 1:1 ratios in a non-competitive manner (*26*). Neither is EMD 57033 binding affected by cTnI$_{128-147}$ nor does EMD 57033 affect cTnI$_{128-147}$ binding. In the end, a stable ternary cTnC•3Ca^{2+}•cTnI$_{128-147}$•EMD 57033 complex is formed. Using the same approach as for cTnI$_{128-147}$ and EMD 57033 binding to cTnC, we analyzed the chemical shift changes as a function of the ligand to protein ratios and determined the binding affinities of cTnI$_{147-163}$ for cNTnC•Ca^{2+} in the absence and presence of bepridil and those of bepridil for cNTnC•Ca^{2+} in the absence and presence of cTnI$_{147-163}$. In contrast to the interaction of EMD 57033 and cTnI$_{128-147}$ with cTnC•3Ca^{2+}, where the affinity of one ligand is not affected by the other, the affinity of cTnI$_{147-163}$ for cNTnC•Ca^{2+} is decreased ~ 3.5 fold (from a K$_D$ of 154 ± 30 μM to a K$_D$ of 550 ± 50 μM) by the presence of bepridil and that of bepridil for cNTnC•Ca^{2+} is also decreased ~ 3.5 fold (from a K$_D$ of 23 ± 5 μM to a K$_D$ of 80 ± 15 μM) by the presence of cTnI$_{147-163}$. This is somewhat surprising because bepridil has been shown to increase both the activity of actomyosin ATPase and force generation *in vitro* (*2, 27*), and this increase was observed in both slow/cardiac and fast skeletal muscle fibers, with the effect being greater in slow/cardiac fibers (*28*). However, this is in agreement with a recent study (*29*) that shows an apparent weaker binding of bepridil to the cTnC regulatory domain in the cTnC-cTnI complex (~ 140 μM) than to the isolated cTnC (~ 10 μM) and bepridil is also shown to inhibit CaM from binding to its target proteins (*30*). Although several possible explanations could account for the apparent difference in binding affinities, the most obvious one would be that the partially positive charged group of bepridil, while binding to cNTnC•3Ca^{2+}, hinder the binding of the positively charged cTnI to cTnC, and *vice versa*. This is what we have observed in the ternary cNTnC•Ca^{2+}•cTnI$_{147-163}$•bepridil complex as described below. The observed negative cooperativity between bepridil and cTnI for cTnC suggests that the effect of bepridil on muscle fibers may result from a combination of many integrated effects within the myofibrillar lattice.

Overall structure of the ternary complex

The 2D {^{1}H, ^{15}N}-HSQC NMR spectrum of cNTnC in the ternary cNTnC•Ca^{2+}•cTnI$_{147-163}$•bepridil complex was highly resolved, allowing the chemical shifts of the backbone and the side chain atoms to be assigned readily using ^{15}N- and/or ^{15}N/^{13}C-labeled protein (Figure III-3). Distance restraints for cNTnC in the ternary

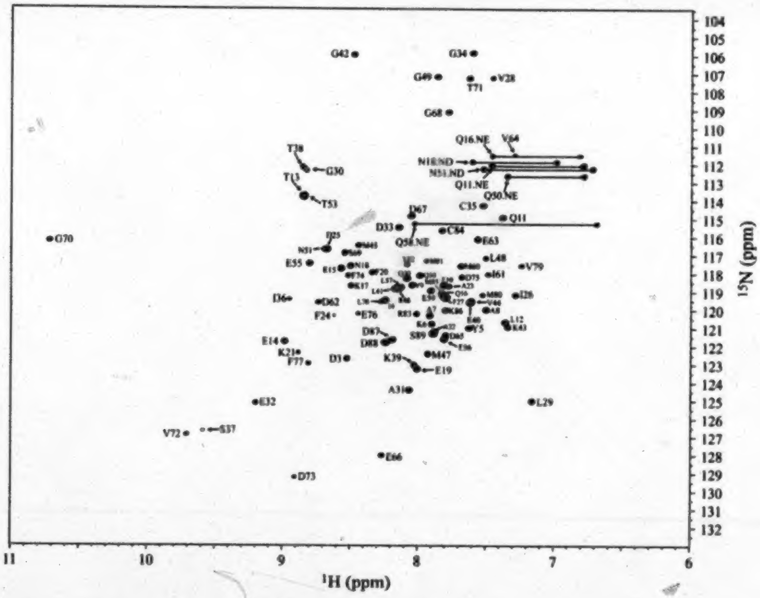

Figure III-3. Assigned HSQC spectrum of the uniformly ^{15}N-labelled cNTnC complexed to cTnI$_{147-163}$ and bepridil. Each signal in the spectrum is labelled with one-letter residue name and number.

complex were obtained by analyzing 3D ^{15}N- or ^{15}N/^{13}C-edited NOESY experiments. Dihedral angle restraints for cNTnC in the ternary complex were obtained from 3D HNHA, 3D HNHB, and ^{15}N-edited NOESY experiments. The NMR experiments performed are summarized in Table III-1.

The proton NMR chemical shift assignments and intramolecular distance restraints for the bound cTnI$_{147-163}$ peptide and bepridil required the collection of ^{15}N/^{13}C filtered 2D-DIPSI and 2D-NOESY experiments using unlabeled cTnI$_{147-163}$ and bepridil in complex with ^{15}N/^{13}C labeled cNTnC. These experiments removed all of the resonance peaks arising from ^{15}N/^{13}C labeled cNTnC. 1D-^{1}H and 2D-DIPSI NMR spectra of free bepridil in DMSO-d$_6$ were also analyzed to aid the assignments of bepridil in the ternary complex. Intermolecular NOEs between cNTnC and cTnI$_{147-163}$ and between cNTnC and bepridil were determined from 3D-^{15}N/^{13}C-filtered, ^{15}N/^{13}C-edited NOESY data. These experiments were optimized for detecting NOEs between protons attached to $^{14}N/^{12}C$ and protons attached to $^{15}N/^{13}C$, thereby editing out all the intramolecular NOEs. A total of 1359 experimental distance restraints (~ 14 restraints per residue for cNTnC) including 1169 intramolecular cNTnC distance restraints, 24 intramolecular cTnI$_{147-163}$ distance restraints, 2 intramolecular bepridil distance restraints, 30 intermolecular contacts between cNTnC and cTnI$_{147-163}$, 28 intermolecular contacts between cNTnC and bepridil, 88 dihedral restraints for cNTnC, 6 dihedral restraints for cTnI$_{147-163}$, and 6 distance restraints to Ca^{2+} were used to calculate the high resolution structure of the ternary cNTnC•Ca^{2+}•cTnI$_{147-163}$•bepridil complex (see Table III-2). Figure III-4a depicts the ensemble of 30 lowest energy structures of the ternary complex in stereo view, with overall structural statistics and conformational energies for the ensemble provided in Table III-2. The ribbon representations of the structure of the ternary complex are shown in Figure III-4b. The structures of cNTnC in the complex are of higher quality than those of cTnI$_{147-163}$ or bepridil, as a result of more restraints for the protein than for the ligands. A close view of the skeleton representations of cTnI$_{147-163}$ and bepridil are shown in Figure III-4c. Figure III-4d shows the ensemble of the bound bepridil molecules in a different orientation from Figure III-4a in order to show that the two aromatic rings of bepridil are better defined than the rest of the molecule.

Structure of cNTnC in the ternary complex

cNTnC in the present structure exhibits an overall fold resembling other Ca^{2+}-bound domains in the EF-hand family, such as the N-domain of sTnC. The secondary structural elements of cNTnC in the ternary cNTnC•Ca^{2+}•cTnI$_{147-163}$•bepridil complex are similar to

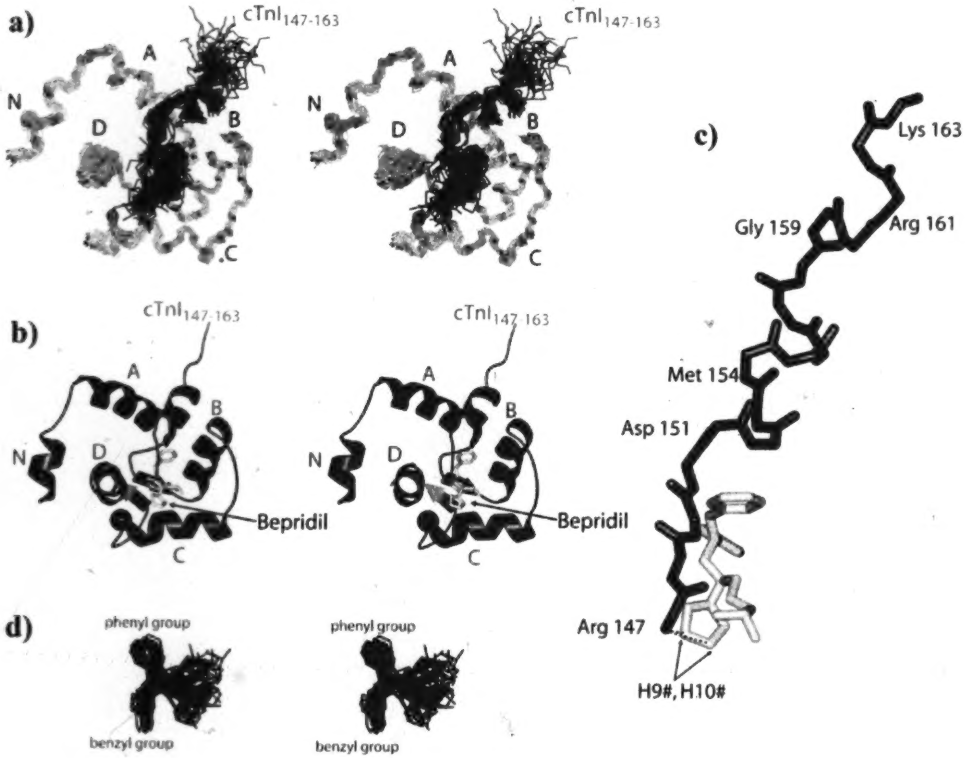
a)
cTnI147-163
cTnI147-163
A
N
D
B
C
b)
cTnI147-163
cTnI147-163
A
B
N
D
C
Bepridil
Bepridil
c)
Lys 163
Gly 159
Arg 161
Met 154
Asp 151
Arg 147
H9#, H10#
d)
phenyl group
phenyl group
benzyl group
benzyl group

Figure III-4. a) The solution structure of the cNTnC•Ca^{2+}•cTnI$_{147-163}$•bepridil complex in stereo view. The backbones (N, Cα, C') of a family of 30 structures are shown in gray. The assembly of the cTnI$_{147-163}$ structures is shown in red. The assembly of bepridil is shown in blue. The Ca^{2+} ions are shown as green spheres. b) The ribbon representation of the ternary complex in stereo view. The protein is shown in green and Ca^{2+} ions are shown as black spheres. Heavy atom skeleton of bepridil is shown in gold. The cTnI$_{147-163}$ peptide is shown in purple. c) A close view of the skeleton representation of the cTnI$_{147-163}$ peptide backbone and bepridil. The bonds of the peptide backbone are colored according to atom, *i.e.*, nitrogen is blue, carbon is gray, and oxygen is red. Bepridil bonds are colored gold. Selective labeling of six residues indicates the orientation of the peptide. d) A closer view of the bepridil heavy atom skeleton assembly. The aromatic rings are better defined than other parts of the molecule in the ensemble. The molecule is shown in a different viewing perspective compared to a).

those in the cNTnC•Ca^{2+}•cTnI$_{147-163}$ complex (*8*) and the cNTnC•Ca^{2+}•bepridil complex (*5*). The five helices, N, A, B, C, and D, are well-defined, superimposing with individual backbone RMSDs of 0.17±0.04Å for helix N (residues 5-11), 0.35±0.07 Å for helix A (residues 14-27), 0.23±0.05Å for helix B (residues 38-47), 0.22±0.03Å for helix C (residues 58-68), and 0.26±0.05Å for helix D (residues 74-83). The two EF hands Ca^{2+}-binding sites are joined by a short antiparallel β-sheet. The β-sheet (residues 35-37, 71-73) is well-defined with a backbone RMSD of 0.22±0.04Å, while the Ca^{2+}-binding sites have a slightly more flexible structure (a backbone RMSD of 0.41±0.08Å). The N- and C-terminal residues (residues 1-4 and 86-89) are less well defined than the helices or the β-sheet.

The global fold of cNTnC in the ternary cNTnC•Ca^{2+}•cTnI$_{147-163}$•bepridil complex is similar to the open cNTnC•Ca^{2+}•cTnI$_{147-163}$ structure as determined by NMR spectroscopy (*8*) and the cNTnC•Ca^{2+}•bepridil structure as determined by X-ray crystallography (*5*). The orientations of the five helices are similar to those in the two binary complexes, cNTnC•Ca^{2+}•cTnI$_{147-163}$ and cNTnC•Ca^{2+}•bepridil complex. The A/B and C/D interhelical angles are 118° ± 3° and 90° ± 3°, respectively, representing nearly perpendicular orientations for the A/B and C/D helix pairs, characteristic of an open conformation for an EF hand domain. However, interhelical angle analysis (see Table III-3) indicates that although cNTnC in the ternary complex is open as compared to the closed cNTnC•apo (exhibiting A/B and C/D interhelical angles of 136° ± 3° and 129° ± 5°, respectively) or cNTnC•Ca^{2+} (exhibiting A/B and C/D interhelical angles of 132° ± 3° and 117° ± 3°, respectively), it is slightly more closed than cNTnC•Ca^{2+}•cTnI$_{147-163}$ (exhibiting A/B and C/D interhelical angles of 102° ± 5° and 96° ± 5°, respectively) or cNTnC•Ca^{2+}•bepridil (exhibiting A/B and C/D interhelical angles of 92° and 89°, respectively). Thus, although either cTnI$_{147-163}$ or bepridil alone can induce and stabilize the open conformation of cNTnC•Ca^{2+}, the hindrance between the two resulted in a less stable open conformation for cNTnC•Ca^{2+}. This hindrance is evident in the ternary structure as discussed below and it explains the observed negative cooperativity between the two ligands.

Structure of bepridil in the ternary complex

The chemical formula and chemical shift assignments of bepridil are shown in Figure III-5a and the NOESY NMR spectra for assigning cTnI$_{147-163}$ or bepridil are shown in Figure III-5b. Bepridil consists of three main organic groups, the phenyl, the benzyl, and the pyrrolidine groups, in addition to the isopropyl ether moiety. The bepridil in the present ternary structure has a similar conformation and shares a similar binding site on cNTnC as the bepridil in the X-ray structure of cNTnC•Ca^{2+}•bepridil complex (*5*). The relative orientations of the four bepridil groups are mainly determined by the intermolecular NOEs between cNTnC and the drug since very few intramolecular NOEs for bepridil were obtained. Strip plots taken from the 3D $^{15}N/^{13}C$ F_1-filtered, F_3-edited spectrum of cNTnC•Ca^{2+}•cTnI$_{147-163}$•bepridil complex are shown in Figure III-6. In this spectrum, only NOEs arising from the ^{12}C-attached protons in the cTnI$_{147-163}$ and bepridil and terminating on ^{13}C-attached protons in cNTnC are observed. The two aromatic rings of the bepridil made significant hydrophobic contact to the protein. In particular, the benzyl ring made hydrophobic contacts with the methyl groups on residues of the B-helix (residues Leu 41, Val 44, Met 45, and Leu 48) and the phenyl ring made contacts to

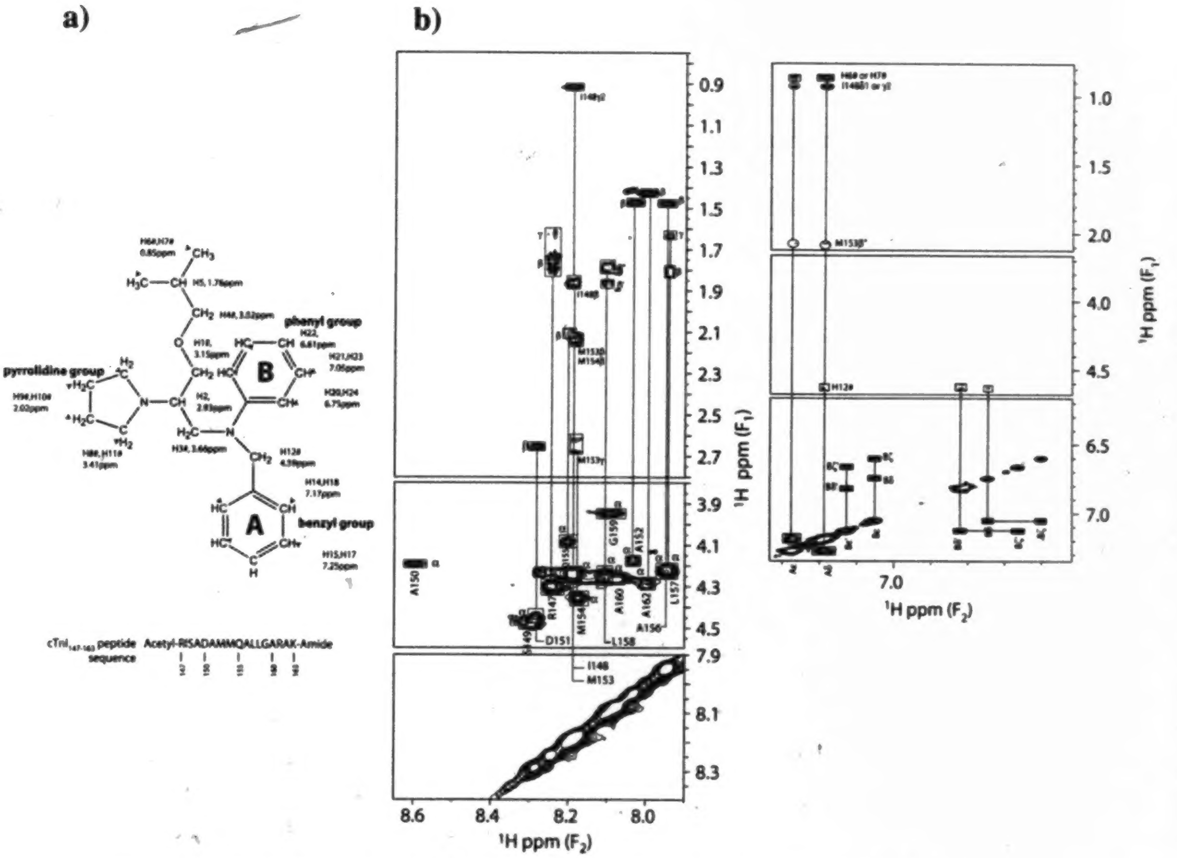

Figure III-5. a) The chemical structure of bepridil and the sequence of cTnI$_{147-163}$. The major functional groups (*i.e.* the phenyl ring, the benzyl group and the pyrrolidine group) are labeled. The number designation and the chemical shift assignments of most protons of the drug are indicated. The "A" and "B" designation of aromatic rings are used in panel b). b) Strips from the 2D-$^{15}N/^{13}C$-filtered-NOESY NMR experiments showing the intramolecular NOE contacts of the cTnI$_{147-163}$ and bepridil, as well as intermolecular contacts between bepridil and the peptide. The amide region of the spectrum is consisted of mainly intramolecular peptide contacts, where as the aromatic region is dominated by intramolecular contacts in bepridil. Notice that the phenyl ring of bepridil actually produces two spin systems in the spectrum. Peaks representing intraresidue contacts are highlighted in boxes whereas peaks representing interresidue contacts are highlighted in circles.

residues of the C-helix (methyl groups of Met 60 and Ile 61) as well as the residues composing the Ca^{2+}-binding loops (methyl groups of Ile 36, Val 64, and Val 72). As a result, the two aromatic rings of bepridil are inserted as a "wedge" between the A/D and B/C units, sterically hindering the closing of cNTnC. The pyrrolidine ring and the isopropyl moieties made little contacts to the protein. The only NOEs observed between the pyrrolidine ring and the protein is between H8# and H11# protons of bepridil (see Figure III-5a) and the methyl Hε# group of Ile 60 in the C-helix of cNTnC. Similarly, only weak NOEs between side chains of Ser 84 in the end of the D-helix of cNTnC and the two methyls of the isopropyl group on bepridil were observed. Due to a lack of unambiguous NOE correlations involving the pyrrolidine ring and the isopropyl group with the protein, those two parts of bepridil are not as well defined as the aromatic rings in the ternary structure (Figure III-4). When the heavy atoms of bepridil superimpose onto the average structure in the ternary complex, the average RMSDs for the benzyl and phenyl groups are 0.9 ± 0.2 Å, while that for the pyrrolidine ring and the isopropyl group is 3 ± 1 Å. Interestingly, we also identified a NOE between the H9# and H10# (degenerate) protons in the pyrrolidine ring of bepridil and the N-terminus residue Arg 147 of cTnI$_{147-163}$ (illustrated in Figure III-4c). Since Arg 147 is positively charged and the nitrogen in the pyrrolidine ring is partially positively charged at neutral pH, the two moieties repel each other to create a hindrance effect. As a result, the two ligands reorient their positions slightly relative to those in the binary cNTnC•Ca^{2+}•cTnI$_{147-163}$ or the cNTnC•Ca^{2+}•bepridil complex to accommodate each other in the hydrophobic pocket of cNTnC•Ca^{2+} (see below).

Structure of cTnI$_{147-163}$ in the ternary complex

In the structure of the cNTnC•Ca^{2+}•cTnI$_{147-163}$ binary complex published previously, there were no intramolecular NOE restraints observed and the secondary structure was solely based on the chemical shift index (*8*). In the present structure, 24 intramolecular NOEs including 3 d_{NN} and 6 $d_{\alpha N}(i,i+3)$ (the hallmark of a helical structure) restraints for the 17 residue cTnI$_{147-163}$ peptide were assigned. As a result, the peptide is slightly better defined in the present structure. In the ensemble of solution structures (Figure III-4a), the backbone atoms of the 17 residues superimpose on to the average peptide structure with a RMSD of 1.5 Å as compared to that of 2.0 Å in the cNTnC•Ca^{2+}•cTnI$_{147-163}$ binary complex. However, if only the α-helical region (residues 150-156) is compared, the backbone RMSDs are almost identical for the two structures. This is because that the helical structure is mainly determined by ϕ and ψ dihedral restraints. The orientation of the cTnI$_{147-163}$ peptide in the ternary complex was determined using the same approach as for cNTnC•Ca^{2+}•cTnI$_{147-163}$ (*8*). NOEs between peptide methyl groups with degenerate chemical shifts and cNTnC were unambiguously assigned by using a specifically deuterated cTnI$_{147-163}$ peptide, containing deuterated methyl groups at Ala 150, Met 154, Leu 158, and Ala 162 located on one side of the helical peptide. The assigned intermolecular NOEs between cNTnC and cTnI$_{147-163}$ are summarized in Figure III-6. These NOE contacts dictate a similar orientation for the cTnI$_{147-163}$ in the ternary cNTnC•Ca^{2+}•cTnI$_{147-163}$•bepridil complex as compared to that in the binary cNTnC•Ca^{2+}•cTnI$_{147-163}$ complex. The peptide inserts between the A and B helices in cNTnC with the N-terminus (residues 147-149) and the helical region interacts with the protein, while the C-terminus does not interact with the protein and remains disordered in

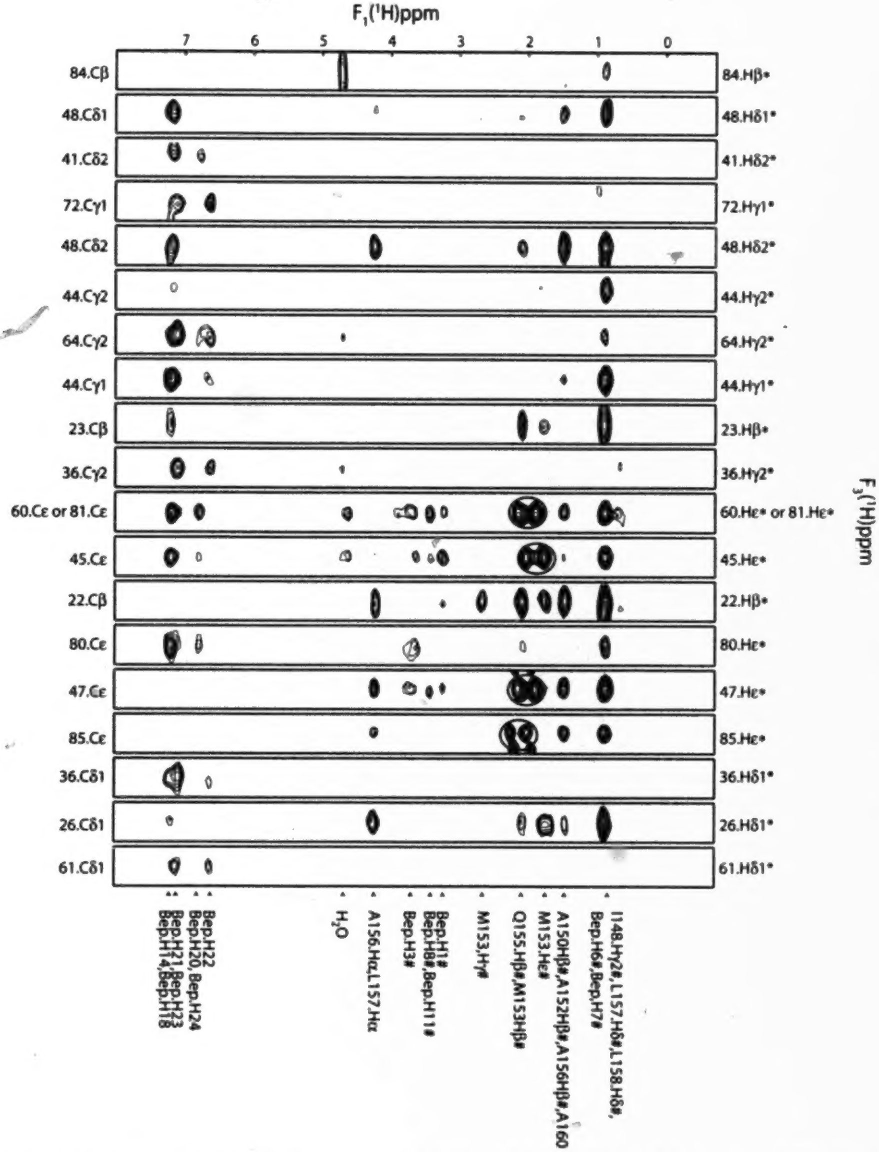

Figure III-6. NOE contacts between cNTnC and bepridil, and between cNTnC and the cTnI$_{147-163}$ peptide. Strip plots from ^{13}C portion of the 3D-^{15}N/^{13}C-filtered/edited-NOESY NMR experiments illustrating the NOEs between cNTnC and the two ligands. The carbon dimension is shown on the left. The cNTnC proton to which the strip corresponds to is labeled on the right. The proton chemical shifts of the drug and peptide are indicated at the bottom. The circled peaks are artifacts in the spectrum.

the ensemble of the solution structures (Figure III-4a). Specifically, the helical portion of the peptide (residues 150-156) sits between the A-B helical interface, contacting the methyl group of residues Ala 22 and Ala 23 in the A-helix and Val 44, Met 45, Met 47 and Leu 48 in the B-helix. The N-terminus of the peptide extends into the hydrophobic pocket of cNTnC, making contacts to the methyl groups of Met 60, Met 80 and Met 85 in cNTnC. As discussed above, the N-terminal residue Arg 147 of the peptide contacts protons attached to C9 and C10 of the pyrrolidine ring of bepridil (Figures III-4c and 5). Thus, in the presence of bepridil, the cTnI$_{147-163}$ peptide retained its basic secondary structure and orientation as adopted in the cNTnC•Ca^{2+}•cTnI$_{147-163}$ binary complex, however, its position in the A/B helical interface is shifted to accommodate the drug molecule (see below).

Comparison of the ternary cNTnC•Ca^{2+}•cTnI$_{147-163}$•bepridil structure with the binary cNTnC•Ca^{2+}•cTnI$_{147-163}$ and cNTnC•Ca^{2+}•bepridil structures

The conformational change in cNTnC•Ca^{2+} that occurs upon binding cTnI$_{147-163}$ (*8*) or bepridil (*5*) involves the straightening of the B-helix and the BC unit moving away from the NAD unit, consisting of a 'closed' to 'open' structural transition. This peptide or drug induced structural change in cNTnC•Ca^{2+} is similar to that observed for the apo to Ca^{2+}-saturated transition observed for sNTnC (*31*). A somewhat surprising finding from the current study is that despite the simultaneous presence of the two ligands that are capable of inducing the opening of cNTnC•Ca^{2+}, cNTnC•Ca^{2+} is, in fact, more closed than if either one of the ligands was complexed to cNTnC•Ca^{2+} alone. This is demonstrated in Figure III-7. When the NAD unit of cNTnC in cNTnC•Ca^{2+}•cTnI$_{147-}$

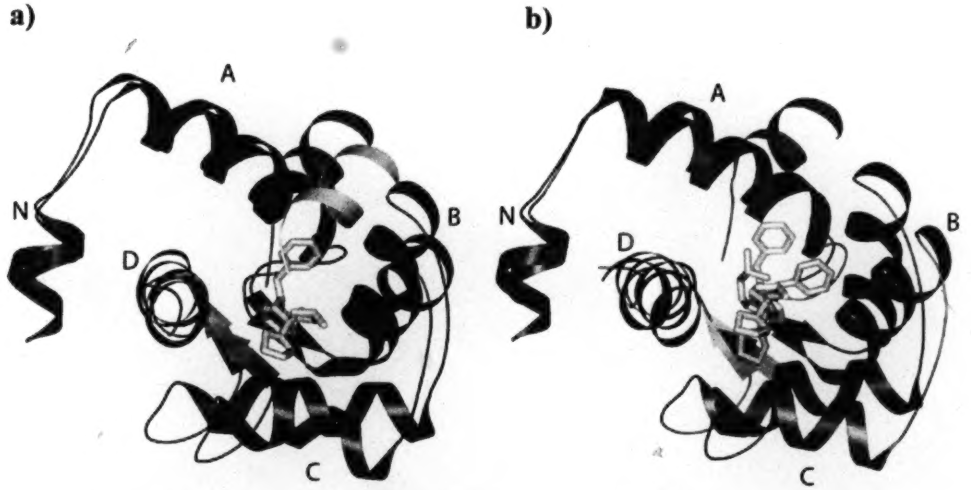

Figure III-7. a) Backbone overlay of cNTnC in the cNTnC•Ca^{2+}•cTnI$_{147-163}$•bepridil complex (green) and cNTnC in the cNTnC•Ca^{2+}•cTnI$_{147-163}$ complex (purple), PDB accession code 1MXL. Note the position shift of the peptide from gray to blue. b) Backbone overlay of cNTnC in the cNTnC•Ca^{2+}•cTnI$_{147-163}$•bepridil complex (green) and cNTnC in the cNTnC•Ca^{2+}•bepridil complex (red), PDB accession code 1DTL. Note the position shift of the bepridil molecule from pink to yellow.

$_{163}$•bepridil superimposes onto the NAD unit of cNTnC in cNTnC•Ca^{2+}•cTnI$_{147-163}$, the BC unit moved up 3.9±0.7 Å (Figure III-7a). This change is also reflected in the A/B and C/D interhelical angle changes (see above and Table III-3). This is a result of altered NOE contacts between cNTnC and cTnI$_{147-163}$ from cNTnC•Ca^{2+}•cTnI$_{147-163}$ to cNTnC•Ca^{2+}•cTnI$_{147-163}$•bepridil. For instance, in cNTnC•Ca^{2+}•cTnI$_{147-163}$, Ala 23 but not Ala 22 on the A-helix of cNTnC makes strong contact to Leu 157 of cTnI$_{147-163}$ peptide, while both Ala 22 and Ala 23 make strong contacts to Leu 157 in cNTnC•Ca^{2+}•cTnI$_{147-163}$•bepridil. The cTnI$_{147-163}$ peptide also moved up 4±1 Å toward the A-helix. The bulky side chain of Leu 158 on the cTnI$_{147-163}$ peptide is pushed away toward outside from its original position in the cNTnC•Ca^{2+}•cTnI$_{147-163}$ binary structure, and adopts a relatively more flexible conformation, free from any contacts with cNTnC. The overall effect is that the N-terminal of the peptide is shifted slightly away from the hydrophobic pocket of cNTnC, likely due to both the steric hindrance with bepridil and repelling force between the N-terminus of the peptide and the pyrrolidine group of bepridil. Similarly, when the NAD unit of cNTnC in cNTnC•Ca^{2+}•cTnI$_{147-163}$•bepridil superimpose onto the NAD unit of cNTnC in cNTnC•Ca^{2+}•bepridil, the BC unit moved up 6 ± 1 Å (Figure III-7b). This change is also reflected in the A/B and C/D interhelical angle changes (see above and Table III-3). In the present structure, the strong contacts between the hydrophobic residues in cNTnC and the two aromatic rings of bepridil serve as the primary anchoring site for this molecule in the hydrophobic core of the protein. The pyrrolidine and isopropyl groups protrude toward the outside. This is similar to the binding of bepridil in the X-ray structure of cNTnC•Ca^{2+}•bepridil. It appears that the bepridil molecule reorients itself in order to accommodate cTnI$_{147-163}$ and minimize both the steric hindrance with the peptide and the repelling force between the N-terminus of the peptide and the pyrrolidine group of bepridil. As a result, the phenyl ring of bepridil in the ternary structure has a similar conformation and binding site as that of bepridil in the cTnC•Ca^{2+}•bepridil structure, but the aromatic ring of the benzyl group has shifted (4.7±0.7Å) its position closer to the A-helix of cNTnC, which pulls the A-helix down to accommodate cTnI$_{147-163}$ and resulted in a more closed structure for cNTnC. The isopropyl group has also showed a small movement, but this movement is not well defined due to a lack of unambiguous NOEs involving the isopropyl group.

In summary, the clashing between the cTnI$_{147-163}$ peptide and bepridil in the cNTnC•Ca^{2+}•cTnI$_{147-163}$•bepridil ternary complex makes the two ligands reorient their positions relative to those in the cNTnC•Ca^{2+}•cTnI$_{147-163}$ or cNTnC•Ca^{2+}•bepridil complexes. The consequence is a reduced degree of 'openness' for cNTnC in the ternary complex than in the binary complexes. This clashing helps to explain the apparent weaker binding of bepridil to the cTnC regulatory domain in the cTnC-cTnI complex than in cTnC alone (*29*) and the observed negative cooperativity between cTnI$_{147-163}$ and bepridil in this work. This may in part explain the poor pharmacological effects of bepridil in heart failure (*32*).

Table III-3. Interhelical angles of various EF hands.

Calcium Binding Protein	Interhelical angles(°)[a] A-B	C-D	Accession Code (PDB)
cNTnC·apo (NMR)	136±3	129±5	1SPY
cNTnC·Ca^{2+} (NMR)	132±3	117±3	1AP4
cNTnC·Ca^{2+}·cTnI$_{147-163}$ (NMR)	102±5	96±5	1MXL
cTnC·3Ca^{2+}·bepridil (X-RAY)	92	89	1DTL
cNTnC·3Ca^{2+}·bepridil·cTnI$_{147-163}$ (NMR)	118±3	90±3	1LXF

[a] A large angle defines a "closed" conformation, whereas a small angle defines an "open" conformation. The axis for an α-helix is defined by two points, taken as the average coordinates of the first and last 11 backbone atoms of the α-helix.

Bepridil's Ca^{2+}-sensitizing activity

Based on results from this and other studies (*3*), bepridil should lead to Ca^{2+}-desensitization in myofibrils, but it has been shown to have weak but definite Ca^{2+}-sensitizing effect on cardiac myofibrils (Figure III-1) (*1*). One way to reconcile the contradiction is by considering the possibility of multiple myofibril targets for bepridil. Bepridil is known to interact with so many proteins that it won't be a surprise if the drug is capable of interacting with other targets on the myofibril. In particular, the fact that the regulatory light chain on the thick filament is structurally similar to cTnC means it could well be an alternative binding site for bepridil. Solaro et al. also showed that bepridil enhanced the Ca^{2+} affinity of cTnC (*1*). Therefore, it is plausible that the enhancement in Ca^{2+} affinity helped to compensate the bepridil-induced reduction in cTnI's cTnC affinity, producing weak Ca^{2+}-sensitization in myofibrils.

Conclusion

Despite many medical advances, heart disease remains the leading cause of death in Western society. The role of myofilament contractile proteins in heart disease is just beginning to be recognized. Many identified cardiac dysfunctions are associated with the changes in the myofilament response to Ca^{2+} as well as altered myofilament structures (for reviews, see (*33-35*)). Studies on the structure and function of myofilament proteins have contributed a great deal to the understanding of the molecular mechanism of cardiac muscle contraction as the information has been exploited to develop possible therapeutic intervention and diagnostics. For example, the release of cTnI from the heart is now used clinically as a key indicator of myocardial ischemia (*36*). Ischemia and other cardiovascular conditions are also associated with changes in cTnI phosphorylation state (*37*). Work in transgenic animals has shown that removal of 17 amino acids at the C-terminus of cTnI is sufficient to produce myocardial stunning (*38*). Moreover, multiple mutations on the myofilament proteins have been associated with familial hypertrophic cardiomyopathy, one of the most frequently occurring hereditary cardiac disorders, affecting up to 1 in 500 of the population (*34*).

Targeting the myofilaments for designing new drugs remains an important objective in the development of experimental tools and inotropic agents. As the Ca^{2+}-binding component in the myofilament of cardiac muscle, cTnC is an attractive target for the design of cardiotonic drugs, which may be used to modulate the altered Ca^{2+}-response of the myofilaments in diseased heart. For example, a group of so-called Ca^{2+}-sensitizers has been developed. These drugs have been shown to increase the myocardial contractility by generating more force for a given amount of cytosolic free Ca^{2+} (for reviews, see (*39-41*)). In fact, we have shown that a Ca^{2+}-sensitizer, EMD 57033, interacts with the C-domain of cTnC without interfering with the interaction between cTnC and the inhibitory region of cTnI (*26, 42*). It is important to put the results of this study into perspective with respect to the design of Ca^{2+}-sensitizers. In Figure III-8, we summarized the effects of Ca^{2+}, cTnI$_{147-163}$, and bepridil on cNTnC. Ca^{2+} binding to cNTnC induces little

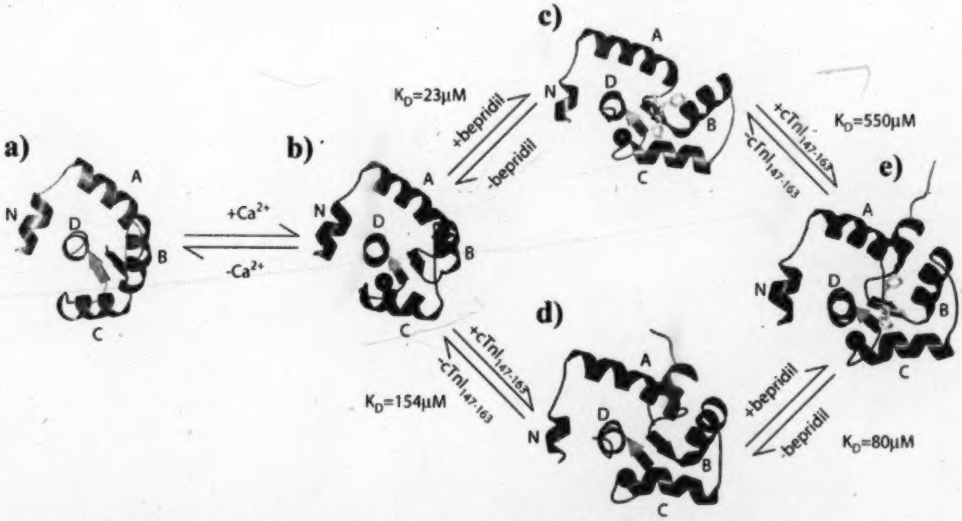
c)
A
K$_D$=23μM
+bepridil
-bepridil
N
D
B
C
+cTnI$_{147-163}$
-cTnI$_{147-163}$
K$_D$=550μM
a)
b)
e)
A
N
D
B
C
+Ca^{2+}
-Ca^{2+}
A
N
D
B
C
A
N
D
B
C
d)
+cTnI$_{147-163}$
-cTnI$_{147-163}$
K$_D$=154μM
A
N
D
B
C
+bepridil
-bepridil
K$_D$=80μM

Figure III-8. An overview of the effects of bepridil and the cTnI$_{147-163}$ peptide on cNTnC. a) The cNTnC•apo, b) cNTnC•Ca^{2+}, c) cNTnC•Ca^{2+}•bepridil, d) cNTnC•Ca^{2+}•cTnI$_{147-163}$, and e) cNTnC•Ca^{2+}•cTnI$_{147-163}$•bepridil. For the corresponding equilibria, the dissociation constants (K$_D$s) are also shown.

structural change but sets the stage for cTnI$_{147-163}$ binding (A to B). A large 'closed' to 'open' conformational transition occurs in cNTnC•Ca^{2+} upon binding cTnI$_{147-163}$ (B to D) or bepridil (B to C). In spite of the simultaneous presence of the two ligands that are capable of inducing the opening of cNTnC•Ca^{2+}, the domain is, in fact, more closed than if either one of the ligands was complexed to cNTnC•Ca^{2+} alone. This is the result of the negative cooperativity and the clashing between the two ligands, as discussed earlier. Ideally, a Ca^{2+}-sensitizer would increase the Ca^{2+}-binding affinity of cTnC and enhance the cTnC-cTnI interaction, corresponding to driving the equilibrium to the right (Figure III-8, from A to B to C/D to E). Clearly, bepridil itself is not an ideal Ca^{2+}-sensitizer since it decreases the binding affinity of cTnI$_{147-163}$ for cNTnC•Ca^{2+}. To avoid such an inhibitory effect, neutral agents resembling bepridil could be designed to enhance the cTnC-cTnI interactions. On the other hand, bepridil itself or agents resembling bepridil could be used as a Ca^{2+}-desensitizer. These agents would be beneficial for the treatment of many cardiac dysfunctions associated with increased Ca^{2+}-sensitivity and increased contractility as well as impairment of diastolic relaxation, such as in certain cases of familial hypertrophic cardiomyopathy (*35*). Thus, although bepridil by itself is not a good pharmacological agent for heart failure (*32*), the current high resolution NMR solution structure of the cNTnC•Ca^{2+}•cTnI$_{147-163}$•bepridil ternary complex provides a structural basis into the features that may be important for the design of cTnC-specific cardiotonic drugs.

References

1. Solaro, R. J., Bousquet, P., and Johnson, J. D. (1986) *J Pharmacol Exp Ther 238*, 502-7.
2. Solaro, R. J., Bousquet, P., and Johnson, J. D. (1986) *J. Pharmacol. Exp. Ther. 238*, 502-507.
3. Abusamhadneh, E., Abbott, M. B., Dvoretsky, A., Finley, N., Sasi, S., and Rosevear, P. R. (2001) *FEBS Lett 506*, 51-4.
4. Kleerekoper, Q., Liu, W., Choi, D., and Putkey, J. A. (1998) *Journal of Biological Chemistry 273*, 8153-60.
5. Li, Y., Love, M. L., Putkey, J. A., and Cohen, C. (2000) *Proc. Natl. Acad. Sci. U. S. A. 97*, 5140-5.
6. Chandra, M., Dong, W. J., Pan, B. S., Cheung, H. C., and Solaro, R. J. (1997) *Biochemistry 36*, 13305-13311.
7. Li, M. X., Gagné, S. M., Spyracopoulos, L., Kloks, C. P. A. M., Audette, G., Chandra, M., Solaro, R. J., Smillie, L. B., and Sykes, B. D. (1997) *Biochemistry*, 12519-12525.
8. Li, M. X., Spyracopoulos, L., and Sykes, B. D. (1999) *Biochemistry 38*, 8289-98.
9. Kay, L. E., Keifer, P., and Saarinen, T. (1992) *J. Am. Chem. Soc. 114*, 10663-10665.
10. Zhang, O., Kay, L. E., Olivier, J. P., and Forman-Kay, J. D. (1994) *J. Biomol. NMR 4*, 845-858.
11. Ogura, K., Terasawa, H., and Inagaki, F. (1996) *J. Biomol. NMR 8*, 492-498.
12. Zwahlen, C., Legault, P., Vincent, S. J. F., Greenblatt, J., Konrat, R., and Kay, L. E. (1997) *J. Am. Chem. Soc. 119*, 6711-6721.
13. Delaglio, F., Grzesiek, S., Vuister, G. W., Zhu, G., Pfeifer, J., and Bax, A. (1995) *J. Biomol. NMR 6*, 277-293.
14. Johnson, B. A., and Blevins, R. A. (1994) *J. Biomol. NMR 4*, 603-614.
15. Gagné, S. M., Li, M. X., and Sykes, B. D. (1997) *Biochemistry 36*, 4386-4392.
16. Sia, S. K., Li, M. X., Spyracopoulos, L., Gagné, S. M., Liu, W., Putkey, J. A., and Sykes, B. D. (1997) *J. Biol. Chem. 272*, 18216-18221.
17. Wishart, D. S., and Sykes, B. D. (1994) *Methods in Enzymology 239*, 363-392.
18. Brünger, A. T. (1992) *X-PLOR Version 3.1 A system for X-ray Crystallography and NMR*, Yale University Press, New Haven.
19. Kuboniwa, H., Grzesiek, S., Delaglio, F., and Bax, A. (1994) *J. Biomol. NMR 4*, 871-8.
20. Archer, S. J., Ikura, N. I., Torchia, D. A., and Bax, A. (1991) *J. Magn. Reson. 95*, 636-641.
21. Muhandiram, D. R., and Kay, L. E. (1994) *J. Magn. Reson. B103*, 203-216.
22. Kay, L. E., Xu, G. Y., Singer, A. U., Muhandiram, D. R., and Forman-Kay, J. D. (1993) *J. Magn. Reson. B101*, 333-337.
23. Pascal, S. M., Muhandiram, D. R., Yamazaki, T., Forman-Kay, J. D., and Kay, L. E. (1994) *J. Magn. Reson. B103*, 197-201.
24. Laskowski, R. A., MacArthur, M. W., Moss, D. S., and Thorton, J. M. (1993) *J. Appl. Crystallogr. 26*, 283-290.

25. Spyracopoulos, L., Li, M. X., Sia, S. K., Gagné, S. M., Chandra, M., Solaro, R. J., and Sykes, B. D. (1997) *Biochemistry 36*, 12138-12146.
26. Li, M. X., Spyracopoulos, L., Beier, N., Putkey, J. A., and Sykes, B. D. (2000) *Biochemistry 39*, 8782-90.
27. MacLachlan, L. K., Reid, D. G., Mitchell, R. C., Salter, C. J., and Smith, S. J. (1990) *J Biol Chem 265*, 9764-70.
28. Kischel, P., Bastide, B., Potter, J. D., and Mounier, Y. (2000) *Br J Pharmacol 131*, 1496-502.
29. Abusamhadneh, E., Abbott, M. B., Dvoretsky, A., Finley, N., Sasi, S., and Rosevear, P. R. (2001) *FEBS. Lett. 506*, 51-54.
30. Itoh, H., Ishikawa, T., and Hidaka, H. (1984) *J. Pharmacol. Exp. Ther. 230*, 737-41.
31. Gagné, S. M., Tsuda, S., Li, M. X., Smillie, L. B., and Sykes, B. D. (1995) *Nat. Struct. Biol. 2*, 784-789.
32. Gill, A., Flaim, S. F., Damiano, B. P., Sit, S. P., and Brannan, M. D. (1992) *Am. J. Cardiol. 69*, 11D-16D.
33. Solaro, R. J., and Rarick, H. M. (1998) *Circ. Res. 83*, 471-80.
34. Redwood, C. S., Moolman-Smook, J. C., and Watkins, H. (1999) *Cardiovasc. Res. 44*, 20-36.
35. Hernandez, O. M., Housmans, P. R., and Potter, J. D. (2001) *J. Appl. Physiol. 90*, 1125-1136.
36. Chapelle, J. P. (1999) *Clin. Chem. Lab. Med. 37*, 11-20.
37. Zakhary, D. R., Moravec, C. S., Stewart, R. W., and Bond, M. (1999) *Circulation 99*, 505-510.
38. Murphy, A. M., Kogler, H., Georgakopoulos, D., McDonough, J. L., Kass, D. A., Van Eyk, J. E., and Marban, E. (2000) *Science 287*, 488-491.
39. Endoh, M. (1995) *Gen. Pharmacol. 26*, 1-31.
40. Varro, A., and Papp, J. G. (1995) *J. Cardiovasc. Pharmacol. 26*, S32-44.
41. Nielsen-Kudsk, J. E., and Aldershvile, J. (1995) *J. Cardiovasc. Pharmacol. 26*, S77-84.
42. Wang, X., Li, M. X., Spyracopoulos, L., Beier, N., Chandra, M., Solaro, R. J., and Sykes, B. D. (2001) *J. Biol. Chem. 276*, 25456-25466.

Chapter IV

Effects of S41/ S43, S149 Phosphorylations and R161W Mutation on cTnI-cTnC Interactions[†]

Introduction

Phosphorylation of cTnI by kinases involved in intracellular signaling pathways has been increasingly recognized as a vital part of myofilament activity modulation(for a review, see (*3*)). So far, six phosphorylation sites have been identified. Two serine residues in the N-terminal extension of cTnI, S22 and S23, are identified as substrates for protein kinase A (PKA) while residues S41, S43 and T142 are targets for protein kinase C (PKC) (Figure IV-1). The effect of cTnI phosphorylation by these kinases is primarily a downward modulation of cardiac contractility, either by decreased acto-myosin ATPase activity, which is mediated by PKC, or by enhanced Ca^{2+} dissociation from cTnC and reduced myofilament Ca^{2+} sensitivity, mediated by PKA. Recently, a study has shown that p21-activated kinase (PAK) increases the Ca^{2+}-sensitivity of triton-skinned cardiac muscle fiber bundles via a mechanism potentially involving the phosphorylation of cTnI at S149 (*4*) (Figure IV-1), representing a novel cTnI phosphorylation site in addition to the PKA and PKC sites.

Mutations in cTnI also occupy a prominent role in cardiology. cTnI mutations have been implicated in various cardiac diseases, including familial hypertrophic cardiomyopathy (FHC), one of the most frequently occurring hereditary cardiac disorders associated with mutations in contractile protein genes (for reviews, see (*5, 6*)). To date,

---

[†] The results from this chapter are taken in part from Li, M. X., Wang, X., Lindhout, D. A., Buscemi, N., Van Eyk, J. E. and Sykes, B. D. *Biochemistry*, 42(49):14460-8, 2003.

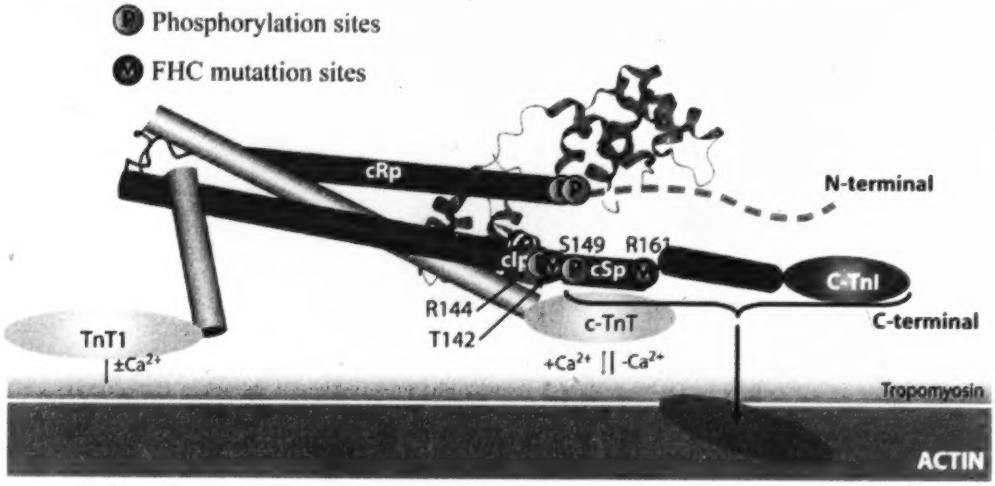

Figure IV-1. A schematic representation of the interaction of cTnC with the cRp, cIp, and cSp regions of cTnI. The phosphorylation sites and mutation site investigated in this study are indicated.

six FHC mutations [R144G, R144Q, R161W, S198N, G202S, and K207Q][‡] on cTnI have been reported along with mutations causing the deletion of one codon (K182) and a deletion of Exon8 (Δexon8) (*6*). Among those, R144G and R144Q are located in the key inhibitory region and R161W is located in the important switch region of cTnI (Figure IV-1). A truncation of cTnI has been associated with myocardial stunning (*7, 8*) and measuring the serum level of cTnI has become the standard of care in the diagnosis of myocardial injury (*9-12*).

In order to understand how alterations in cTnI are involved in disease, it is important to elucidate the effects of cTnI modifications on its interaction with cTnC. Although many functional and animal model experiments have revealed the functional differences between native and modified cTnI that may underline the pathogenesis of cardiac disease

---

[‡] S41, S43, T142, R144, S149, and R161 in recombinant human cTnI correspond to S42, S44, T143, R145, S150, and R162, respectively, in the wild-type protein, which has an extra N-terminal Met residue. In this article, the sequence numbering of cTnI follows that of recombinant cTnI.

(*8*, *13-18*), there is little data available concerning the structural consequences of cTnI modification with regard to the interaction of cTnI with cTnC or cTnI with actin-tropomyosin, especially on the combined effects of FHC mutation with phosphorylation of cTnI. In this study, we have utilized 2D {^{1}H, ^{15}N}-HSQC NMR spectroscopy to elucidate the binding of two segments (cRp, and cSp) of cTnI in native, S41/S43 phosphorylated, S149 phosphorylated, and R161W mutated states to cTnC. While S41/S43 phosphorylation of cRp had minimal disruption in the interaction of cRp and cTnC•3Ca^{2+}, the affinity of cSp for cNTnC•Ca^{2+} was reduced by the modifications in all cases. An important and novel finding of this work was that the FHC mutation R161W suppresses the effect of S149 phosphorylation on the interaction of cSp and cNTnC•Ca^{2+}, demonstrating linkages between FHC mutation and phosphorylation of cTnI. The observed alterations corroborate well with the structural data. These results suggest that while the modifications in the cRp region have minimal influence, those in the key functional cTnI region, in this case cSp, have a pronounced effect on the interaction of cTnI and cTnC, which may correlate with the altered myofilament function and cardiac muscle contraction under pathophysiological conditions.

Experimental Procedures

Protein Sample Preparation. In this work, recombinant human cTnC(1-161) and cNTnC(1-89) with the mutations C35S and C84S were used. The engineering of the expression vector of cTnC(C35S/C84S) and cNTnC(C35S/C84S) was as described elsewhere (*19, 20*). For the purpose of clarity, (C35S/C84S) is omitted in the following sections. Protocols for transformation, expression in BL21(DE3)pLysS cells and purification of ^{15}N-cNTnC were as described in Chapter III. The protocol for expressing ^{15}N-cTnC in *E. coli* strain BL21(DE3)pLysS was the same as that for the ^{15}N-cNTnC. The first step in the purification of ^{15}N-cTnC used the same DEAE-sephadex (A25) column as that for the purification of ^{15}N-cNTnC, also under the same condition. After the protein has been partially purified by the DEAE-sephadex column, all fractions containing the protein are pooled and lyophilized. The dried protein powder dissolved in 25ml of a buffer containing 5mM $CaCl_2$, 1mM MgCl and 50mM KCl, pH 7.5 and loaded onto a phenyl-sepharose column (Pharmacia) without desalting. The column is washed with the aforementioned buffer for at least one column volume at a flow rate of ~1ml/min. The protein is eluted with an EDTA buffer containing 50mM Tris and 1mM EDTA, pH 7.5. The phenyl-sepharose purification step utilizes cTnC's unique Ca^{2+}-dependent binding to hydrophobic-interaction column to separate the protein from impurities. The 5mM $CaCl_2$ in the buffer is crucial for the proper functioning of the column. Without the Ca^{2+}, the apo cTnC will not possess the unique hydrophobic patch that allows it to bind to hydrophobic media in the column. Two NMR samples of ^{15}N-cTnC•3Ca^{2+} were prepared for the titrations of cRp and cRp-S41P/S43P, and four NMR samples of ^{15}N-cNTnC•Ca^{2+} were prepared for the titrations of cSp, cSp-S149P, cSp-

R161W, and cSp-S149P-R161W. Standard NMR buffer [100 mM KCl, 10 mM imidazole, 0.2 mM 2,2-dimethyl-2-silapentanesulfonic acid (DSS), and 0.01% NaN_3 in 90% H_2O/10% D_2O] was used in all cases. The sample concentrations were determined by amino acid analysis. To each sample was added 5 μL of 1 M $CaCl_2$ to ensure that the protein was Ca^{2+}-saturated, and the pH was adjusted to 6.7 by 1 M HCl and/or 1 M NaOH.

Synthetic Peptides. acetyl-AKKKSKI**S**A**S**RKLQLKTLLLQIAKQELEREAEERRGEK-amide (cRp), acetyl-RI**S**ADAMMQALLGARAK-amide (cSp) and acetyl-RI**S**ADAMMQALLGAWAK-amide (cSp-R161W) were prepared using standard methodology for a typical TnI peptide (*21*). Standard methodology was also used to synthesize cRp-S41P/S43P, cSp-S149P and cSp-S149P-R161W except that phosphorylated amino acid (bold and underlined in the sequences) is incorporated. The sequences were confirmed by amino acid analysis and the mass verified by electrospray mass spectrometry.

Titration of ^{15}N-cTnC•3Ca^{2+} with cRp and cRp-S41P/S43P. Both cRp and cRp-S41P/S43P peptides are highly soluble in water, which allows the preparation of a 35 mM stock solution of cRp and a 40 mM stock solution of cRp-S41P/S43P. A 500 μL NMR sample of 0.6 mM ^{15}N-cTnC•3Ca^{2+} was used for the titration with cRp and a 500 μL NMR sample of 0.7 mM ^{15}N-cTnC•3Ca^{2+} was used for the titration with cRp-S41P/S43P. Each titration was done by adding consecutive aliquots of 1 μL of cRp or cRp-S41P/S43P stock solutions. The sample was mixed thoroughly with each addition. The change in protein concentration due to dilution was taken into account for data analysis. The decrease in pH associated with cRp or cRp-S41P/S43P addition was adjusted by 1M NaOH to pH 6.7 at every titration point. Both 1D ^{1}H and 2D {^{1}H, ^{15}N}-HSQC NMR spectra were acquired at every titration point.

Titration of ^{15}N-cNTnC•Ca^{2+} with cSp, cSp-S149P, cSp-R161W, and cSp-S149P-R161W. cSp peptide is slightly soluble in aqueous solution and tends to form a gel at high concentrations (> 50 mM), likely due to aggregation. Thus, no stock peptide solution was prepared; instead, solid peptide was added directly to the NMR tube at every titration point. A 500 μL 0.6 mM sample of ^{15}N-cNTnC•Ca^{2+} was used for the cSp titration, a 500 μL 0.5 mM sample was used for the cSp-S149P titration, a 500 μL 0.7 mM sample was used for the cSp-R161W titration, and a 500 μL 0.6 mM sample was used for the cSp-S149P-R161W titration. The sample was mixed thoroughly with each addition. 2 μL of sample in duplicate were taken at every titration point for amino acid analysis to determine the peptide/protein ratios. Changes in pH associated with cSp additions were compensated by adjusting to pH 6.7 at every titration point. Both 1D ^{1}H and 2D {^{1}H, ^{15}N}-HSQC NMR spectra were acquired at every titration point.

NMR Spectroscopy. All of the NMR spectra were obtained using a Unity INOVA 500 MHz spectrometer at 30°C. All 1D ^{1}H NMR spectra were acquired with a sweep width of 6000 Hz or 7000 Hz with 128 transients. All 2D {^{1}H, ^{15}N}-HSQC spectra were acquired using the sensitivity-enhanced gradient pulse scheme developed by Lewis E. Kay and co-workers (*22, 23*). The ^{1}H and ^{15}N sweep widths were 6000 Hz or 7000 Hz and 1500 Hz, with 16 transients and 128 increments, respectively. Spectral processing and analyses were accomplished with the program VNMR (Varian Associates), NMRPipe (*24*), and NMRView (*25*).

Results

Effect of S41/S43 phosphorylation on the interaction of cRp with cTnC•3Ca^{2+}

Previously, we have shown that cRp binds cCTnC•2Ca^{2+} in a 1:1 stoichiometry to form a tight cCTnC•2Ca^{2+}•cRp complex ($K_D \leq 1$ μM) and the interaction of cRp with cCTnC•2Ca^{2+} occurs with slow exchange kinetics on the NMR time scale (*26*). A similar binding behavior of cRp for cTnC•3Ca^{2+} indicates that the interaction of this region of cTnI binds specifically to the C-domain of cTnC•3Ca^{2+} regardless of the presence of the N-domain (*20*). Here we compare the binding behavior of cRp and cRp-S41P/S43P. Figure IV-2a shows a superimposition of the 2D {^{1}H, ^{15}N}-HSQC NMR spectra of cTnC•3Ca^{2+} and cTnC•3Ca^{2+}•cRp complex and Figure IV-2b shows a superimposition of the 2D {^{1}H, ^{15}N}-HSQC NMR spectra of cTnC•3Ca^{2+} and cTnC•3Ca^{2+}•cRp-S41P/S43P complex. The 2D {^{1}H, ^{15}N}-HSQC NMR spectrum of cTnC•3Ca^{2+} is completely assigned (*27*) and is used as a guide in assigning some of the residues in the cRp or cRp-S41P/S43P bound states. In both cases, the C-domain residues underwent significant changes and several C-domain residues including G110 and G146 are labeled in Figure IV-2a and 2b as examples. As the titration progresses, the resonance peaks corresponding to cTnC•3Ca^{2+} become less intense while those corresponding to the cTnC•3Ca^{2+}•cRp or cTnC•3Ca^{2+}•cRp-S41P/S43P complex grow. When the protein:peptide ratio reaches 1:1, all cross peaks corresponding to cTnC•3Ca^{2+} completely disappears, while those corresponding to the complex attain maximum intensity. When the intensity changes as a function of peptide to protein ratios were plotted, the curve levels off after protein:peptide ratio reaches 1:1. Figure IV-2c and 2d show the respective binding curves of cRp and cRp-S41P/S43P for cTnC•3Ca^{2+}. In both

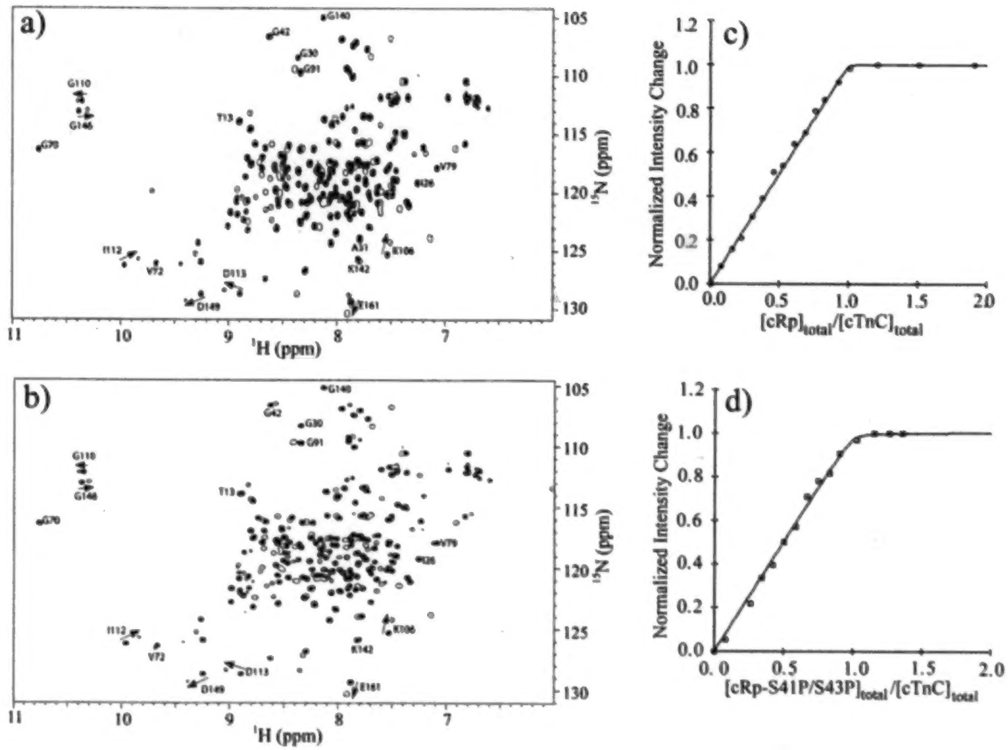

Figure IV-2. Titration of ^{15}N-cTnC•3Ca^{2+} with cRp (a) and cRp-S41P/S43P (b). In the expanded contour plots of the 2D {^{1}H, ^{15}N}-HSQC spectra, the cross-peaks corresponding to free cTnC•3Ca^{2+} are shown as multiple contours, whereas the peaks corresponding to the protein•peptide complexes are shown as single contours. The titration curves for cRp and cRp-S41P/S43P binding are shown in c) and d), respectively. Each curve is normalized according to $(I_{obs} - I_{initial})/(I_{final} - I_{initial})$, where I represents the cross peak intensity changes. A solid line represents the best fit to the data.

cases, curve fitting yielded a dissociation constant $K_D \leq 1$ μM. It is important to point out that since the K_D values of ≤ 1 μM are far less than the concentrations of protein used in the NMR experiments, the affinity less than 1 μM becomes difficult to determine from a titration curve, *i.e.*, it is hard to distinguish between K_Ds of 1 μM, 0.1 μM, and 0.01 μM. Thus, our result indicates that the phosphorylation of S41/S43 did not destabilize the tight association of cRp with cTnC•3Ca^{2+} as the K_D is still equal or below 1 μM (indicative of high affinity between ligand and protein). The X-ray crystal structure of the cTnC•3Ca^{2+}•cTnI$_{31\text{-}210}$•cTnT$_{183\text{-}288}$ complex solved in 2003 (*2*) shows that cRp region forms a long α-helix interacting primarily with the C-domain of cTnC•3Ca^{2+} via multiple

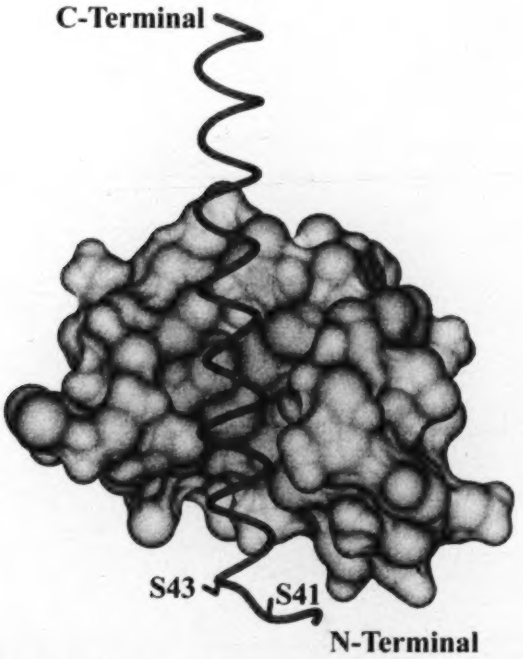

Figure IV-3. Ribbon and surface representations of the structure of cCTnC•2Ca^{2+}•cRp in the cTnC•3Ca^{2+}•cTnI$_{31\text{-}210}$•cTnT$_{183\text{-}288}$ complex (PDB accession code 1J1E) (*2*). The positions of S41 and S43 phosphoylation sites are indicated.

polar and van der Waals interactions, similar to the earlier structure of sTnC•2Ca^{2+}•sTnI$_{1-47}$ (*28*). As shown in Figure IV-3, the α-helix enters the C-domain of cTnC hydrophobic cleft near helices G/H and exits near helices E/F and the S41/S43 phosphorylation sites are located approximately in the beginning of the α-helix with almost no direct contacts with the protein hydrophobic cleft. Thus, it is unlikely that the introduction of two negatively charged phosphate groups at S41P/S43P would exert much influence on the extensive contacts between the long α-helix of cRp and the C-domain of cTnC. Interestingly, in both the sTnC•2Ca^{2+}•sTnI$_{1-47}$ and cTnC•3Ca^{2+}•cTnI$_{31-210}$•cTnT$_{183-288}$ structures, TnC adopts a collapsed conformation as such the N-terminus of the cRp α-helix makes several weak contacts with the N-lobe of cTnC. This is reflected in our observation that some of the N-domain peaks (e.g., G42, V72, V79) underwent slight chemical shift changes in the titration of cRp-S41P/S43P to cTnC•3Ca^{2+} (Figure IV-2a,b). It is possible that the two negative charged phosphate groups at S41P/S43P caused minor conformational alterations in the N-domain of cTnC.

Effect of S149 phosphorylation and R161W mutation on the interaction of cSp with cNTnC•Ca^{2+}.

Some of the resonance peaks in the 2D {^{1}H, ^{15}N}-HSQC spectrum of ^{15}N-cNTnC(C35S/C84S)•Ca^{2+} were assigned based on the assignments of wild type ^{15}N-cNTnC•Ca^{2+} (*29*). The complete assignments were achieved using CBCA(CO)NNH and HNCACB experiments (*30*) analyzed with the automated assignment program smartnotebook (*31*). The 2D {^{1}H, ^{15}N}-HSQC NMR spectrum of cNTnC•Ca^{2+} was used as a starting point to monitor the cSp peptides induced chemical shift changes. The cSp

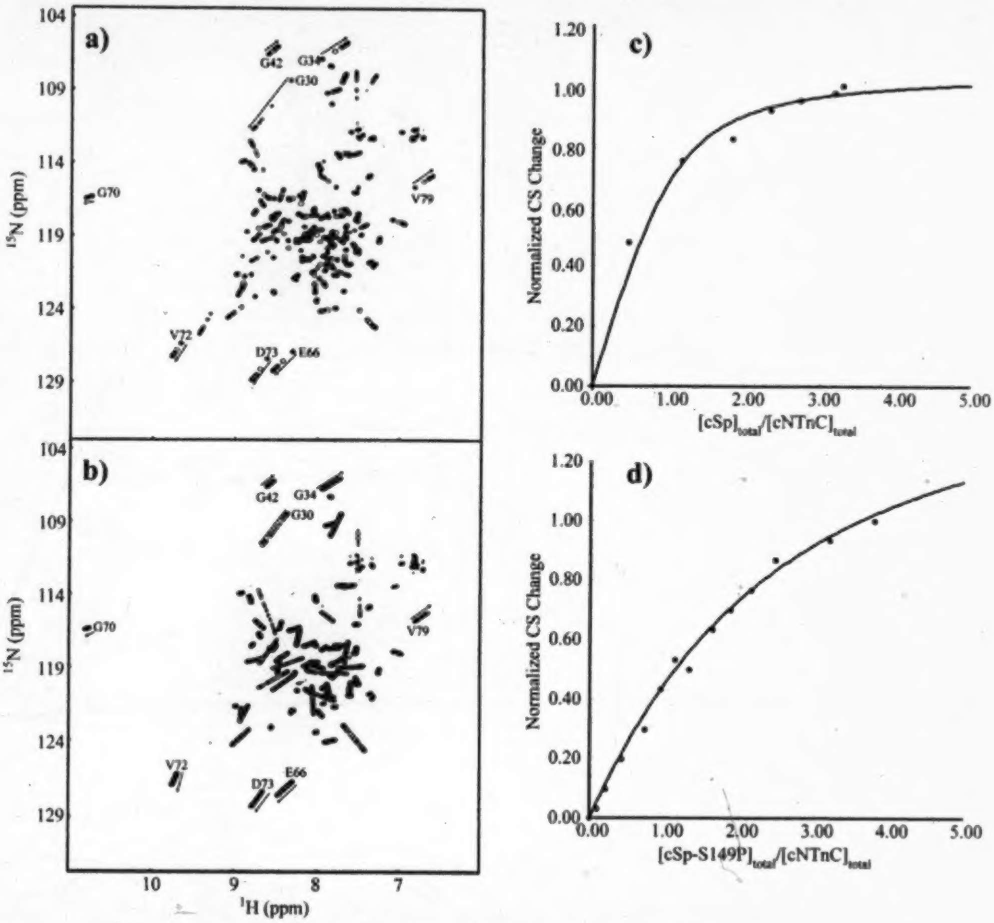

Figure IV-4, Part I. Titration of ^{15}N-cNTnC•Ca^{2+} with wild type cSp (a, c), cSp-S149P (b, d). (a, b) Overlays of {^{1}H, ^{15}N}-HSQC spectra of cNTnC•Ca^{2+} at various peptide additions are superimposed. Solid contours represent the starting point of the titration. Hollow contours represent the progressive shifts of peaks with increasing peptide concentrations. (c, d) Titration curves representing the average of all residues followed in (a, b). The curves are normalized according to $(\delta_{obs} - \delta_{initial}) / (\delta_{complex} - \delta_{initial})$. A solid line represents the best fit to the data.

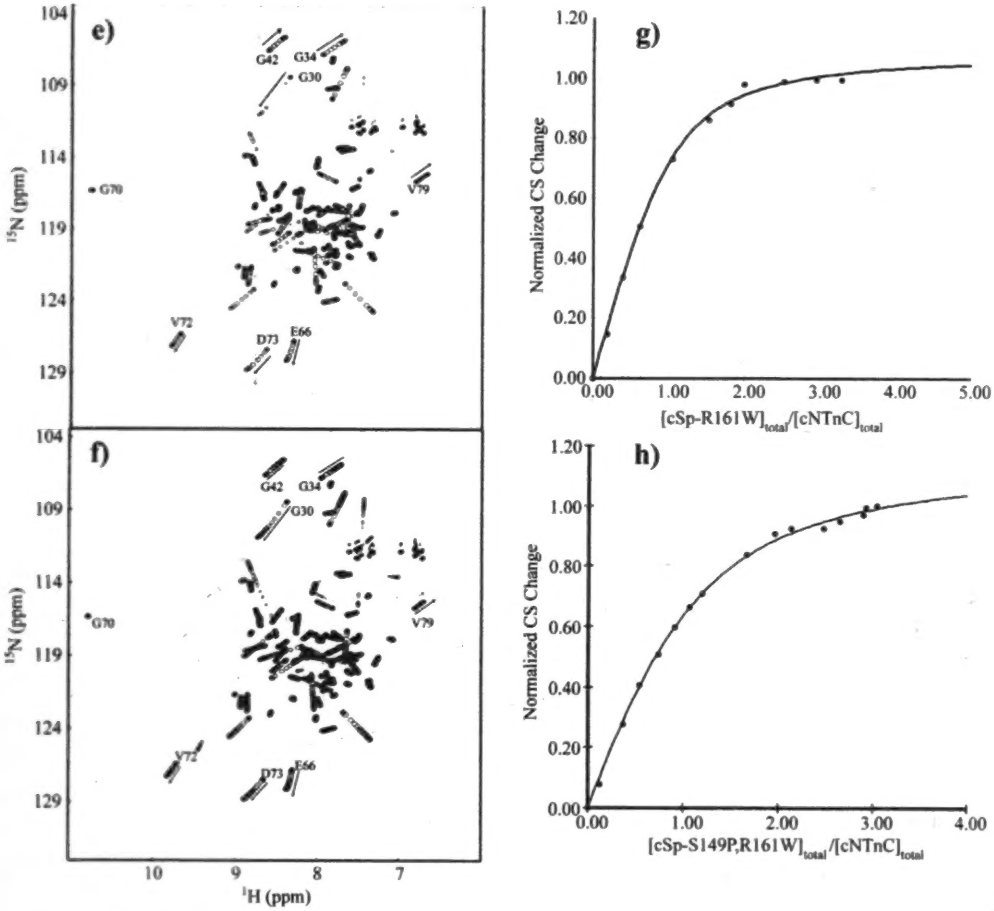

Figure IV-4, Part II. Titration of ^{15}N-cNTnC•Ca^{2+} cSp-R161W (e, g), cSp-S149P-R161W (f, h). (e, f) Overlays of {^{1}H, ^{15}N}-HSQC spectra of cNTnC•Ca^{2+} at various peptide additions are superimposed. Solid contours represent the starting point of the titration. Hollow contours represent the progressive shifts of peaks with increasing peptide concentrations. (g, h) Titration curves representing the average of all residues followed in (e, f). The curves are normalized according to $(\delta_{obs} - \delta_{initial}) / (\delta_{complex} - \delta_{initial})$. A solid line represents the best fit to the data.

induced 2D {^{1}H, ^{15}N}-HSQC NMR spectral change of ^{15}N-cNTnC•Ca^{2+} is very similar to that reported previously (*1*). The overlays of {^{1}H, ^{15}N}-HSQC spectra taken during the titrations of ^{15}N-cNTnC•Ca^{2+} with cSp-S149P, cSp-R161W, and cSp-S149P-R161W are shown in Figure IV-4(a, b, e, f). Comparison of the 2D {^{1}H, ^{15}N}-HSQC NMR spectral changes induced by the four cSp peptides reveal that all four peptides induced similar patterns of backbone amide resonance changes of cNTnC•Ca^{2+}. Typical examples are G30, G34, and G42. In all cases, chemical shift changes fall into the fast exchange limit on the NMR time scale and the linear movement of the resonance peaks indicates that the binding occurs with a 1:1 stoichiometry.

Resonances which undergo backbone amide ^{1}H$_N$ and/or ^{15}N chemical shift changes during titrations were followed to monitor peptide binding to protein. For each titration, the peptide induced chemical shift changes of individual amide resonance as a function of the peptide:protein ratio was plotted, and the average curves are shown in Figure IV-4. The curve fitting yielded dissociation constants (K$_D$) of 130 ± 20 μM for cSp, 1.25 ± 0.2 mM for cSp-S149P, 176 ± 33 μM for cSp-R161W, and 394 ± 32 for cSp-S149P-R161W. This corresponds to an affinity reduction of ~10-fold by the S149 phosphorylation, ~1.4-fold by the mutation R161W, and ~4-fold by a combination of S149 phosphorylation and mutation R161W.

To compare the four cSp peptides induced chemical shift changes of cNTnC, the normalized values for amide ^{1}H$_N$ and ^{15}N were averaged and plotted against the protein sequence with different colors coding four cTnI peptides (Figure IV-5). The important point of this plot is that the patterns induced by four peptides are very similar although to a slightly different extent. Although most of the residues throughout the sequence are

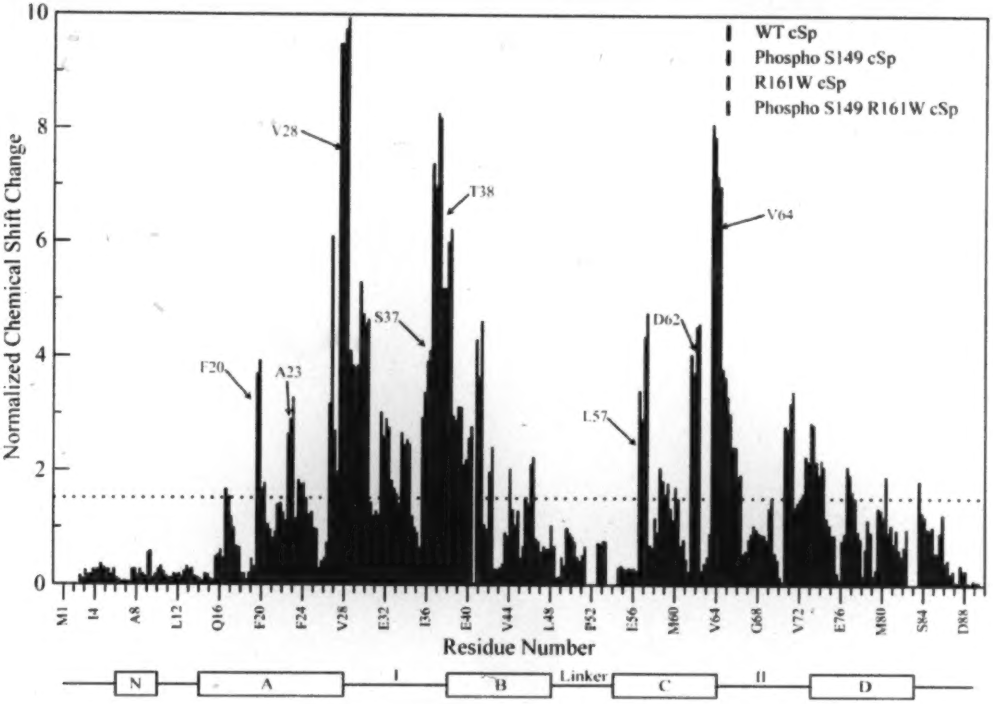

Figure IV-5. Comparison of induced chemical shift changes of cNTnC•Ca^{2+} upon the addition of cSp (maroon), cSp-S149P (blue), cSp-R161W (green), and cSp-S149P-161W (red). The chemical shift changes for each residue were calculated by averaging the normalized chemical shift changes of the backbone ^1H_N and ^{15}N chemical shifts. For a particular nucleus, the normalized chemical shift change of a residue is obtained by dividing the observed shift change by the average shift change for all residues. Thus, $\Delta\delta_{ppm} = 1$ indicates that the chemical shift change for a given residue is equal to the average change for all residues. The secondary structure of the protein is represented schematically below the horizontal axis with boxes representing helical regions and lines representing coil regions.

more or less affected by peptides binding, 26 residues undergo significant ($\Delta\delta_{ppm} \geq 1.5$) peptide-induced chemical shift perturbations. Mapping those residues on the structure of cNTnC in the cNTnC•Ca^{2+}•cSp complex (Figure IV-6a) reveals that the peptide-induced chemical shift perturbations arise primarily from the A, B, and C-helices and the β-sheet regions. This is not surprising considering that these regions are directly involved in binding cSp and undergo large conformational changes in the cSp-induced 'closed' to 'open' structural transition of cNTnC. The fact that these residues are identical in all four cases indicates that neither the S149 phosphorylation, the mutation R161W, nor the combination of both, abolish the ability of cSp to induce a 'closed' to 'open' structural transition in cNTnC•Ca^{2+}. It is important to point out that when the 26 residues were mapped to the surface of cNTnC in the cNTnC•Ca^{2+}•cSp complex, it did not reveal a binding patch matching the hydrophobic surface as shown in Figure IV-6b. This is probably owing to the fact that the major conformational perturbation caused by cSp is on the 'closed' to 'open' structural transition, but not on the binding surface of cNTnC.

In the high resolution structure of the cNTnC•Ca^{2+}•cSp complex (*1*), the α-helical segment (residues 151-156) of the 17 residue cSp peptide inserts between the A/B interhelical interface and the N-terminus (residues 147-149) interacts with the hydrophobic core of cNTnC and S149 is located in the center of the core (Figure IV-6b). As such two negative charges introduced by S149 phosphorylation would be expected to disrupt the hydrophobic force and lead to weaker binding of cSp for cNTnC•Ca^{2+} as observed in the current study. It is interesting to note that the affinity of cSp for cNTnC•Ca^{2+} is also weakened by the presence of bepridil in the hydrophobic core although to a smaller extent (~ 3.5 fold reduction in affinity) (*32*). This indicates that hydrophobic interaction is the primary anchoring force for cSp binding to cNTnC and disruption of this hydrophobic interaction by the introduction of a negatively charged phosphate group or a small organic molecule would have tremendous impact on cSp's affinity for cTnC. On the other hand, mutation R161W involves a basic to hydrophobic charge change and can be postulated to result in an energetically more favorable interaction of the tryptophan side chain with the hydrophobic patch on cNTnC.

Unfortunately, in the structure of the cNTnC•Ca^{2+}•cSp complex, the C-terminal residues (A160, R161, A162, and K163) of cSp do not interact with cNTnC•Ca^{2+} and extends out of the protein surface (Figure IV-6a). Thus, the mutation R161W may only have minimal effect on the interaction of cSp and cNTnC•Ca^{2+} as reflected in the observed ~1.4-fold affinity decrease. The subtle affinity alteration observed herein is in accordance with a recent surface plasmon resonance-based (SPR) study showing that the affinity of R161W mutant for cTnC is only ~ 2.6 times that of wild type cTnI (*13*). Somewhat surprisingly, the effect of S149 phosphorylation is compromised in the presence of the R161W mutation, i.e. a ~4-fold affinity decrease by cSp-S149P-R161W as compared to a ~10-fold one by cSp-S149P. It is possible that the ~10-fold weakening caused by the

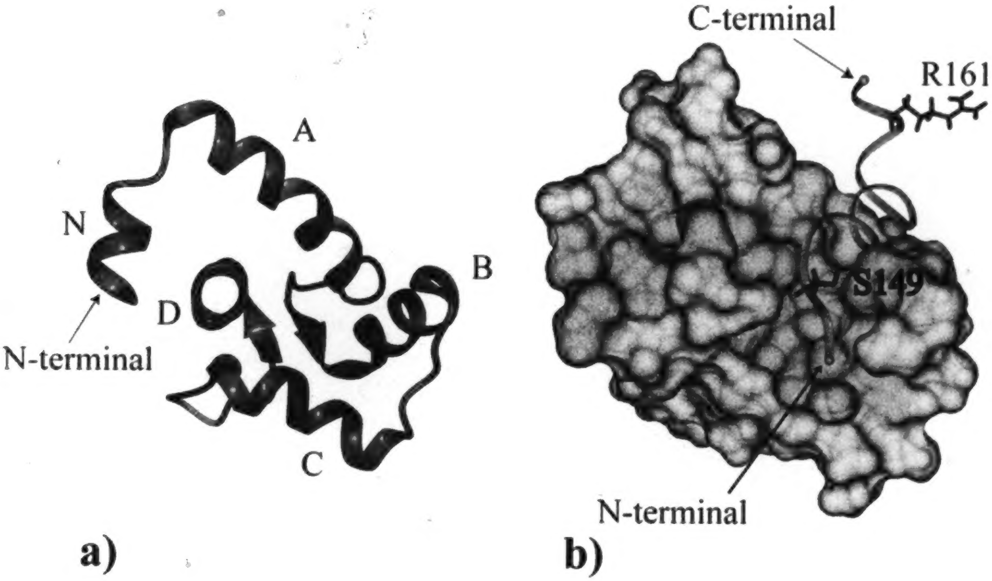

Figure IV-6. a) Chemical shift mapping on the structure of cNTnC in the cNTnC•Ca^{2+}•cSp complex (PDB accession code 1MXL) (*1*): the residues experience major chemical shift changes ($\Delta\delta_{ppm} \geq 1.5$) are colored red. b) Residues S149 and R161 are shown on the structure of cNTnC•Ca^{2+}•cSp. The molecular surface of cNTnC•Ca^{2+} (residues 5-84) in the complex is shown with the hydrophobic surface colored yellow, the structure of cSp is shown in the "coil" representation.

phosphorylation of S149 allows the tryptophan side chain of the R161W cSp peptide to rearrange its position slightly so it can make more energetically favorable interactions with cNTnC•Ca^{2+} and therefore increasing the apparent affinity. At present, there is no compelling data for this rationalization.

Discussion

This study is directed toward an evaluation of the consequences caused by the phosphorylation of S41, S43, and S149 and FHC mutation R161W on the interaction of cTnI with cTnC. We have utilized 2D {^{1}H, ^{15}N}-HSQC NMR spectroscopy as a tool to monitor and compare the chemical shift and spectral intensity changes in cTnC•Ca^{2+} caused by cRp in native or modified states, and in cNTnC•Ca^{2+} caused by cSp in native or modified states. This allows us to systematically assess the influences of these alterations on the binding location, stoichiometry, and affinity of three key regions of cTnI to cTnC. The binding constants for cRp peptides binding cTnC•3Ca^{2+}, and cSp peptides binding to cNTnC•Ca^{2+} are summarized in Table IV-1.

Three specific PKC phosphorylation sites on cTnI have been identified at residues S41, S43, and T142. The relative contribution of the phosphorylation of three sites to the accelerated relaxation and decreased acto-myosin ATPase activity has been the focus of several recent studies. For example, Burkart et al. reported that phosphorylation of S41/S43 dominates regulation of the level of maximum tension, while phosphorylation of T142 appears to be required for regulation of thin filament sliding speed (*18*). The data presented here demonstrated that the phosphorylation of S41/S43 plays a minor role in destabilizing the cTnI-cTnC interaction, which leads to diminished acto-myosin ATPase activity and depressed contractility. Since S41/S43 are located in the structural domain of the troponin complex based on the recent proposed model (*2*), the phosphorylation of S41/S43 may be involved in the global conformational changes of troponin in the thin filament rather than in the cTnI-cTnC interface. In particular, The core domain structure places the N-terminus of the cTnI in close proximity with cNTnC such that S43 is found to interact with E10 in the N-helix of cTnC, indicating that phosphorylation of S43 may disrupt the cTnI interaction with cNTnC and have direct impact on the Ca^{2+} binding to the regulatory site of cTnC. This is supported by recent studies showing that pseudophosphorylation (replacement of S with E) of S41 and S43 significantly reduces myofilament response to Ca^{2+} (*18*) and that phosphorylation of S41 and S43 are responsible for the accelerated relaxation observed in cardiomyocytes (*33*). Residue S149 in the cSp region has been recently identified to be the site of p21-activated kinase (PAK), a kinase potentially involved in Ca^{2+}-sensitization of cardiac muscle contraction and cardiac hypertrophy. This study has demonstrated that S149 phosphorylation reduced the affinity of cSp for cNTnC•Ca^{2+} by ~10-fold. Since S149 of cTnI is located in the center of the hydrophobic core of cNTnC•Ca^{2+} (*1*), introduction of a negatively charged phosphate group in this region of cTnI would certainly destabilize its binding to cNTnC•Ca^{2+} and result in reduced affinities. Given that the phosphorylation of S149 in cTnI may be involved in a mechanism of Ca^{2+}-sensitization of triton-skinned cardiac muscle fiber (*4*) and considering that cTnI toggles between cTnC and actin-tropomyosin during the systolic-diastolic cycle, these results suggest a greater reduction in affinity of S149 phosphorylated cTnI for actin-tropomyosin as compared to cTnC. Thus cTnI-cTnC interactions would be favored compared to cTnI-actin-tropomyosin interaction resulting in an increase of the Ca^{2+}-affinity for cTnC and thereby the Ca^{2+}-sensitization of the myofilaments. Nonetheless, the dramatic affinity reduction of cTnI for cTnC by the phosphorylation of S149 strongly suggests that PAK modulate cardiac muscle contraction by modifying myofilament protein-protein interaction, contributing to depressed contractility in certain cases and compromised relaxation in others.

Table IV-1: K_{D}s (μM) and $\Delta G_{binding}$ (kcal/mol) for peptides binding to cTnC.

Peptide	cTnC isoform		$\Delta G_{binding}$
	cTnC•3Ca^{2+}	cNTnC•Ca^{2+}	
cRp	≤ 1		≤ -8.3
cRp-S41P/S43P	≤ 1		≤ -8.3
cSp		130 ± 20	-5.4 ± 0.1
cSp-S149P		1250 ± 200	-4.0 ± 0.1
cSp-R161W		176 ± 33	-5.2 ± 0.1
cSp-S149P-R161W		394 ± 32	-4.7 ± 0.1

In addition to phosphorylation, the cIp-cSp region of cTnI is also prone to missense mutations in diseased heart. One of the mutations, R161W is located in the cSp region and co-segregates with FHC (*6*). The substitution of Arg by Trp constitutes not only a change in charge, but also the introduction of a large aromatic side chain, a potentially crippling mutation. Functional studies revealed that the R161W mutation produced a reduction in cTnI's ability to inhibit actomyosin ATPase and an increase in Ca^{2+} sensitivity of actomyosin ATPase regulation (*13-17*). If these functional differences manifest themselves *in vivo* there will be impairment of relaxation of cardiac muscle and this altered contractility may provide a hypertrophic stimulus eventually leading to cardiac dysfunction. Because cTnI toggles between cTnC and actin-tropomyosin, it seems likely that an important mechanism of cTnI-induced cardiac dysfunction by the R161W mutation lies in altered cTnI interactions with cTnC, actin-tropomyosin or both. The binding of cTnI to actin-tropomyosin inhibits actomyosin ATPase activity, depresses cross-bridge cycling, and prevents contraction. The inhibition is released as cTnI binding shifts from actin-tropomyosin to cTnC, an action favored by an increase in cytosolic Ca^{2+} concentration during systole, when Ca^{2+} binds to the N-domain of cTnC. Thus, it seems that the R161W mutation either reduced cTnI's affinity for actin-tropomyosin or enhanced its affinity for cTnC. The net effect would be diminished inhibition of actomyosin ATPase activity. Interestingly, our present results indicate that the affinity of cSp for $cNTnC{\bullet}Ca^{2+}$ is reduced by only ~1.4-fold by the mutation R161W. In light of the above argument, these results suggest a greater reduction in affinity of the R161W mutant for actin-tropomyosin compared to cTnC, such that cTnI-cTnC interaction is favored over cTnI-actin-tropomyosin interaction, similar as in the case of S149 phosphorylation.

The fact that the cSp segment of cTnI are subject to modifications by both phosphorylation and mutation prompted us to examine the binding of cSp-S149P-R161W to $cNTnC{\bullet}Ca^{2+}$. The results showed that the destabilizing factor introduced by S149 phosphorylation on the interactions of cSp with $cNTnC{\bullet}Ca^{2+}$ is compromised somehow by the R161W mutation. Thus, it seems that the FHC mutations can either enhance or suppress the effect of phosphorylation depending on the specificity of the interactions. So far there is limited functional data available from the literature linking the FHC mutations with cTnI phosphorylation. One study has compared the *in vitro* function of R144G mutation in nonphosphorylated and S22/S23 (PKA sites) bisphosphorylated cTnI and revealed that S22P/S23P and R144G exhibit mutual suppressing effect on the acto-myosin ATPase activity (*16*). Another study has probed the effects of R144G mutation and pseudo-phosphorylation of cTnI PKC sites on Ca^{2+}-signaling at the cTnC-cTnI interface and on tension developments (*34*). Compared to cTnI controls, cTnC-cTnI binary complexes with either cTnI-R144G or cTnI-S41E-S43E-T142E has a small effect on Ca^{2+}-dependnent structural opening of the N-domain of cTnC as measured by FRET, however, this structural change was significantly reduced in the cTnC-cTnI-R144G-S41E-S43E-T142E complex. In skinned fiber bundles, exchange of cTnI with cTnI-R144G induced enhanced Ca^{2+}-sensitivity and exchange of cTnI with cTnI-S41E-S43E-T142E induced decreased Ca^{2+}-sensitivity, however, cTnI-R144G-S41E-S43E-T142E had little additional effects over cTnI-R144G.

It is difficult to fully rationalize the effect of the R161W mutation on the cTnC affinity of the S149-phosphorylated cSp peptide without more data. Table IV-1 lists the ΔG of cNTnC-binding for all four versions of the cSp peptide to cNTnC. It is obvious that the binding energetics of the doubly-modified peptide (cSp-S142P-R161W) can not be expressed simply as a linear addition of two non-interacting modifications. Instead, the ΔG of binding for the doubly-modified peptide is more appropriately represented as:

$$\Delta G_{DM} = \Delta G_{WT} + \Delta\Delta G_{S149-P} + \Delta\Delta G_{R161W} + \Delta\Delta G_{coupling},$$

where ΔG_{DM} represents ΔG of cNTnC-binding for the doubly modified cSp peptide, ΔG_{WT} represents ΔG of cNTnC-binding for the wild type cSp peptide, $\Delta\Delta G_{S149-P}$ represents the change in ΔG owing to the S149 phosphorylation, $\Delta\Delta G_{R161W}$ represents the change in ΔG owing to the R161W mutation and $\Delta\Delta G_{coupling}$ represents the change in ΔG brought about by the interaction of the phosphate group with the Trp side chain. The exact value of $\Delta\Delta G_{coupling}$ can not be logically quantified without structural and dynamic data on the peptides. One possible explanation for the observed binding energetics is that owing to geometrical and conformational restraints, cNTnC's interactions with the N-terminal and the C-terminal of the cSp are mutually exclusive. That is the C-terminal Trp side chain in the R161W cSp peptide can not make meaningful contacts with cNTnC because the N-terminal of cSp binds tightly to the hydrophobic pocket on cNTnC. But once cSp's N-terminal interactions with cNTnC is weakened by the phosphorylation, the Trp side chain at the C-terminal of cSp will be able to interact more with its binding site on cNTnC.

In summary, we have employed a very feasible system by the use of cTnI peptides to examine the consequences of cTnI modification on its interaction with cTnC. The results indicate that a given modification of cTnI can have a pronounced effect on the binding affinity of cTnI for cTnC. These perturbations in protein affinity may correlate with the impairment of cTnI function in heart muscle contraction. Clearly, future explorations involving the use of the intact cTnI protein, the entire troponin complex, and even the entire thin filament are needed to generate a more complete picture in the understanding of the mechanism by which myofilament protein modifications promote cardiac dysfunction.

References

1. Li, M. X., Spyracopoulos, L., and Sykes, B. D. (1999) *Biochemistry 38*, 8289-98.
2. Takeda, S., Yamashita, A., Maeda, K., and Maeda, Y. (2003) *Nature 424*, 35-41.
3. Solaro, R. J., and Rarick, H. M. (1998) *Circ. Res. 83*, 471-80.
4. Buscemi, N., Foster, D. B., Neverova, I., and Van Eyk, J. E. (2002) *Circ Res 91*, 509-16.
5. Redwood, C. S., Moolman-Smook, J. C., and Watkins, H. (1999) *Cardiovasc Res 44*, 20-36.
6. Hernandez, O. M., Housmans, P. R., and Potter, J. D. (2001) *J Appl Physiol 90*, 1125-36.
7. McDonough, J. L., Arrell, D. K., and Van Eyk, J. E. (1999) *Circ Res 84*, 9-20.
8. Murphy, A. M., Kogler, H., Georgakopoulos, D., McDonough, J. L., Kass, D. A., Van Eyk, J. E., and Marban, E. (2000) *Science 287*, 488-491.
9. D'Costa, M., Fleming, E., and Patterson, M. C. (1997) *Am. J. Clin. Pathol. 108*, 550-555.
10. Van Eyk, J. E., Powers, F., Law, W., Larue, C., Hodges, R. S., and Solaro, R. J. (1998) *Circ. Res. 82*, 261-271.
11. McDonough, J. L., Labugger, R., Pickett, W., Tse, M. Y., MacKenzie, S., Pang, S. C., Atar, D., Ropchan, G., and Van Eyk, J. E. (2001) *Circulation 103*, 58-64.
12. Lee, T. H., and Goldman, L. (2000) *N. Engl. J. Med. 342*, 1187-1195.
13. Elliott, K., Watkins, H., and Redwood, C. S. (2000) *J. Biol. Chem. 275*, 22069-22074.
14. James, J., Zhang, Y., Osinska, H., Sanbe, A., Klevitsky, R., Hewett, T. E., and Robbins, J. (2000) *Circ. Res. 87*, 805-811.
15. Takahashi-Yanaga, F., Morimoto, S., Harada, K., Minakami, R., Shiraishi, F., Ohta, M., Lu, Q. W., Sasaguri, T., and Ohtsuki, I. (2001) *J. Mol. Cell Cardiol. 33*, 2095-2107.
16. Deng, Y., Schmidtmann, A., Redlich, A., Westerdorf, B., Jaquet, K., and Thieleczek, R. (2001) *Biochemistry 40*, 14593-14602.
17. Lang, R., Gomes, A. V., Zhao, J., Housmans, P. R., Miller, T., and Potter, J. D. (2002) *J. Biol. Chem. 277*, 11670-11678.
18. Burkart, E. M., Arteaga, G. M., Sumandea, M. P., Prabhakar, R., Wieczorek, D. F., and Solaro, R. J. (2003) *J Mol Cell Cardiol 35*, 1285-93.
19. Pearlstone, J. R., Chandra, M., Sorenson, M. M., and Smillie, L. B. (2000) *J Biol Chem 275*, 35106-15.
20. Li, M. X., Saude, E. J., Wang, X., Pearlstone, J. R., Smillie, L. B., and Sykes, B. D. (2002) *Eur Biophys J 31*, 245-56.
21. Tripet, B. P., Van Eyk, J. E., and Hodges, R. S. (1997) *J. Mol. Biol. 271*, 728-750.
22. Kay, L. E., Keifer, P., and Saarinen, T. (1992) *J. Am. Chem. Soc. 114*, 10663-10665.
23. Zhang, O., Kay, L. E., Olivier, J. P., and Forman-Kay, J. D. (1994) *J. Biomol. NMR 4*, 845-858.
24. Delaglio, F., Grzesiek, S., Vuister, G. W., Zhu, G., Pfeifer, J., and Bax, A. (1995) *J. Biomol. NMR 6*, 277-293.

25. Johnson, B. A., and Blevins, R. A. (1994) *J. Biomol. NMR 4*, 603-614.
26. Wang, X., Li, M. X., Spyracopoulos, L., Beier, N., Chandra, M., Solaro, R. J., and Sykes, B. D. (2001) *J Biol Chem 276*, 25456-66.
27. Sia, S. K., Li, M. X., Spyracopoulos, L., Gagné, S. M., Liu, W., Putkey, J. A., and Sykes, B. D. (1997) *J. Biol. Chem. 272*, 18216-18221.
28. Vassylyev, D. G., Takeda, S., Wakatsuki, S., Maeda, K., and Maeda, Y. (1998) *Proc. Natl. Acad. Sci. U.S.A. 95*, 4847-4852.
29. Spyracopoulos, L., Li, M. X., Sia, S. K., Gagné, S. M., Chandra, M., Solaro, R. J., and Sykes, B. D. (1997) *Biochemistry 36*, 12138-12146.
30. Muhandiram, D. R., and Kay, L. E. (1994) *J. Magn. Reson. B103*, 203-216.
31. Slupsky, C. M., Boyko, R. F., Booth, V. K., and Sykes, B. D. (2003) *Journal of Biomolecular NMR 27*, 313-321.
32. Wang, X., Li, M. X., and Sykes, B. D. (2002) *J Biol Chem 277*, 31124-33.
33. Westfall, M. V., and Borton, A. R. (2003) *J. Biol. Chem. 278*, 33694-33700.
34. Kobayashi, T., Dong, W. J., Burkart, E. M., Cheung, H. C., and Solaro, R. J. (2004) *J. Biol. Chem. 43*, 5996-6004.

Chapter V

Introduction to in situ ^{19}F NMR of myofibrils

Introduction

Structural biology has come a long way since the determination of the double helical DNA structure by Watson & Crick. Now, elucidating the structure of a medium size soluble protein is straight forward enough that it can almost be considered as routine. However, in many instances, the knowledge of a single structure of an isolated protein offers little in way of answering the relevant biological question. The development of protein structure determination by NMR has helped to fill in some inadequacies by looking at dynamics of the protein as well as detecting interactions that would have been missed by crystal structures. But fundamentally, structural biologists must recognize the fact that studying isolated proteins has limited relevance. Most biologically relevant events take place when proteins interact with other proteins and many proteins exist naturally as a component in a large complex. Conclusions deduced from structures of these proteins in isolation will often be found to contradict the biochemical data. Therefore, investigations of protein interactions *in situ* are inevitable if meaningful biological questions were to be answered. This is especially true in the field of muscle regulatory proteins in which interactions with filamentous protein assemblies are the norm. In this thesis alone, three major topics can be advanced enormously by studying Tn as part of a large assembly of proteins, namely, the myofibril. The first topic concerns the active sites of Ca^{2+}-sensitizers *in vivo*. cTnC is a logical choice for these drugs and *in vitro* studies indicate they are able to affect cTnC's interaction with cTnI (see Chapters II and III). However, none of the drugs studied so far binds to cTnC with nM affinity and no direct experimental evidence exists to prove that these drugs do indeed interact with cTnC in the muscle. Naturally, evidence of this sort can be obtained only by studying drug-cTnC interactions in intact myofibrils. The second topic pertains to the rational explanation for the effects of phosphorylations and FHC mutations on physiological function of myofibril. Studies conducted with cTnC and cTnI alone *in vitro* often do not fully explain physiological observations. The full picture can not be elucidated without studying Tn proteins in the presence of other thin filament proteins, especially actin. The third topic concerns the structural details of Tn-mediated muscle activation mechanism. Although the basic underlying Tn protein interaction cascades during the Ca^{2+}-activation of muscle is extensively studied (*2-7*), the question of how this leads to movements in Tm has never been properly answered. To answer such a question, detailed movements of Tn proteins upon binding Ca^{2+} must be studied with Tn complex *in situ*. As stated in chapter I, the only information on movements of Tn proteins in thin filaments are from fluorescence polarization as well as cryoelectron microscopy studies of myofibril and constituted thin filaments (*1, 8*). Thus it has long been one of our goals to make a significant contribution to the area of *in situ* studies of Tn proteins. What role can NMR play in this field?

Cryoelectron microscopy has impacted structural studies of large macromolecule assemblies greatly. The technique is virtually impervious to the size of the assembly and the requirement for regular repeats in its samples is much less stringent than X-ray crystallography. But most importantly, many filamentous polymers, resistant to crystallization, can be studied readily using cryoEM. X-ray has also made a number of inroads into this area. The elucidation of the ribosome structure has advanced the understanding of the RNA translation process tremendously. Compared to the former two techniques, NMR has been a relative new comer to the field of *in situ* protein investigation. Its adoption has been hampered by several inherent difficulties in the technique. The sensitivity of NMR is relative low compared to other techniques and this is exacerbated by the signal broadening inherent to large molecules. The increase in spectral complexity is also an issue with large protein-protein complexes, rendering the unambiguous analysis of the data difficult. Although a number of strategies are formulated to improve the resolution and sensitivity of NMR, they only alleviate the problems, not eliminating them (*9, 10*). Thus, in order to make NMR study of intact myofibrils viable, a different strategy needs to be adopted.

Although myofibrils are large and insoluble, one feature in the myofibril structure makes the application of NMR to myofibrils possible: the myofibril consists of regular-repeating units all arranged in the same orientation. This naturally aligns the proteins in the myofibril, greatly simplifying the analysis of NMR spectra and improves the signal to noise ratio by reducing signal dispersion due to anisotropic chemical shift and dipolar interactions. Because many interactions in NMR are orientation specific, the natural alignment of proteins also allows us to gain information regarding the orientation of the protein relative to the fibril axis. Structural information gained from conventional studies of TnC and Tn complex can be utilized to simplify the data analysis even further. The structure of TnC in different Ca^{2+}-saturated states has been extensively studied, both in isolation and in complex with other Tn proteins (*5, 7, 11-14*). And it is reasonable to assume no additional conformation change is associated with the protein's incorporation into the thin filament. This implies that TnC's domains can be treated as rigid bodies and determining the orientations of a few well defined bond vectors in the domain is all that is needed to fix the orientation of TnC in muscle fibres. In fact, the idea of determining protein orientation using bond vector orientations has been already been put into practice by the solid state NMR field. A good example comes from a study Anne Ulrich's group has done on the orientation of helical transmembrane peptide in orientated membrane bilayers (*15*). In this study, stacks of oriented membrane bilayers containing the membrane-binding peptide are created on glass plates. Each peptide is labelled with a 5fW residue whose side chain indole ring orientation relative to the peptide helical axis is known. The orientation of the helix with respect to the bilayer normal was obtained by analyzing the line shape of the ^{19}F signal at different orientation of the membrane. The choice of ^{19}F nucleus in this study is not an accident. Several unique properties of fluorine make it an ideal reporter atom for NMR studies of biological systems (*16*). Its inherent absence in most organisms reduces its background noise in NMR spectra. The high gyromagnetic ratio of this spin ½ nucleus coupled with 100% natural abundance means the detection of fluorine signal is much easier than those of ^{13}C or ^{15}N atoms. The electronic structure of the fluorine atom makes its resonance frequency far more sensitive to its magnetic environment than most other atoms, leading to a wide chemical shift spread and higher sensitivity to variations in protein orientation and dynamics. There are, however, several difficulties associated with ^{19}F solid state NMR. These include the need for wide spectral width at high field, difficulty implementing ^{1}H decoupling and contamination from ^{19}F-containing probe components. But all the difficulties can be overcome through the use of special NMR equipment.

Because TnC in muscle fibre is also aligned with respect to the filament axis, there is no reason why this methodology can not be applied to the investigation of TnC orientation change in muscle fibres. Our strategy is to produce a biologically functional ^{19}F-labelled TnC and incorporate it into intact myofibrils. Then by observing the ^{19}F signal during different physiological states of the muscle, changes in orientations of TnC domains during muscle activation and relaxation can be elucidated. For almost half of my graduate career I have worked on the development of the *in situ* ^{19}F NMR methodology for investigating cTnC's orientation in myofibrils. I must admit it has been a much more challenging project than I originally envisioned. Most difficulties arose because I am a biochemist inexperienced with the physiology of muscle fibres. A few details regarding biochemical properties of ^{19}F-labelled cTnC mutants also managed to side track me for a period of time. But, I now believe that enough experimental results have been collected to give this technique an entirely realistic chance of success. In this chapter, I will outline the theoretical background for the determination of protein orientation using chemical shift anisotropy, and the feasibility as well as the expected results of the experiment. I will also present our strategy for constructing such a ^{19}F-labelled cTnC. And in Chapters VI and VII, the specific details of constructing these mutants along with their structural and functional properties will be examined.

Theoretical Background

Excellent expositions on the general theory of NMR are so numerous that the reader would benefit far more by referring to one of those works rather than by reading an abridged version written by me (For a gentle and insightful introduction, please refer to the book by Malcolm Levitt (*17*), more in-depth discussion of the NMR theory can be found in Slichter (*18*). Detailed treatise on chemical shift anisotropy in NMR can be found in Mehring (*19*)). However, certain aspects of NMR theory are crucial to the understanding of how protein orientation can be extrapolated from shapes of ^{19}F signal, therefore I will focus my analysis on those topics relevant to our discussion.

The resonance frequency of any nucleus is determined primarily by the electronic configuration around the nucleus as well as the electrons interaction with the external magnetic field. In most cases, electronic orbitals around a nucleus are not isotropic. This leads to an orientation-dependent variation in the local magnetic environment. Since the local magnetic environment determines the precise resonance frequency of any nucleus (the Zeeman interaction), the final result is a correlation between a nucleus' resonance frequency and the orientation of its electron orbitals relative to the main magnetic field. This effect is commonly referred to as Chemical Shift Anisotropy (CSA). The orientation of electron orbitals surrounding any nucleus is in turn correlated with the geometry of the molecule containing the atom, therefore, in practice, it is often convenient to describe orientation dependency of the resonance frequency in terms of relative orientation between the molecule containing the atom and the external magnetic field.

Mathematically, the relationship between chemical shift and local electronic configuration can be stated as

$$H_{CS} = \gamma\hbar \mathbf{I}\,\tilde{\sigma}\,\mathbf{B}_0$$

where H_{cs} is the contribution to the system Hamiltonian by the chemical shift effect, **I** is the vector representing the angular momentum of the nucleus. $\mathbf{B}_0$ is the vector representing the direction of the magnetic field and $\tilde{\sigma}$ is the second-rank tensor relating the orientation of the magnetic field and nucleus angular momentum with properties of the local electronic orbitals. A second-rank tensor is any bilinear function that takes two vectors as its arguments and returns a scalar value. All second-rank tensors can be represented as 3×3 matrices. The tensor $\tilde{\sigma}$ is commonly referred to as the magnetic shielding tensor. There is no *a priori* reason for the 3×3 matrix representation of the shielding tensor to be symmetric. However, the anti-symmetric portion of the shielding tensor contributes little to the determination of the resonance frequency, therefore we will assume all shielding tensors are symmetric for the sake of simplicity.

The reason for our fondness of symmetric tensors is because eigenvectors of any symmetric matrix form an orthogonal coordinate system (referred to as the principal axis frame). The orientation of the principal axis frame relative to the laboratory coordinate frame can be described using a set of three angles (αβγ) known as the Euler angles. The Euler angles are the rotational angles required to align the principal axis frame with the laboratory frame. In this discussion, we will also adopt the traditional ZYZ convention for specifying Euler angles, i.e. the first angle specifies the rotation around the Z-axis, the second angle specifies the rotation around the new Y-axis and the third angle specifies the rotation around the final Z-axis. If $\mathbf{I} = (0,0,\mathrm{I}_z)$ and $\mathbf{B}_0 = (0,0,\mathrm{B}_0)$ in the laboratory frame (this is the case in most experimental setup if only the part of nuclear angular momentum commuting with the Zeeman operator is considered) and (α,β,γ) are the Euler angles aligning the principal axis frame with the laboratory frame, then in the coordinates of the shielding tensor frame, the two vector will be represented as:

$$\begin{aligned}\mathbf{I} &= \mathrm{I}_z(\cos\alpha\sin\beta, \sin\alpha\sin\beta, \cos\beta)\\ \mathbf{B} &= \mathrm{B}_0(\cos\alpha\sin\beta, \sin\alpha\sin\beta, \cos\beta)\end{aligned}$$

In the principal axis frame, $\tilde{\sigma}$ will be a diagonal matrix of the form

$$\tilde{\sigma} = \begin{bmatrix} \sigma_{xx} & 0 & 0 \\ 0 & \sigma_{yy} & 0 \\ 0 & 0 & \sigma_{zz} \end{bmatrix}$$

The three non-zero diagonal components are known as principal axis components. Substituting these equations into the representation for H_{cs} gives

$$H_{CS} = \gamma\hbar I_z B_0 (\sigma_{xx} \cos^2 \alpha \sin^2 \beta + \sigma_{yy} \sin^2 \alpha \sin^2 \beta + \sigma_{zz} \cos^2 \beta).$$

For a spin ½ nucleus this implies that the deviation in transition frequency is represented by

$$\omega = \omega_0 (\sigma_{xx} \cos^2 \alpha \sin^2 \beta + \sigma_{yy} \sin^2 \alpha \sin^2 \beta + \sigma_{zz} \cos^2 \beta)$$

where $\omega_0 = \gamma B_0$. This equation is central to our discussion because it is the equation that links the orientation of a molecule with the chemical shift and the line shape of the signal. If the orientation of a fluorinated molecule with respect to the rest of the protein is fixed and known, e. g. the molecule is a fluorinated side chain of one of the residues in the protein, then the orientation of the protein with respect to the laboratory frame can be extrapolated from the tensor frame. Since the orientation of the myofibrils in the laboratory frame can be easily manipulated, the orientation of the protein in the filament can be deduced through a series of coordinate transformations (Figure V-1).

However, determining the full shielding tensor (the values of the three principal axis components and the three Euler angles relating the principal axis frame to the laboratory frame) using the equation above directly is difficult because non-linearities and degeneracies in the equation. Traditionally, the six unknowns are transformed into a new set of six variables that vary linearly with the chemical shift. Then by rotating the aligned

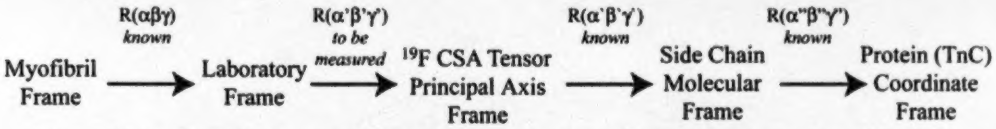
R(αβγ)
known
R(α'β'γ')
to be measured
R(α'β'γ')
known
R(α"β"γ")
known
Myofibril Frame
Laboratory Frame
^{19}F CSA Tensor Principal Axis Frame
Side Chain Molecular Frame
Protein (TnC) Coordinate Frame

Figure V-1. Coordinate transformations required to obtain the orientation of TnC in myofibrils. R(αβγ) denotes the Euler angle-specified rotational matrix needed to align the frame of reference on the left of the arrow with that on the right side of the arrow. The only rotational matrix not known is that aligning the laboratory frame with the ^{19}F shielding tensor principal axis frame.

molecule (usually in the form of 3D crystal) around three orthogonal axis, a set of linear equations relating the chemical shift to the six variables can be obtained and solved. The determination of protein orientation from chemical shifts is similar to that for determination of the full shielding tensor. However, the task is simplified enormously because usually the shielding tensor for the ^{19}F atom in question is already determined, thus the three principal axis components in the equation are already known and only the two Euler angles remain to be resolved. However, the traditional method is unsuited for our purpose owing to the distribution of Tn around the thin filaments. In particular, the last Euler angle, γ, may have a random distribution rather than a singular value. As a result only two Euler angles can be determined unambiguously. So far, the most reliable method for solving the two angles is to explicitly search for the best combination of two angles that produce simulated spectra in good agreement with the experimental results (*15, 20*). To overcome the degeneracy in the equation and improve the certainty of the fitting, spectra of filament at different orientations relative the external magnetic field need to be taken.

Distribution of Tn on the thin filament

Crucial to the feasibility of our experiment is the structure of the thin filament, in particular the arrangement of Tn on the filament. G-actin (globular actin) spontaneously

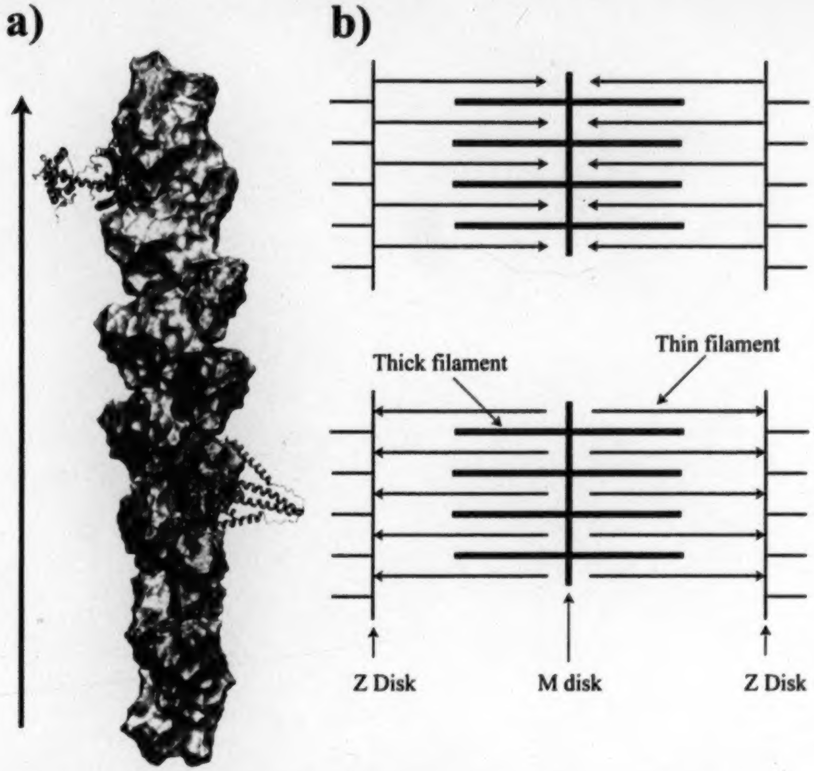

Figure V-2. a) Model of Tn complex (blue and red ribbon) on the actin filament. Tn complex is taken from Ca^{2+}-saturated skeletal Tn complex core structure (PDB access code 1YTZ) and oriented onto the filament according to the orientation specified by Ferguson et al. (*1*). The arrow on the left identifies the polarity of the actin filament. For details on the construction of the actin filament, please consult the Methods section. b) Two possible orientations of the thin filaments in the sarcomere. The orientation of the thin filament is indicated by the direction of the arrow. Both orientations give identical NMR spectra thus are considered equivalent.

polymerizes in the presence of ATP to filamentous actin, or F-actin. The polymer formed is consisted of ADP-bound actins arranged in a helical fashion (Figure V-2a). Each unit of actin can be transformed into the actin at the next position in the filament by a twist of -166.2° and a vertical offset of 27.5Å. The actin filament is a polar entity. That is its two ends are not equivalent. However, the structure of the sarcomere dictates that actin filaments attached to opposite sides of the Z-disk be arranged in anti-parallel fashion.

Thus two possible arrangements of thin filaments in myofibrils are possible and both are equivalent on the macroscopic scale (Figure V-2b). The interaction of Tn with actin filaments also rests on the polarity of the filament. Biochemical studies have shown that one unit of Tn is attached to every seven units of actin molecules. Based on the geometry of the actin filament, this implies each unit of Tn is separated from the next unit by a twist of 83° around the filament as well as an vertical offset of 192.5Å. This helical arrangement of Tn on the filament implies that if ($\alpha\beta\gamma$) are the Euler angles determining the orientation of the Tn complex relative to the myofibrils, all units of Tn in the fibre have identical values for the angles α and β, but different values of the angle γ. Tn attached to anti-parallel actin filaments are related by a change of 180° in the angle α and $(180-2\beta)°$ in the angle β. Because the degeneracy in the equation relating chemical shifts to the Euler angles, both orientations produce the same chemical shift. This is in fact a great advantage since the spectrum will be easier to analyze with only a single signal.

Fluorine-labelling of TnC

By the methodology described above, TnC's orientation in the thin filament can be determined if a fluorine-labelled molecule is attached to TnC with well defined orientation relative to the protein. The label must offer minimal perturbation to protein's structure and function, and to simplify the interpretation of the spectra, only a single label per molecule of protein should be present. It is with these requirements in mind when we decided to used 5-fluorotryptophan (5fW) as our fluorine label.

TnC is naturally devoid of Trp. Our intention is to mutate one of the Phe residues to Trp without disrupting the structure of TnC. Then through special protein expression methods, fluorotryptophan can be incorporated into Trp mutants of TnC. Most EF-hand motifs follow the consensus sequence of h_1**h_2(x)*(y)*(z)*G($-y$)I($-x$)**($-z$)h_3**h_4, where, x, y, z, $-x$, $-y$, $-z$ represent Ca^{2+}-chelating amino acids, * represents any amino acid and h represents hydrophobic amino acids. For the C-terminal domain of cTnC, h_1 and h_2 of the first EF-hand motif, as well as h_3 and h_4 of the second EF-hand motif are Phe. Our decision was to mutate the h_2 of the first EF-hand motif, which is residue 104, and the h_3 of the second EF-hand motif, which is residue 153, to Trp. By putting the mutations on two non-parallel helices near two different Ca^{2+}-binding loops, we reduce the chance of protein misfolding induced by having two mutations on the same helix. The skeletal troponin C equivalents of both mutants containing L-Trp have been studied before (*21, 22*), and the mutations are found to have minimal effects on the biological function of the protein. The advantage of having multiple Trp mutants is that as long as each indole ring possesses an unique orientation, each one can act as an additional restraint on the possible value of α and β angles, reducing the problem of degeneracy. However, spectra of the myofibrils at different orientations may still be needed.

Although 4-fluorotryptophan (4fW) is known to produce less perturbation to protein structures (*23, 24*), 5fW is more popular among investigators because of its modest price tag. As a result, far more information is available about the chemical properties of 5fW than 4fW. In particular, the shielding tensor of the fluorine on 5fW is fully determined. Work by Grage et al. (*15*) and Graether et al. (submitted for publication) showed that the three principal axis components, δ_{11}, δ_{22}, δ_{33}, possess values of 2.3ppm, -73.7ppm and -78.7ppm, respectively, with the Y-axis of the principal axis parallel to the CF bond vector and the positive X-axis of the principal axis on the same side as the amide nitrogen on the indole ring. Figure V-3 shows the simulated powder spectrum of 5fW as well as the expected spectra of myofibrils containing the F104(5fW) and the F153(5fW) mutants. As for the toxicity of 5fW, next chapter will show that by carefully choosing the *E. coli*-expression system used to express the protein, the toxicity of 5fW can be minimized, making the expression of 5fW-containing protein much easier.

Concentration of TnC in Myofibrils

One of the weaknesses of NMR is its lack of sensitivity. This weakness is especially fatal when working with large assemblies such as myofibrils, where the presence of active spins is very dilute. The estimate of TnC concentration in muscle fibres is ~85nmol per cubic centimetre of muscle fibre. Most of native TnC will be extracted by washing myofibrils with EDTA solution so that fluorinated TnC can be inserted by incubating the

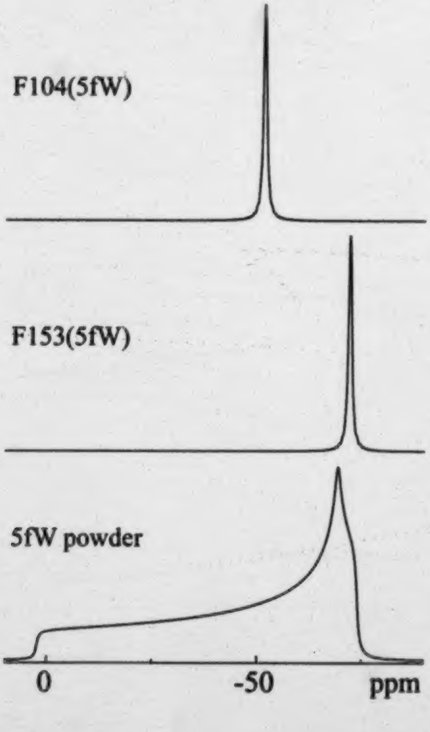

Figure V-3. Simulated ^{19}F NMR spectra of the 5fW powder pattern and myofibrils containing either the F104(5fW) TnC mutant or the F153(5fW) TnC mutant. The myofibril axis is assumed to be parallel to the external magnetic field.

TnC-deficient myofibrils in a buffer containing the fluorinated TnC. This extraction procedure will not completely replace all native Tn in the fibre, therefore the concentration of fluorinated TnC in the fibre can be even lower. However, advancements in NMR spectrometer hardware, such as the advent of microcoil NMR probes, mean the detection of compounds at μM is not impossible. Since only 1D spectra are needed in these experiments, signal-to-noise ratio can be improved if enough number of transients are taken. Thus, although significant challenges are present, we believe NMR is developed enough to overcome it.

Effects of Distribution of Tn on Signal Shape

Although the shape of ^{19}F signal is insensitive to the distribution of Tn on the thin filament when the myofibril axis is parallel to the magnetic field, spectra of the myofibril at different orientations in the magnetic field are needed to obtain unambiguous fit for the Euler angles. To simulate the effect of Tn distribution on the ^{19}F signal when myofibrils are at non-parallel orientations with respect to the magnetic field, we used the *in situ* TnC orientation information obtained by polarized fluorescence to construct a model of Tn complex on the actin filament using the crystal structure of the Ca^{2+}-saturated skeletal Tn core structure (Figure V-2a). From this model, we extracted the Euler angles required to align the shielding tensor frame with the laboratory frame, taking into consideration both the orientation of the myofibril with respect to the magnetic field as well as all the possible arrangement of Tn on the thin filament. Figure V-4 shows the simulated ^{19}F spectra of myofibrils containing the F104(5fW) TnC mutant at various orientations with respect to the magnetic field. The panel of spectra on the left are simulated assuming all

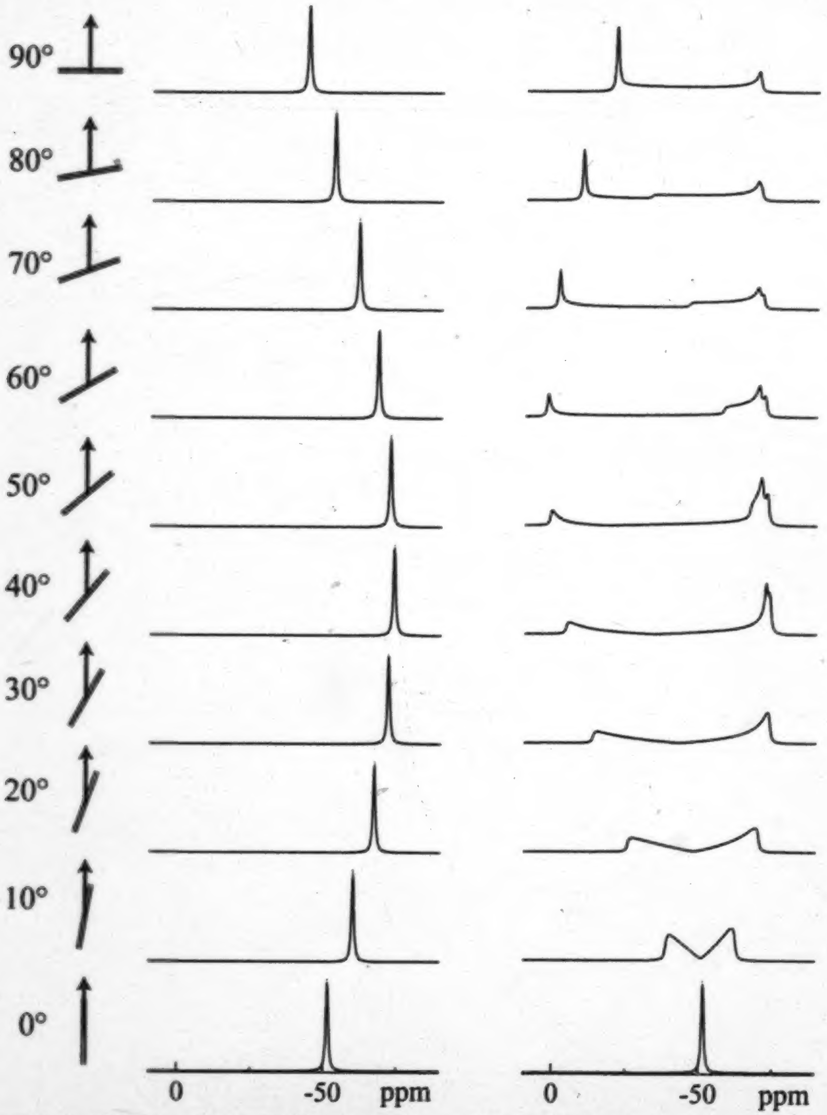

Figure V-4. Effects of myofibril orientation and helical Tn distribution on simulated ^{19}F spectra of myofibrils labelled with the F104(5fW) TnC mutant. The angle between the myofibril axis and the main magnetic field (the arrow) is indicated on the left. The panel of spectra on the left are simulated spectra of the myofibril assuming all Tn are arranged in a line on the thin filament. The panel of spectra on the right are simulated after taking into consideration the helical distribution of Tn on the thin filament. The bottom spectrum of the right hand panel is scaled down by 350% compared to the rest of spectra in the panel.

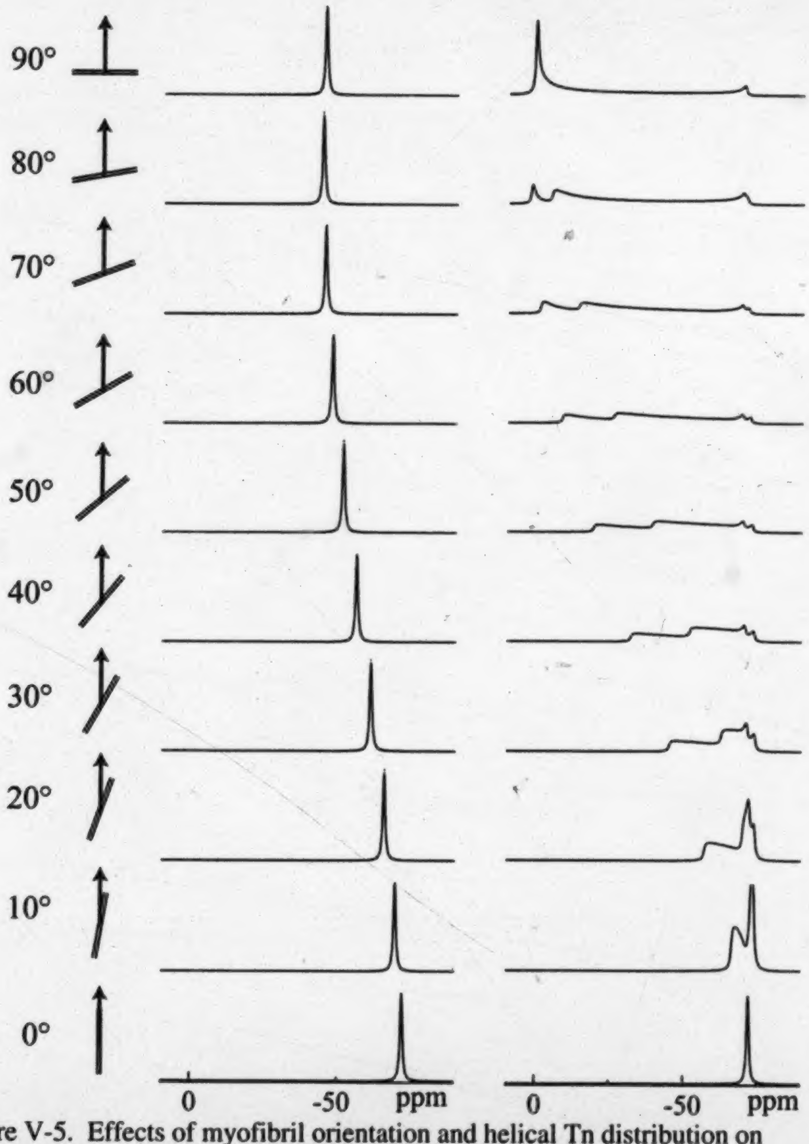

Figure V-5. Effects of myofibril orientation and helical Tn distribution on simulated ^{19}F spectra of myofibrils labelled with the F153(5fW) TnC mutant. The angle between the myofibril axis and the main magnetic field (the arrow) is indicated on the left. The panel of spectra on the left are simulated spectra of the myofibril assuming all Tn are arranged in a line on the thin filament. The panel of spectra on the right are simulated after taking into consideration the helical distribution of Tn on the thin filament. The bottom spectrum of the right hand panel is scaled down by 350% compared to the rest of spectra in the panel.

Tn are arranged on the thin filament in a perfect line and the panel of spectra on the right are simulated by taking into consideration helical distribution of Tn on the thin filament. It is evident that the signals are considerably broadened when the myofibril axis is not aligned with the magnetic field. Figure V-5 shows the same two sets of spectra for myofibrils containing the F153(5fW) mutant. Although the signal shapes are considerably degraded in the figures, the shapes of the signal at different tilt angles are dependent on the orientation of the shielding tensor in the laboratory frame as well as its orientation relative to the protein. Thus by fitting the progression of change in the signal shape, orientation of the shielding tensor relative the myofibril axis, and therefore the orientation of TnC in the myofibril can be obtained.

Effects of side chain dihedral angle fluctuations on signal shape

Another factor that could have an impact on the signal shape is the variations in the side chain dihedral angles of the 5fW residue. Although fluoroindole rings in the F104(5fW) and F153(5fW) mutants do not freely rotate, they do oscillate in a range of side chain conformations. In the ensembles of the experimentally determined structures, both χ^1 and χ^2 angles of the 5fW fluctuate, although the magnitude of change is far bigger for the F104(5fW) mutant than for the F153(5fW) mutant. For the sake simplicity, we will examine only the variation of χ^2 on the signal shape. The fluoroindole ring of the F104(5fW) mutant sweeps out a χ^2 range of 88° while the fluoroindole ring of the F153(5fW) mutant sweeps out a χ^2 range of 22°. Tn proteins likely experience restricted movements in their *in situ* environment, but proteins on the thin filament are still hydrated, thus should still be able to undergo side chain motions such as ring oscillations.

If the ring oscillations occur at a frequency faster than that can be detected with NMR, then only the average conformation will be detected and the spectra would look as if no variations in dihedral angles existed. However, if the motion of the side chain occurs on slow NMR time scale, considerable changes in line shape would be seen. Figure V-6 shows the simulated spectra for ^{19}F-labelled myofibrils at different orientations with respect to the magnetic field. In these simulations, both the helical distributions of Tn complexes as well as variations in χ^2 angles of the 5fW side chain are considered. In the case of the F153(5fW) mutant, the spectra largely resembles those in the right panel of Figure V-5 except line shapes are more spread out due to variations in χ^2. The broadening effect is far more severe in the case of the F104(5fW) mutant, whose χ^2 angle oscillation covers a range four times the size covered by the F153(5fW) mutant (Figure V-6). Overall, the variation in ring orientation offers no extra information while causing severe decrease in signal-to-noise ratio. However, molecular dynamics simulation of the F104(5fW) mutant seems to indicate that the oscillations of its indole ring takes place at a frequency far higher than the range detectable by NMR. Thus, the severe degradation in line shape due to variations in side chain dihedral angles may not be seen.

Other application of the *in situ* NMR system

The *in situ* NMR system of fluorinated TnC embedded in myofibrils described above may have more uses than obtaining the orientations of proteins *in situ*. Another important application of the system may lay in investigations of drug-protein interactions *in situ*. As mentioned in Chapters I to III, Ca^{2+}-sensitizers occupy an important place in modulating cardiac muscle activity. However, no direct experimental evidence exists to

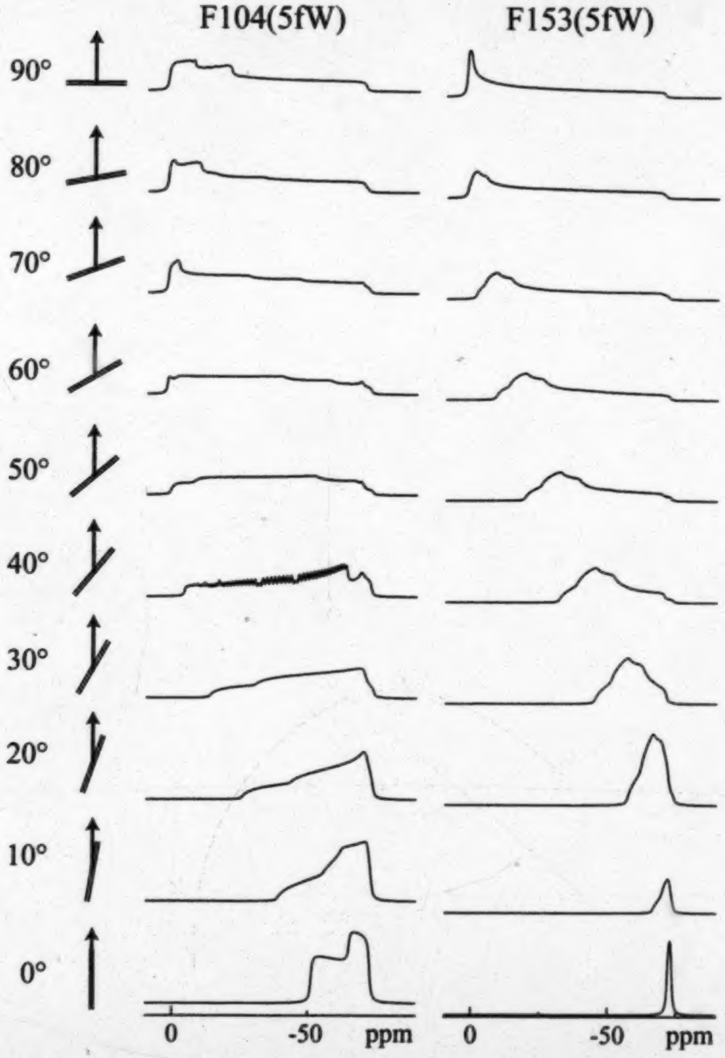

Figure V-6. Effects of side chain dihedral angle χ^2 on spectra of myofibrils. Simulated spectra of fluorine-labelled myofibrils taking into consideration both the helical distribution of Tn around the thin filament as well as variations in χ^2 angle of 5fW. The panel of spectra on the left is simulated assuming myofibril is labelled with the F104(5fW) mutant and the panel of spectra on the right is simulated assuming myofibrils is labelled with the F153(5fW) mutant. The bottom two spectra of the right hand panel are scaled down 300% compared to ~~the rest of the~~ spectra in the panel.

prove that these drugs do interact with TnC *in situ*. Many of the drugs either already contain fluorine or can be easily fluorinated. If the fluorinated drugs are titrated into myofibrils containing fluorinated TnC, the dipolar interaction between the ^{19}F on the protein and ^{19}F on the drug can be easily measured. Theoretically, both the distance between the two fluorines as well as the orientation of the internuclear vector with respect to the magnetic field can be obtained from dipolar coupling measurements. For our purpose, the distance information alone is enough to show direct interactions between the protein and the drug. However, if the interaction between the protein and drug is able to induce weak alignment in drug molecules, the resulting ^{19}F-^{19}F homonuclear residue dipolar coupling constant can be measured easily for the drug and used to model the orientation of interaction between the drug and the protein.

Methods

Construction of Tn-actin filament model: The model of actin filament is constructed using the software package FilaSitus (situs.biomachina.org) using the G-actin structure describes in Wriggers & Schulten (*25*). The axis of the actin filament is arranged to be parallel with the Z-axis of the laboratory frame. The Ca^{2+}-saturated skeletal Tn complex core structure (*7*) is positioned onto the actin filament with TnC in the same orientation described by Ferguson et al. (*1*). The C-terminal domains of the F104(5fW) and the F153(5fW) mutants are then superimposed with the C-terminal domain of the sTnC in the model.

Spectral simulation: Using the coordinates from the above model, Euler angles required to align the ^{19}F CSA principal axis frame of the 5fW in either the F104(5fW) or the

F153(5fW) mutants are calculated using the software package VMD (*26*) and a home-written Tcl script. Euler angles at different orientations of myofibrils are obtained by first rotating the entire model around the Y-axis at 10° intervals and calculating the Euler angles after each rotation. To simulate the helical distribution of Tn around the thin filament, TnC is rotated around the actin filament axis and Euler angles aligning the principal axis frame with the laboratory frame is calculated at each position. To simulate the variations in χ^2 angle of 5fW, the indole ring is rotated around the C_β-C_γ bond through the range seen in experimental structures of the F104(5fW) and the F153(5fW) mutants and Euler angles calculated after each rotation. Sets of Euler angles are then weighted according to the size of solid angle occupied by each point and used as crystallite orientations input files for the software simulation package SIMPSON (*27*). The spectra are simulated as static powder pattern in SIMPSON by specifying a rotor spin rate of 0 and sampling gamma angle of 1.

References

1. Ferguson, R. E., Sun, Y. B., Mercier, P., Brack, A. S., Sykes, B. D., Corrie, J. E., Trentham, D. R., and Irving, M. (2003) *Mol Cell 11*, 865-74.
2. Li, M. X., Spyracopoulos, L., and Sykes, B. D. (1999) *Biochemistry 38*, 8289-98.
3. McKay, R. T., Tripet, B. P., Hodges, R. S., and Sykes, B. D. (1997) *J. Biol. Chem.* 272, 28494-28500.
4. McKay, R. T., Tripet, B. P., Pearlstone, J. R., Smillie, L. B., and Sykes, B. D. (1999) *Biochemistry 38*, 5478-89.
5. Takeda, S., Yamashita, A., Maeda, K., and Maeda, Y. (2003) *Nature 424*, 35-41.
6. Tripet, B. P., Van Eyk, J. E., and Hodges, R. S. (1997) *J. Mol. Biol. 271*, 728-750.
7. Vinogradova, M. V., Stone, D. B., Malanina, G. G., Karatzaferi, C., Cooke, R., Mendelson, R. A., and Fletterick, R. J. (2005) *Proc Natl Acad Sci U S A 102*, 5038-43.
8. Pirani, A., Xu, C., Hatch, V., Craig, R., Tobacman, L. S., and Lehman, W. (2005) *J Mol Biol 346*, 761-72.
9. Pervushin, K., Riek, R., Wider, G., and Wuthrich, K. (1997) *Proc Natl Acad Sci U S A 94*, 12366-71.
10. Gardner, K. H., and Kay, L. E. (1998) *Annu Rev Biophys Biomol Struct 27*, 357-406.
11. Herzberg, O., and James, M. N. G. (1985) *Nature 313*, 653-659.
12. Li, M. X., Spyracopoulos, L., and Sykes, B. D. (1998) *Biophysical Journal 74*, A51.
13. Sia, S. K., Li, M. X., Spyracopoulos, L., Gagné, S. M., Liu, W., Putkey, J. A., and Sykes, B. D. (1997) *J. Biol. Chem. 272*, 18216-18221.
14. Spyracopoulos, L., Li, M. X., Sia, S. K., Gagné, S. M., Chandra, M., Solaro, R. J., and Sykes, B. D. (1997) *Biochemistry 36*, 12138-12146.
15. Grage, S. L., Wang, J., Cross, T. A., and Ulrich, A. S. (2002) *Biophys J 83*, 3336-50.
16. Hull, W. E., and Sykes, B. D. (1975) *J Mol Biol 98*, 121-53.
17. Levitt, M. H. (2001) *Spin Dynamics: Basics of Nuclear Magnetic Resonance*, 1st edition ed., John Wiley & Sons.
18. Slichter, C. P. (1990) *Principles of Magnetic Resonance*, 3rd ed. ed., Springer-Verlag, New York.
19. Mehring, M. (1983) *Principles of High Resolution NMR in Solids*, 2nd ed. ed., Springer-Verlag, Berlin.
20. Ulrich, A. S. (2005) *Progress in Nuclear Magnetic Resonance Spectroscopy 46*, 1-21.
21. Trigo-Gonzalez, G., Racher, K., Burtnick, L., and Borgford, T. (1992) *Biochemistry 31*, 7009-15.
22. Chandra, M., McCubbin, W. D., Oikawa, K., Kay, C. M., and Smillie, L. B. (1994) *Biochemistry 33*, 2961-9.
23. Pratt, E. A., and Ho, C. (1975) *Biochemistry 14*, 3035-40.
24. Browne, D. R., Kenyon, G. L., and Hegeman, G. D. (1970) *Biochem Biophys Res Commun 39*, 13-9.
25. Wriggers, W., and Schulten, K. (1999) *Proteins 35*, 262-73.

26. Humphrey, W., Dalke, A., and Schulten, K. (1996) *J Mol Graph 14*, 33-8, 27-8.
27. Bak, M., Rasmussen, J. T., and Nielsen, N. C. (2000) *J Magn Reson 147*, 296-330.

Chapter VI

Expression of Fluorinated Proteins and The Effect of Expression System on Expression Level and Protein Structural Integrity

Introduction

The unique properties of fluorine make it an ideal reporter atom for NMR studies of biological systems (*1*). Its inherent absence in most natural organisms reduces its background noise in NMR spectra. The high gyromagnetic ratio of this spin ½ nucleus coupled with 100% natural abundance make the detection of fluorine signal much easier than those of ^{13}C or ^{15}N atoms. The electronic structure of the fluorine atom makes its resonance frequency far more sensitive to its magnetic environment than most other atoms, leading to a wide chemical shift spread. Although in most cases this property would be an advantage, the wide chemical shift spread also implies an increase in transverse relaxation in solution due to a large CSA. In some instances, this will partially cancel out the sensitivity gain from having the high gyromagnetic ratio.

The history of fluorine in protein NMR is a long and productive one. It has found useful application in both organic and inorganic chemistry (*2-4*). In the field of protein chemistry, ^{19}F NMR spectroscopy is used to probe conformation changes, denaturation events as well as dynamics. Many reagents are used to fluorine label the protein of interest (*5*). Biosynthetic incorporation of fluorinated-amino acids is amongst the most popular schemes used for this purpose. The advantage of this method is that the fluorinated amino acids often resemble the natural amino acid in both form and chemical property, thus eliciting minimal disruption to the protein's structure and function. On the other hand, many fluorinated compounds carry considerable toxicity to bacteria. This does not come as a surprise as fluorine can produce unpredictable properties in common chemicals. A good example would be fluoroacetic acid, a plant toxin known to be lethal at only milligram doses. Toxicity of fluorinated amino acids means that special care would be needed to ensure the incorporation of fluorinated amino acids into the protein of interest without killing the host bacterium. Usually this implies that bacteria are exposed to high concentration of fluorinated amino acids only during the induction period. The down side to this strategy is that it is difficult to achieve 100% ^{19}F-labelling consistently. Another popular scheme used to ^{19}F-label proteins involves chemical modification of reactive residue side chains. Cysteine and lysine side chains are usually the candidate in these schemes owing to their chemically active side chain groups. The chemical reactions involved in attaching the fluorine label to the residue side chain are quite robust in general, which means 100% fluorine-labelling of the target side chains are often attainable. And since only normal proteins are required, the inconvenience and time consuming procedure used to fluorine-label proteins biosynthetically need not be applied. The disadvantage of this method is that the ^{19}F-label is often large and bulky, increasing the possibility of label-induced modification to protein structure and function. Most labels also incorporate many freely rotatable bonds, which lead to increased dynamics and flexibility of the label. This diminishes the information content obtainable from ^{19}F reporter atoms because the most important information revealed by these labels is often distance- and orientation-related. For these reasons, it is usually preferable to use fluorinated amino acid as the fluorine label rather than attaching the label by chemical modifications.

Early in the days of ^{19}F NMR of proteins, a number of studies have been conducted to find the optimum condition for biosynthetic incorporation of fluorinated amino acids into proteins. Pratt et al.(*6*) and Browne et al.(*7*) have independently examined the relative toxicity of fluorotryptophans. Both found that 4-fluorotryptophan (4fW) supported bacterial growth better compared to 5- (5fW) or 6-fluorotryptophan (6fW) (for an illustration of the indole ring carbon numbering system and proton nomenclature, see Figure VI-1b). They also examined the specific activity of fluorotryptophan-containing β-galactosidase and found, once again, 4fW-containing isomers of the enzyme have far higher activity compared to 5fW and 6fW. Despite the early hints implicating 5fW's role in inducing misfolding in proteins, 5fW continues to enjoy wide spread usage in the community (*8-11*). A number of subsequent studies (both theoretical and experimental) proved that in some proteins, the perturbation is minimal. The most interesting observation was that a polar ^{19}F atom can sit comfortably inside a hydrophobic pocket

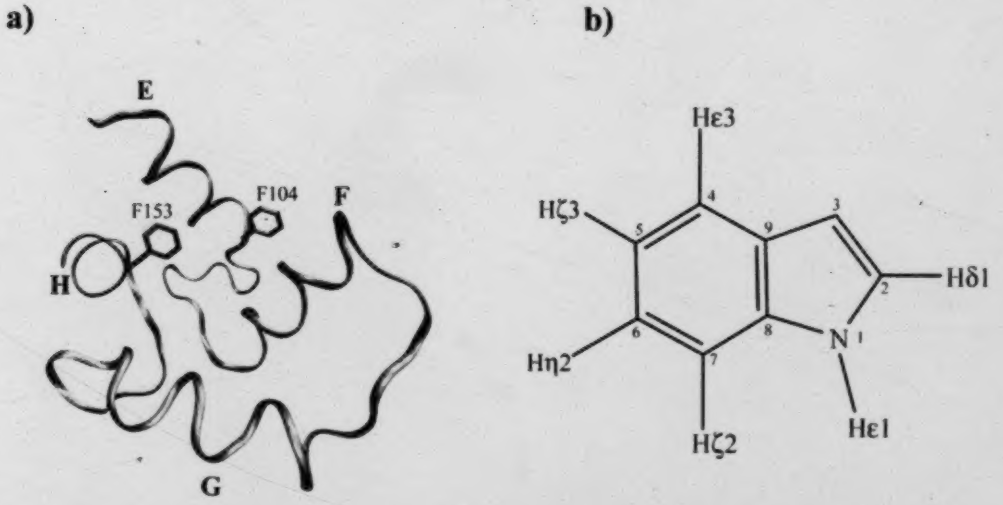

Figure VI-1. a) Ribbon representation of the C-domain of the wild type chicken cTnC. Side chains of F104 and F153 (sites of mutation) are labelled red and blue. b) Indole ring of Tryptophan. Numbering of the carbon is illustrated. Each proton is labelled using nomenclature used in the paper. In 5fW, Hζ3 is replaced with a ^{19}F atom.

without disturbing the hydrophobic core packing (*9*).

However, even with results from these studies, expressing fluorinated proteins biosynthetically can be a frustrating affair. Practical knowledge on how different fluorinated amino acids affect bacterial growth and protein structure as well as which strain of *E. coli* is the best host for expressing proteins in the presence of fluorinated amino acids is limited. In this study, I systematically investigated the effect of 4fW and 5fW on the folding properties of F104W and F153W cTnC mutants, as well as the effect of different *E. coli* strains (BL21 vs. W3110TrpA33) on the expression level and property of the protein. Overall, I found that BL21 had very low tolerance for 5fW and produced proteins that exhibited abnormal Ca^{2+} binding behaviour. BL21 tolerated 4fW better and the observation of abnormal Ca^{2+}-binding has diminished considerably for the 4fW-containing proteins, which isn't a surprise considering the early studies done by Pratt et al. and Browne et al. The *E. coli* Trp-auxotroph W3110TrpA33 was found to be very tolerant of 5fW and produced a much higher yield of protein, which exhibited the same Ca^{2+}-binding behaviour as normal cTnC. The 5fW incorporation efficiency of the Trp-auxotroph is also believed to be higher since Trp-auxotroph is unable to convert other aromatic amino acids to Trp the way fully competent strains are able to. Thus this study has shown that not only is it important to choose the appropriate fluorinated amino acids for a project, the strain of bacteria used to express the fluorine-labelled protein is also a crucial factor.

Experimental Details

Site directed mutagenesis: cloned A-Cys human cardiac troponin C cDNA in a pET3a vector was used as the template in the construction of the F104W and F153W mutants by site directed mutagenesis. F104W mutant was produced using the method of site-directed mutagenesis by overlap primer extension(*12*). Primers 5'-CCCGCGCCCCGCCATATGGATGACATCTACAAGGCT-3' (cTnC-5') and 5'-TTTGTCCCACATGCGGAAGAGGTC-3' (F104-3') were used to clone one half of the mutant cDNA while primers 5'-TGACCTCTTCCGCATGTGGGACAAA-3' (F104-5') and 5'-ACGACAGTGGATCCTCAGCATCTACTCCACAC-3' (cTnC-3') were used to clone the second half of the cDNA. The two halves were subsequently connected by performing PCR using the products from the first round as templates and primers cTnC-5' and cTnC-3' as extending primers. The full length mutant cDNA is then digested with NdeI and BamHI and ligated into pET3a fragments that were pre-cut with NdeI and BamHI. F153W mutant was produced by PCR using primers cTnC-5' and 5'-ACGACAGTGGATCCCTACTCCACACCCTTCATGAACTCCAGCCACTCATCATAG-3' (F153-3') and wild type cDNA as template. In all cases the underlined bases in the primer sequences are the mismatching bases that introduced the mutation into the protein. All primers were synthesized by the DNA core facility at Department of Biochemistry, University of Alberta.

Expression of 5fW- and 4fW-labelled F104W and F153W mutants in BL21(DE3)pLysS: In this study, a combination of unlabelled and $^{15}N/^{13}C$-labelled proteins containing either

L-tryptophan, 5fW, 4fW have been used. Proteins containing normal tryptophan was expressed in *E. coli* strain BL21(DE3)pLysS using the procedure described in Chapter V.

Incorporation of 4fW and 5fW into the expressed protein was promoted by first inhibiting the aromatic amino acid synthesis using 1g/L glyphosate, an inhibitor of the 5-enolpyruvylshikimic acid-3-phosphate synthase (*13, 14*). Aromatic amino acids Tyr, Phe and Trp are then supplemented exogenously at a concentration of 100mg/L. When the culture has reached an OD_{600} between 0.8 to 1.0, 150mg of either D,L-5fW (Sigma, F0896) or D,L-4fW (Sigma, F7376) was added. Half hour later, the culture was induced using 120mg/L IPTG. And the induction was carried out for 3 hours before the culture is harvested.

Expression of 5fW- and 4fW-labelled F104W and F153W mutants in W3110TrpA33: To achieve a high fluorine incorporation efficiency, 5fW-containing mutants were also expressed in Trp auxotrophic strain W3110TrpA33. The cells was infected with phage DE3 and transformed with plasmid pLysS to provide the bacteria with the appropriate RNA polymerase for protein expression (*15*). In this procedure, 1 litre of minimal M9 medium containing 100mg of L-Trp was seeded with 10ml of overnight culture grown in LB at 37°C and grown at the same temperature. When the cells have reached an OD_{600} of ~1.0, they were spun down at 4°C for 10min with a 4400g centrifugal force and the pellet was re-suspended in fresh M9 media containing no Trp and grown for 30 minutes at 37°C. 150mg/L of D,L-5fW was then added at the end of the 30 minutes. After which cells were grown for another 30mins before induction was initiated with 120mg/L of IPTG. The culture was then harvested 3 hours after induction.

Purification of the mutants: The harvested cells were pelleted and then re-suspended in 25mM Tris buffer with 1mM PMSF, pH 8.0. The re-suspended cells were French pressed with a pressure of 11000psi and debris removed by centrifugation at 31000g. Expressed proteins were found mostly in the supernatant. The undiluted supernatant was then applied to a DEAE-sephadex (A25) column equilibrated with a buffer of 50mM Tris, 0.1M NaCl, pH 8.0. The column was washed extensively with the equilibration buffer at a flow rate of 0.6ml/min before the protein was eluted with a 0.1M to 0.45M NaCl salt gradient. The fractions containing the expressed proteins were pooled and lyophilized and re-dissolved in approximately 30ml of a buffer containing 5mM $CaCl_2$, 50mM KCl, 50mM Tris and 1mM MgCl, pH 7.5. The sample solution was loaded onto a phenyl-sepharose column equilibrated with the same buffer. The column was washed with the same buffer for 5 to 8 hours at a flow rate of 0.6ml/min before an elution buffer containing 50mM Tris and 1mM EDTA, pH 7.5 is applied. The intact TnC was eluted as a single sharp peak.

Sample Preparation and Calcium titrations: All samples used for data collection contained 1.0 to 1.5mM of protein, 100mM KCl, 10mM imidazole, 1.5mM DSS, 10% D_2O, and 0.05% NaN_3. The sample pH was around 6.7. If a Ca^{2+}-saturated sample was required, $CaCl_2$ stock solution was added until Ca^{2+} concentration has reached 10mM. To evaluate ^{19}F's effect on protein, qualitative Ca^{2+} titrations of the protein were performed as follows: either 0.5μl or 1μl aliquot of 100mM $CaCl_2$ was added to a 500μl sample containing ~1mM of apo protein, pH 6.7 and 100mM KCl, 10mM imidazole, 0.2mM DSS. The titration was monitored with either {^{1}H, ^{15}N}-HSQC or one dimensional ^{19}F spectroscopy, or both. The titration was stopped when the chemical shift and the line shape of the signal have stopped changing.

Data acquisition and analysis: All data were acquired either on a Varian Inova 500 or an Inova 600 spectrometer equipped with 5mm triple resonance probes with *z*-axis pulse field gradients at 30°C. All pulse sequences were obtained from the BioPack pulse sequence package distributed by Varian Inc. and processed using the software package NMRPipe(*16*) and analyzed using NMRView(*17*).

Results

Expression of 5fW-labelled F104W and F153W mutants in BL21 and Their Properties

5fW had a detrimental effect on the growth of BL21 cells. 100mg of 5fW per litre of cell culture is enough to induce complete lysis of all cells during early stage of growth (O.D.$_{600} \leq 0.6$). At higher O.D.$_{600}$, the same amount of 5fW did not stop the bacterial growth completely, but the doubling time of the culture was considerably elongated. To increase fluorotryptophan incorporation efficiency, aromatic amino acid synthesis was first inhibited using glyphosate and exogenous sources of Phe, Tyr and Trp are used to supplement the media. Owing to the toxic nature of 5fW, the culture was grown to an approx OD$_{600}$ of 1.0 before 150mg to 200mg of the racemic mixture of D- and L-5fW was added. During the expression and the purification stages of these mutants, Mg^{2+} and/or Ca^{2+} are constantly present at mM concentrations. As a result, proteins extracted from cell cultures are partially Ca^{2+}- or Mg^{2+}-saturated. Figure VI-2 shows the 1D ^{19}F spectra of BL21-expressed F104(5fW) and F153(5fW) mutants dissolved in a buffer containing no Ca^{2+} or EDTA immediately after purification. In both spectra, two signals are visible with one being slightly broader than the other. EDTA titration of the sample revealed that the broad peak corresponded to the ^{19}F-signal from the Ca^{2+}-saturated and structured form of the C-terminal domain while the sharp peak came from the apo form of the protein. However, when the BL21-expressed apo F104(5fW) mutant was depleted of metal ions and re-titrated with Ca^{2+}, it became obvious that the Ca^{2+} affinity of the protein's C-domain was reduced relative to its N-domain and the most likely cause was 5fW-induced misfolding during the transition from apo to Ca^{2+}-saturated state. Normally, because TnC's C-domain has much higher Ca^{2+} affinity compared to the N-

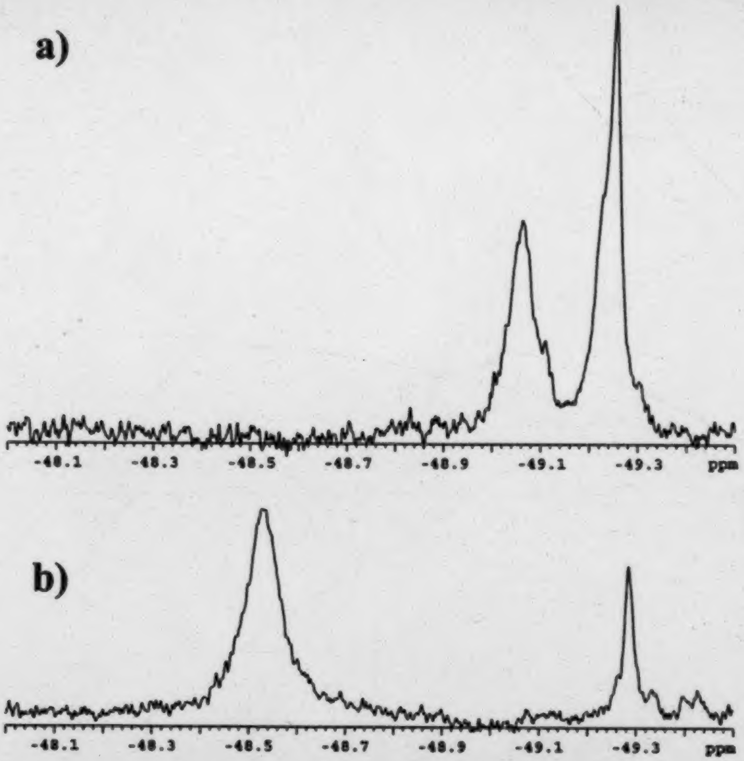

Figure VI-2. 1D ^{19}F NMR spectra of non-Ca^{2+}-depeleted samples of a) the F104(5fW) mutant and b) the F153(5fW) mutant. In both spectra, the broad signal is from the Ca^{2+}-saturated C-terminal domain and the sharp signal is from the apo C-terminal domain.

domain, wild type TnC becomes Ca^{2+}-saturated in the C-domain before significant Ca^{2+}-binding is detected in the N-domain (*18*). This is exemplified by the NMR-monitored Ca^{2+} titration of the F104W mutant presented in Figure VI-3a. However, in BL21-expressed F104(5fW) mutant the N-domain binds Ca^{2+} before the C-domain. This is indicated by the migration of the N-domain G70 amide proton signal upon Ca^{2+} addition before the signal corresponding to amide proton of residue G146 in the Ca^{2+}-saturated C-domain begins to grow in intensity (Figure VI-3b). It was also noted that the final intensities of most signals from the Ca^{2+}-saturated C-domain are only half the size of their counterparts from N-domain. This is in contrast to cTnC isoforms that fold

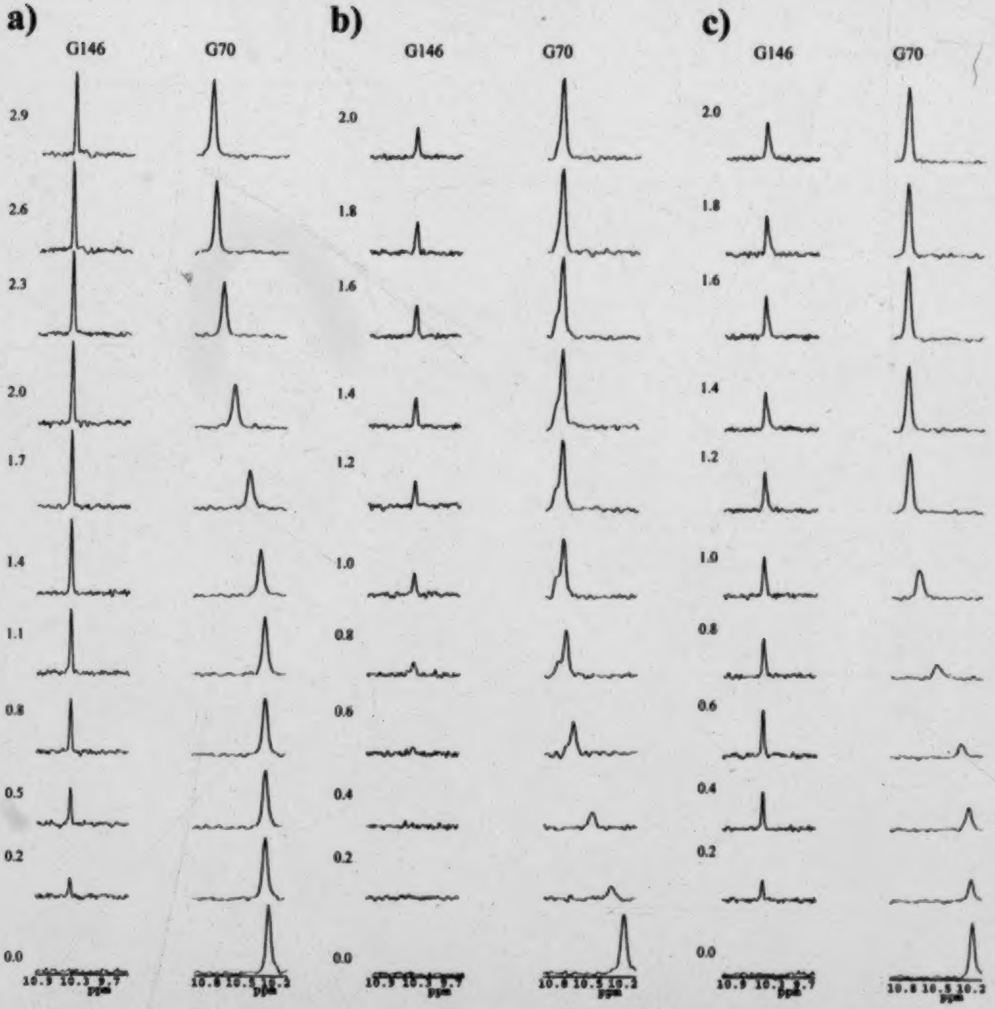

Figure VI-3. 1D traces from {^{1}H, ^{15}N}-HSQC spectra taken during the Ca^{2+} titrations of a) the F104W mutant, b) the BL21-expressed F104(5fW) mutant and c) the BL21-expressed F153(5fW) mutant. In all panels, the strip on the left is the amide proton of residue 146 and the strip on the right is the amide proton of residue 70. In the case of the F104W mutant titration, C-domain was Ca^{2+}-saturated before N-domain is. But in the case of BL21-expressed F104(5fW), the trend is the opposite. The numbers shown on the left side of each panel are the total Ca^{2+} concentration at each point in mM.

normally. In those cases, signals from the Ca^{2+}-saturated C-domain are the same size as those from the N-domain (Figure VI-3a). This indicates that not only is Ca^{2+} affinity of the C-domain reduced, C-terminal domains from a portion of the protein is not folding properly. This hypothesis was further confirmed by 1D ^{19}F spectra taken during the titration, which showed the ^{19}F signal corresponding to the apo state of the C-domain disappear as Ca^{2+} is added, but no single peak arose in its place, as is expected for a protein in two-state slow conformational exchange. Instead, multiple broad signals appeared, an indication that many conformational states of the protein existed (data not shown). To ensure the abnormality is not caused by the mutation from Phe to Trp, I performed Ca^{2+} titrations on mutants containing L-Trp. Both F153W and F104W mutants showed normal pattern of Ca^{2+} binding (a representative set of data from the Ca^{2+} titration of the F104W mutant is shown in Figure VI-3a). Even though the $\{^1H, ^{15}N\}$-HSQC NMR spectra of these Phe-to-Trp mutants in their Ca^{2+}-saturated state are not identical to that of the wild type cTnC (Figure VI-4), the patterns of chemical shift changes upon metal binding are very similar to the wild type and the presence of minor populations or misfolded proteins are not observed. Originally, I thought the observed reduction in the Ca^{2+} affinity and misfolding I saw in the F104(5fW) mutant's C-domain was a consequence of 5fW incorporation. However, the same mutant expressed in *E. coli* Trp auxotrophic strain W3110TrpA33 exhibited normal Ca^{2+} binding patterns (Figure VI-8), thus the phenomenon observed seem to be restricted to the F104(5fW) mutant produced in BL21 cells.

Several hypotheses can be formulated to explain this observation. The 5fW could be modified by enzymes expressed by BL21 but not in W3110TrpA33. However, the ^{19}F

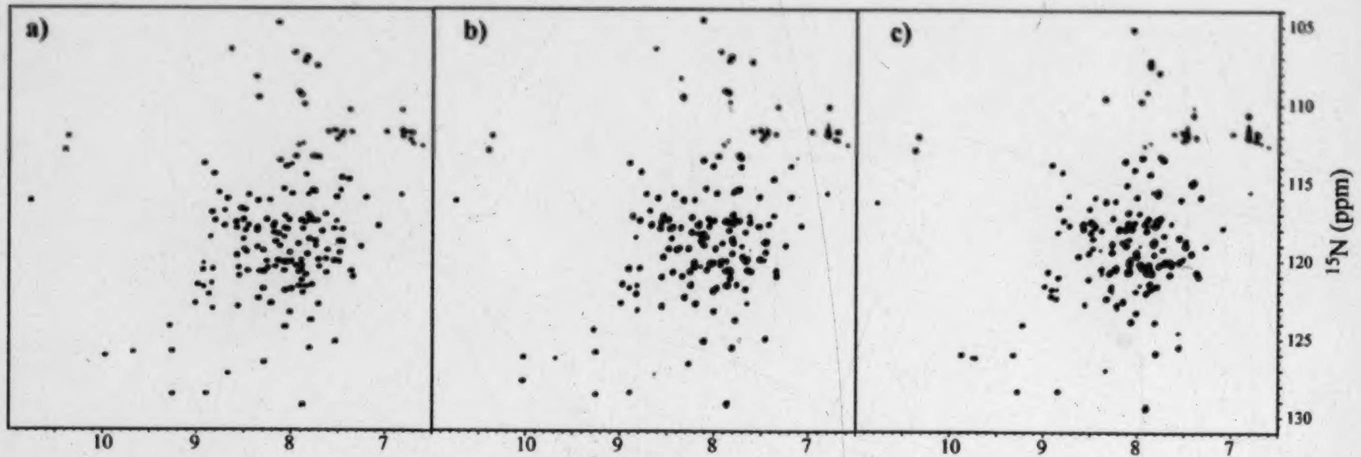

Figure VI-4. {^{1}H, ^{15}N}-HSQC spectra of a) wild type cTnC, b) the F104W mutant and c) the F153W mutant. Peak patterns in all three HSQC spectra are very similar.

chemical shift for both BL21 and W3110TrpA33-expressed apo proteins are similar, indicating that the chemical structure of the indole ring is not significantly altered. Mass spectrometry of the samples showed that the BL21-expressed F104(5fW) mutant sample contained a 14kDa degradation product of TnC, whereas the proteins produced by W3110TrpA33 are intact (Figure VI-5). Combined with the observation that W3110TrpA33 grew much more robustly in the presence of 5fW than BL21, I think that 5fW had far more severe adverse effects on BL21 cells than on W3110TrpA33 cells, leading to the production of higher amount of proteases in BL21. Since the C-domain of TnC is unstructured in its apo state, proteolytic cleavage likely occurred in the C-terminal domain, hampering its ability to bind Ca^{2+}.

The BL21-expressed F153(5fW) mutant also exhibited some signs of abnormal Ca^{2+}-binding. However, the BL21-expressed F153(5fW) mutant was not affected to the same extent as the BL21-expressed F104(5fW) mutant. In particular, {^{1}H, ^{15}N}-HSQC

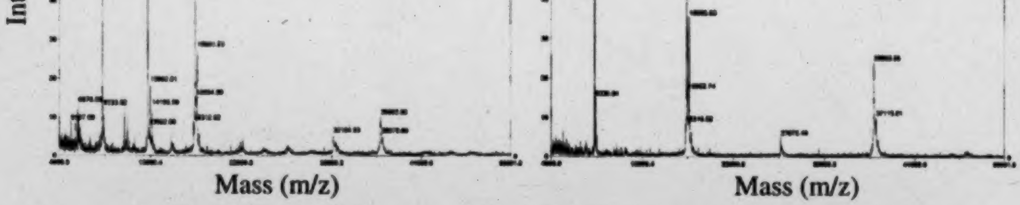

Figure VI-5. Mass spectrometry results for a) BL21-expressed F104(5fW) mutant and b)W3110TrpA33-expressed F104(5fW) mutant. The BL21-expressed mutant contains a sizable signal from a 13.7kDa degradation product of cTnC. Also note the signal produced by the dimer of cTnC at 33kDa.

spectrum signals for C-terminal domain residues exhibited Ca^{2+}-induced chemical shift changes before signals in the N-domain showed any Ca^{2+}-induced chemical shift migration, just like the case with normal cTnC isoforms (Figure VI-3c). However, the signals representing residues from the Ca^{2+}-saturated C-domain is still only half the size as signals from the Ca^{2+}-saturated N-domain. This implies that although the presence of 5fW at position 153 did not change Ca^{2+}-affinity of the C-terminal domain as much as the F104(5fW) mutant, it did induce a noticeable amount of misfolding in the C-terminal domain. In the light of the mass spectrometry information for the BL21-expressed F104(5fW) mutant, this is most likely caused by degradation of the C-terminal domain.

Expression of 4fW-labelled F104W and F153W mutants in BL21 and Their Properties

To study how different fluorotryptophans perturb protein structures, I also produced F104W and the F153W mutants containing 4fW rather than 5fW. As shown by previous investigations, 4fW is less toxic to *E. coli* than 5fW and β-galatosidase containing 4fW had higher activity than isoforms of the same enzyme with 5fW (*6, 7*). Our results seem to collaborate with their conclusions. Figure VI-6 showed 1D traces from $\{^1H, ^{15}N\}$-HSQC spectra taken during the Ca^{2+}-titrations of the F104(4fW) and F153(4fW) mutants. In both cases, C-terminal peaks (G146 is shown in Figure VI-6 as an example) exhibited Ca^{2+}-induced chemical shift changes before the same effect was observed in N-terminal domain peaks. Not only is the Ca^{2+}-binding order preserved in the case of 4fW-containing mutants, signals from residues in Ca^{2+}-saturated C-terminal domain also have about the same intensity as signals from residues in Ca^{2+}-saturated N-terminal domain.

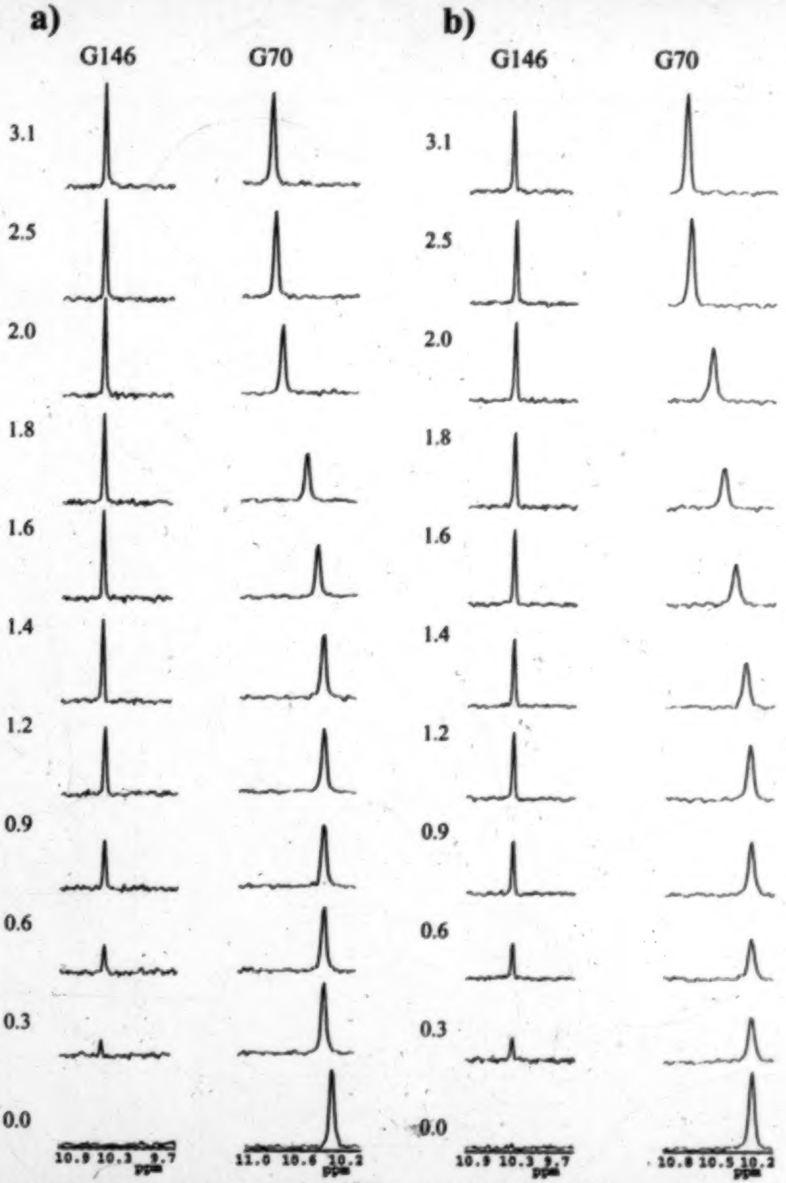

Figure VI-6. 1D traces from {^{1}H, ^{15}N}-HSQC spectra taken during the Ca^{2+} titrations of the BL21-expressed F104(4fW) mutant and b) the BL21-expressed F153(4fW) mutant. The strip on the left is the amide proton of residue 146 and the strip on the right is the amide proton of residue 70. The numbers shown on the left side of each panel are the total Ca^{2+} concentration at each point in mM.

This implies a big portion of the protein has properly folded C-terminal domains, a statement that can not be said for any of the 5fW-containing mutants.

A detailed examination revealed that many residues in 4fW-containing mutants have given rise to two signals in {^{1}H, ^{15}N}-HSQC. Figure VI-7 shows {^{1}H, ^{15}N}-HSQC signals from a representative subset of these residues. After comparing with {^{1}H, ^{15}N}-HSQC spectrum of the mutant containing L-Trp, it became obvious that the phenomenon is caused by incomplete fluorotryptophan incorporation. For each pair of signals, one peak always corresponds exactly to a signal in the {^{1}H, ^{15}N}-HSQC spectrum of L-Trp labelled protein, thus this peak represents the isoform containing L-Trp while its neighbouring peak represents the isoform containing 4fW. For this particular sample of the F104(4fW) mutant, the intensities of the two peaks in the pair are approximately equal, implying only 50% of the protein contain 4fW.

Expression of 5fW-labelled F104W and F153W mutants in W3110TrpA33 and Their Properties

W3110TrpA33 is a strain of *E. coli* that has been rendered Trp auxotrophic by the E48M mutation in its Trp synthetase A protein (*19*). Compared to BL21 cells, W3110TrpA33 cells were considerably more robust when grown in the presence of 5fW. Yields of 5fW-labelled mutants expressed in W3110TrpA33 are as good as that of BL21 cells grown in the presence of L-Trp. This robustness made expressing uniformly ^{15}N, ^{13}C-labelled protein possible. Figure VI-8 shows 1D traces from HSQC spectra taken during Ca^{2+}-titration of W3110TrpA33-expressed F104(5fW) mutant. Both the Ca^{2+}-binding order of the domains as well as the peak intensities from Ca^{2+}-saturated isoforms

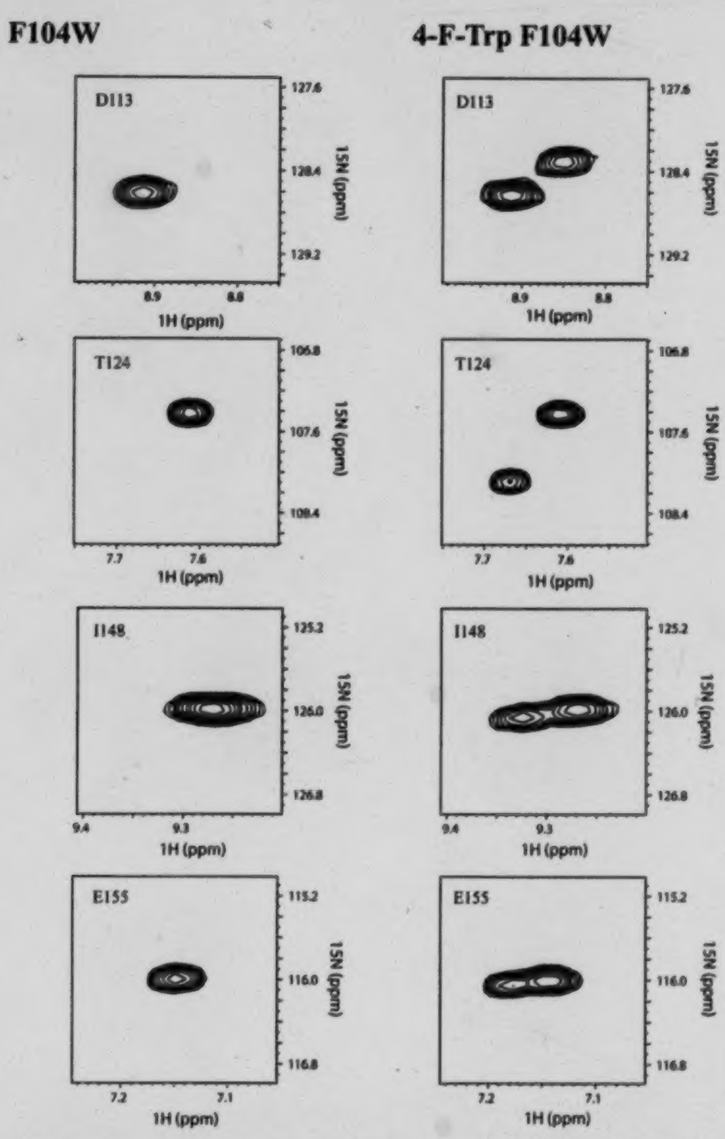

Figure VI-7. Comparisons between portions of {^{1}H, ^{15}N}-HSQC spectra for F104W and F104(4fW) mutants. One peak in the F104(4fW) mutant {^{1}H, ^{15}N}-HSQC spectrum corresponds exactly to a signal in the F104W spectrum, thus represents the Trp-labelled form of the mutant, while the additional signal represents the 4fW-labelled version of the mutant.

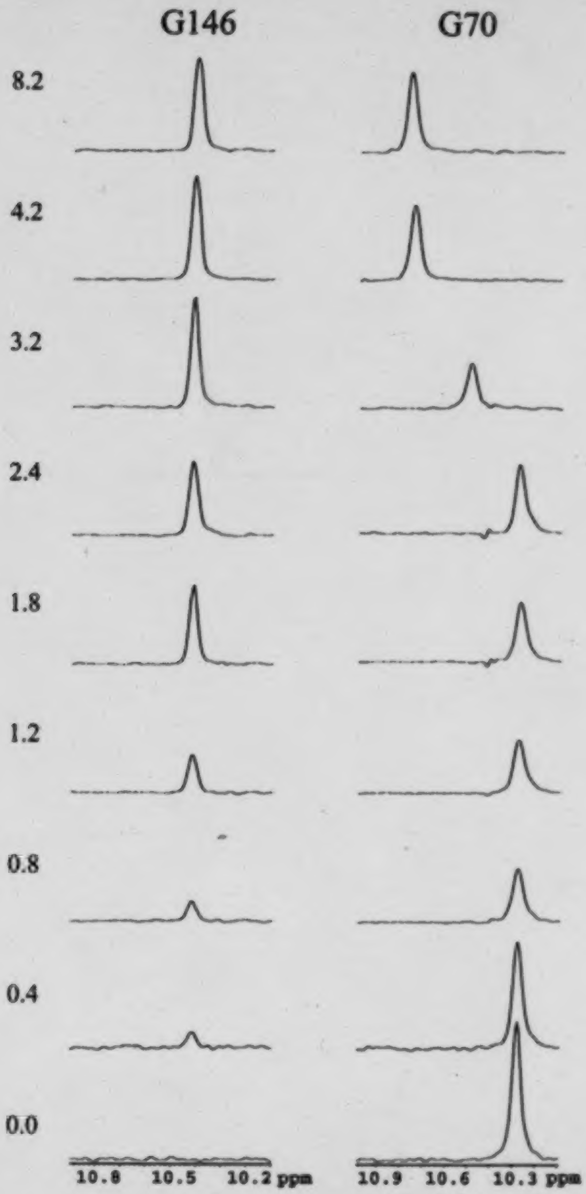

Figure VI-8. 1D traces from {^{1}H, ^{15}N}-HSQC spectrum taken during the Ca^{2+} titrations of the W3110TrpA33-expressed F104(4fW) mutant. The strip on the left is the amide proton of residue 146 and the strip on the right is the amide proton of residue 70. The numbers shown on the left side of each panel are the total Ca^{2+} concentration at each point.

are identical to L-Trp labelled proteins. This is in contrast to the same mutant expressed in BL21 cells, which showed neither the correct Ca^{2+}-binding order nor the appropriate signal intensities expected from a sample with the fully folded C-terminal domain. This demonstrates that not only is the form of fluorotryptophan being used a determining factor in whether expression of fluorine-labelled protein can be successful, the *E. coli* system used to express the protein can also be an important factor. Although the data is not shown in Figure VI-8, the F153(5fW) mutant expressed in W3110TrpA33 cells also exhibited the same Ca^{2+}-binding behaviour as that of wild type cTnC.

Discussion

Although Trp auxotrophic *E. coli* strains are the most convenient system for producing fluorotryptophan-labelled proteins, in many instances genetic manipulations are required to prepare the strain as a proper expression host for the protein. This is a skill beyond the expertise of most ordinary protein chemists, therefore normal *E. coli* strains are often recruited to express fluorotryptophan-labelled proteins when no appropriate Trp auxotrophic strain is available. To increase bacteria's uptake of fluorotryptophans, the endogenous production of Trp is often shutdown by adding excess fluorotryptophan to the medium. A variation of this strategy, which is employed in this study, used the 5-enolpyruvylshikimic acid-3-phosphate synthase inhibitor glyphosate to stop aromatic amino acid synthesis, creating a pseudo-auxotrophic strain which requires exogenous sources of aromatic amino acids. It is not a perfect Trp-auxotrophic strain since the bacteria is still capable of converting Phe or Tyr to Trp. Nonetheless, this study demonstrated that there are disadvantages to this approach. Inhibition of the natural amino acid synthesis can induce the expression of other enzymes. These changes in bacterial metabolism can lead to degradation and modification of the protein of interest, leading to lower yield and modified protein properties. The results also revealed the importance of screening for an *E. coli* strain with a high tolerance to the fluorinated amino acid being used. BL21, which is robust and adaptable in most scenarios, has very low tolerance for 5fW. The presence of 5fW at a concentration of 100mg/L was enough to stop bacterial growth when O.D.$_{600}$ was less than 0.6. At higher O.D.$_{600}$, although bacteria did continue to grow, the stressed cells produced higher levels of proteases that degraded the protein of interest.

Although the mass spectrometry results clarifies nicely the differences in signal intensities observed between F104(5fW) mutants expressed in BL21 and W3110TrpA33, it does not necessarily reveal why the Ca^{2+}-binding order of the domains is also disrupted in the case of BL21 cells. One of the possible reasons is that the presence of 5fW triggered the expression of a number of metabolic enzymes in BL21, leading to the modifications of the fluorinated amino acid into a form that is more perturbing to protein structure than the native 5fW. The reason as to why the strain W3110TrpA33 is more tolerant of 5fW than BL21 cells most likely lay in the differences in their genetic makeup, a topic beyond the scope of discussion.

The suitability of 4fW as a ^{19}F-label for proteins has been confirmed once again by this study. Its effect on bacterial growth is much more benign compared to 5fW and 4fW-containing mutants exhibited neither Ca^{2+}-binding abnormality nor any sign of protein degradation. The rational reason behind 4fW's inertness has not been thoroughly investigated and the effort it takes to understand this phenomenon is probably greater than the reward. But the reason behind 4fW's lack of popularity amongst the ^{19}F NMR community is most likely its prohibitively expensive price tag, which is almost 10 times that of 5fW.

Conclusion

In this study, I used NMR spectroscopy to investigate the effects of 4fW and 5fW incorporation, as well as different *E. coli* expression systems on the Ca^{2+}-binding properties of cTnC, with the aim of developing a functional ^{19}F-labelled cTnC for use in *in situ* ^{19}F NMR. I found that BL21 cells have very low tolerance of 5fW, leading to significant protein degradation and abnormal Ca^{2+}-binding behaviour. 4fW is found to be more benign to BL21 cells than 5fW. Ca^{2+}-binding behaviours of 4fW-containing mutants are identical to that containing L-Trp and no excessive protein degradation was detected. Interestingly, the *E. coli* Trp auxotrophic strain W3110TrpA33 was much more tolerant of 5fW than BL21 and produced 5fW-containing mutants that exhibited the same kind of Ca^{2+}-binding behaviour as wild type cTnC. Overall, this study has shown that not only is the choice of fluorotryptophan important to the success of obtaining fluorine-labelled protein, the strain of bacteria used in the expression system is also crucial.

References

1. Hull, W. E., and Sykes, B. D. (1975) *J Mol Biol 98*, 121-53.
2. Cornelissen, G., Van Noort, P. C. M., Nachtegaal, G., and Kentgens, A. P. M. (2000) *Environmental Science & Technology 34*, 645-649.
3. Sobolev, A. V., Krupoder, S. A., Liskovskaya, T. I., and Danilovich, V. S. (2000) *Journal of Structural Chemistry 41*, 338-339.
4. Dalvit, C., Flocco, M., Veronesi, M., and Stockman, B. J. (2002) *Combinatorial Chemistry & High Throughput Screening 5*, 605-611.
5. Sykes, B. D., and Weiner, J. H. (1980) in *Magnetic Resonance in Biology* (Cohen, J. S., Ed.) pp 171-196, John Wiley & Sons, New York.
6. Pratt, E. A., and Ho, C. (1975) *Biochemistry 14*, 3035-40.
7. Browne, D. R., Kenyon, G. L., and Hegeman, G. D. (1970) *Biochem Biophys Res Commun 39*, 13-9.
8. Salopek-Sondi, B., Vaughan, M. D., Skeels, M. C., Honek, J. F., and Luck, L. A. (2003) *J Biomol Struct Dyn 21*, 235-46.
9. Campos-Olivas, R., Aziz, R., Helms, G. L., Evans, J. N., and Gronenborn, A. M. (2002) *FEBS Lett 517*, 55-60.
10. Anderluh, G., Razpotnik, A., Podlesek, Z., Macek, P., Separovic, F., and Norton, R. S. (2005) *J Mol Biol 347*, 27-39.
11. Abbott, G. L., Blouse, G. E., Perron, M. J., Shore, J. D., Luck, L. A., and Szabo, A. G. (2004) *Biochemistry 43*, 1507-19.
12. Ho, S. N., Hunt, H. D., Horton, R. M., Pullen, J. K., and Pease, L. R. (1989) *Gene 77*, 51-9.
13. Steinrucken, H. C., and Amrhein, N. (1980) *Biochemical and Biophysical Research Communications 94*, 1207-1212.
14. Comai, L., Sen, L. C., and Stalker, D. M. (1983) *Science 221*, 370-371.
15. Valencia, F. F., Paulucci, A. A., Quaggio, R. B., Da Silva, A. C., Farah, C. S., and Reinach, F. C. (2003) *J Biol Chem 278*, 11007-14.
16. Delaglio, F., Grzesiek, S., Vuister, G. W., Zhu, G., Pfeifer, J., and Bax, A. (1995) *J. Biomol. NMR 6*, 277-293.
17. Johnson, B. A., and Blevins, R. A. (1994) *J. Biomol. NMR 4*, 603-614.
18. Li, M. X., Saude, E. J., Wang, X., Pearlstone, J. R., Smillie, L. B., and Sykes, B. D. (2002) *Eur Biophys J 31*, 245-56.
19. Drapeau, G. R., Brammar, W. J., and Yanofsky, C. (1968) *J Mol Biol 35*, 357-67.

Chapter VII

Effects of Phe-to-Trp Mutations and 5fW-Incorporation on the Solution Structure of Cardiac Troponin C

Introduction

As the determination of high-resolution protein structures becomes easier and information in structural biology begins to accumulate, many scientists have come to the realization that knowing the structure of a single protein is no longer adequate in many situations. Far more insight can be gained by understanding how proteins interact with each other. Thus, researchers are switching their focus to investigating the behaviour of proteins in complex with other macromolecules in their *in situ* environment. However, owing to the sizes of these complexes, conventional structural biology techniques often are not applicable. As a result, a new approach is often used to investigate these large complexes: structures of proteins composing the complex are first solved individually, then by obtaining a few crucial pieces of information regarding their relative distances and orientations to each other in the complex, the structure of the entire complex can be constructed(*1*). NMR has been an indispensable tool in structural biology(*2, 3*). Besides being useful in elucidating high-resolution protein structures in solution, solid-state NMR can also be an effective tool for *in situ* investigations(*4-6*). By strategically placing only a few receptor atoms in the complex, much information can be obtained regarding the orientation and the motions of the proteins in the complex. In particular, the technique of ^{19}F NMR spectroscopy can be an excellent medium to implement this methodology.

The history of fluorine in protein NMR is a long and productive one. It has found useful applications in both organic and inorganic chemistry(*7-9*). In the field of protein chemistry, ^{19}F NMR spectroscopy is used to probe conformation changes, denaturation events as well as dynamics. Many reagents are used to fluorine label the protein of interest(*10*). Biosynthetic incorporation of fluorinated amino acids is amongst the most popular schemes used. However, despite the wide spread use of these compounds, very few systematic studies have been conducted to investigate fluorine's perturbation on protein structures.

In the early days of ^{19}F NMR of proteins, a number of studies have been conducted to find the optimum conditions for biosynthetic incorporation of fluorinated amino acids into proteins. Pratt et al.(*11*) and Browne et al.(*12*) have independently examined the relative toxicity of fluorotryptophans. Both found that 4-fluorotryptophan (4fW) supported bacterial growth better than 5- (5fW) or 6-fluorotryptophan (6fW) (for an illustration of the indole ring carbon numbering system and proton nomenclature, see Figure VII-1b). They also examined the specific activity of fluorotryptophan-containing β-galactosidase and found, once again, 4fW-containing isomers of the enzyme have far higher activity compared to 5fW and 6fW. Despite the early hints implicating 5fW's role in inducing misfolding in proteins, 5fW continues to enjoy wide spread usage in the community(*13-16*). A number of subsequent studies (both theoretical and experimental) proved that in some proteins, the perturbation is minimal. The most interesting observation was that a polar ^{19}F atom can sit comfortably inside a hydrophobic pocket without disturbing the hydrophobic core packing(*14*).

In this paper, we studied the effects of fluorinated amino acid 5fW on the structure of human cardiac troponin C, a classic Ca^{2+}-binding EF-hand protein responsible for regulating muscle contraction. Our motive for studying the ^{19}F-labelled cTnC comes from a desire to investigate the mechanism of TnC-mediated muscle regulation. With a

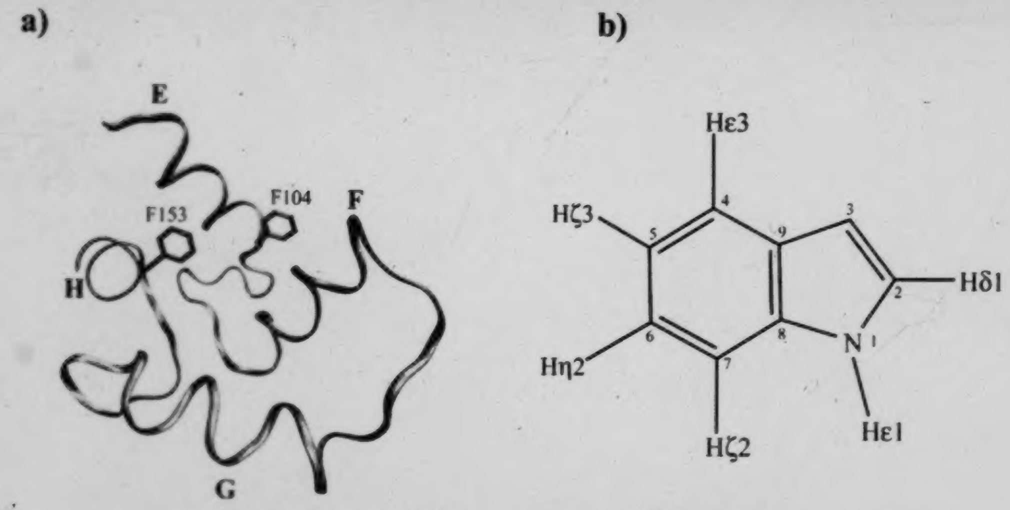

Figure VII-1. a) Ribbon representation of the C-domain of the wild type chicken cTnC. Side chains of F104 and F153 (sites of mutation) are labelled red and blue. b) Indole ring of Tryptophan. Numbering of the carbon is illustrated. Each proton is labelled using nomenclature used in the paper. In 5fW, Hζ3 is replaced with a ^{19}F atom.

^{19}F-labelled cTnC, solid-state NMR techniques can be applied to obtain orientational information for the protein(*17*). Knowing how cTnC changes its orientation as muscle contracts and relaxes will be valuable to the construction of the muscle regulatory model. To engineer such a ^{19}F-labelled TnC isoform, we utilized the lack of Trp in wild type TnC's sequence to construct F104W and F153W mutants of cTnC that can be labelled with fluorotryptophans (Figure VII-1a). A study done on the F105W mutant of skeletal TnC (the skeletal analog of the F104W mutant) by Trigo-Gonzalez reasoned, from an observed red shift in the absorbance spectrum of the F105W mutant, that Ca^{2+}-binding caused the tryptophan ring to become more buried(*18*). No changes in Ca^{2+}-binding affinity of the C-domain was observed by them. Chandra et al. did a thorough study on the sTnC analog of the F153W mutant and found the mutant to have comparable biological activity and secondary structure as the wild type sTnC. Interestingly, they observed a 2-fold decrease in the Ca^{2+}-binding affinity of the mutant. They attributed this to the destabilization of sTnC's hydrophobic pocket packing by the bulky side chains of tryptophan. In this study, we closely scrutinized the effects of Phe-to-Trp substitutions as well as 5fW incorporation on the structure of cTnC. Using NMR techniques, we determined the high resolution structures of all four isoforms of the protein, putting the emphasis on the structure of the C-domain where the substitutions reside. The orientation of the indole ring in each isoform is also carefully determined using data from homonuclear NOE as well as ^{19}F-^{1}H heteronuclear NOE experiments.

Experimental Details

Site directed mutagenesis: cloned A-Cys human cardiac troponin C cDNA in a pET3a vector was used as the template in the construction of the F104W and F153W mutants by site directed mutagenesis. The F104W mutant was produced using the method of site-directed mutagenesis by overlap primer extension(*19*). Primers 5'-CCCGCGCCCCGCCATATGGATGACATCTACAAGGCT-3' (cTnC-5') and 5'-TTTGTCCCACATGCGGAAGAGGTC-3' (F104-3') were used to clone one half of the mutant cDNA while primers 5'-TGACCTCTTCCGCATGTGGGACAAA-3' (F104-5') and 5'-ACGACAGTGGATCCTCAGCATCTACTCCACAC-3' (cTnC-3') were used to clone the second half of the cDNA. The two halves were subsequently connected by performing PCR using the products from the first round as templates and primers cTnC-5' and cTnC-3' as extending primers. The full length mutant cDNA was then digested with NdeI and BamHI and ligated into pET3a fragments that were pre-cut with NdeI and BamHI. The F153W mutant was produced by PCR using primers cTnC-5' and 5'-ACGACAGTGGATCCCTACTCCACACCCTTCATGAACTCCAGCCACTCATCATAG-3' (F153-3') and wild type cDNA as template. In all cases the underlined bases in the primer sequences are the mismatching bases that introduced the mutation into the protein. All primers were synthesized by the DNA core facility at Department of Biochemistry, University of Alberta.

Expression of the protein and incorporation of fluorotryptophan into F153W and F104W mutants: To achieve a high fluorine incorporation efficiency, 5fW-containing mutants were also expressed in *E. coli* Trp auxotrophic strain W3110TrpA33 that was infected with phage DE3 and transformed with plasmid pLysS(*20*). In this procedure, 1 litre of minimal M9 medium containing 100mg of L-Trp was seeded with 10ml of overnight culture grown in LB at 37°C and grown at the same temperature. When the cells have reached an OD_{600} of ~1.0, they were spun down at 4°C for 10min with a 4400g centrifugal force and the pellet was re-suspended in fresh M9 media containing no Trp and grown for 30 minutes at 37°C. 150mg/L of D,L-5fW was then added at the end of the 30 minutes. After which cells were grown for another 30mins before induction is initiated with 120mg/L of IPTG. The culture is then harvested 3 hours after induction.

Purification of the mutants: The harvested cells are pelleted and then re-suspended in 25mM Tris buffer with 1mM PMSF, pH 8.0. The re-suspended cells were French pressed with a pressure of 11000psi and debris removed by centrifugation at 31000g. Expressed proteins were found mostly in the supernatant. The undiluted supernatant was then applied to a DEAE-sephadex (A25) column equilibrated with a buffer of 50mM Tris, 0.1M NaCl, pH 8.0. The column was washed extensively with the equilibration buffer at a flow rate of 0.6ml/min before the protein was eluted with a 0.1M to 0.45M NaCl salt gradient. The fractions containing the expressed proteins were pooled and lyophilized and re-dissolved in approximately 30ml of a buffer containing 5mM $CaCl_2$, 50mM KCl, 50mM Tris and 1mM MgCl, pH 7.5. The sample solution was loaded onto a phenyl-sepharose column equilibrated with the same buffer. The column was washed with the same buffer for 5 to 8 hours at a flow rate of 0.6ml/min before an elution buffer containing 50mM Tris and 1mM EDTA, pH 7.5 was applied. The intact TnC will be eluted as a single sharp peak.

Sample Preparation and Calcium titrations: All samples used for data collection contained 1.0 to 1.5mM of protein, 100mM KCl, 10mM imidazole, 1.5mM DSS, 10% D_2O, and 0.05% NaN_3. The sample pH was around 6.7. If a Ca^{2+}-saturated sample was required, $CaCl_2$ stock solution is added until Ca^{2+} concentration has reached 10mM. To evaluate ^{19}F's effect on protein, qualitative Ca^{2+} titrations of the protein were performed as follows: either 0.5μl or 1μl aliquot of 100mM $CaCl_2$ was added to a 500μl sample containing ~1mM of apo protein, pH 6.7 and 100mM KCl, 10mM imidazole, 0.2mM DSS. The titration was monitored with either {^{1}H, ^{15}N}-HSQC or one dimensional ^{19}F spectroscopy, or both. The titration was stopped when the chemical shift and the line shape of the signal have stopped changing.

Data acquisition and analysis: All data were acquired either on a Varian Inova 500 or an Inova 600 spectrometer at 30°C except the 3D aliphatic ^{13}C-edited NOESY for the F153W, which was collected on the Inova 800 spectrometer equipped with 5mm triple resonance probe with triple axis gradients. The 500- and 600-MHz spectrometers were equipped with 5mm triple resonance probes with *z*-axis pulse field gradients. With the exception of the ^{19}F-^{1}H heteronuclear NOE experiment, all pulse sequences were obtained from the BioPack pulse sequence package distributed by Varian Inc. A mixing time of 75ms was used for all 3D NOESY experiments used to derive distance restraints for structure calculations. All data were processed using the software package NMRPipe(*21*) and analyzed using NMRView(*22*). Backbone assignments were done using data from HNCO, HNCACB(*23*), CBCACONNH(*24*) spectra. The software package Smartnotebook(*25*) was used to expedite the process. Since most secondary structures in cTnC are α-helices, d_{NN} contacts from the 3D ^{15}N-edited NOESY experiment were also used to establish sequential assignments along the back bone. Side chain assignments were done using data from conventional HCCHTOCSY(*26*), HCCONH(*27*) and CCONH(*28*) experiments. The β-methylene protons and the methyl groups on Val and Leu in the mutants were not stereo-specifically assigned.

Structural determination: All proton distance restraints used in determining structures are derived from 3D aliphatic and aromatic ^{13}C-edited NOESY and ^{15}N edited NOESY automatically using CYANA version 2 (*29*). NMRView was first used to automatically generate a peak list for each NOESY spectrum. The lists were then manually edited to remove spectral artefacts and noise. Some unambiguous peaks representing long range contacts were also assigned manually before the lists are supplied to CYANA. Dihedral angle restraints obtained using TALOS(*30*) were also included in the calculation. The automatic NOE assignments in CYANA were carried out using a tolerance of 0.025ppm for the directly-detected dimension, 0.04ppm for the indirectly-detected proton dimension and 0.5ppm for the ^{13}C or ^{15}N dimension. No distance restraints were allowed to be shorter than 1.8Å or longer than 6Å. Distance calibration in CYANA was done using a simple but robust scheme: peaks with median intensity were assumed to represent a distance of 3.1Å. Distance restraints from peaks with other intensities were extrapolated from this standard using the R^6 distance relationship commonly used for calibrating NOE distances. 24 crystal structure-derived distance restraints between Ca^{2+} ions and chelating side chains were also used in the structure calculation. The automatic NOE assignment module in CYANA uses an 8-round iterative structure refinement protocol in which 100 random structures were calculated in the first round with no restraints applied and 50 structures were calculated for each successive round using NOE assignments based on previous round's structures. After 8 rounds, 20 minimum energy structures were chosen from the 50 calculated as the final ensemble. Because the two globular domains of cTnC were known to be independent of each other, the default NOE assignment script was modified to eliminate any possible NOE assignments connecting C-terminal domain atoms with N-terminal domain atoms. The automatic back bone dihedral angle estimation feature of CYANA was not used since experimentally determined back bone dihedral angles were available. The set of CYANA-optimized structures was further refined using a water-refinement protocol (*31*) implemented under the software package Xplor-NIH (*32*). For CYANA calculations, the force field parameter and topology for 5fW were defined exactly the same way as those for L-Trp. The force field parameter and topology for 5fW in Xplor-NIH calculations were adapted from those for L-Trp by changing atom type for atom HZ3 to fluorine and modifying the charges on HZ3 and CZ3 to -0.25 and 0.25, respectively. Bond angles, bond lengths as well as improper dihedral angles concerning these two atoms were not changed.

^{19}F-^{1}H Heteronuclear NOE Determination: The distance restraints between ^{19}F and ^{1}H were determined using data from a ^{19}F-^{1}H heteronuclear NOESY experiment (FHOESY), whose pulse sequence was adapted from a pulse sequence designed to measure heteronuclear NOEs (*33, 34*) for use with ^{19}F. In particular, ^{19}F was the indirectly-detected nucleus and ^{1}H was the observed nucleus. No decoupling of ^{19}F was necessary

during the acquisition since there is only one ^{19}F atom per molecule. Mixing times of 150ms and 75ms were used for the F104(5fW) and the F153(5fW) mutants, respectively.

Molecular dynamics simulations of Ca^{2+}-saturated F104(5fW) and F153(5fW) mutants

To gauge the dynamic behaviour of the 5-fluoroindole rings, 10ns molecular dynamics simulations of both F104(5fW) and F153(5fW) mutants were conducted. Both simulations were carried out using the GROMACS software package (http://www.gromacs.org) with a simulation temperature of 300K and a time step of 2fs. GROMOS96 force field parameters were used for the protein and SPC model of water was used for the solvent. Force field parameters for 5fW were modified from those for L-Trp by changing the mass as well as the non-bonded parameters for the HZ3 atom of the residue to that for the fluorine atom. Charges on HZ3 and CZ3 are also modified to -0.25 and 0.25 to reflect the increased dipole moment for the CF bond. Long range electrostatic interactions were treated using particle mesh- Ewald algorithm with a range of 1nm. The protein was first solvated in a solvent-filled box with the dimension 5.635nm×5.635nm ×5.635nm. Eleven Na$^+$ ions were also added to neutralize the total system charge. Orientation changes of the 5-fluoroindole ring during the simulations were analyzed using the g_sgangle program, which is also part of the GROMACS software package.

Results

Effects of ^{19}F incorporation on Backbone Amide Proton/Nitrogen Chemical Shifts

In many situations, the replacement of a proton by a ^{19}F atom is considered a conservative substitution. Presence of only a single ^{19}F atom often changes little in the way of steric and electrostatic interactions in the region. However ^{19}F does possess a different electronic configuration than a proton. Under the right circumstances, this can induce a change in the local magnetic environment, which can manifest itself as changes in the chemical shifts of nuclei surrounding it. The HSQC spectrum of the F104(5fW) mutant largely resembles that of the F104W mutant (Figure VII-2). With the exception of the backbone amide nitrogen chemical shifts of a few residues on the F helix, no other significant chemical shift differences between the two mutants were observed. However, many residues in the F153(5fW) mutant give two signals in the $\{^1H, ^{15}N\}$-HSQC (Figure VII-2). All of these residues are found in the C-domain of the protein. Each pair of signals consist of a strong and a weak peak with the weak peak having exactly the same chemical shifts as a peak in the F153W mutant $\{^1H, ^{15}N\}$-HSQC. Besides residue 153 itself, other residues exhibiting discernable signal doubling included residues 98, 100, 119, 121, 136, 137, 148, 154 to 158. All the residues are mapped to a region close to the location of the ^{19}F atom (Figure VII-3). This signal doubling is a manifestation of the incomplete 5fW-labelling of the protein. For residues close to the indole ring, the amide nitrogen and amide proton chemical shifts are sensitive enough to detect the difference between a ^{19}F atom and a proton. The fact that signal doubling was not seen with the F104(5fW) mutant means that either the ^{19}F incorporation is more complete for the F104(5fW) mutant, or the side chain of 5fW in the F104(5fW) mutant is not close

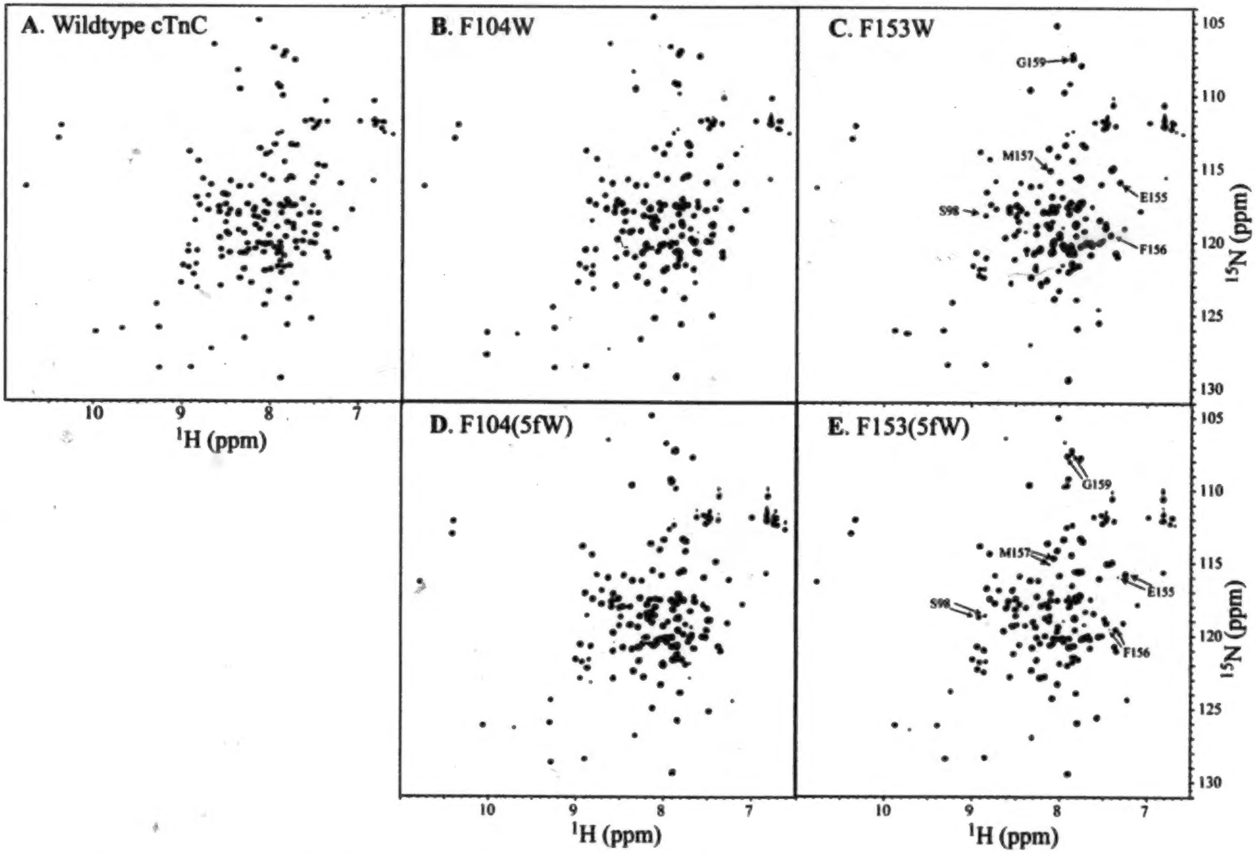

Figure VII-2. {^{1}H, ^{15}N}-HSQC spectra of a) wild type cTnC, b) the F104W mutant, c) the F153W mutant, d) the F104(5fW) mutant, E) the F153(5fW) mutant. Peak patterns in all five HSQC spectra are very similar. Signals from some residues exhibiting signal doubling in the {^{1}H, ^{15}N}-HSQC spectrum of the F153(5FW) mutant are labelled in panels C) and E).

enough to any residue to produce a significant change in the chemical shifts of amide protons and nitrogens. However, even in the case of F153(5fW) mutant, not every residue close to the ^{19}F atom exhibited signal doubling. In particular, residues 112 and 117 showed no change in their amide nitrogen/proton chemical shifts. No signal doubling was observed in any atom other than the amide nitrogen and amide proton. This is not surprising since amide nitrogen and amide proton are known to be much more sensitive to the environment than the side chain atoms.

Structures of the mutants

To evaluate the effects of the mutations and the 5fW-incorporation on the structure of TnC, we determined the solution structures of all four mutants using NMR techniques; and compared them to the structure of the wild type chicken cTnC (PDB access code 1AJ4) determined by Sia et al.(*35*). To solve the structures, conventional methodology

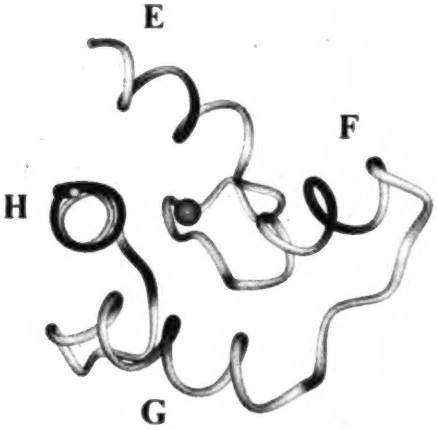

Figure VII-3. Visual representation of the ^{19}F-induced signal doubling in {^{1}H, ^{15}N}-HSQC of the F153(5fW) mutant. Residues exhibiting the signal doubling phenomenon are coloured red on the ribbon representation of the backbone structure of the F153(5fW) mutant. The ^{19}F atom is shown as an orange sphere. All residues are found in the vicinity of the ^{19}F atom.

used in multidimensional protein NMR was followed. In particular, chemical shift assignments of the backbone atoms (N, C_{α}, HN) were first established using data from the HNCACB(*23*)and CBCACONNH(*36*) experiments. Chemical shifts of the side chain ^{13}C and ^{1}H were then assigned using data from the HCCHTOCSY(*26*), HCCONH(*27*) and CCONH(*37*) experiments. Once the proton chemical shifts were known unambiguously, data from 3D aliphatic and aromatic ^{13}C-edited NOESY as well as 3D ^{15}N-edited NOESY experiments were automatically analyzed using CYANA. Distance and dihedral restraints derived from the data were then used to generate structures using both CYANA and Xplor-NIH. For more details on this procedure, please consult the experimental section.

Of all the structures solved in this study, none had a significantly different N-domain structure compared to the wild type chicken cTnC. This is not surprising since the N-domain sequence of the mutants (residues 1 to 90) shares 100% identity with the N-domain sequence of wild type chicken cTnC. Together with the fact that the two domains of cTnC do not interact at all in solution, substitutions localized to the C-domain should have no effect on the N-domain. Therefore, the following analysis on the structures of the mutants will focus entirely on the C-domain, with the emphasis on the orientations of the indole ring in each structure.

(1) Structures of F104W and F104(5fW) mutants

The Phe-to-Trp mutation at position 104 resulted in a change of approx. 2.5ppm and 2.6ppm in the residue's amide nitrogen and alpha carbon chemical shifts, respectively (1.5ppm and 2.2ppm after correcting for the change in residue type and assuming random structure(*38*)) as compared to the wild type cTnC. The replacement of L-Trp with 5fW in the mutant did not induce additional perturbation judging by the small amide proton/nitrogen chemical shift differences between the F104W and the F104(5fW) mutants. The only significant amide nitrogen chemical shift changes induced by the incorporation of 5fW occurred to a few residues on the F helix (residues 119, 120, 121 and 124). This is not surprising since the side chains of these residues are very close to atom Hζ3 of the indole ring. However, no significant chemical shift changes were seen with any other atoms in these residues.

In this study CYANA was used to automatically assign and calibrate the signals in all 3D NOESY spectra. The procedure is very robust if a carefully filtered peak list and accurate backbone dihedral angles are supplied. For the F104W mutant, CYANA was able to find a total of 1545 unambiguous distance restraints with 183 of them long range restraints. Structure calculation carried out using these restraints and the dihedral angle restraints derived using TALOS revealed that the structure of the F104W mutant is very similar to that of the wild type cTnC (Figure VII-4a). The 20 lowest energy structures from a total of 50 structures calculated superimposed with a backbone RMSD of 0.80±0.14Å while the backbone of the well defined region superimposed with a RMSD of 0.62±0.11Å (see Table VII-1 for definition of well-defined region). A total of 89.8% of all back bone dihedral angles are in the most favoured region of the Ramachandran map (Table VII-1). The major difference between the wild type cTnC and the F104W mutant lies in the interhelical angles between helices E and F, as well as helices G and H, with the F104W mutant being slightly more "open" compared to the wild type (Table VII-2, Figure VII-5a). The situation for the F104(5fW) mutant is similar. CYANA found 1272 unambiguous distance restraints for this protein, the least of all mutants. Out

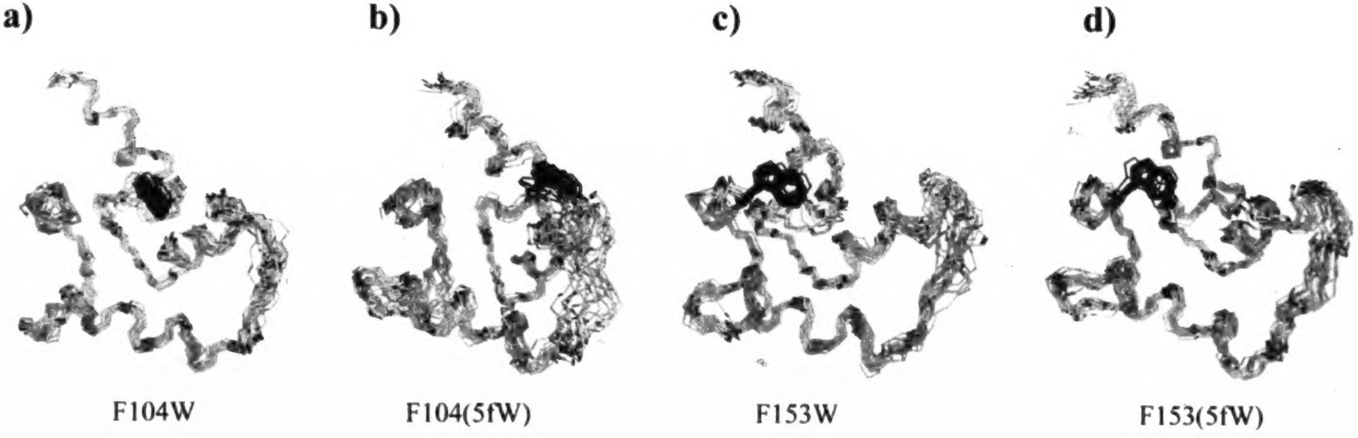

F104W F104(5fW) F153W F153(5fW)

Figure VII-4. Ensembles of back bone structures of a) the F104W mutant, b) the F104(5fW) mutant, c) the F153W mutant and d) the F153(5fW) mutant. Each ensemble contains the superimposition of 20 lowest energy structures from the 50 calculated. Only residue from 95 to 158 is shown in each ensemble.

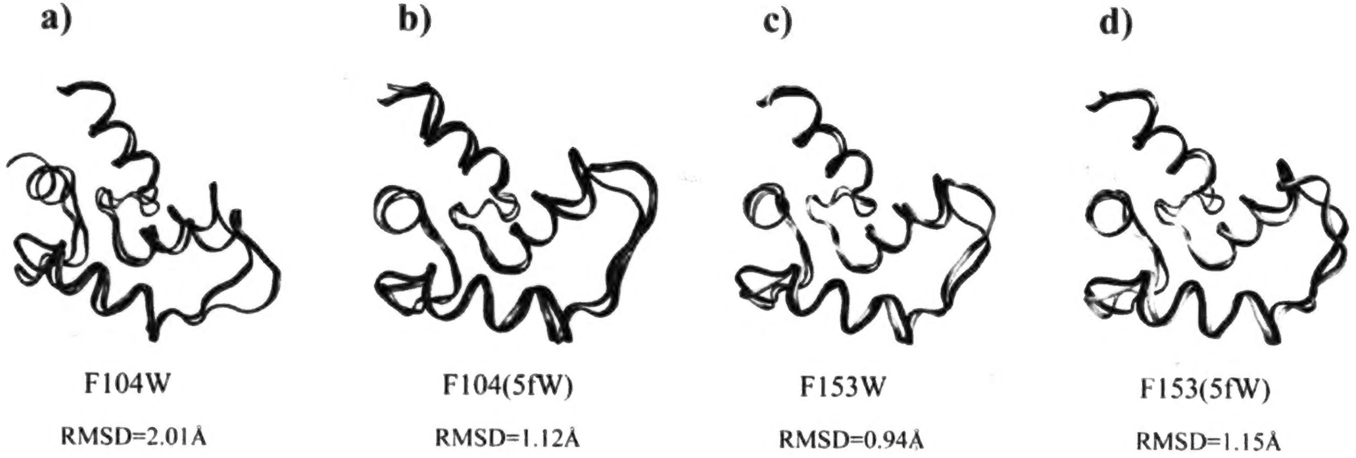

a) F104W RMSD=2.01Å

b) F104(5fW) RMSD=1.12Å

c) F153W RMSD=0.94Å

d) F153(5fW) RMSD=1.15Å

Figure VII-5. Ribbon representations of back bone superimposition of the wild type chicken cTnC structure (PDB code 1AJ4) with a) the F104W structure (red), b) the F104(5fW) structure (grey), c) the F153W structure (orange), d) the F153(5fW) structure (yellow). The wild type structure is shown in blue in all superimpositions. RMSDs between the mutant structures and the wild type structure are shown below each ribbon representation. In all panels, the

of all the restraints, 122 are long range restraints. Despite the smaller number of restraints, the backbone RMSD of 20 lowest energy structures superimposed is 0.94±0.15Å, with the well-defined region having a RMSD of 0.61±0.12Å, almost as good as the F104W structure. In fact, the structure of the F104(5fW) mutant agrees with the wild type cTnC structure slightly better than the F104W mutant (Figure VII-5b).

For both the F104W and the F104(5fW) mutants, the hydrophobic packing around the indole ring is not significantly disturbed. This is not surprising since the side chain of residue 104 is not deeply buried in the hydrophobic core. It lies above the hydrophobic core, with fewer packing constraints compared to the side chain of residue 153. In the F104 mutant structures, variations in the orientation of the indole ring are mostly determined by changes in the χ^2 angle for the Trp residue. From the 3D aromatic ^{13}C-edited NOESY data, a number of unambiguous distance restraints involving indole ring protons were obtained (Figure VII-6a). Structure calculations showed all restraints are consistent with each other and a single, well defined orientation of the indole ring, with side chain χ^2 dihedral angle of ~96° (Table VII-3), was able to satisfy all the restraints. The orientation of the ring is similar but not identical to that of wild type F104 side chain. The Hζ3 atom is pointed down toward the F helix while the Hε1 points toward the side chains of residues 97 and 100. Interestingly, even if no distance restraints are used for any indole ring protons but atoms Hζ3 and Hε1, the ring orientation is still well defined and agrees with the ring orientation obtained with a full set of restraints. This fact turned out to be relevant in defining the 5fW indole orientation in the F104(5fW) mutant. Owing to the lack of ^{13}C-labelling on the ring, we can only obtain NOE data for the fluorine and the Hε1 proton (thanks to its distinct proton chemical shift) on the indole

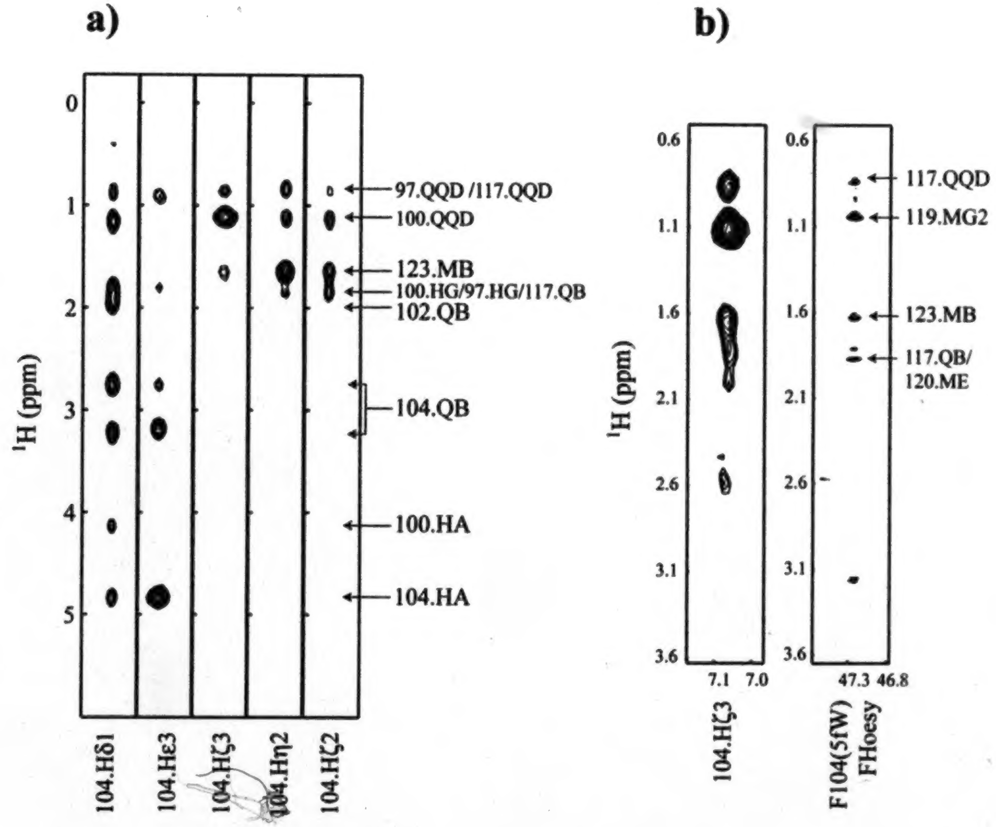

Figure VII-6. a) Strips taken from the 3D aromatic ^{13}C-edited NOESY spectrum of the F104W mutant, illustrating the intramolecular contacts made by the indole ring protons. b) Detailed comparison between the NOE contacts made by the Hζ3 proton on the Trp of the F104W mutant and the ^{19}F atom on the 5fW of the F104(5fW). The NOE contact patterns are virtually identical between the two. Although the intensities of heteronuclear NOE are weaker than that of the homonuclear NOEs, the resolution of the ^{19}F-^{1}H heteronuclear NOE experiment is much higher, allowing to the identification of many unambiguous NOEs.

ring. However, the distance information from the FHoesy experiment is of much higher quality compared to the conventional 3D ^{13}C-edited NOESY because of the higher resolution and lack of spectral overlap in the heteronuclear NOE experiment. Comparing the NOE contact pattern made by the proton Hζ3 on the indole ring with the ^{19}F atom's heteronuclear NOE contact pattern, we see little, if any, difference (Figure VII-6b). This is only possible if the orientation of the 5-fluoroindole ring in the F104(5fW) mutant is similar to that of the indole ring in the F104W mutant. Just as in the F104W case, specifying only distance restraints involving the ^{19}F and Hε1 is enough to produce a well defined ring orientation that is very similar to that of the F104W mutant. In fact, although we were able to obtain the chemical shift assignments for protons Hη2 and Hε3 using the FHoesy experiment, adding distance restraints from these two atoms did not improve the definition of the 5-fluoroindole ring orientation.

(2) Structure of F153W and F153(5fW) mutants

Compared to the F104W mutant, the mutation of Phe to Trp at position 153 produced no change in amide nitrogen and relatively small change in alpha carbon chemical shifts. Since there is no sign of secondary structure change at either position, the difference in mutation-induced chemical shift changes between the two mutation sites could be purely due to differences in dynamics or exposure to solvents at the two sites. The side chain of the F153 residue is a more integrated part of the hydrophobic core than that of F104. Replacing the Phe with the bulky Trp, and subsequently the bulkier 5fW, could be potentially disruptive to the overall packing of the core. However, the physiological study done by Chandra et al. showed that the mutant has the same physiological activity as the wild type while the Ca^{2+} affinity is decreased only by half(*39*). Inspection of the {^{1}H, ^{15}N}-HSQC of either the F153W mutant or the F153(5fW) mutant showed that both have well folded C-domains.

The 3D aliphatic ^{13}C-edited NOESY spectrum of the F153W mutant was collected on the INOVA 800 MHz spectrometer. The better sensitivity and the high resolution of the spectrum are reflected in the large number of distance restraints CYANA was able to derive from the data. A total of 2111 unambiguous restraints were found with 273 of them being long range restraints, the most of all mutants. The 20 lowest energy structures, of a total of 50 calculated, superimposed with a back bone RMSD of 0.82±0.10Å, 0.62±0.12Å for the well-defined regions. Almost 92% of all back bone dihedral angles are found in the most favoured region of the Ramachandran map. The interhelical angles between helices E and F, and helices G and H of the F153W mutant also agreed well with the wild type C-domain structure. The back bone RMSD between the F153W mutant and the wild type C-domain structure is only 0.94Å for the well defined regions. For the F153(5fW) mutant, a total of 1709 unambiguous distance restraints were found. 216 of them were long range restraints. The RMSD between the 20 lowest energy structures (out of 50 calculated) after superimposition is 0.91±0.22Å. The well defined regions in these structures superimposed with a RMSD of 0.60±0.17Å. Just like the other mutants, almost 90% of all backbone dihedral angles are found in the most favoured region of the Ramachandran map. There is a slight difference in the interhelical angle of helices E and F between the F153(5fW) mutant and the wild type cTnC (Table VII-2), with the F153(5fW) mutant being slightly more "open" than the wild type cTnC. As a result the two structures superimposed with a slightly higher back bone RMSD for well defined regions.

The hydrophobic packing of the F153W and the F153(5W) mutants are little disturbed by the replacement of the phenyl ring with the bulkier indole ring. Superimposition of the C-domain of the F153W mutant with the C-domain of the wild type protein revealed that the conformations of all the hydrophobic side chains in the core are in good agreement between the two structures. For the F153W mutant, the 3D aromatic ^{13}C NOESY allowed the extraction of close to 30 unambiguous NOEs for the 6 protons on the indole ring. Qualitative examination of each indole proton's NOE contact patterns alone was enough to define the orientation of the ring unequivocally (Figure VII-7a). The orientation of the indole ring is such that the amide proton on the ring points away from the hydrophobic pocket and towards the E helix, making several contacts with the side chains of Leu 100 and Leu 97. The Hζ3 on the indole ring points deep into the hydrophobic pocket, contacting side chains of the Ile residues in the middle of the short

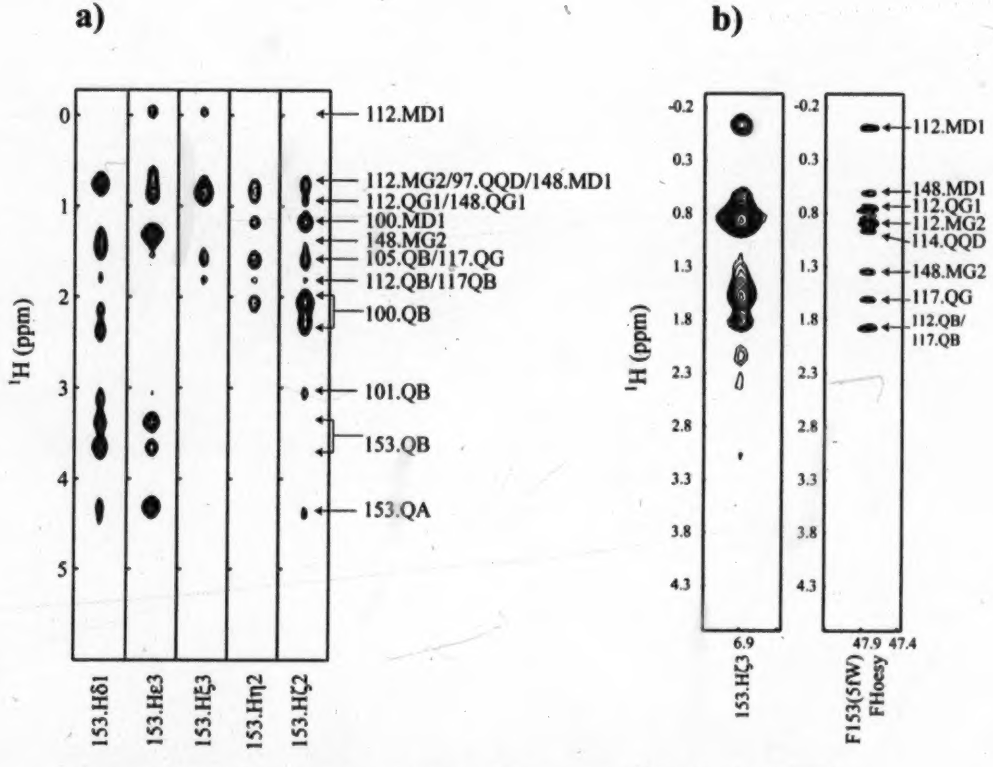

Figure VII-7. a) Strips taken from the 3D aromatic ^{13}C-edited NOESY spectrum of the F153W mutant, illustrating the intramolecular contacts made by the indole ring protons. b) Detailed comparison between the NOE contacts made by the Hζ3 proton on the Trp of the F153W mutant and the ^{19}F atom on the 5fW of the F153(5fW). The NOE contact patterns are virtually identical between the two.

anti-parallel β-sheet that forms the back of the hydrophobic pocket. The χ^2 angle for the residue is ~-95° (Table VII-3). The normal of the indole ring plane is roughly parallel to the helical axis of helix G.

The orientation of the F153(5fW) mutant's fluoroindole ring is determined using the NOE contacts involving only the ^{19}F atom and the amide proton. The NOE contact pattern made by the fluorine agreed well with that of the Hζ3 proton in the F153W mutant (Figure VII-7b). Thus it was not a big surprise when structure refinements done using the distance restraints from the heteronuclear experiment revealed an orientation of the fluoroindole ring that is almost identical to the orientation of the indole ring in the F153W mutant.

Owing to the larger number of restraints that were found for the ^{19}F atom, the fluoroindole ring orientation of the F153(5fW) mutant is much better defined compared to the F104(5fW) mutant. The average value of the χ^2 angle for the 5fW is ~-106° with a standard deviation of only 6° (Table VII-3).

Discussion

Potential use of the mutants as probes in in situ NMR

Studies have demonstrated the applicability of ^{19}F chemical shifts to obtain transmembrane helix orientation in aligned membrane bilayers(*6*). We want to extend this approach to proteins in naturally aligned macromolecular complexes, in particular, skinned muscle fibres. In this methodology, knowledge of the precise orientation of the indole ring in the structure is crucial to acquiring accurate protein orientation. Our study showed that, in all mutants, the indole rings have well-defined orientations. The 5fW in the F104(5fW) mutant possessed an average χ^2 of 83±22° while the 5fW in the F153(5fW) mutant had an average χ^2 of -106±6°. The fact that the 5fW in the F104(5fW) mutant has larger χ^1 and χ^2 diheral angle spreads than the F153(5fW) mutant could be a reflection of its more dynamic indole ring motions. Molecular dynamics simulations conducted for both mutants showed that the indole ring in the F104(5fW) mutant undergoes ring oscillations of considerably larger magnitude than that of the F153(5fW) mutant, which experiences almost no movement (Figure VII-8). However, the motions experienced by the F104(5fW) indole ring are at a much higher frequency than the NMR time scale, thus will have no bearing on the results of the NMR experiments. Owing to the inherent degeneracy in the process of orientation determination using the CSA tensor, two or more CF bond vectors, all of which must have different orientation in the protein, will be needed to solve the protein's orientation. The CF bond vectors in the two mutants are at an average angle of 24° with each other. This implies, with the exceptions of a few situations, that the two vectors will reveal non-

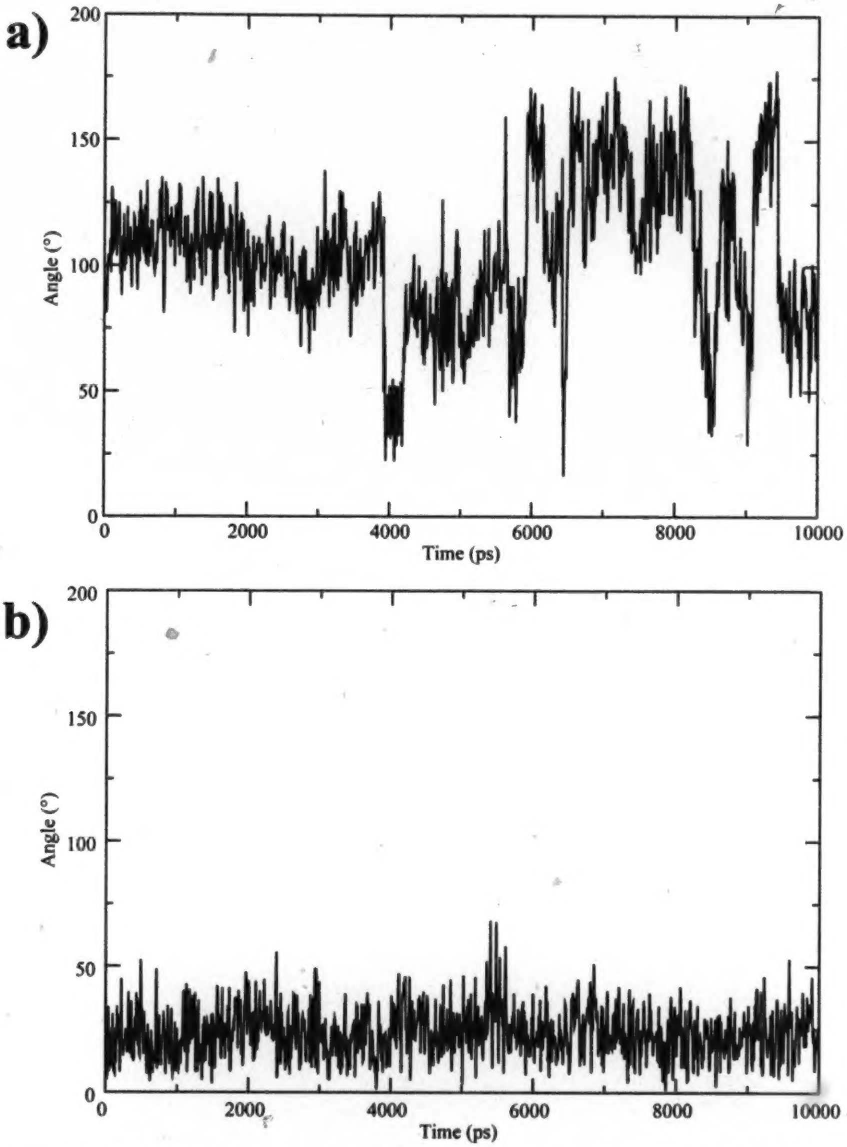

Figure VII-8. 5fW indole ring orientation changes during the 10ns molecular dynamics simulations of a) the F104(5fW) mutant and b) the F153(5fW) mutant. Orientation changes are characterized as changes in the angle between helical axis of the helix containing the 5fW residue and the normal of the fluoroindole ring plane.

degenerate information, an important detail in the case where protein orientation was to be determined using axially symmetric chemical shift tensors.

Structures of the F104 and F153 mutants

In all mutants, the secondary structures are well preserved. The major difference between the mutant structures and the wild type structure lies in the difference in interhelical angles. Determination of interhelical angles using NOE derived distance restraints alone is not always a robust process(*40*). The presence of one or two long range restraints is enough to change the interhelical angle by 20° or more. For this reason, some ambiguous NOE signals from long range contacts were manually assigned before applying the CYANA automatic assignment protocol. It is also evident from the {^{1}H, ^{15}N}-HSQC spectra as well as the presence of important long range NOE signals in the 3D ^{13}C-edited NOESY spectra that all mutants are well folded and adopt the "open" conformation of the wild type cTnC C-domain. Given the above information, we believe the differences in the interhelical angles between the F104W mutant and the wild type structure, as well as that between the F153(5fW) mutant and the wild type structure are not significant enough to be an indicator of major structural change in the mutants.

Signal doubling in the F153(5fW) mutant

Fluorotryptophan incorporation in a protein is never 100% even using the most carefully controlled protocols. The exact percentage of incorporation can be estimated using a number of methods(*14, 20*). If the protein is produced for use in ^{19}F NMR applications, our study shows that the {^{1}H, ^{15}N}-HSQC can be used as supplementary proof of the fluorine incorporation efficiency. In the case of the F153(5fW) mutant, we were able to calculate the ratio between the intensities of the peak produced by the fluorinated isoform and the peak produced by the non-fluorinated isoform. Of the 12 residues showing the signal doubling phenomenon, 10 residues had clear and non-overlapping peaks. For all 10 peaks, the intensity ratio of the strong and the weak peaks came to around 4:1. This implies that about 80% of protein is 5fW-labelled, a number that agrees well with the estimation done using fluorescence measurements. However, this method is much easier to apply once the NMR data is collected and the result is much less ambiguous than the fluorescence method. On the other hand, the methodology is limited to proteins exhibiting the peak doubling phenomenon, and a decent number of residues would have to be looked at to achieve a statistical certainty.

Conclusion

In this study, we used NMR spectroscopy to investigate the effects of Phe-to-Trp mutations and 5fW incorporation on the structure of cTnC, with the aim of developing a functional ^{19}F-labelled cTnC for use in *in situ* ^{19}F NMR. We found that the overall fold of the protein is not significantly affected by either the F104W mutation or the F153W mutation. The hydrophobic core remained intact even when a residue in the core was replaced by the bulkier Trp. The indole ring in the F104W mutants adopted a side chain χ^2 angle of 96±6° while the indole ring in the F153W mutant adopted a χ^2 angle of -96±3°. The replacement of L-Trp with 5fW in these mutants changed neither the protein conformation nor the indole ring orientation. ^{19}F-induced signal doubling in $\{^1H, ^{15}N\}$-HSQC was seen for the F153(5fW) mutant but not for the F104(5fW) mutant. Overall, both mutants would be excellent candidates to serve as probes in the investigation of TnC orientation in skinned muscle fibres.

Table VII-1. Structural Statistics for the C-domain structures of F104W, F104(5fW), F153W, F153(5fW) mutants.

Isoform	F104W	F104(5fW)	F153W	F153(5fW)
NOE Restraints				
total	1545	1272	2111	1709
intraresidue	683	497	695	570
sequential	424	409	637	534
medium range	255	264	496	389
long range	183	122	273	216
Backbone dihedral restraints				
ϕ	98	119	91	106
ψ	101	116	86	106
Restraints violations				
Distance > 0.1Å	8	11	5	7
Dihedral > 1°	0	0	0	0
RMSD to average structure				
Well-defined regions[a]	0.62±0.11Å	0.61±0.12Å	0.62±0.12Å	0.60±0.17Å
All regions[b]	0.80±0.14Å	0.94±0.15Å	0.82±0.10Å	0.91±0.22Å
ϕ,ψ angle stats[c]				
Percentage in most favoured region	89.8	89.4	91.7	89.9
Percentage in additional allowed region	8.0	8.6	7.0	7.9

---

[a] Using residues in the range of 95 to 158 with back bone RMSD smaller than 1.00.
[b] Using all residues in the range of 95 to 158.
[c] Using residues in the range of 95 to 158 as determined by the program Procheck.

Table VII-2. Interhelical angles for the C-domains of wild type and mutant cTnC.

	E/F(°)	G/H(°)
Wild type chicken cTnC[a]	115±4	121±4
F104W	82±9	89±11
F104(5fW)	106±8	111±6
F153W	108±8	115±5
F153(5fW)	92±9	116±6

[a]PDB access code 1AJ4.

Table VII-3. Trp and 5fW side chain dihedral angles of the mutants.

	χ^1(°)	χ^2(°)
F104W	-67±4	96±6
F104(5fW)	-70±14	83±23
F153W	177±4	-96±3
F153(5fW)	-175±6	-106±6

References

1. Corrie, J. E., Brandmeier, B. D., Ferguson, R. E., Trentham, D. R., Kendrick-Jones, J., Hopkins, S. C., van der Heide, U. A., Goldman, Y. E., Sabido-David, C., Dale, R. E., Criddle, S., and Irving, M. (1999) *Nature 400*, 425-30.
2. Wuthrich, K. (2001) *Nat Struct Biol 8*, 923-5.
3. Wuthrich, K. (1998) *Nat Struct Biol 5 Suppl*, 492-5.
4. Opella, S. J., and Marassi, F. M. (2004) *Chem Rev 104*, 3587-606.
5. Opella, S. J., Ma, C., and Marassi, F. M. (2001) *Methods Enzymol 339*, 285-313.
6. Grage, S. L., Wang, J., Cross, T. A., and Ulrich, A. S. (2002) *Biophys J 83*, 3336-50.
7. Cornelissen, G., Van Noort, P. C. M., Nachtegaal, G., and Kentgens, A. P. M. (2000) *Environmental Science & Technology 34*, 645-649.
8. Sobolev, A. V., Krupoder, S. A., Liskovskaya, T. I., and Danilovich, V. S. (2000) *Journal of Structural Chemistry 41*, 338-339.
9. Dalvit, C., Flocco, M., Veronesi, M., and Stockman, B. J. (2002) *Combinatorial Chemistry & High Throughput Screening 5*, 605-611.
10. Sykes, B. D., and Weiner, J. H. (1980) in *Magnetic Resonance in Biology* (Cohen, J. S., Ed.) pp 171-196, John Wiley & Sons, New York.
11. Pratt, E. A., and Ho, C. (1975) *Biochemistry 14*, 3035-40.
12. Browne, D. R., Kenyon, G. L., and Hegeman, G. D. (1970) *Biochem Biophys Res Commun 39*, 13-9.
13. Salopek-Sondi, B., Vaughan, M. D., Skeels, M. C., Honek, J. F., and Luck, L. A. (2003) *J Biomol Struct Dyn 21*, 235-46.
14. Campos-Olivas, R., Aziz, R., Helms, G. L., Evans, J. N., and Gronenborn, A. M. (2002) *FEBS Lett 517*, 55-60.
15. Anderluh, G., Razpotnik, A., Podlesek, Z., Macek, P., Separovic, F., and Norton, R. S. (2005) *J Mol Biol 347*, 27-39.
16. Abbott, G. L., Blouse, G. E., Perron, M. J., Shore, J. D., Luck, L. A., and Szabo, A. G. (2004) *Biochemistry 43*, 1507-19.
17. Ulrich, A. S. (2005) *Progress in Nuclear Magnetic Resonance Spectroscopy 46*, 1-21.
18. Trigo-Gonzalez, G., Racher, K., Burtnick, L., and Borgford, T. (1992) *Biochemistry 31*, 7009-15.
19. Ho, S. N., Hunt, H. D., Horton, R. M., Pullen, J. K., and Pease, L. R. (1989) *Gene 77*, 51-9.
20. Valencia, F. F., Paulucci, A. A., Quaggio, R. B., Da Silva, A. C., Farah, C. S., and Reinach, F. C. (2003) *J Biol Chem 278*, 11007-14.
21. Delaglio, F., Grzesiek, S., Vuister, G. W., Zhu, G., Pfeifer, J., and Bax, A. (1995) *J. Biomol. NMR 6*, 277-293.
22. Johnson, B. A., and Blevins, R. A. (1994) *J. Biomol. NMR 4*, 603-614.
23. Wittekind, M., and Mueller, L. (1993) *Journal of Magnetic Resonance B 101*, 201-205.
24. Grzesiek, S., and Bax, A. (1992) *Journal of the American Chemical Society 114*, 6291-6293.

25. Slupsky, C. M., Boyko, R. F., Booth, V. K., and Sykes, B. D. (2003) *Journal of Biomolecular NMR 27*, 313-321.
26. Sattler, M., Schwendinger, M. G., Schleucher, J., and Griesinger, C. (1995) *Journal of Biomolecular Nmr 6*, 11-22.
27. Lyons, B. A., and Montelione, G. T. (1993) *Journal of Magnetic Resonance Series B 101*, 206-209.
28. Grzesiek, S., Anglister, J., and Bax, A. (1993) *Journal of Magnetic Resonance Series B 101*, 114-119.
29. Guntert, P. (2004) *Methods Mol Biol 278*, 353-78.
30. Cornilescu, G., Delaglio, F., and Bax, A. (1999) *Journal of Biomolecular Nmr 13*, 289-302.
31. Linge, J. P., Williams, M. A., Spronk, C. A., Bonvin, A. M., and Nilges, M. (2003) *Proteins 50*, 496-506.
32. Schwieters, C. D., Kuszewski, J. J., Tjandra, N., and Clore, G. M. (2003) *Journal of Magnetic Resonance 160*, 65-73.
33. Kover, K. E., and Batta, G. (1987) *Progress in Nuclear Magnetic Resonance Spectroscopy 19*, 223-266.
34. Rinaldi, P. L. (1983) *Journal of the American Chemical Society 105*, 5167-5168.
35. Sia, S. K., Li, M. X., Spyracopoulos, L., Gagné, S. M., Liu, W., Putkey, J. A., and Sykes, B. D. (1997) *J. Biol. Chem. 272*, 18216-18221.
36. Grzesiek, S., and Bax, A. (1992) *J. Magn. Reson. 96*, 432-440.
37. Grzesiek, S., Anglister, J., Ren, H., and Bax, A. (1993) *Journal of the American Chemical Society 115*, 4369-4370.
38. Wishart, D. S., Sykes, B. D., and Richards, F. M. (1991) *Journal of Molecular Biology 222*, 311-333.
39. Chandra, M., McCubbin, W. D., Oikawa, K., Kay, C. M., and Smillie, L. B. (1994) *Biochemistry 33*, 2961-9.
40. Chou, J. J., Li, S., Klee, C. B., and Bax, A. (2001) *Nat Struct Biol 8*, 990-7.

Chapter VIII

Conclusion

This thesis is devoted to expanding our knowledge on the role played by Tn proteins in muscle regulation in general and cardiac muscle regulation in particular. Much focus has been put on understanding how drugs such as Ca^{2+}-sensitizers modulate the cardiac muscle function by interacting with cTnC (Chapters II and III) as well as how phosphorylations and mutations in Tn proteins lead to changes in cardiac muscle behaviour (Chapter IV). In the latter part of my thesis, I tried to bring the research in muscle regulatory proteins into an *in situ* setting where movements and conformational changes of Tn proteins as well as their interactions with other ligands can be evaluated in a realistic environment. This chapter will not summarize the results from other chapters (each chapter already has its own conclusions). Instead I will focus on the significance of the results as well as unanswered questions and future projects worth conducting.

Role of Ca^{2+}-sensitizers in modulating cardiac function

Ca^{2+}-sensitizers are poised to play an important clinical role in the future. Results from this thesis have shed some light on how Ca^{2+}-sensitizers interact with cTnC. The importance of the hydrophobic grooves in mediating drug-cTnC interactions is immediately evident from the structure of EMD 57033 and bepridil complexed to cTnC. Of all TnC-binding compounds for which high-resolution structural information is available (EMD 57033, bepridil, W7, TFP), all interact with the hydrophobic patches on TnC. Knowing this general trend will help the designers of such compounds to focus on only the interactions that matter. However, a good many questions about the interactions between TnC and Ca^{2+}-sensitizers still remain. One of them is regarding the specificity of EMD 57033 for cCTnC but not cNTnC. Although there is no experimental data to explain this, differences between EMD 57033's and bepridil's interactions with cTnC do offer a possible hypothesis. The binding of bepridil to cNTnC converts the protein to its active conformation (*1, 2*) by inserting two aromatic rings into the hydrophobic core of the N-terminal domain. This involves extensive interactions between the two aromatic rings of bepridil and the residues composing the hydrophobic core. Compared to bepridil, EMD 57033 contacts a less number of residues in the core, thus EMD 57033 may not be able to "open" the N-terminal domain on its own. Since the exposure of the hydrophobic surface is important to EMD 57033's interaction to the C-terminal domain of TnC, it is plausible that EMD 57033 is unable to bind to the isolated cNTnC simply because cNTnC adopts the "closed" conformation that hides the hydrophobic surface. It remains to be seen whether EMD 57033 can bind to the N-terminal domain when it is in the "open" conformation and stabilize it. Another reason supporting the notion of the N-terminal-binding EMD 57033 is the fact that the N-terminal region of cTnI binds the hydrophobic groove of cCTnC with high affinity and is expected to be immobilized on the cCTnC during both activated and relaxed state of the muscle. With the cTnI bound to cCTnC, the likelihood of small molecules such as EMD 57033 gaining access to the C-terminal domain is effectively nullified. In fact, this has been demonstrated experimentally for both EMD 57033 and levosimendan (*3, 4*).

Given the highly homologous structure between cTnC and sTnC, whether EMD 57033 has the same effect in skeletal muscle as in cardiac muscle is another question researchers are interested in. Lipscomb et al. showed that EMD 57033 produced bigger

Ca^{2+}-sensitizing effect in cTnC-containing skeletal muscle fibres than sTnC-containing skeletal muscle fibres (*5*), implying EMD 57033 interacted differently with sTnC than cTnC. The sequence alignment between cTnC and sTnC shows their hydrophobic core structures are almost identical. The few non-conservative amino acid substitutions between them are not close to the area where these drugs interact with the protein. Because our understanding of ligand-protein interactions is still incomplete, we can only speculate as to what the possible explanations maybe. If steric clashes or electrostatic repulsions are ruled out, there only remain entropic reasons to explain the difference we see, and this can only be proved using dynamic data from both the protein and the ligand. The differential interaction of EMD 57033 with cTnC and sTnC is a good example of some of the troubling inconsistencies I have encountered during my graduate studies. And this type of inconsistencies can be found in many structural biology projects. I think our inability to rationalize experimental observations, especially when it comes to predicting the affinity of proteins for its ligands, illustrates the incompleteness of our knowledge of protein behaviour. Sometimes, weak and subtle interactions, which are usually not seen in crystal structures or even in solution structures, can have dire consequences on how proteins interact with other compounds. Although NMR is not the only technique in the field of biochemistry, I believe its ability to probe site-specific dynamics of proteins, at the time scale relevant to these interactions make it a promising tool for cracking these tough questions.

Besides EMD 57033, levosimendan is also a member of the family of thiadiazinone-derived Ca^{2+}-sensitizers. It is also the only commercially available Ca^{2+}-sensitizer. However, because levosimendan's instability in solution, its interaction with cTnC was never thoroughly investigated. A series of studies conducted by Sorsa et al. showed it binds cCTnC only marginally but interacts with cNTnC on slow NMR time scale (*6*). Interestingly, levosimendan's interaction with cNTnC is dependent on the presence of Cys 84 residue of cNTnC. Given that levosimendan is also known to react with DTT, this raises the possibility that levosimendan might be covalently linked to cNTnC by reacting with the SH group of Cys 84. This would also explain why EMD 57033, whose structure is very similar to levosimendan, is not shown to interact with cNTnC while levosimendan is.

Phosphorylations and mutations in cTnI and their effects on cTnI-cTnC interactions

Modulations of cardiac muscle function by phosphorylation as well as disease-associated mutations in Tn proteins are gathering more attention in the field because of their medical applications. However, most attempts to rationalize their physiological impact using available structural information have come up with ambiguous, if not all together contradictory, conclusions. The phosphorylation of residue S149 of cTnI studied in this thesis is a good example. The NMR study clearly shows the phosphorylation weakens cTnI's interaction with cTnC, which would imply decreased Ca^{2+}-sensitivity and reduced muscle activity. But physiological study shows the phosphorylation, in fact, sensitizes the muscle to Ca^{2+} (*7*). The cTnI FHC mutation R161W investigated in Chapter IV is in a similar situation. Although *in vitro* study shows the R161W mutation in cTnI produced only nominal changes in its interaction with cTnC, the physiological study clearly shows it decreases acto-myosin ATPase inhibition and increases Ca^{2+}-sensitivity. In both cases the result can only be rationalized by assuming the modification changes cTnI-actin interactions more than it does cTnI-cTnC interactions. This highlights the fact that although our understanding of TnC-TnI interaction is quite thorough, our knowledge of how Tn proteins interact with Tm and actin is still inadequate. Eventually Tn protein interactions with Tm and actin and their impact on muscle regulation would have to be investigated. And I hope the *in situ* NMR technique developed in the last part of this thesis will play an important role in it.

Another notable implication from this study concerns the role played by cTnI's switch region in mediating cTnI-actin interaction. The conventional wisdom is that only the inhibitory region and the region down stream from the switch region are important for cTnI's affinity for actin. However, if the above assumption regarding the effects of cTnI's modifications on cTnI-actin interaction is true, then cTnI's switch region must also play a pivotal role in mediating cTnI-actin interaction. The interplay between phosphorylations and mutations of cTnI revealed by this and other studies may also warrant further investigations. The fact that FHC mutations causes sudden cardiac failure rather than a chronic condition maybe a sign that the effects of FHC mutations maybe exaggerated greatly when the heart is under stress, which also happens to be the occasion when some of the cTnI phosphorylations take place. The changes produced by cTnI's R161W mutation on S149-phosphorylated cTnI's affinity for cTnC might offer some rational explanation to this trend.

in situ ^{19}F NMR of myofibrils

I believe *in situ* NMR of myofibrils discussed in the previous three chapters holds great promise in answering many of the questions just raised. The methodology doesn't have to be restricted to the C-terminal of cTnC, it can be equally applied to any rigid domains of TnI, TnT, even Tm and actin. To investigate the orientation of cNTnC using this methodology, Phe-to-Trp mutations in cNTnC would need to be made. F27 and F77 are counterparts of F104 and F153 in the N-terminal. F27 has been studied before and shown to have minimal impact on the structure (*8*). F77W mutant of TnC is currently being investigated (Julien et al., unpublished data). It will be very interesting to see whether the mutation, which is in the hydrophobic core of cTnC has any impact on the more flexible structure of cNTnC. Besides obtaining orientational information, this technique can also be used to detect changes in protein dynamics and protein ligand interactions. However, CSA tensor doesn't have to be our only source of information. Dipolar coupling interactions through space are also orientation dependent. The fact most proteins in a myofibril are aligned means, theoretically, the orientation of the protein can be elucidated through experiments such as PISEMA (*9*). In practice, the experiment is complicated by the fact that PISEMA is usually applied to ^{15}N-^{1}H pair in aligned membrane bilayers, where nitrogen containing compounds are rare. However, myofibril is almost consisted entirely of protein. The background noise due to natural abundance ^{15}N from other proteins is enough to overwhelm even the signal from ^{15}N-enriched cTnC. ^{19}F-^{13}C pair is another possible PISEMA combination. However, obtaining custom fluorinated ^{13}C-enriched compounds is beyond the financial reach of most laboratories.

One of the advantages of working with proteins embedded in myofibrils is that fibre proteins are aligned with respect to the laboratory frame, giving reduced spectral complexity, higher information content and better signal-to-noise ratio. However, myofibril isn't the only way to induce protein alignment. Proteins in liquid crystalline medium such as phage and lipids, as well as those embedded in stressed polyacrylamide gel, often show weak alignment owing to restricted movement. This weak alignment can change the value of some coupling constants and the magnitude of the change is dependent on the orientation of the vector connecting the two coupled atoms with respect to the magnetic field, similar to the relationship between CSA tensor of an atom and the magnetic field. The technique has found wide spread application in protein NMR, especially for defining protein-protein interactions. In the field of muscle regulation, this technique can be readily applied to solving one of the outstanding problems concerning the structure of TnC: in the crystal structure of skeletal Tn core domain, the central linker of sTnC adopts a rigid helical conformation where as the cTnC in the crystal structure of cardiac Tn core domain has an unstructured central linker. Since the linker region is implicated in the interaction with the inhibitory region of cTnI, knowing its conformation as well as how it changes its conformation during muscle activation will help to shed light on how cTnC is able to attract cTnI from actin onto cTnC. Because the orientation of the N-terminal domain would be quite different depending on whether the central linker is rigid or flexible, the question of central linker conformation can be answered easily by obtaining the orientation of the N-terminal domain. The easiest way to accomplish this is by aligning the soluble form of Tn core complex in stressed gel or liquid crystalline medium and compare the differences in the orientation between the C-terminal domain of cTnC and the N-terminal domain of cTnC.

References

1. Li, Y., Love, M. L., Putkey, J. A., and Cohen, C. (2000) *Proc. Natl. Acad. Sci. U. S. A. 97*, 5140-5.
2. Wang, X., Li, M. X., and Sykes, B. D. (2002) *J Biol Chem 277*, 31124-33.
3. Wang, X., Li, M. X., Spyracopoulos, L., Beier, N., Chandra, M., Solaro, R. J., and Sykes, B. D. (2001) *J Biol Chem 276*, 25456-66.
4. Sorsa, T., Pollesello, P., Permi, P., Drakenberg, T., and Kilpelainen, I. (2003) *J Mol Cell Cardiol 35*, 1055-61.
5. Lipscomb, S., Preston, L. C., Robinson, P., Redwood, C. S., Mulligan, I. P., and Ashley, C. C. (2005) *Biochem J.*
6. Sorsa, T., Heikkinen, S., Abbott, M. B., Abusamhadneh, E., Laakso, T., Tilgmann, C., Serimaa, R., Annila, A., Rosevear, P. R., Drakenberg, T., Pollesello, P., and Kilpelainen, I. (2001) *J Biol Chem 276*, 9337-43.
7. Buscemi, N., Foster, D. B., Neverova, I., and Van Eyk, J. E. (2002) *Circ Res 91*, 509-16.
8. Chandra, M., da Silva, E. F., Sorenson, M. M., Ferro, J. A., Pearlstone, J. R., Nash, B. E., Borgford, T., Kay, C. M., and Smillie, L. B. (1994) *J Biol Chem 269*, 14988-94.
9. Ramamoorthy, A., and Opella, S. J. (1995) *Solid State Nucl Magn Reson 4*, 387-92.